PLACEMENT OF PHASOR MEASUREMENT UNITS AND CONTROL OF ROTOR ANGLE STABILITY IN POWER SYSTEMS

Ph. D. THESIS

by

CHARU SHARMA

DEPARTMENT OF ELECTRICAL ENGINEERING
INDIAN INSTITUTE OF TECHNOLOGY ROORKEE
ROORKEE-247667 (INDIA)

OCTOBER, 2014

PLACEMENT OF PHASOR MEASUREMENT UNITS AND CONTROL OF ROTOR ANGLE STABILITY IN POWER SYSTEMS

A THESIS

Submitted in partial fulfilment of the requirements for the award of the degree of

DOCTOR OF PHILOSOPHY

in

ELECTRICAL ENGINEERING

by

CHARU SHARMA

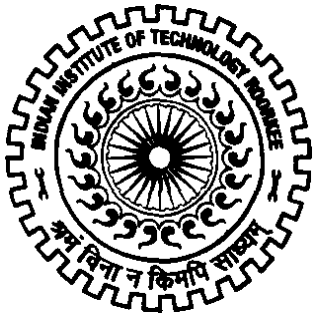

DEPARTMENT OF ELECTRICAL ENGINEERING
INDIAN INSTITUTE OF TECHNOLOGY ROORKEE
ROORKEE-247 667 (INDIA)

OCTOBER, 2014

INDIAN INSTITUTE OF TECHNOLOGY ROORKEE
ROORKEE

CANDIDATE'S DECLARATION

I hereby certify that the work which is being presented in the thesis entitled "**PLACEMENT OF PHASOR MEASUREMENT UNITS AND CONTROL OF ROTOR ANGLE STABILITY IN POWER SYSTEMS**" in partial fulfilment of the requirements for the award of the Degree of Doctor of Philosophy and submitted in the Department of Electrical Engineering of the Indian Institute of Technology Roorkee is an authentic record of my own work carried out during a period from December, 2009 to October, 2014 under the supervision of Dr. Barjeev Tyagi, Associate Professor, Department of Electrical Engineering, Indian Institute of Technology Roorkee, Roorkee.

The matter presented in this thesis has not been submitted by me for the award of any other degree of this or any other Institute.

(Charu Sharma)

This is to certify that the above statement made by the candidate is correct to the best of my knowledge.

(Barjeev Tyagi)
Supervisor

Date: _____

ABSTRACT

For secure and reliable operation of an interconnected power system, it is required to monitor wide area system and its stability in real time. The recent development of synchro phasor technology has brought a paradigm shift in real time analysis of power system. Phasor Measurement Unit (PMU) is the backbone of this Synchronized Measurement Technology (SMT). PMU measures the instantaneous voltage, current, and frequency from dispersed locations of a wide network. These analog system parameters are sampled 20 or more times per cycle. Phasor values are computed from these sampled values, and more than 30 phasor values are reported per second. Precise time stamp is added to each phasor value. Therefore, phasor measurement provides an electrical real-time picture with high resolution. This high-resolution picture aids in all kinds of monitoring, control, and protection applications. This thesis primarily focuses on application of PMU measurements in wide area monitoring and control of rotor-angle/dynamic stability.

In wide area monitoring, the very first step, is to install phasor measurement units in the system. The prime objective of PMU installation is to make given system observable, either completely or incompletely. In practical scenario, PMU deployment requires large expenditure on its installation. Proper site preparation, establishment of adequate communication and Global Positioning System (GPS) are other essential requirements, which increase these financial constraints more. As a solution, PMU placement locations are selected optimally. Rich literature is available on various placement methodologies, such as Integer programming, depth-first search, and spanning tree methods. Intelligent techniques like genetic algorithm, Tabu search, simulated annealing, particle swarm optimization techniques are also reported. Presence of conventional measurements and loss of line or PMU are also extensively studied. However, placement methodology dealing simultaneously with three objectives i.e. observability, conventional measurements and redundancy is a requirement.

In present work, all three objectives are formulated using quadratic programming approach. This quadratic problem is solved using Binary Particle Swarm Optimization (BPSO) technique to obtain optimal PMU locations. Further, to confirm efficiency of the

approach, optimal results of BPSO are compared with locations obtained through GAMS-MIP solver.

Today utilities are planning to place PMUs in large amount. In near future synchro-phasor number in the grid will increase substantially. With increase in number of synchro phasors, apart from topological and numerical observability, new methodologies are required to explore more benefits from PMU placement. In few power system applications, flow connectivity plays an important role, for example in congestion management. Therefore, it is essential to have a methodology to identify those PMU locations, through which maximum amount of power flow can be monitored. Since, power flow in the network depends on the load / demand of the network. Therefore, identification of those demand nodes, which affect maximum flow connectivity in a smart grid, is still an unanswered question.

To address aforesaid problem, sequential placement scheme is suggested in present work. Proposed technique is based on power flow patterns and demand of the given system. Therefore, demand and flow coverage concept is introduced to formulate PMU placement. Formulation for multiple flow patterns is also addressed, which considers variable operating scenarios of power systems.

PMU placement in phases or stages is another widely used approach for Optimal PMU Placement (OPP) problem. PMU placement in stages using Integer Linear Programming (ILP) and depth first search are reported in past. Few authors have considered phased placement with additional benefits in terms of bus and tie line observability. However, PMU placement based on control scheme for rotor-angle stability is not yet reported. As stated before, PMU placement is done to make system complete observable. For rotor angle stability, real time angular information is required, which means PMUs should be placed at generator buses. With limited number of PMUs, placement scheme dealing simultaneously with these two different issues is a need of time.

In this thesis, a method is developed to identify and rank those PMU locations, which are important for rotor-angle stability. First, Eigen value analysis is carried out to determine inter-area modes. For these inter-area modes, control scheme is proposed. Based on control scheme, selection criteria namely, Generator bus observability criterion, tie-line observability criterion and bus observability criterion are introduced. Critical buses are

identified based on these criteria and ranking of PMU locations is carried out using Analytical Hierarchical Process.

Stability of power system is that property of the system, which governs continuance of intact operation following a disturbance. Stability of power system is characterized by its time varying nature. Traditionally performance of the system can be judged under a particular set of conditions. According to IEEE-CIGRE joint working group, power system stability is broadly classified into Rotor angle Stability, Voltage Stability and Frequency Stability. Rotor angle stability can be further divided into small-signal rotor angle stability and large-disturbance rotor angle stability or transient stability.

Small-signal rotor angle stability is the ability of power system to maintain synchronism under small disturbances. These disturbances are considered significantly small, such that system can be analyzed by linearized equations. This instability is further sub divided into local and global. Local instability results due to presence of local mode, which are having frequencies from 1-10Hz. Power system stabilizers, are conventionally provided with each generator to control local mode. Global problems are caused by inter area modes having frequency between 0.1 to 1 Hz and have more widespread effects. To identify these local and inter area modes, which are responsible for oscillations usually Eigen value analysis is performed. These Eigen value based techniques are offline methods and does not work well for geographically large dynamic systems. Introduction of synchro phasor technology has encouraged utilization of direct measurements based techniques for mode identification. These measurement based techniques offers a real time solution to identify inter area modes.

This thesis provides a real-time approach to analyze inter-area modes based on Continuous Wavelet Transform (CWT). Modal frequency and damping are estimated using Morlet based CWT with good accuracy. Results of CWT are verified through conventional Eigen value analysis.

Presence of these inter area modes in an interconnected network has wide spread effects. These inter area modes results into inter area oscillations, which have adverse effects on transmission corridors. To enhance transmission through tie lines in near-by areas, additional damping is required. Recently, it is explored that remote machine can be used to provide this additional damping. With advent of phasor technology, it is easier to obtain remote machine

speed signals with the help of PMUs. These remote machine signals are used to design wide area damping controllers. Literature reveals that robust and intelligent damping controllers are widely used for inter area oscillations. In a large practical system, it is important to select appropriate location of these damping controllers. Further, proper selection of feedback signals from generators is of immense importance. Since feedback, signals are communicated from remote locations, so they carry communication latencies or delays. In past, very few researchers have considered selection of controller location and feedback signals in detail. However, time delays are not reported in their work.

In present work, first low frequency modes are identified. For identified modes, control scheme is proposed to select suitable controller location and input signal based on participation factors and controllability indices respectively. Wide area controllers based on Mamdani fuzzy inference system and Adaptive Neuro Fuzzy inference System (ANFIS) are designed to compensate time latencies and low frequency oscillations. Robustness of designed controllers is checked by varying various system parameters.

According to IEEE 1344-1995 synchro-phasor standard, PMU data are uncertain due to errors in measurement of magnitude or angle of the phasor or due to error in time synchronization of synchro-phasors. Total vector error for PMUs should be less than 1%, which means measurements can have a maximum error of 1%. According to literature, PMU measurements are uncertain due to routing and packet delay. Further, PMUs cannot directly measure the internal states like rotor angle. These rotor angles are generally estimated through various rotor-estimating algorithms. Therefore, rotor angle measurements provided by PMUs depends on accuracy of these algorithms. Practically, accurate estimating algorithms also have few estimating errors, which make PMU measurements more uncertain and noisy. Therefore, for small signal stability problem a wide area-damping controller considering communication delay and measurement uncertainties is a requirement.

As a solution, in this work, interval-type-2 fuzzy controllers are designed. To compensate measurement uncertainty, a method is introduced to model Foot of Uncertainty (FOU) of type-2 membership function from type-1 membership function. FOU is varied in gradual steps to test controller performance. Further, robustness of controller is verified by adding noise in the communicated signal.

In large power systems, sometimes superposition of local modes and inter area modes or occurrence of severe disturbances like three-phase to ground fault or loss of transmission lines, causes large excursions of generator rotor angles resulting into transient instability. Conventionally, time domain simulations are used for transient stability analysis. However, this technique is time consuming and requires accurate system information. As time- frame of interest in transient stability studies is usually 3-5 seconds following a disturbance which itself is of small duration. Therefore, fast and accurate transient predictor is needed to have secure operation of the system. A predictor having small prediction- time provides more time to utilities to take corrective and preventative actions. Since synchro-phasors are able to provide real time voltage and current information of the bus on which they are placed. Therefore, a transient predictor utilizing these précised information is essential for reliable performance of power system.

Present thesis describes about transient stability predictor based on relevance vector machine. Three different features are considered in the work, for training predictor. These features are obtained from sampled values of generator bus voltage and angle profiles. To validate effectiveness of the predictor, sample values are gradually increased from 2 to 7 samples. Later, RVM predictor is compared with SVM predictor for different number of samples.

ACKNOWLEDGEMENTS

My foremost and profound gratitude goes to my guide **Dr. Barjeev Tyagi**, Associate Professor, Department of Electrical Engineering, Indian Institute of Technology Roorkee, India, for his proficient and enthusiastic guidance, useful criticism, moral support, continuous encouragement, and immense help throughout the research and believing in me all the time. With his wide experience, sharp and incisive intellect, maestro ability combined with astute research methodology, and deep insight of the subject have unerringly steered the work on smooth and steady course. I sincerely appreciate his pronounced individuality, humanistic and warm personal approach, which has given me the strength and will to carry this research work. I humbly acknowledge a lifetime gratitude to my mentor.

I express my deep sense of gratitude to the Dr. S.P. Srivastava, Professor and Head, Department of Electrical Engineering, for providing the necessary facilities and healthy environment to carry out the research work. I extend my thanks to all members of the Department of the Electrical Engineering, with its diverse nature of the faculty that has constituted the strength of the department.

I express my sincere thanks to Prof. G. N. Pillai, Chairman D.R.C. and Prof. B. Das, Chairman S.R.C., Department of Electrical Engineering and Dr. Ravi Kumar, Professor, Department of Mechanical Engineering for sparing their valuable time in reviewing and critically examining the work.

My heartfelt thanks are due to the families of Dr. Barjeev Tyagi for providing the moral support and co-operations.

I wish to thank my M. Tech. friend Miss Pooja Bharadwaj, Mrs Sarita Mishra, Miss Yati Sharma for giving me support and energy in realizing my thoughts as successful research work.

I am indebted to my father Sh. K.C Sharma and my mother Smt. Bala Devi for their eternal support and everlasting blessings. I gratefully acknowledge the inspiration and unflagging support of my parents. I wish to express my deepest gratitude to my brother, Mr. Ashutosh Sharma, Mr. Dinanath Prasad and their families. I wish to express my wholeheartedly thanks to my sister Mrs. Vibhuti Mishra and her family.

I express my sincere appreciation and gratitude to my parents and for bearing joyfully all the sorts of inconvenience and hard ship during my involvement in this work. I thank my fiancé

Dr. Pawan Sharma for his patience, encouragement and close cooperation during the tenure of this work. I wish to express my sincere thanks to my father-in-law and mother- in-law for their blessings.

I would like to dedicate this research work to my parents.

My special thanks are due to all my senior, fellow, and junior research scholars Satish Kansal, Sweta Tripathi, Megha Aggarwal, Himanshu Chaudhary, K.S. Sajan, Nagendra Gautam, Mrs. Sandeep Kaur, Afzal Sikander, Harikrishanan Muda, Sandeep Hanwate, Sahaj Saxena and Swati Sodhi at IIT Roorkee, for their cooperation and moral support from time to time. I am thankful to non-teaching staff of the Department of Electrical Engineering for their help and support.

Lastly, I owe a deep sense of gratitude to the All-Pervading, All-Sustaining Spirit whose divine light and warmth provided me the perseverance, guidance, inspiration, faith, and strength to carry on even when the going got tough.

(Charu Sharma)

CONTENTS

LIST OF FIGURES

LIST OF TABLES

LIST OF SYMBOLS

The list of principle symbols used in the text and their abbreviations are given below. For the sake of clarity and similarity of symbols used in the text, some symbols are redundantly abbreviated.

Symbol	Stands for
I_{MXM}	Identity matrix
$pbest_i^k$	Personal best value of particle i at iteration k
v_i^k	Velocity of particle at iteration k
$gbest^k$	Global best at iteration k
φ_1	Acceleration constant
$s(v_{ij})$	Sigmoid function of velocity vij
w_1	weights
$F(x)$	Fitness function
G	Transformation matrix
N_G	Redundancy level
$F(9,2)$	Fractional flow from node i to node j
d_i	Demand at node i
$\overline{C}_{i,j}$	Transpose of FCM
d_{ip}	Demand at node i for pattern P
$\overline{C}_{i,j}^p$	Transpose of Flow-coverage-matrix (*FCM*) for p^{th} pattern
q_{ki}	Left Eigen vector of the i^{th} mode of the k^{th} state variable
ρ_{ki}	Participation factor of the i^{th} mode of the k^{th} state variable
p_{ki}	Right Eigen vector of the i^{th} mode of the k^{th} state variable
NI_{kj}	Normalized value of j^{th} crierion for k^{th} optimal location
U_{gen}^k	Number of generator buses connected to k^{th} bus

U_{Ngen}^{k}	Number of neighboring generator buses connected to k^{th} bus
U_{NNgen}^{k}	Neighbor to neighboring buses connected to k^{th} bus
e	Error
de	Derivative of error
σ	Standard deviation
ω	Speed deviation
$d\omega/dt$	Derivative of Speed
$\mu_A(x)$	Membership function of Fuzzy set A
$\widetilde{A}$	Type-2 Fuzzy set A
$\widetilde{\mu}_A(x)$	Membership grade of x in the type-2 Fuzzy set $\widetilde{A}$
$\widetilde{\mu}_A(x,u)$	Membership function of type-2 Fuzzy set A
s_{noise}	Noise in communicated signal
$\lvert d_{\max} \rvert$	Maximum angle of separation between any two machines
$P(t_j/x_j)$	Probability of obtaining the output t_j when input x_j is given
$\in_j$	Noise in prediction
σ^2	Variance
α	Vector of hyper-parameters
β	Inverse of Variance

LIST OF ABBREVIATIONS

The abbreviations used in the text have been defined at appropriate places, however, for easy reference, the list of abbreviations are being given below.

Abbreviations	Stands for
AHP	Analytical Hierarchical Process
ANFIS	Adaptive Neuro Fuzzy Inference Systems
BOI	Bus Observability Index
BPSO	Binary Particle Swarm Optimization
CWT	Continuous Wavelet Transform
eq	Equation
et al.	and others
etc	et cetera
FCM	Flow Coverage Matrix
FFM	Flow Fraction Matrix
Fig	Figure
FLC	Fuzzy Logic Controller
FOU	Foot of Uncertainty
FPI	Final Priority Indices
GAMS	Generic Algebraic Modeling Systems
GBOI	Generator Bus Observability Index
i.e	that is to say
IEEE	Institute of Electrical and Electronics Engineers
KCL	Kirchhoff's Current Law
MFs	Membership Functions
MIP	Mixed Integer Programming
OPP	Optimal PMU Placement
p.u	Per unit
PM	Pair wise Matrix
PMU	Phasor Measurement Units

PSO	Particle Swarm Optimization
RVM	Relevance Vector Machine
s	second
SCADA	Supervisory Control and Data Acquisition System
SNR	Signal to Noise Ratio
SVM	Support Vector Machine
TLBOI	Tie Line Bus Observability Index
WAFC	Wide area Fuzzy Controller
WAMS	Wide area Measurement Systems
WT	Wavelet Transform

CHAPTER – 1
INTRODUCTION

1.1 OVERVIEW

Today electric power systems are continuously expanding. This dynamic expansion has made power systems more complex, unpredictable, and uncertain. Consequently, monitoring and control of power systems is becoming more and more challenging. Conventional methods like Supervisory Control and Data Acquisition (SCADA) systems provide system information, typically at an interval of 5-10 minutes. With this information, it becomes difficult to have real-time realization of the system. With advent of Synchronized Measurement Technology (SMT), it is easy to obtain real time picture of the system. SMT comprises of Phasor Measurement units (PMU), which provides time synchronized measurements from widely dispersed locations. These measurements are highly accurate and provide phasor information more than once in one cycle. Such Precise information represents dynamic information of the network. This dynamic information facilitates real time wide area monitoring and control.

In a wide area network, it is essential to place PMUs judicially in the system. Efficient PMU placement is a prerequisite for complete observability of the system. Further, it can also benefit in various control and stability applications. Recently, it is established that PMU measurements can enhance Rotor angle stability analysis. These measurements can assist in real time identification of various causes, which lead to rotor angle instability. As well as they also help in designing various preventive and control measures for the same. Therefore, this thesis explores various issues regarding PMU placement and their application in field of rotor angle stability.

1.1.1 Phasor Measurement Units and Power System Monitoring

In past years, it has been recognized that many problems that led to power system failure could have been prevented if more robust and accurate Energy Management System (EMS) was used. Conventional EMS obtains information from Supervisory Control and Data Acquisition System (SCADA). SCADA system comprises of Remote Terminal Units (RTU) for measuring voltage and current magnitudes. However, RTUs are unable to provide phasor values of these

measurements. RTU measurements have refresh rate of 2-10 seconds. Further, data preprocessing and state estimation takes complete 5-10 minutes. With such reporting rate SCADA measurements are only good for steady state analysis and have limited applications.

Introduction of Wide Area Monitoring System (WAM) based on phasor telemetry, has greatly enhanced EMS performance. A wide area monitoring system consists of geographically dispersed Phasor measurement units. Phasor measurement units provides both magnitude and phase values of the bus voltages and currents. These PMU measurements are time synchronized via Global Positioning System (GPS) with an accuracy of 1 micro-second. Since PMU is the prime functional unit of WAM. Therefore, its architecture is discussed here in detail.

Phasor Measurement Unit (PMU)

According to North American Synchro Phasor Initiative (NASPI), PMU is "a device that provides, as a minimum, synchro phasor measurement for one or more phases of an AC voltage and /or current waveform. The synchro phasor can be single phase or symmetrical component values."

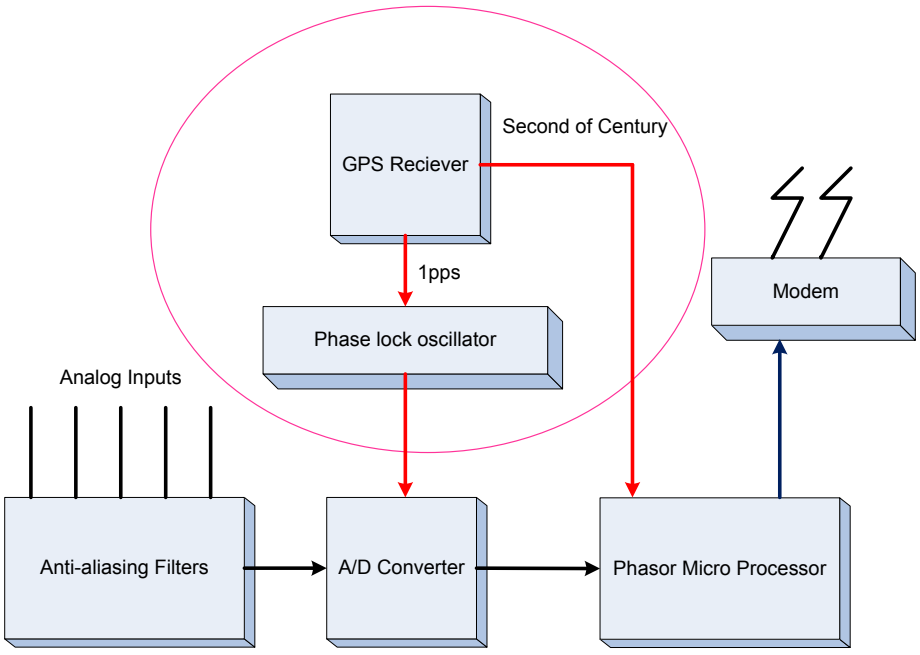

Figure 1.1 Generic Phasor Measurement Unit [64]

The PMUs manufactured by different manufacturers differ from each other in many aspects. According to [47] standard, PMUs are categorized into two classes of (i.e. P and M). P class PMUs are meant for protection applications and M class PMUs are designed for measurement

applications. However, Fig 1.1 shows the generic PMU structure depicting its principal components.

In Fig 1.1, anti-aliasing filters, analog to digital converter and phasor microprocessor are involved in phasor computation. GPS receiver and phase lock oscillator helps in synchronizing these phasors. However, modem is used to transmit the generated phasors to Phasor Data Concentrators (PDC).

In a wide area network, analog voltage and current signals are obtained from secondary side of potential and current transformers respectively. These signals are fed to PMUs as analog inputs. These analog inputs are pre-processed by anti-aliasing filter to remove alias of the reconstructed signals. The analog to digital converter samples the pre-processed analog data according to Nyquist criterion. These data samples uses standard time signal (GPS time signal) as a reference for sampling process. These time-synchronized samples are further processed by microprocessor based phasor estimator. Estimated phasors are time tagged with the synchronizing signal. These time tagged phasors or synchrophasor are finally send to PDC using IEEEC37.118 data format.

Synchronization

In Fig 1.1, PMU utilizes GPS as synchronizing source, which performs two functions. First, GPS receiver provides synchronizing signal, in form of Pulse Per Second (PPS). Second, it provides time-tag to computed phasors by Second of Century (SOC). 1PPS signal is usually divided by phase locked oscillator into required number of pulses per second for sampling the analog signal. Further, pulses that trigger data sampling shall be locked in phase with IPPS signal within1 μs of Coordinated Universal Time (UTC) to have desired level of accuracy.

Computed phasors are time tagged based on the time of UTC time reference with GPS signal. These Time tag defines the time instant at which sample was taken. Therefore, Time stamp is a 8 byte message consisting of 4 byte "SOC-Second of Century", a 3 byte "Fraction of Second" and 1 byte "Quality Indicator". SOC-time tag, counts the number of seconds that have occurred since 1 January 1970. With 3-bytes for the Fraction of Second, one second can be broken down into 16,777,216 counts or about 59.6 nsec/count. Finally, the time quality byte contains information about the status and relative accuracy of the source clock as well as an indication of pending leap seconds and their direction (plus or minus). Based on these time tags, events occurring simultaneously in power systems are recorded. Recorded measurements from given network can be precisely aligned for comparison against one another.

According to IEEE standards, accuracy of phasor measurements are expressed by a term called Total Vector Error (TVE). It is desired that PMUs should have TVE not more than 1%, which corresponds to phase error of 0.01 radian or 0.57degrees. Other few desired specifications of PMU are given in Table 1.1.

Table 1.1 Specifications of Phasor measurement units

Time Tagging of PMUs should have accuracy of 50 micro second
Synchronizing source should have accuracy of 1 micro second
Phase angle calculation should have accuracy of 1 degree
Analog to Digital converter should have resolution of 16 bits or more.

Architecture of wide area monitoring system

Wide area monitoring system consists of PMUs, PDC, and communication network and application software in its architecture as shown in Fig 1.2. PMUs are installed at various substations in given power system. These PMUs measure current-phasor, voltage-phasor, and frequency from distant locations. PMU communicates with Phasor Data Concentrator (PDC) generally with IEEE C37.118 data format. PDC is central monitoring station, which collect data from various PMUs and creates record of simultaneously measured data from remote locations of power systems. PDC completes this task by rejecting bad data and aligning time-stamps of data provided by PMUs. Super PDC (SPDC) is also incorporated in large WAMS. Super PDC is a central PDC that collects and correlates phasor information from all PMUs and PDCs. SPDC is connected to central database for long term archiving of collected data. This data is later utilized by application software's like RTDMS, to carry out one-line operations.

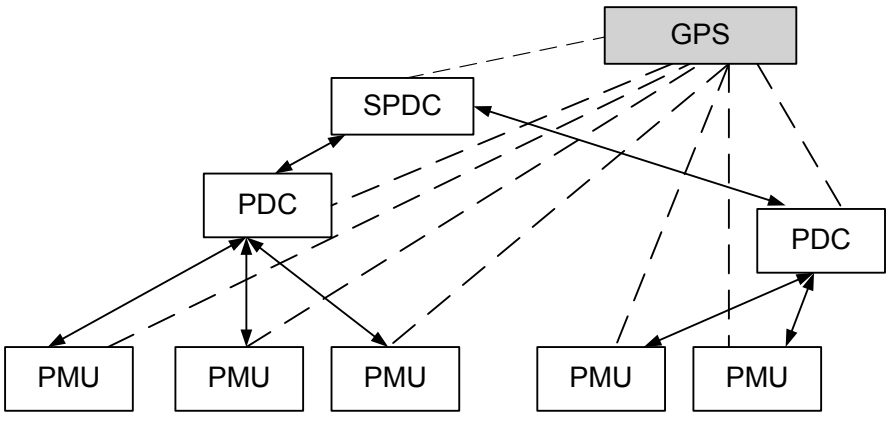

Figure 1.2 Architecture of Wide Area Monitoring Systems

In a wide area monitoring system, communication networks play significant roles [11]. Authors in [121, 79] have mentioned the requirements of the communication systems for all wide area applications. Today, different types of communication links are available for PMUs. Some of them are telephone lines, power lines, microwave links and fiber links. Satellite based communication is also utilized. Choice of suitable communication medium depends on two factors. First factor is the infrastructure cost associated with the communication medium. Second factor is the communication delay. Communication delay is generally introduced along transmission path, when PMU sends data from point of measurement to the point of application. Depending upon the location of PMUs, PDCs, and application point, delay across communication medium is directly proportional to distance between them. Communication delays for various links is summarized Table1.2. In WAMS, due to security reasons data is often encrypted and is passed through security gateways or firewalls. Time delay across these security devices varies greatly depending on type and number of the devices. Further, PDC also introduces time delay. This delay is the processing time of PDC to generate concentrated data. In addition to above, fixed delays associated with multiplexing, processing are also present. Causes of these delays and their ranges are given in Table 1.3.

Table 1.2 Delays in Various Communication Medium [11]

Communication link	**Associated delay(one way)**
Fiber optic cables	~ 100-150 ms
Microwave links	~100-150 ms
Power lines	~150-350 ms
Telephone lines	~200-300 ms
Satellite links	~500-700 ms
Fixed delay (PMU processing)	75 ms
PDC wait time	1-4 sec

Table 1.3 Causes and Range of Fixed Communication Delay

Cause of delay	**Typical range of delay**
Sampling window	17ms-100ms
Measurement filtering	8ms-100ms
PMU processing	0.005ms-30ms
PDC processing &alignment	2ms-2s
Serializing output	0.05ms-20ms
COMMUNICATION system I/O	0.05-30ms
Communication system buffering and error correction	0.05-8s
Application input	0.05ms-5ms

1.1.3 Power System Stability

Due to continuous growth in the size and technology, different types of instabilities have emerged in the power system. Power system instability largely depends upon network topology, system operating conditions, and nature of disturbance. According to IEEE and CIGRE Joint Task Force power system stability is defined as "the ability of an electric power system, for a given initial operating condition, to regain a state of operating equilibrium after being subjected to a physical disturbance, with most system variables bounded so that practically the entire system remains intact"[95].

Since, power system is continuously subjected to variety of disturbances. Depending on the physical nature of disturbance, power system stability is broadly classified into Rotor angle stability, Voltage Stability and Frequency stability. Voltage stability is the "ability of power system to maintain steady voltages at all buses in the system after being subjected to a disturbance from a given initial operating condition". Voltage stability is primarily caused because of inability of power system to meet the demand for reactive power. This instability causes progressive drop or fall in voltage of buses. In a similar manner, Frequency stability refers to "the ability of a power system to maintain steady frequency following a severe system upset". It depends on balance between load and demand requirements of the system.

Both of the stabilities are further divided into small and large depending on the size and time of study of disturbances. Apart from above two instabilities, power system is also subjected to Rotor angle stability. Details regarding rotor angle stability are presented in following section.

Rotor Angle Stability

Rotor angle stability "is the ability of power system to maintain synchronism after being subjected to the disturbance". This stability maintains equilibrium between mechanical and eletromagnetic torque of each synchronous machine. When system is disturbed from steady state, the equilibrium between torques is upset. This results into angular separation between the machines. Since, power-angle relationship of synchronous machines is non-linear, this angular separation is further increased with decrease in power. Electromagnetic torque of synchronous machine can be resolved into two components namely synchronizing torque and damping torque components respectively. Therefore, when synchronizing torque is insufficient in the system, aperiodic oscillation occurs. On the other hand, if damping torque is less, oscillatory instability takes place.

Depending on the magnitude of the disturbance, rotor angle stability is further divided into two instabilities. These are

- Small signal stability
- Large signal stability

Small signal stability: When disturbance is very small such that system can be linearized for the purpose of analysis, then rotor angle stability is called as small-disturbance rotor-angle stability or small signal stability. In small signal stability, resulting instability can be either aperiodic or periodic depending upon type of insufficient torque. Aperiodic instability problem in power systems are generally eliminated by voltage regulators. Periodic oscillations are generally encountered in power systems and increases with increase in size of the system. These small-signal periodic-oscillations can be either local or inter area depending on nature of their mode.
Local modes are caused by interaction of mechanical and electrical modes of turbine-generator system. Therefore, Local modes occur when a generator (group of generators) is swinging against rest of the system. On other hand, Inter area modes are caused by either high-gain exciters or heavy power transfer across weak tie line. In inter area oscillations one part or group of generators oscillate against another group of machines. These oscillations are enhanced, when power system is subjected to ever changing stressed operating conditions. Sometimes, large disturbances also encourage inter-area oscillations in the system. This stability studies generally have time- frame from 10-20s following a disturbance.

Transient stability: When disturbance is large and severe, which results into large angle excursions, is called as large-disturbance rotor-angle stability or Transient stability. Unlike, small signal stability, transient stability is usually aperiodic in nature. They may or may not occur as first swing instabilities. Sometimes they occur due to superposition of local and inter-area modes. Transient stability largely depends on initial operating conditions of the system, type, and nature of the disturbances. Fault clearing time and generator loading also plays significant role. Since, the rotor angle response becomes non-linear in case of transients. Therefore, linear methods used in small-signal instability cannot be used for large angle excursions. Time of study for transient stability is generally between 3 to 5 seconds following a fault.

1.2 LITERATURE SURVEY

Synchronized phasor technology has wide applications in power sector. Synchronized measurements can be utilized for power system monitoring, control and protection. Therefore, references available on this topic are extensive. This thesis is primarily focused on comprehensive study of monitoring and control application of wide area measurement systems, involving optimal placement of phasor measurement units and rotor angular stability analysis of power system. Three different placement methodologies are introduced in this work, to select suitable locations for phasor measurement units. Angular stability analysis consists of inter area mode identification, controller design for small signal stability and transient stability prediction scheme. A literature review is presented below discussing some of the major techniques used in judicious placement of PMUs and control of rotor angle stability using synchro-phasor measurements.

1.2.1 Review on PMU Placement Methods

Implementation of wide area monitoring starts with optimal PMU placement.PMU deployment helps in observing the dynamics of interconnected power system. PMUs are capable of measuring voltage and current phasors of its adjacent buses and bus on which it is located. Therefore, PMUs required are very less as compared to other measuring devices for the given system.

J.S Throp et al. in [64] described analytically, expression for phasors and their computations through phasor measurement units using Discrete Fourier Transform (DFT) from three phase voltage and current waveforms. They also described working and structure of PMUs in greater-details. A.G Phadke et al. [5] derived analytically linear state estimator using synchrophasors. Authors in [84] discussed various applications of phasor measurements in power systems. They also described benefits of synchrophasor in power system angular stability.

Significant research has been done in the past to deploy phasor measurement units in power systems. A.G Phadke et al. [106] presented a procedure by which PMU locations are systematically determined in order to render an observable system. They described the concept of pseudo–observability/unobservability. Depth-of-unobservability is defined as a situation in which all of the neighboring buses of any unobservable bus must be observable. They further explained that when a bus is not directly observed by the PMU, then it has to be estimated.

A. bur et al. in [6] presented a novel approach for PMU placement problem. They formulated PMU placement problem as an optimization problem. Solution for this optimization problem is obtained through integer programming approach. Further, cases regarding conventional measurements like injection measurements and flow measurements are described by same authors in [9, 1]. They also established that by considering conventional measurements the number of PMUs is reduced. However, suggested ILP method becomes non-linear under conventional measurement or zero injection.

B. Gou [17] proposed another formulation for the optimal placement of PMU, which is linear for both conventional and non-conventional cases. Author expanded same formulation in [16] for depth-one and depth–two observability cases, with and without zero injections.

S. Chakrabarti et al. [108] explained that multiple objectives such as minimizing number of PMUs and maximizing the measurement redundancy cannot be handled simultaneously by integer programming. They explained that maximizing redundancy means that each bus is observed by more than one PMU. Therefore, they proposed an exhaustive binary search approach for the same. S. Chakrabarti et al. in another reference [114] utilized Integer quadratic approach for placement problem. Same author in [109] used Binary Particle Swarm Optimization (BPSO) technique for solving integer quadratic formulation for optimal PMU sites. Presented formulation also maximizes the redundancy. However, presence of conventional measurements and depth of observability are not considered by them.

C.Su.et al [26] formulated optimal PMU placement problem with new cost considerations. They discussed that cost of installation of a PMU is always not equal to another, PMUs with larger number of branches are more important than one with less number of branches. Authors in [66] developed heuristically algorithms such as Bacterial Foraging Algorithm based on mixed integer non-linear programming for placement problem.

Literature shows that PMU allocations are primarily done according to topological observability. R. Sodhi et al. [104] considered both for complete topological and numerical observability in PMU placement algorithm. R.F. Nuqui et al. [106] reported that economic constraints associated with PMU technology, compels utilities to place the limited number of PMUs in the system. As a solution, they considered PMU placement in stages/phases. They utilized the concept of depth of observability to place PMUs in stages. D. Dua et al [28] formulated PMU placement in stages in such a manner that placement results after final stage are identical to single stage PMU placement using ILP approach. R. Sodhi et al. [103] used multi criteria decision making

approach to place PMUs considering various criteria like bus, tie line, and voltage observability. They utilized ILP and Analytical Hierarchy Process (AHP) to place PMUs in stages.

Recently few researchers have utilized probabilistic approaches to locate significant PMU locations in a given system. J.C. Cepeda et al. [52] utilized analytical reliability methods to improve probability of observability for given system under random power outages. They considered topological observability concept for placement of PMU. In another reference [70] Gaussian Markov Random Field (GMRF) model of power system is proposed. They employed greedy algorithm to find optimal PMU sites, which provides maximum information gain.

1.2.2 Review on Application of PMU Measurements for Small Signal Stability Analysis and Control

Past researches have claimed that Rotor angle stability problems are due to presence of the local and inter-area modes. Conventionally, linearization based Eigen value analysis is utilized to determine frequency and damping parameters of these modes. This technique is based on state-space representation of the system, linearized about a given operating point. Therefore, this technique is applicable only where linear approximation is valid [93, 39, 95, 87]. P.Kundur in [93] explained other algorithms like Analysis of Essential Spontaneous Oscillations in Power system (AESOPS) and Modified Arnoldi Method (MAM) for instability problems of larger systems. However, aforesaid methods are offline methods and do not provide real-time information.

Several measurement-based techniques for extraction of oscillation parameters are reported in literature [10, 50, 43, 88, 49, 29, and 9]. These techniques are a good complement to model-based Eigen value analysis, and are based on the actual response of a power system. D.J Trudnowski et al. [50] discussed various direct measurement based techniques to identify and estimate electromagnetic modes of the power system. Author further described that measurement data of PMUs are divided into three types i.e. Ring Down, Ambient data and Probing data. Ring down data is generated when the system is disturbed by some large events like addition or subtraction of large loads, tripping of generators or when the short circuit occurs. In this type of data, transient response can be analyzed. The transient response is considered as sum of more than one-damped signals. Ambient data occurs due the switching of load in one day and its nature is random. Magnitude of ambient data is small and is generally considered as noise. Thus, it is not easy to differentiate them by the noise found in measurements. However,

probing data occurs, when the low-level pseudo random noise is added to check the performance of the system.

D.J Trudnowski in another work [29] established the relationship between Eigen value analysis and mode shapes identified from direct measurements. Author utilized welch's periodogram for computing power spectral density and cross correlation density. Y.Chompoobutrgool et al. [129] establishes that measurements from PMUS contains "actual" system modes as they are able to capture modal frequencies and damping in real time. They utilized both ambient and ring down data to identify inter area modes. Author has also identified dominant oscillation paths to benefit various control and protection applications. Researchers of [88] have utilized regularized robust recursive least squares (R3LS) method for online estimation of power-system electromechanical modes.

According to [50], few direct measurement techniques are appropriate for ring-down analysis and some others for ambient and probing. Therefore, mode identification methods are categorized as ring down, mode meter methods and probing methods. In ring down analysis, most widely used algorithm is prony [49, 97]. J.F Haufer in [49] derived frequency, damping and phase of measured signal utilizing prony analysis. Authors of [97] have shown that these prony methods and its variants are sensitive towards noise. Few other algorithms like Hankel Total Least Squares (HTLS) and Eigen value Ralization (ERA) are discussed in [50] as ring down methods.

In mode meter methods, stochastic framework is generally considered. N. ZJou et al. discussed various mode meter methods based on robust least square method to extract modal quantities [89] [88]. Auto-regressive (AR), Auto Regressive Moving Average Exogenous (ARMAX) and stochastic subspace are other mode meter methods, which are reported in literature [105, 50]. R.W. Wines et al. [105] considered Auto-Regressive Moving Average (ARMA) method to estimate low frequency components of power system. H. Ghasemi et al. [43] derived critical modes from ambient data using stochastic subspace identification methods. Recently, in [97] Noise space decomposition based, low frequency mode identification technique is presented.

Wavelets have multi resolution properties and have wide applications [96]. S. Avdakovic et al. [107] discussed various applications of wavelets in power system field. They presented potential benefits of wavelets in mode identification. Authors of [110] utilized continuous wavelet transform (CWT) to identify various parameters of the mechanical dynamic systems. J.L. Rueda et al [56] derived modal frequencies and damping ratios, utilizing CWT on measurements

obtained through PMUs. They have also presented guidelines to select various wavelet parameters. A.R Messina et al. [10] provided a method to identify trend from directly measured power system oscillations. They utilized Hilbert transform and wavelet shrinkage method to analyze non-stationary signals. They checked the performance of two methods against Moving Average technique.

P. Kundur [93] derived analytically that in power system presence of inter area modes, causes small signal oscillations. To prevent system from these oscillations, additional damping is required. Conventionally, Power System Stabilizers (PSS) provides required damping torque to damp out oscillations prevailing in the system. Author, further derived an analytical expression, which shows that local controllers/PSS are tuned in a non-optimum fashion to damp inter area oscillatory modes. According to another reference [39], sometimes stabilizers themselves interact with each other to produce new modes. The effectiveness of PSS in damping inter-area modes is limited because inter-area modes are not as controllable and observable in the generator's local signals as local modes. As a solution, several alternative techniques like, adding FACTS devices for voltage control or addition of local signals to existing devices, are used to damp inter-area modes [123]. M.J Gibbard et al [76] outline an algorithm to coordinate PSS and FACTS device together for damping. R. Gupta et al. [101] designed Linear Quadratic Regulator (LQR) based robust power system stabilizer for single machine system to damp inter area oscillations. Recent investigations have demonstrated that cost of FACTs devices is quite high [15]. Therefore, their wide use in power systems is restricted.

J.D.L. Ree et al. [53] discussed various applications of synchrophasors in power system monitoring, control and protection. They highlighted use of PMU measurements for Transient and electromagnetic oscillations. J.S. Throp et al. [61] demonstrated detection of instability in a two area four machine using PMU measurements. A.G. Phadke [64] described analytically that in a wide area monitoring system, certain remote signals measured at electrical centers of the group of generators separated from the rest of the system provide effective control. Remote signals derived from PMUs are measured and transmitted to distant PSS/ FACTS controller to damp out the oscillation. This led to the development of "Wide area damping controllers" for inter area oscillations.

Rich literature is available on design of damping controller [15, 13, 44, 128, 113, 24, 125, 122, 45, 35, 123, 119, 85, 124, and 41]. In previous work, H-infinity based robust controllers are widely used for designing damping controllers [41, 15, 44, 24, 45, and 119]. B.C. Pal et al. [13] designed a robust controller based on H∞ norm for a Thyristor Controlled Series Compensator

(TCSC) to enhance the damping of inter-area oscillations. They utilized remote measurements obtained through PMUs as feedback input to controller. Hui Ni et al. [44] designed supervisory robust Power system stabilizer (SPSS) using H-infinity norm with wide area measurements. They utilized multi-agent system theory to coordinate local PSS and centralized SPSS with the help of fuzzy logic switch. The controller is capable of compensating for the nonlinear dynamic operation of power systems and uncertain disturbances. According to Researchers of [14], LQR and H-infinity based robust controllers are of high order. Linear Matrix Inequalities (LMI) based robust controllers are able to solve high order problem of H-infinity controllers to some extent.

Time latency is an important factor, which greatly affects performance of the damping controller. Time latency majorly depends on communication network. Ruofei Ma et al. [78] described various types of communication mediums for wide area networks. They explained that proper communication-network topology, type of communication medium, and protocols plays significant role in any power system application. M. Shahraeini et al in [79] explained that communication structure depends on application and control scheme employed. Therefore, time delay for different systems will be different depending on the practical PMU settings and communication media [11, 75].

G. Yu et al [41] reported various reasons for communication delays and data incompleteness. They also highlighted impact of communication delay-uncertainties on various monitoring and control applications. Communication traffic can also have a significant effect on the time delay [55,121]. S. Wang et al. [121] highlights significance of network induced delays, data packet drop out and disordering in various control schemes. In [55] described effect of communication traffic on transmission delays. Further, they proposed hybrid technique to monitor and control this traffic. Authors of [75] and [79] formulate these transmission uncertainties as routing and packet size delay. Therefore, communication delays are uncertain.

S.K Seethalakshmi et al. [67] described three topologies for implementing control in wide area network. They discussed De-Centralized, Centralized and Multi-agent control schemes according to their architecture. M. Shahraeini et al [79] compared communication latencies and uncertainties for centralized and decentralized control schemes. They described that for same infrastructure investment, decentralized control scheme is more reliable and have less latency.

W.Hongia et al. [119] shows that for designing damping controllers, even small communication delays can also make the system unstable. R. Majumder et al. in [14] implemented a real time smith predictor based robust H-infinity controller. They modeled delayed PMU measurements

present in the system as a dead-time system. Further, they checked robustness of the controller for constant current, constant power and constant type loads. Smith predictor based approach fails to provide sufficient damping in plant, which have lightly damped poles in their open-loop configuration. B.C Pal et al. [15] designed a centralized LMI based H∞ robust controller for delayed PMU measurements. They utilized unified smith predictor approach. They checked performance of controller for maximum delay of 0.7 seconds.

W. Hauren et al. [122] designed a robust controller for delayed signals. They have utilized proportional and derivative control structure to control delays in the system. They modeled time delays using Pade approximation. However, Designed controller performs well for time delays not more than 0.25 seconds. Y. Ye et al. [128] modeled transmission delays in state space form. They utilized genetic algorithm to compute feedback gain of controller. Also effect of time delays on phase lag and gain amplification are shown. Designed controller is able to work for 0.8 seconds delay. W.Yao et al. [124] designed an embedded robust controller for inter-tie oscillations. They have considered time delays, which are varying with time. Recent studies have shown that LMIs based aforesaid techniques are numerically complex for large system and require good model-order reduction techniques [15, 45, 128, 124].

Measurement based, intelligent controllers are also reported by few researchers as an alternative method to design damping controllers [12]. Intelligent approaches do not require system description and are easier to implement. S. Ray et al. [113] designed single simultaneous recurrent neural network based adaptive controllers for rotor-angle stability problem. Designed controllers are trained in forward mode utilizing adaptive control method. In reverse mode, controller generate control signals to provide necessary damping. D. Molina et al. [85] utilized Recurrent Neural Network and dynamic programming to damp oscillations. Power system network is simplified using virtual generators concept. Authors of [45] have modeled transmission delay as structured uncertainty with linear fractional transformation (LFT) approach. They designed an adaptive supervisory controller. According to literature [85], performance of these adaptive controllers largely depends on training algorithm. H. Dongchen et al. [42] derived analytical expressions for rotor angle deviations from synchrophasors to detect angular instability. P. Tripathi et al. [98] described rotor angle estimation method based on divide by difference method.

Y. Chompoobutrgool et al. [125] described various other issues regarding rotor angle stability. They have give survey of existed methodologies for damping controllers. Authors explained importance of appropriate selection of control signals and control algorithms for single and multi

input controllers. They also discussed various methods, which are utilized for selecting control signals. B. Padhy et al. [24] proposed a methodology for selection of input and output signals, and a robust fuzzy controller is designed by them. Authors have further extended the work in [23] and Sequential Orthogonalisation Algorithm is utilized to select optimal input /output signals. Authors have also presented in their work, Principal Component Analysis (PCA) based clustering method, to select the signals. Further, they compared the effectiveness of the two proposed techniques.

In recent series of publications, few probabilistic based methods are explored to quantify the uncertainties for small signal analysis [57] J.C. Cepeda et al. in [57] developed Monte Carlo based Probabilistic Eigen value analysis for various operating conditions and uncertainties, to increase reliability of the given system. Past works have shown that it is difficult to assign probability distributions for all system parameters. Moreover, for large power systems probabilistic methods become computationally heavy.

Zadeh in [71] derived that fuzzy logic provides much easier way to handle randomness /uncertainty. H.M. Behbehani et al. [46] designed a Fuzzy PSS based on Mamdani inference systems. They have considered triangular membership functions to design PSS. They have also considered presence of time delays in the communicated signals. In [24] authors have designed robust fuzzy controller based on Takagi-Sugeno inference systems. They have also proposed a method to convert Bilinear matrix inequality problem of Lyapunov stability criterion into set of LMIs. They have compared H-infinity and fuzzy controller performance for three systems. They established that fuzzy controller performs better than traditional controller. Literature shows that [92, 72, 59, 90] type-2 fuzzy systems are able to handle uncertain information more appropriately by handling them in their membership functions. M. Mendel et al. [59] described that fuzzy type-1 represents a general case of type-2. They also described analytically Foot of Uncertainty of type-2 system. O. Castilo in [92] described designing of type-2 fuzzy controller in detail. Author also explained application of type-2 systems for practical control systems.

1.2.3 Review on Application of PMU Measurements for Transient Analysis and Prediction

Since 1920, vast literature has been reported to accurately predict large rotor angle instability. P Kundur [93] described various causes of large rotor angle stability. Author presented analytically that time domain techniques based on nonlinear differential equations are most widely used for transient analysis. However, this technique requires accurate system information and exhaustive

mathematical modeling of the system. According to authors of [80, 77] Equal area criterion (EAC) is another important method based on the energy principle. This method provides transient stability of a multi-machine system, without solving the differential equations. In this technique, given system is represented by a single machine connected to an infinite bus (SMIB).Hence, EAC requires equivalent machine model/classical generator model, which represents only the mechanical dynamics of the generator [127]. Y. Xue et al. proposed the extended equal area criterion (EEAC), which is hybrid of the time-domain simulation and energy functions. This method is less accurate than time-domain simulation, but computationally more efficient. Author of [80] described Transient-energy-function (TEF) method based on Lyapunov stability to determine angular stability in large. Author also established that, in TEF method it is difficult to determine kinetic and potential energy under certain disturbances when applied for practical power networks.

Y.V. Markov et al [130] described concept of transient stability in a wide area network. They also highlighted benefits of incorporating phasor measurements for transient analysis. They also discussed various problems and existing solutions for transient analysis. B.K. Saha et al. [22] described a method to detect power system stability using synchrophasors. Similar work is reported in [53].

C.W. Lui et al. [27] established difference between offline and online transient stability assessment techniques with basic assumption that the PMU's are placed at each bus. Based on the various factors like voltage dip, frequency deviation, rotor angle deviation etc, a constraint region is formed by authors. Power system is modeled, as constant ZIP model. Based on Runge-kutta interpolation technique, piecewise linearized prediction is performed based on swing equation. C.Li et al. [69] utilized rolling optimizing algorithm and extended equal area criterion to predict and analyze the stability. They also developed a scheme for generator shedding based on the predicted trajectory and indices. These indices are derived from acceleration energy, angular speed, and rotor angle.

Many researches are conducted in past utilizing intelligent techniques for transient stability studies [34, 112, 100, 4, 73, 3, 38]. F. Hashiesh et al. in [34] used ANN to predict real-time stability. Rate of change of bus voltages and angles are used to train the ANN network. They also proposed a controlled islanding scheme based on coherent groups of generators as a remedial measure.

In references [112,100] authors have used Decision Trees (DT) for stability studies. K. Sun et al. [112] designed a DT based security assessment scheme for very large systems. DTs are

trained with 24 hours ahead time simulations to derive critical attributes. They also proposed a new-path based DT classification method to regulate DTs according to changing operating conditions. Authors in [100] developed a DT based predictor to determine the stability. They have also proposed a response based control scheme, in which one-shot control is triggered when DT classifies measurement as Unstable.

Literature reveals that machine-learning techniques are widely used to predict the transient stability status after a fault [73, 3, 38, 18]. L.S Moulin et al. [73] compared the performance of Multi layer perceptrons (MLP) and Support vector machine (SVM) as transient stability predictors for large systems. They established that SVMs performed well in comparison to MLP. A.E. Gavoyiannis et al. [4] developed a stability classification algorithm using class pattern recognition with a system of combined classifiers. They used fuzzy C-means clustering algorithm (FCM) and SVM based classifier.

A.D Rajapakse et al [3] utilized Support Vector Machine (SVM) classifier and a set of pre identified voltage-variation trajectory templates to predict the transient stability status. Measured voltages obtained through phasors are compared with template to evaluate fuzzy membership. This fuzzy membership indicates similarity between two voltage measurements. Angular separation between generator rotor angles is generally utilized as indicator for transient instability. Since voltage, measurements can be directly obtained from synchro phasors. R. Gomez et al. [38] extended their work, in which they carried analysis with sampled values of voltages. They also compared performance of voltage inputs with other inputs like generator speed and rotor angle measurements. They also established that voltage magnitude phasor with four sample values (taking one sample per cycle) are able to predict transient stability with desired accuracy.

1.3 MOTIVATION AND OBJECTIVES

Reliable and uninterruptible operation of large interconnected power system is a prime need of present time. Traditional measurement and data acquisition systems are unable to provide dynamic information. Therefore, synchronized phasor measurement technology is gaining wide attention. PMUs are increasingly being installed in different parts of the world. The general objective of these PMU installation activities is to develop more dynamic, robust, and advance metering system so as to have more "situational awareness". This will help utilities to take necessary protection and control action in real time to avoid emergent and severe shutdowns.

Many researchers have investigated and analyzed impacts of PMU placement in power system. PMUs are widely used for power system monitoring, control and protection applications. Recently PMUs are also utilized in post disturbance analysis, monitoring of inter area oscillations and system modeling. Because of large size of power system network and continuous increase in interconnections, PMU placement is a biggest challenge today.

From reviewed literature, it is evident that PMU placement plays significant role in power system monitoring. Therefore, considerable amount of work is carried out in past to place PMUs to achieve complete observability of the system [5,106,6,9,1,17,16,108,114,109,26,66,104,28,103]. Majority of works utilized Integer Linear Programming (ILP) formulation for topological observability. The solutions obtained through ILP, gives optimal number of PMUs. However, it gives multiple solutions for optimal locations. This problem of multiple solutions increases with increase in size of the network. For large systems, ILP and MILP formulations based topological concept gives multiple solutions. Placement methods for incomplete observability are also reported. PMUs are expensive device and their placement in a wide area network involves huge investment. For huge power systems, it is not possible to have PMUs according to complete observability. In such cases, placement is done according to incomplete observability, which requires less number of PMUs.

Reviewed literature depicts that apart from observability, presence of conventional measurements also decreases required quantity of PMUs. Various other factors like loss of transmission line and loss of PMUs are also widely covered in literatures to have redundant placement methods. However, placement scheme considering all these factors simultaneously are very few.

Due to multi benefits of synchrophasors and rapid development of the technology. PMUs are likely to increase substantially in the grid. In such situations, new methodologies are required to assist various power applications apart from primary function of observability. Reviewed literature reveals that most of the approaches so far utilize topological observability concept to place PMU. PMU placement complementing power system applications is a recent need of time.

Significant literature is available, establishing significant benefits of synchrophasors in wide area stability analysis [64, 42, 129, 53]. Large amount of work is carried out in past to identify and control rotor angle stability using dynamic PMU measurements. However, in most of them it is considered that PMUs are installed on generator terminals, which is practically not possible in a wide area network owing to large size and observability requirements. Therefore, a placement method addressing simultaneously, rotor angle stability and observability problem is required today.

Direct measurement based techniques are extensively explored in past to analyze and identify underlying phenomena. With phasor measurements, more dynamic-information can be captured. Reviewed publications [50, 43, 88, 89, 105, 56, 107] depicts that inter area modes, resulting into rotor angle instability are easily identified by these direct measurement methods. Various mode meter and ring down methods are utilized in past to compute modal parameters. According to literature, ring down methods are very sensitivity to noise. On the other hand, estimates obtained through mode-methods takes large computational time. Recently, wavelets are used in various power system applications. However, wavelet based mode identification methods are relatively new and requires more attention.

In a wide area network, effects of inter area modes are more pronounced due to large interconnections. Conventional Local controllers and PSS are unable to provide sufficient damping to these oscillations. Reviewed literature shows that these small-signal oscillations can be controlled through wide area damping controllers. Majority of Available publications have utilized H-infinity based wide area damping controllers. However, these controllers are high of order and are difficult to design. Since, communication link is an important component of wide area monitoring system. Time latencies due to these communication links are another important factor, which affects damping controller. In robust H-infinity based controllers, these delays are either accounted through robustness of the controller or neglected. However, studies have shown that these controllers have poor performance for delayed PMU measurements. To cater this, various LMI based H-infinity controllers having different control schemes are employed. However, LMI based controllers require good model reduction techniques and are computationally heavy.

According to reviewed literature, intelligent controllers are also employed as damping controllers. However, these controllers are designed using offline training data. To design controller for various operating conditions huge amount of training data is required. Therefore, performance of these controllers primarily depends on availability and nature of training data. Fuzzy controllers are extensively used in various power system applications. Since, fuzzy systems are able to give good performance with imprecise information. Recently, few researchers have considered them as damping controllers [24, 46]. However, to explore more benefits from them, they require more concern.

Above literature presents, various methodologies to deal with delayed PMU signals, while designing controllers. According to IEEE standards [47], PMU data are uncertain due to errors in measurement of magnitude or angle of the phasor or due to error in time synchronization of synchro phasors. Total vector error for PMUs should be less than 1%, which means measurements can have a maximum error of 1%. Moreover, in rotor angle analysis it is

assumed that PMUs are placed with generators [42]. Since, PMU cannot directly measure the internal states such as the rotor angle of generators. Therefore, various rotor-angle estimation techniques are employed. Practically, a highly accurate rotor estimation routine also incorporates some estimation errors, which further add uncertainty of the measured signal. Based on aforesaid reasons, it is required to have damping controllers, which can model these uncertainties. Since, Type-2 fuzzy systems are capable of modeling uncertainties both in linguistic variable and in membership function simultaneously. Therefore, damping controllers based on type-2 FIS is a requisite of present practical system.

In large sized network, to have effective control, it is important to select correct location of controllers. Therefore, selection of controller location is another vital issue, which is recently gaining attention among researchers. Recently few publications have addressed this problem. Hence, a suitable methodology is required to select controller location and feedback signals.

To prevent the given system from large rotor angular catastrophes, it is essential to transfer the rotor angular information in real time. So that, preventative measures can be taken as quick as possible. Earlier, most of the tripping systems were based on local measurements and were unable to transmit information. Existed literature shows that with inclusion of synchro phasor measurements these out of step problems could be well predicted and solved. According to past researches, traditional methods like time domain, Equal Area Criterion (EAC), and Transient Energy Function (TEF) are computationally exhaustive in nature. Further, these are relatively slow in conducting protective actions. As a solution, various intelligent predictors are widely used in literature. Recent list of publications revealed that among various intelligent techniques Vector machines are most common. Vector machines require less training data and are more accurate in comparison to other intelligent methods. Past literature reveals that to predict rotor angle stability, generally rotor angle speeds, or deviations are considered as inputs. However, synchrophasors are voltage or current phasors. It is found that, predictors utilizing voltage phasors as their inputs are few. Therefore, an efficient, fast, and simple predictor utilizing less number of synchrophasors is necessary.

Considering aforesaid technical challenges for PMU placement and control of Rotor angle stability, the main objectives behind the research work carried out in this thesis are summarized below:

- A new optimal PMU placement approach has been proposed considering conventional measurements, observability, and redundancy issues simultaneously using quadratic approach.

- A technique has been proposed to select few significant PMU locations; from which maximum amount of power flow of the system can be monitored to assist various power flow applications.
- Phased PMU placement technique to monitor and control the small- signal stability in real time has been proposed. The placement technique is based on rotor-angle stability control scheme. Various observability indices are utilized to rank PMU locations. Based on this ranking PMU are placed in stages, such that after first stage placement, control scheme can be implemented.
- A direct measurement based real time mode identification scheme has been implemented to find those modes, which are responsible for small-signal instability. Results obtained through direct measurements are compared with conventional Eigen value analysis.
- Wide area damping controllers based on Fuzzy Inference System (FIS) and Adaptive Neuro Fuzzy Inference System (ANFIS) have been designed to nullify the constant time delays in a large network. A control scheme to employ these damping controllers in a wide area network is also developed.
- An interval type-2 fuzzy controller has been designed for large practical systems dealing simultaneously with measurement uncertainties and communication delays of synchro-phasor measurements.
- A fast and accurate transient stability predictor based on Relevance Vector Machine (RVM) has been proposed, for secure operation of power system. The proposed approach utilizes phasor measurements for prediction.

1.4 ORGANIZATION OF THE THESIS

The present thesis is organized into seven chapters and the work included in each chapter is presented in the following sequence:

Chapter-1, the current chapter, gives an overview on Phasor measurement Units and application of PMU measurements in Rotor angle stability. Further, it presents brief literature review on the problem area, and finally, outlines the organization of the present thesis.

Chapter-2 deals with PMU placement problem of a wide area network. A single objective function is formulated considering observability, conventional measurements, and redundancy issues simultaneously. Formulated objective function is solved using Binary Particle swarm optimization (BPSO) technique to obtain optimal PMU locations. Proposed technique is

implemented on IEEE-7, 14, 30 and 57 bus systems. Further, results obtained from proposed approach are verified with GAMS-MIP solver.

Chapter-3 describes a sequential PMU placement approach to monitor power flows in a given network. Demand and flow concepts are introduced and based on these concepts coverage matrices are calculated. For a fixed coverage criterion, flow fraction matrices are computed. Placement problem is formulated utilizing flow fraction matrices and demand. Further, proposed formulation is extended for multiple operating conditions.

Chapter-4 presents a novel approach to rank PMU locations in a given network according to control scheme employed for rotor angle stability. First suitable PMU locations are identified for complete observability using ILP approach. Later, inter area modes are identified using mode identification techniques. For identified modes, control scheme is utilized to identify critical generator, tie-lines and load buses of the system. Various observability indices are formulated to prioritize these buses. Analytical Hierarchical Process (AHP) is utilized to rank PMU locations based on developed indices. Further, to explore potential benefits of proposed approach, Continuous Wavelet Transform (CWT) based mode identification is also carried out.

Chapter-5 deals with design of wide area damping controllers for small rotor-angle instability problem. Three different types of fuzzy logic controllers (FLCs) are designed. First, fuzzy controllers based on Mamdani inference systems are designed for delayed PMU signals. Based on data of Mamdani fuzzy controllers, Adaptive Neuro Fuzzy Inference System (ANFIS) based controllers are developed for delayed signals. To incorporate measurement and delay uncertainty in fuzzy model, type-2 fuzzy controllers are designed by changing Foot of Uncertainty (FOU).

Chapter-6 describes about Relevance Vector Machine (RVM) based transient predictor. Three different inputs namely voltage magnitudes, voltage angle and complete voltage phasors are utilized to design the predictor. Performance of the proposed predictor is compared with Support Vector Machine (SVM) Predictor.

Chapter-7 concludes the work contained in the main body of the thesis and presents the suggestion for the future work.

CHAPTER-2
Optimal placement of Phasor Measurement Units

2.1 INTRODUCTION

Phasor measurement units (PMUs) are able to capture system dynamics in real time with reporting time as high as 60 frames per second. Further, PMUs required are very less as compared to other measuring devices for the given system. This is because; PMUs are capable of measuring voltage and current phasors of its adjacent buses and bus on which it is located. Therefore, dynamic monitoring of a wide-area network starts with placement of phasor measurement units in the given system.

PMU locations are generally selected judiciously, considering various factors. Economic constraint is the first and most important factor, which is widely reported in the literature [5,106, 6, 9, 1, 16, 17, 108, 114, 109, 26, 66, and 104]. Strategies are required to select PMU placement sites to meet cost criterion and intended applications. Utilizing phasor measurements in conjunction with existing conventional measurements provided by Supervisory Control And Data Acquisition (SCADA) system, is second big issue. Several approaches are presented in past [106, 9, 1, 17, 108, 114] to enhance monitoring by considering both measurements together. Placement schemes considering existing conventional measurements are necessity. Lastly, for reliable operation, system should have high measurement redundancy. Therefore, it is important to choose only those PMU locations, which results in high redundancy. Considering aforesaid reasons, PMU placement becomes an optimization problem with observability, conventional measurements, and redundancy constraints. In [109] Binary Particle Swarm Optimization (BPSO) based quadratic technique is presented dealing simultaneously with optimal placement and redundancy issues. However, conventional measurements are not considered by authors. This chapter considers optimal placement with observability, redundancy, and conventional measurements together in a single objective function using BPSO.

2.2 POWER SYSTEM OBSERVABILITY

2.2.1 Complete Observability

A power network is observable when sufficient measurements are available such that all states of the system can be determined. In power system, these states are voltage magnitudes and angles. According to [106], given power system is represented as a connected graph, where all

its buses are treated as nodes and lines as edges. The placement of PMUs becomes a problem that finds a minimal set of PMUs such that a bus must be "reached" at least once by the set of the PMUs. This concept is known as complete observability.

2.2.2 Formulation for Complete Observability

The objective of placing PMUs in power systems is to decide a minimal set of PMUs such that the whole system is observable. Hence, for an N-bus system, the PMU placement problem is formulated as:

$$\text{Minimize} \quad \sum_{k=1}^{n} x_k \tag{2.1}$$

Where *x* is a binary variable vector, whose entries are defined as:

$$x_i = \begin{cases} 1 & \text{if a PMU is installed at bus i} \\ 0 & \text{otherwise} \end{cases} \tag{2.2}$$

$$\text{Subject to} \quad f(x) \geq N \tag{2.3}$$

f(x) is a vector function, whose entries are non-zero if the corresponding bus voltage is solvable using the given measurement set and zero otherwise. *N* represents unity vector. Consider IEEE-7 bus system as an example. Figure 2.1 represents topological connectivity graph of the system. Nodes of the system are represented in bold numbers. However, branch numbers are shown in bubble. Therefore, IEEE-7 bus system has 7 nodes and 8 branches. In given system, 2th node is an injection measurement node.

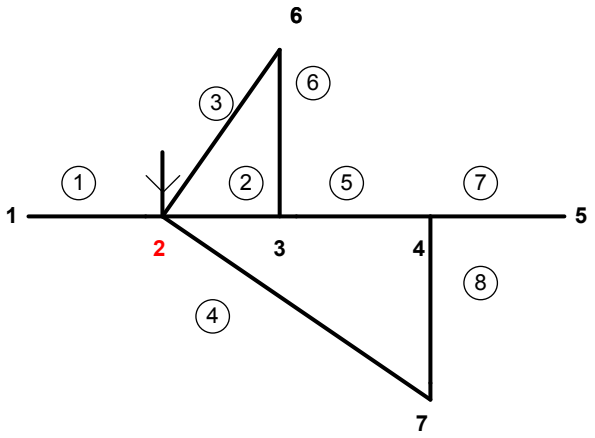

Figure 2.1 IEEE-7 Bus System

For IEEE-7 bus system, the basic objective function is represented as:

$$\text{Minimize} \quad \sum_{k=1}^{n=7} x_k \tag{2.4}$$

The constraints of (2.3) for the system are formulated as

$$f(x) = \begin{cases} f_1 = x_1 + x_2 \geq 1 \\ f_2 = x_1 + x_2 + x_3 + x_6 + x_7 \geq 1 \\ f_3 = x_2 + x_3 + x_4 + x_6 \geq 1 \\ f_4 = x_3 + x_4 + x_5 + x_7 \geq 1 \\ f_5 = x_4 + x_5 \geq 1 \\ f_6 = x_2 + x_3 + x_6 \geq 1 \\ f_7 = x_2 + x_4 + x_7 \geq 1 \end{cases} \tag{2.5}$$

The first constraint f_1 implies that at least one PMU must be placed at either one of buses 1 or 2 (or both) in order to make bus 1 observable. Similarly, the second constraint f_2 indicates that at least one PMU should be installed at any one of the buses 1, 2, 3, 6, or 7 in order to make bus 2 observable. The use of in the right hand side of the inequality ensures that at least one of the variables appearing in the sum will be non-zero. This implies at least one PMU should be placed in any one of the buses (variables) in each inequalities. In matrix form, these constraints are expressed as:

$$\begin{bmatrix} 1 & 1 & 0 & 0 & 0 & 0 & 0 \\ 1 & 1 & 1 & 0 & 0 & 1 & 1 \\ 0 & 1 & 1 & 1 & 0 & 1 & 0 \\ 0 & 0 & 1 & 1 & 1 & 0 & 1 \\ 0 & 0 & 0 & 1 & 1 & 0 & 0 \\ 0 & 1 & 1 & 0 & 0 & 1 & 0 \\ 0 & 1 & 0 & 1 & 0 & 0 & 1 \end{bmatrix} \begin{bmatrix} x_1 \\ x_2 \\ x_3 \\ x_4 \\ x_5 \\ x_6 \\ x_7 \end{bmatrix} \geq \begin{bmatrix} 1 \\ 1 \\ 1 \\ 1 \\ 1 \\ 1 \\ 1 \end{bmatrix} \tag{2.6}$$

Equation (2.6) is further represented as:

$$AX \geq N \tag{2.7}$$

In equation (2.7), matrix *A* is called as bus connectivity matrix, which is obtained directly from the bus admittance matrix by transforming its entries into binary form. *X* is the vector of binary placement variables having length equal to *n* (i.e. number of buses) and *N* is unity vector of dimension *n* X1.

2.2.3 Incomplete Observability

Increase in size of network increases the number of PMUs required for complete observability. According to [106], PMUs needed for complete observability is 20-30% of the total number of system buses. Sometimes, due to financial constraints, available quantity of PMUs is insufficient for complete observability. According to past works [106, 6, 9, 1, 17, 16, 108, 114], in such situations, PMU placement is generally carried out according to incomplete observability.

Incomplete observability refers to the network condition in which number and location of the PMUs are insufficient to determine the complete set of bus voltage phasors. Depth of observability is a measure of an unobserved bus from its observed neighbors. Based on the depth of observability, observability is defined as *Depth-of-One Observability, Depth-of-Two Observability* and so on.

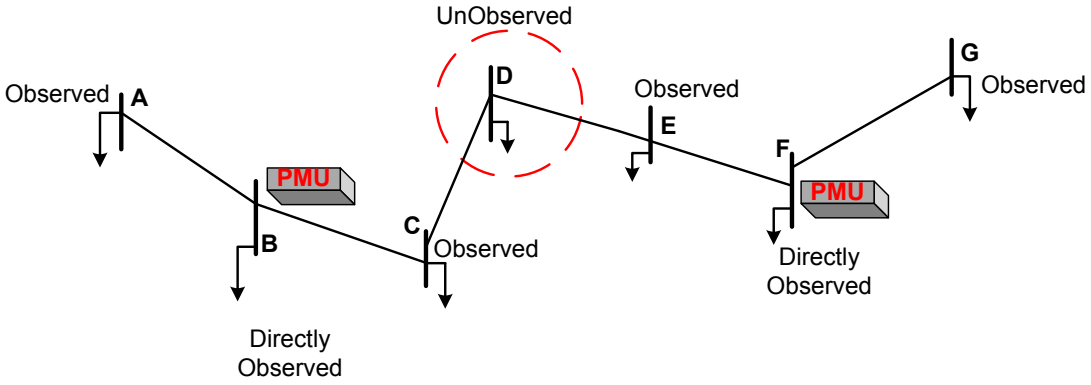

Figure 2.2 Example for Depth-one observability

Depth-of-one observability is defined as a situation in which all of the neighboring buses of any unobservable bus are observable as shown in Figure 2.2. In the figure, D is the bus, which is at depth-one observability from directly observed buses C and E.

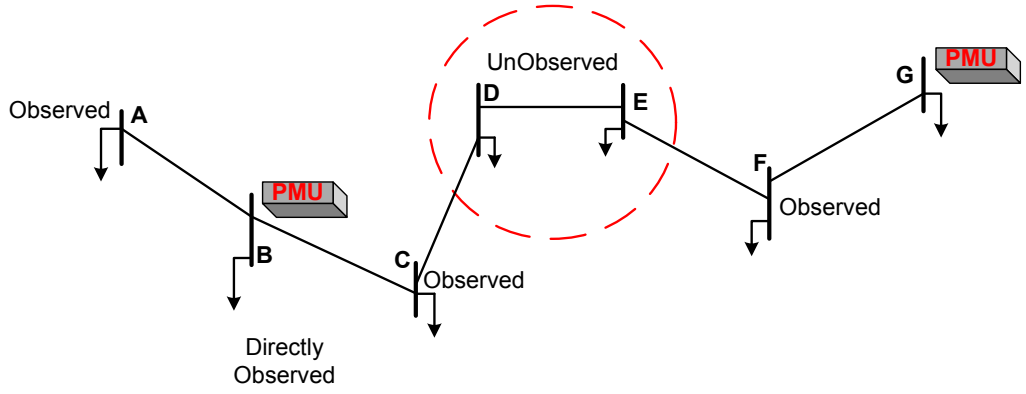

Figure 2.3 Example for Depth-two observability

Similarly, Depth-of-Two observability is defined as a situation in which all of the neighboring buses of any two adjoining unobservable buses are observable. The definition implies that it is impossible for more than two unobservable buses to connect together. This particular case is depicted in Figure 2.3, in which buses D and E are surrounded by all directly observed buses.

2.2.4 Formulation for Incomplete Observability

For incomplete observability, PMU placement problem is formulated utilizing integer linear programming approach according to [17, 16]. Since basic objective function remains unchanged. Therefore, equation (2.1) remains unaltered throughout the chapter. However, constraint equation (2.7) is modified according to depth-one and depth-two observability concept.

PMU placement for Depth-one-Observability

As described in previous section, depth-one observability defines incomplete observability one bus apart. Therefore, constraints of (2.7) are modified by multiplying with matrix *B*, which are given by (2.8).

$$\text{Subject to} \quad BAX \geq b \tag{2.8}$$

Where *B* is branch-to-node incident matrix and defines branch connectivity between various nodes. *B* has dimension *m1*x*n*, where *m1* is total number of branches of the system. Further *b* is a unity vector, which is given as

$$b = \begin{bmatrix} 1 & 1 & \cdots & 1 \end{bmatrix}^{T}_{m1x1} \tag{2.9}$$

For IEEE-7 bus system, Branch to node matrix *B* is given by (2.10). As mentioned before, system has 7 nodes and 8 branches. Therefore, *B* matrix has dimension 8x7 and unity vector *b* has dimension of 8x1. First row of *B* depicts that first branch is between nodes 1 and 2. In similar manner, all other entries are defined.

$$B = \begin{bmatrix} 1 & 1 & 0 & 0 & 0 & 0 & 0 \\ 0 & 1 & 1 & 0 & 0 & 0 & 0 \\ 0 & 1 & 0 & 0 & 0 & 1 & 0 \\ 0 & 1 & 0 & 0 & 0 & 0 & 1 \\ 0 & 0 & 1 & 1 & 0 & 0 & 0 \\ 0 & 0 & 1 & 0 & 0 & 1 & 0 \\ 0 & 0 & 0 & 1 & 1 & 0 & 0 \\ 0 & 0 & 0 & 1 & 0 & 0 & 0 \end{bmatrix} \tag{2.10}$$

PMU placement for Depth -two-Observability

Like depth-one-observability, in depth-two-observability also inequality constraints are modified according depth-two definition. A depth-two observability measure depends on connectivity between three adjacent nodes. From these three nodes, two nodes can be unobserved or observed nodes. Therefore, depth-two formulation involves matrix B', which contains all possible combinations of three connecting buses [16]. Constraints for depth two are formulated as:

$$\text{Subject to} \quad B'AX \geq b' \tag{2.11}$$

$$b' = \begin{bmatrix} 1 & 1 & \cdots & 1 \end{bmatrix}^T_{m2x1} \tag{2.12}$$

In above formulation, *m2* is the total numbers of possible combinations of three connecting buses. For IEEE-7 bus system, total number of combinations for three connecting buses is 15, i.e. *m2*=15. For the system, *B'* is given by (2.13), which has dimension of 15x7. In *B'* matrix, first row represents first combination of three connecting nodes i.e. 1st, 2nd and 3rd nodes. Likewise, other rows represent various other combinations.

$$B' = \begin{bmatrix} 1 & 1 & 1 & 0 & 0 & 0 & 0 \\ 1 & 1 & 0 & 0 & 0 & 1 & 0 \\ 1 & 1 & 0 & 0 & 0 & 0 & 1 \\ 1 & 0 & 1 & 0 & 0 & 1 & 0 \\ 1 & 0 & 1 & 0 & 0 & 0 & 1 \\ 1 & 0 & 0 & 0 & 0 & 1 & 1 \\ 0 & 1 & 1 & 0 & 0 & 1 & 0 \\ 0 & 1 & 0 & 0 & 0 & 1 & 1 \\ 0 & 0 & 1 & 0 & 0 & 1 & 1 \\ 0 & 1 & 1 & 1 & 0 & 0 & 0 \\ 0 & 1 & 1 & 0 & 0 & 1 & 0 \\ 0 & 0 & 1 & 1 & 0 & 1 & 0 \\ 0 & 0 & 1 & 1 & 1 & 0 & 0 \\ 0 & 0 & 1 & 1 & 0 & 0 & 1 \\ 0 & 0 & 0 & 1 & 1 & 0 & 0 \end{bmatrix} \tag{2.13}$$

2.3 POWER SYSTEM CONVENTIONAL MEASUREMENTS

In existing power system, SCADA system provides various conventional measurements. When conventional measurements like real or reactive power injections, real or reactive power flow,

current injection measurements comes into picture, the number of PMUs required reduces. According to B.Gou [16-17], to understand, formulation with conventional measurements, a vector Y is defined as

$$Y = AX \tag{2.14}$$

The element $y_i = A_i X_i$ indicates the number of times for a bus *i* "*reached*" by PMUs, where A_i is the i^{th} row of *A* and x_i is the i^{th} element of X. Figure 2.4 represents an injection measurement at bus *k.* Further, bus *k* connects buses *l*, *p* and *q.* Vector *Y* at individual buses are related with following inequality

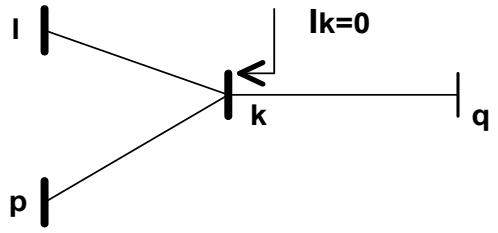

Figure 2.4 Zero Injection Measurement at bus k

$$y_l + y_p + y_k + y_q \geq 3 \tag{2.15}$$

Above inequality indicates that if the voltage phasors at any of the three out of four buses *k, l, p* and *q* are known, and then the fourth is solved using KCL applied at bus where the net injection at *k* is known. Therefore, constraints for the optimal placement of PMUs with conventional measurements are formulated as

$$\text{Subject to} \quad T_C PAX \geq N \tag{2.16}$$

Where, matrix T_C is having structure, $T_C = \begin{bmatrix} I_{MXM} & 0 \\ 0 & T_{con} \end{bmatrix}$, I_{MXM} is an identity matrix and M is the number of buses not associated with conventional measurements. T_{con} is an unity vector having length equal to total number of buses related with conventional measurements. P is the permutation matrix, which contains first all those entries, which are not related with conventional measurements and later having entries for nodes related with conventional measurements.

In the IEEE7-bus system, a current injection measurement is placed at bus 2. Voltage phasors at any four buses out of five buses 1, 2, 3, 6, and 7 are known, and then fifth one is calculated using KCL applied at bus 2 where the net injected current is known.

$$y_1 + y_2 + y_3 + y_6 + y_7 \geq 4$$

Now as buses 1, 2, 3, 6, 7 are associated with conventional measurement and 4, and 5 are not associated with conventional measurement. Therefore

$$I_{MXM} = \begin{bmatrix} 1 & 0 \\ 0 & 1 \end{bmatrix} \tag{2.17}$$

$$T_{con} = \begin{bmatrix} 1 & 1 & 1 & 1 & 1 \end{bmatrix} \tag{2.18}$$

$$P = \begin{bmatrix} 0 & 0 & 0 & 1 & 0 & 0 & 0 \\ 0 & 0 & 0 & 0 & 1 & 0 & 0 \\ 1 & 0 & 0 & 0 & 0 & 0 & 0 \\ 0 & 1 & 0 & 0 & 0 & 0 & 0 \\ 0 & 0 & 1 & 0 & 0 & 0 & 0 \\ 0 & 0 & 0 & 0 & 0 & 1 & 0 \\ 0 & 0 & 0 & 0 & 0 & 0 & 1 \end{bmatrix} \tag{2.19}$$

2.3.1 Formulation for Incomplete Observability

Constraints for incomplete observability, considering conventional measurements are different from constraints for complete observability with conventional measurements, defined in previous section. This section defines constraints for incomplete observability together with conventional measurements.

PMU placement for Depth-of-one observability

For depth-one observability, constraints of equation (2.8) are modified by multiplying expression on both sides of inequality with permutation matrix *P1*. *P1* is the matrix that keeps the branches that are not associated with zero injection measurements and remove the branches that are associated with zero injection measurements. Therefore, constraint equation is given as

$$\text{Subject to} \quad P1BAX \geq P1b \tag{2.20}$$

For IEEE-7 bus system, with a zero injection measurement at bus 2. Branches 1, 2, 3, and 4 are associated with zero injection measurements. Therefore, matrix P1 is given as:

$$P1 = \begin{bmatrix} 0 & 0 & 0 & 0 & 1 & 0 & 0 & 0 \\ 0 & 0 & 0 & 0 & 0 & 1 & 0 & 0 \\ 0 & 0 & 0 & 0 & 0 & 0 & 1 & 0 \\ 0 & 0 & 0 & 0 & 0 & 0 & 0 & 1 \end{bmatrix} \quad (2.21)$$

PMU Placement for Depth-of-Two observability

Depth-two observability constraints (2.11) are further changed to incorporate the conventional measurements. To accomplish this (2.11) is multiplied with permutation matrix P2, like depth-one case and constraints are expressed as:

$$\text{Subject to} \quad P2B'AX \geq P2b' \quad (2.22)$$

Where, *P2* matrix keeps those combinations, which are not associated with zero injection measurements and remove those, which are associated with zero injection measurements.

For IEEE-7 bus system, only three combinations of branches are not associated with the injection node. Therefore, P2 for the system is formulated as:

$$P2 = \begin{bmatrix} 0 & 0 & 0 & 0 & 0 & 0 & 0 & 0 & 0 & 0 & 0 & 0 & 1 & 0 & 0 \\ 0 & 0 & 0 & 0 & 0 & 0 & 0 & 0 & 0 & 0 & 0 & 0 & 0 & 1 & 0 \\ 0 & 0 & 0 & 0 & 0 & 0 & 0 & 0 & 0 & 0 & 0 & 0 & 0 & 0 & 1 \end{bmatrix} \quad (2.23)$$

2.4 BINARY PARTICLE SWARM OPTIMIZATION

Particle swarm optimization (PSO) is inspired from collective movement of a flock of bird, a school of fish, or a swarm of bees [126]. In PSO, members of entire population are maintained throughout the search process. Therefore, PSO is different from other evolutionary techniques like Genetic Algorithm (GA). In PSO, each member/particle is characterized by its position in multi dimensional search space. The i^{th} particle of the population is represented by a *j*-dimensional vector, which is defined as $x_i^k = [x_{i1}^k, x_{i2}^k, \cdots x_{ij}^k]$. Therefore, x_{ij}^k is the position of the i^{th} particle with respect to j^{th} dimension. Complete population at k^{th} iteration having *n* number of particles is presented as $population^k = \left[x_1^k, x_2^k, \cdots x_n^k\right]$.These particles are constantly moving with a velocity in the space. v_i^k is the velocity of the particle at iteration *k*. This velocity is further described as $v_i^k = \left[v_{i1}^k, v_{i2}^k, \cdots v_{ij}^k\right]$, where v_{ij}^k is velocity with respect to j^{th} dimension. The movement

of particles towards finding the optimal solution is guided by individual and social knowledge of the particles. Each particle adjusts its own position towards its previous experience and towards the best previous position of the population. $pbest_i^k$ is the best value of the particle till iteration *k*. It gives best position for individual particle obtained through fitness function. This $pbest_i^k$ is defined for *j* dimension as $pbest_i^k = \left[pbest_{i1}^k, pbest_{i2}^k, \cdots pbest_{ij}^k\right]$. The best position among all particles in the given population is termed as $gbest^k$ until k^{th} iteration, which is expressed as $gbest_i{}^k = \left[gbest_{i1}^k, gbest_{i2}^k, \cdots gbest_{ij}^k\right]$. To find optimal solution, these *pbest* and *gbest* values are utilized to update particle velocity using expression

$$v_{ij}^{k+1} = v_{ij}^k + \varphi_1 . r_1 \left(pbest_i^k - x_{ij}^k\right) + \varphi_2 . r_2 \left(gbest_i^k - x_{ij}^k\right) \tag{2.24}$$

Where φ_1 and φ_2 are adjustable parameters called individual and social acceleration constant respectively. φ_1 and φ_2 are usually defined such that $\varphi_1 + \varphi_2 = 4$. r_1 and r_2 are random numbers in the range [0,1]. After computing new particle velocity, particle position is calculated according to equation (2.25)

$$x_{ij}^{k+1} = x_{ij}^k + v_{ij}^{k+1} \tag{2.25}$$

Therefore, in a PSO algorithm, first population is generated randomly and fitness function is computed to find particle best and global best values. Now these particle and global best values are utilized to update velocity. Based on this current velocity, particle position is also updated as new particle position. Again, fitness function is evaluated and whole process is repeated till stopping criterion is met.

In present work, binary version of PSO algorithm is employed. This means, each element of position vector can take only binary values i.e. 1 or 0. Therefore, at each stage of iteration, the elements of the position vector x_{ij}^k are updated according to following rule:

$$x_{ij}^k = \begin{cases} 1 & \text{if } \rho_{ij} \le s\left(v_{ij}\right) \\ 0 & \text{otherwise} \end{cases} \tag{2.26}$$

Where ρ_{ij} is a random number in the range [0, 1]. $s\left(v_{ij}\right)$ is a sigmoid function defined as

$$s\left(v_{ij}\right) = \frac{1}{1 + \exp\left(-v_{ij}\right)} \tag{2.27}$$

This sigmoid function is used to force real values between 0 and 1. Further, velocity values are also restricted between maximum and minimum values. This limit on velocity enhances local search in provided search space, thus avoiding large oscillations around solutions. Therefore, velocity values are obtained with maximum and minimum values of the velocity as

$$v_{ij}^{\ k} = \begin{cases} -v_{\max}, & v_{ij}^{\ k} \le -v_{\max} \\ v_{\max}, & v_{ij}^{\ k} \ge v_{\min} \end{cases} \tag{2.28}$$

2.4.1 Proposed PMU Placement Using Binary Particle Swarm Optimization

The objective of the PMU placement problem is to minimize the number of PMUs that can make the system observable, considering conventional measurements and maximizing the measurement redundancy in the system. This means, designed fitness function should evaluate following factors, for the position vector of each particle

- Whether the system is observable or unobservable
- For both, complete and incomplete observable cases, with and without conventional measurements, what is number of PMUs employed
- Provide maximum measurement redundancy in each case

For PMU placement problem, the position array X of the BPSO algorithm gives the information of PMU installation location. In other words, j^{th} dimension of position is equal to total number of buses. Therefore, position array is a binary bit array with the length of number of buses in the target power system. Value1 of one-bit means an installation of PMU at corresponding bus, while value 0 means no PMU installation at corresponding bus. The fitness function $F(x)$ for BPSO is formulated as

$$F(x) = \begin{cases} K & \text{if systemis unobservable} \\ w_1 F_1 + w_2 F_2 & \text{if systemis observable} \end{cases} \tag{2.29}$$

Where *K* is a large number assigned to the fitness function if the position vector representing the PMU placement solution is not able to make the system observable. w_1 and w_2 are two weights having values such that $w_1 F_1$ and $w_2 F_2$ are comparable in magnitude.

In present formulation, radial buses are excluded from the list of potential locations. PMUs are pre-assigned to each buses connected to a radial buses. Pre-assigning PMUs to certain buses

in this manner reduces the total number of possible combinations of PMU locations, thereby reducing the computational burden.

Various steps of BPSO placement scheme are as follows:

Step 1: Initialize the swarm, set iteration count *k*=0, where maximum number of iterations is taken equal to 100* number of total buses in the system. Generate *n* number of particles in swarm randomly with *n*= 5* total number of buses in the system.

Step 2: Generate initial velocities of the particles, present in the swarm randomly using $v_{ij} = v_{\min} + (v_{\max} - v_{\min}) * \text{random number}$

Step 2: Calculate the value of objective function according to equation (2.29)

Step 3: For each particle, calculate personal and global best values ($pbest_i^k$ and $gbest_i^k$) of each particle and whole swarm respectively

Step 4: Update iteration counter, and calculate new values of velocity and positions according to (2.24) and (2.26). Further update particle personal and swarm best values

Step 5: Check for observability condition, and if not meet replace initial position and velocity vectors with new one and repeat the process from Step 2

Step 6: Check whether number of iteration exceeds the maximum number of iteration, if yes stop, otherwise go to Step 4.

2.4.2 Proposed BPSO Placement without Conventional Measurements

In given fitness function (2.29), F_1 and F_2 represents the total number of PMUs and the measurement constraints along with redundancy respectively. These two sub-parts are defined as follows:

$$F_1 = x^T x \tag{2.30}$$

$$F_2 = (N - Ax)^T (N - Ax) \tag{2.31}$$

The elements of binary vector *x* are described as follows:

$$x_i = \begin{cases} 1 & \text{if PMU is placed at bus i} \\ 0 & \text{otherwise} \end{cases} \tag{2.32}$$

The elements of binary connectivity vector *A* are defined as follows:

$$A(i,j)=\begin{cases}1 & \text{if i = j}\\ 1 & \text{if bus i and j are connected}\\ 0 & \text{otherwise}\end{cases} \tag{2.33}$$

If number of buses in the given system is *M*, then *A* is an *MXM* matrix and *N* is an *MX1*dimension matrix. Further, vector *N* is chosen according to the desired level of measurement redundancy.

The entries of the product Ax in (2.31), represents the number of times a bus is observed by the PMU placement set defined by x. Therefore, the proposed fitness function, not only gives optimal locations for PMUs but also considers the required measurement redundancy i.e. maintain system integrity even when system is subjected to loss of single line or PMU.

2.4.3 Proposed BPSO Placement with Conventional Measurements

Incomplete observability and Zero-injection measurements are introduced in the above formulation by making slight changes in the fitness function F_2. In equation (2.31), matrix *A* and *N* are replaced with *GA* and N_G respectively. *G* matrix is the transformation matrix, which transforms matrix according to full observability, incomplete observability, and zero injections. N_G represents the redundancy level considered for the system.

$$F_2=\left(N_G-Gx\right)^T\left(N_G-Gx\right) \tag{2.34}$$

Both *G* and N_G take different values according to different cases described in previous section 2.3.

When zero injections are not considered, the transformation matrix *G* and N_G will take values according to (2.35) and (2.36).

$$G=\begin{cases}B*A & \text{for depth one}\\ B'*A & \text{for depth two}\end{cases} \tag{2.35}$$

$$N_G=\begin{cases}b & \text{for depth one}\\ b' & \text{for depth two}\end{cases} \tag{2.36}$$

However, for zero injections measurements (2.34) are given by (2.37) and (2.38) expressions.

$$G=\begin{cases}P1B*A & \text{for depth one}\\ P2B'*A & \text{for depth two}\end{cases} \tag{2.37}$$

$$N_G=\begin{cases}P1b & \text{for depth one}\\ P2b' & \text{for depth two}\end{cases} \tag{2.38}$$

Where *B*, *B'*, *b*, *b'*, *P1*, and *P2* are formulated as described in section 2.3.

2.5 GAMS-MIP SOLVER BASED FORMULATION

Using Formulation equations of (2.5), connectivity matrix A and constraints are formed, which are directly solved by MIP solver of Generic Algebraic Modelling Systems (GAMS).

2.6 SIMULATION RESULTS

The proposed formulation is successfully tested on various IEEE test systems and results are shown in the Table 2.1 for complete observability and measurement redundancy 2. The number of radial buses for the given test systems are 1, 3 and 1, for IEEE 14, 30, and 57 bus systems respectively [8-9]. Number of constraints becomes too large in GAMS-MIP-solver (student version) for depth-one and depth-two observability cases. Therefore, results obtained through BPSO are only reported. A comparative study is carried out between BPSO and GAMS for complete observability. Optimization results for various systems are tabulated in Table 2.2 and Table 2.3.

Table 2.1

Number and Locations of PMUs for complete observability by BPSO and GAMS

Test Systems	**BPSO results**		**GAMS Results**	
	Locations of PMUs	Number of PMUs	Locations of PMUs	Number of PMUs
IEEE -14	2,6,7,9	4	2,7,10,13	4
IEEE-30	1,2,6,9,10,12,15,19,25,27	10	1,2,6,9,10,12,15,18,26,27	10
IEEE-57	1,6,9,15,18,26,29,30,32, 35,36,38,42,46,50,54,57	17	1,6,9,15,19,22,25,27,28, 32,36,41,45,47,50,53,57.	17

From results, it is observed that, though the locations obtained are not unique but the optimized value of objective function and numbers of PMUs obtained are same.

Further, results are obtained for incomplete observability without zero injections and with zero injections. In proposed formulation, numbers of zero injections are taken as 1, 7 and 17 in IEEE-14, 30, and 57 bus systems respectively. Table 2.2 shows results without zero injections. However, Table 2.3 shows results with zero injections.

Table 2.2

Number and Locations of PMU for observability cases without zero injections

Test Systems	Complete Observability		Depth-one observability		Depth-two observability	
	Number of PMUs	Locations of PMUs	Number of PMUs	Locations of PMUs	Number of PMUs	Locations of PMUs
IEEE14	4	2,6,7,9	2	4,6	2	4,13
IEEE30	10	1,2,6,9,10,12, 15,19,25,27	4	2,10,15,27	3	6,15,7
IEEE57	17	1,6,9,15,18,26, 29,30,32,35,36,38, 42,46,50,54,57	11	1,6,19,22,30, 33,35,39,43, 47,54	8	8,17,21,27,32,44, 53,56

Table 2.3

Number and Locations of PMU for various observability cases with zero injections

Test Systems	Complete Observability		Depth-one observability		Depth-two observability	
	Number of PMUs	Locations of PMUs	Number of PMUs	Locations of PMUs	Number of PMUs	Locations of PMUs
IEEE14	3	2,6,9	2	4,6	2	4,6
IEEE30	7	3,5,10,11, 12,18,24,27	4	2,10,15,30	3	6,15,27
IEEE57	11	8,10,15,23,25, 33,34,40,49,54,57	9	2,10,19,23,24, 26,34,35,48	8	4,16,23,33, 35,38,52,54

From results, it is concluded that number of PMUs are reduced for complete observability and depth of one observability when zero injections are considered. However, in case of depth-two observability amount of PMUs are same for with and without conventional measurements.

Further, it is observed that the obtained results are in complete agreement with the results of [17], [16] and [108].

2.7 CONCLUSION

Based on above analysis and results following points are concluded

- Proposed objective function considers observability, conventional measurements, and redundancy simultaneously.
- Proposed method based on BPSO accurately computes the optimal number of PMU locations for complete and in complete observability. Results obtained are in complete accord with references [16, 17, and108]. Further, solutions obtained through GAMS-MIP solver also support proposed technique.
- From obtained results, it is concluded that with topological based observability concept gives multiple solutions for same number of PMU locations. Moreover, this difference in locations increases with increase in size of the network.

CHAPTER-3
Sequential placement of Phasor Measurement Units to monitor power flows

3.1 INTRODUCTION

Majority work for solution of the PMU placement problem is based on topological observability considering various factors like cost of PMUs, redundancy, loss of PMUs and lines, presence of injection and conventional measurements as described in previous chapter. However, according to [5,106,6,9,1,17,16,108,114,109,26,66,104,28,103,65,51] PMUs should be placed strategically in system according to some criterion to get maximum benefit from placement and to aid various applications. Observability is one such criterion, which provides complete state information with minimum number of PMUs. From results obtained in previous chapter, it is observed that topological observability based methods gives multiple solutions. Sometimes for simple networks also, observability fails to give optimal solution. For example, consider a small network as shown in Fig 3.1. A, B, and C are three interconnected nodes and each node is connected with two other nodes. To place two PMUs in given network according to topological observability, placing PMU's either at A, B or B, C or C, A will be of same significance. In such ambiguous situation other criteria is required to select optimal PMU site.

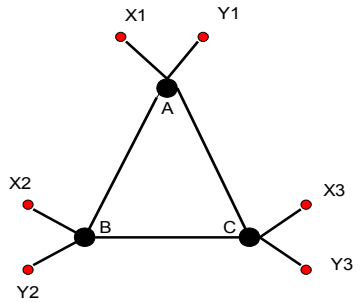

Figure 3.1 Example of small network

Moreover, any change in topology of the network, will results in change of solution. Recently, few researchers have reported techniques to place PMUs considering practical aspects of power systems [65, 51, 37, 32, 70]. In this chapter, a new approach is presented to sequentially place the PMU's in a given power system under normal conditions (without considering contingent situations). It is to be noted here that proposed technique is no way replacement for conventional observability based methods. However, proposed method is suggested as one

possible way to select PMU locations sequentially to benefit those applications where power flow patterns and demand variations plays important role. Further, proposed technique is useful when utilities are planning to place PMUs in large amounts, where this placement scheme can serve as secondary placement approach after achieving topological observability.

3.2 BACKGROUND

Any interconnected system whether a power system or a water distribution system [20], is generally denoted as connected graph having nodes and edges. Therefore, a given power system can be represented as a connected graph/network, where all its buses are treated as nodes and lines as edges. Each node in this network will be either a load/demand node or a generation node or both. This connected graph becomes directed graph by considering active and reactive power flow directions. These power flows depend on load and generation of the system, a small change in either of them will be reflected in the power flows. Further, each node is connected to other nodes via edges (line flows), which means effect of one individual node on other is accounted by line power-flow-pattern. Therefore, in this work coverage concept is introduced, which includes demand-coverage and flow-coverage. Next section deals with coverage concept in detail.

3.2.1 Coverage Concept

In a power-network, load is connected to various nodes. Each load node represents a certain amount of total load, in the system. If the node *i* has a demand of d_i and the total demand of the system is *D*. Load on the node *i* is represented as fraction $(d_i/D) \times 100\ \%$ of total demand *D*. Therefore, a single demand node is fractional representative of total demand of the system. For example, if total demand in the system is say, 100 units and demand on an individual node is 5 units, then that bus is representative of 5% of total demand, this representativeness is termed as 'demand-coverage'.

For a given operating condition, the power flow in the system has a fixed pattern, which is obtained by the conventional load flow techniques. In an interconnected power system, power flow through any node is influenced by flow through other nodes. Therefore, 'flow-coverage' concept is introduced. Flow-coverage is defined as fractional contribution of real flow from any node *i* to another node *j*. In other words, node *i* is contributing to some fraction of total flow of node *j.* This fractional representativeness of flow by other node on node under consideration is termed as flow-coverage.

PMUs when placed at a particular node provide synchronized voltage and current phasors of that node. Due to interconnection of nodes, voltage and current phasors of neighboring nodes are inferred by flow-coverage and if node under consideration has certain load associated with it, then certain fraction of demand is also covered. Therefore, PMU placement problem reduces to selection of only those demand points, which will maximize the demand-coverage as well as flow-coverage, or finding out those demand nodes, which will affect the flow-pattern most. To formulate the placement problem, coverage concept is utilized. As described, coverage concept includes demand-coverage and flow-coverage. The term coverage will be used to convey that by placing a PMU at a certain node, voltage and current phasors along with demand are known (demand-coverage) at that particular node. Voltage and current phasors of other nodes can be determined based on flow pattern (flow-coverage). It is to be noted here that inflow to a node, is an outflow to another node. Furthermore, at a particular node, all inflows and outflows are balanced following Kirchhoff's law. Therefore, in this work, to make formulation simple, only inflows to a particular node from other nodes are considered.

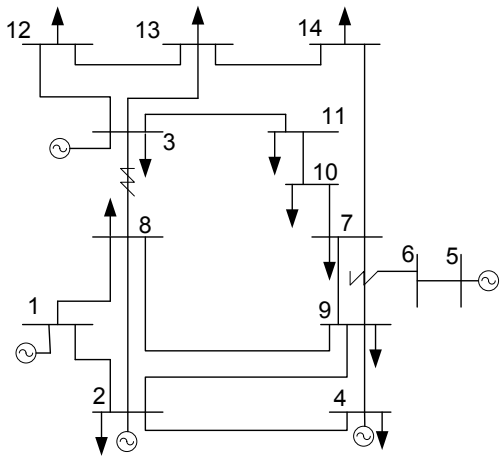

Figure 3.2 IEEE-14 Bus Systems

3.2.2 Coverage Matrix Formation

To understand the coverage concept in detail, let us consider IEEE-14 bus system of Fig 3.2, which shows that 1, 2, 3, 4, and 5 are generation nodes and remaining nodes are demand nodes. Generator 1, 2, and 3 are only responsible for real power generation. Nodes 2 and 3 are having both real load and generation. For the given system real and reactive power flows is determined using conventional load flow. Results obtained for line flows and bus solutions are given in Table 3.1 and Table 3.2.

Based on the conventional load–flow analysis a directed graph is developed which depicts the real power flow pattern in the system at a given load. For IEEE 14 bus system, flow-pattern is shown in Fig.3.3

Table 3.1

Line flows for IEEE-14 bus system

Line	From bus	To bus	Real	Reactive
1	8	3	0.2822	0.0978
2	9	6	0.2404	0.0400
3	9	7	0.1394	0.0463
4	1	8	0.5446	-0.0453
5	2	8	0.3893	-0.0322
6	9	4	0.2226	0.1881
7	8	9	0.5529	0.1371
8	1	2	0.8501	-0.2791
9	2	4	0.7214	-0.1373
10	2	9	0.5202	-0.0577
11	5	6	0.0000	-0.0218
12	6	7	0.2427	0.0584
13	7	10	0.0209	0.0649
14	3	11	0.1034	0.0117
15	3	12	0.0797	0.0203
16	3	13	0.1892	0.0575
17	7	14	0.0717	0.0502
18	11	10	0.0670	0.0076
19	12	13	0.0189	0.0035
20	13	14	0.0723	0.0019

Table 3.2

Bus solution for IEEE-14 bus system

			GENERATION		LOAD	
Bus	**Volts**	**Angle**	**Real**	**Reactive**	**Real**	**Reactive**
1	1.0000	0	1.3946	-0.3244	0	0
2	1.0000	-3.1641	1.0132	0.1726	0.2170	0.1270
3	1.0000	-11.1554	0.2021	0.0882	0.1120	0.0750
4	1.0000	-11.6895	0	0.4000	0.9189	0.0127
5	1.0000	-11.5447	0	0.0219	0	0
6	0.9961	-11.5447	0	0	0.000	-0.0089
7	0.9901	-13.0957	0	0	0.2894	0.1572
8	0.9829	-7.1642	0	0	0.0696	-0.0510
9	0.9812	-8.6613	0	0	0.4488	-0.0860
10	0.9839	-13.0780	0	0	0.0855	0.0569
11	0.9881	-12.2835	0	0	0.0350	0.0162
12	0.9852	-12.1957	0	0	0.0600	0.0151
13	0.9802	-12.3736	0	0	0.1331	0.0539
14	0.9673	-13.8741	0	0	0.1421	0.0481

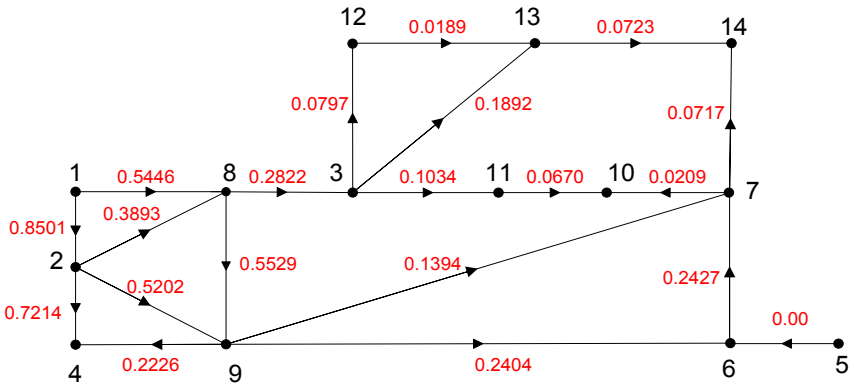

Figure 3.3 Flow pattern in IEEE-14 bus system

According to the definition of the flow-coverage, one can infer how much other nodes are contributing to each node. For this, a fractional flow *F* (*i,j*) is defined as the contribution of real power flow at node *i* from node *j*.

This fractional flow is computed by a simple formula, which is given below

$$Fractional\ flow F(i,j) = \frac{(Inflow\ from\ node\ j\ to\ node\ i)}{(Total\ in-flow\ at\ node\ i)}$$

Based on this simple formula and load-flow pattern, fractional flow for each-and-every node in the given network is computed. From Fig 3.3, It is observed that 2nd and 8th node is directly contributing to 9th node. Therefore, $F(9,2)$ represents power flow at 9th node contributed by the 2nd node. Likewise, computation is carried out to determine the effect of power flow contribution at an individual system node from the other system nodes.

For example

$$F(9,2) = \frac{0.5202}{0.5529 + 0.5202} = 0.484$$

This means that 48.4% of the power flow on 9th node is contributed by 2nd node. Similarly, 51.5% flow on same node is contributed from 8th node is

$$F(9,8) = \frac{0.5529}{0.5529 + 0.5202} = 0.515$$

In the given pattern, it is observed that every node is not directly contributing to 9th node, in such case all paths from every other node to 9th node are taken into account. Consider the case of fractional flow $F(9,1)$ i.e. contribution of 1st node to 9th node. As node-1 is not directly contributing to node-9, in such a case, consider all the paths from node-1 to node-9. According to Fig 3.3, there are three paths from node-1 to node-9, first path is 1-2-9, second path is 1-8-9, and third path is 1-2-8-9. However, third path shows that both directly connected nodes are interconnected. So flow fraction in such case will be calculated as

$$F(9,1) = F(9,2) * F(2,1) + F(9,8) * F(8,1) + F(9,8) * F(8,2) * F(2,1)$$

Where, $F(2,1) = 1$ because 2nd node is getting all its flow from 1st node and

$$F(8,1)=\frac{0.5446}{0.5446+0.3893}=0.583$$

$$F(8,2)=\frac{0.3893}{0.5446+0.3893}=0.417$$

Further, $F(i,i)=1, F(1,1)=F(2,2)\ldots=F(14,14)=1$

Fractional flows are arranged in a matrix form called as Fractional Flow Matrix (FFM). FFM for IEEE-14 bus system is shown in Table 3.3.

Table 3.3

Flow Fraction Matrix (FFM)

	1	**2**	**3**	**4**	**5**	**6**	**7**	**8**	**9**	**10**	**11**	**12**	**13**	**14**
1	1	0	0	0	0	0	0	0	0	0	0	0	0	0
2	1	1	0	0	0	0	0	0	0	0	0	0	0	0
3	1	0.416	1	0	0	0	0	1	0	0	0	0	0	0
4	1	0.878	0	1	0	0	0	0.121	0.235	0	0	0	0	0
5	0	0	0	0	1	0	0	0	0	0	0	0	0	0
6	0.98	0.699	0	0	0	1	0	0.515	1	0	0	0	0	0
7	0.97	0.255	0	0	0	0.635	1	0.188	0.364	0	0	0	0	0
8	1	0.416	0	0	0	0	0	1	0	0	0	0	0	0
9	1	0.699	0	0	0	0	0	0.515	1	0	0	0	0	0
10	0.99	0.378	0.762	0	0	0.151	0.237	0.762	0.086	1	0.762	0	0	0
11	1	0.416	1	0	0	0	0	1	0	0	1	0	0	0
12	1	0.416	1	0	0	0	0	1	0	0	0	1	0	0
13	1	0.416	1	0	0	0	0	0.999	0	0	0	0.098	1	0
14	1	0.336	0.502	0	0	0.316	0.497	0.595	0.181	0	0	0.045	0.502	1

After computing flow fractions, flow-coverage-criterion is defined. Flow-coverage-criterion is the minimum fractional percentage of flow under which a node is assumed to be covered. Since it is a selection criterion, it can take any value. To understand flow-coverage criteria, consider the case, when a PMU is placed at bus 4. According to FFM node 1, 2, 8, and 9 contributed to flow at node-4 (i.e. 4th row of FFM). Flow fraction values of nodes 1, 2, 8, and 9 are 1, 0.878, 0.121,

and 0.235 respectively. Every flow fraction value carries certain amount of knowledge regarding flow. Suppose a flow-coverage-criterion of 0.75 is considered. This means that only those nodes are taken into account, which contributes more than 75% of the flow at that particular node. Therefore, with flow-coverage-criteria, a Flow-Coverage-Matrix (FCM) is obtained from FFM. In other words, FCM defines those nodes, which has flow-coverage greater than or equal to the flow-coverage-criterion. For IEEE-14 bus system, a coverage criterion of 75% is considered. A FCM for 14-bus system is obtained by changing the elements of FFM with values 0.75 or more, equal to unity and other elements to zero. Therefore, elements of FCM are defined as

$$FCM(i,j)=\begin{cases}1, if\ \ FFM(i,j)\geq \text{coverage criterion}\ i,\ j=1,2,3,\cdots n\\ 0,\quad otherwise\end{cases}$$

Where *n* is total number of buses in the given system.

Based on FFM of Table 3.3, FCM for IEEE-14 bus system is given in Table 3.4.

TABLE 3.4

Flow-Coverage-Matrix (FCM) by 75% criterion-base case

	1	**2**	**3**	**4**	**5**	**6**	**7**	**8**	**9**	**10**	**11**	**12**	**13**	**14**
1	1	0	0	0	0	0	0	0	0	0	0	0	0	0
2	1	1	0	0	0	0	0	0	0	0	0	0	0	0
3	1	0	1	0	0	0	0	1	0	0	0	0	0	0
4	1	1	0	1	0	0	0	0	0	0	0	0	0	0
5	0	0	0	0	1	0	0	0	0	0	0	0	0	0
6	1	0	0	0	0	1	0	0	1	0	0	0	0	0
7	1	0	0	0	0	0	1	0	0	0	0	0	0	0
8	1	0	0	0	0	0	0	1	0	0	0	0	0	0
9	1	0	0	0	0	0	0	0	1	0	0	0	0	0
10	1	0	1	0	0	0	0	1	0	1	1	0	0	0
11	1	0	1	0	0	0	0	1	0	0	1	0	0	0
12	1	0	1	0	0	0	0	1	0	0	0	1	0	0
13	1	0	1	0	0	0	0	1	0	0	0	0	1	0
14	1	0	0	0	0	0	0	0	0	0	0	0	0	1

A wide area network is always subjected to demand variation, which results in ever changing flow patterns. Any change in flow patterns results into changed FCM. Hence, FCM of Table 3.4

will change with change in load. To generate various flow and demand patterns for IEEE-14 bus system, load at individual node is increased by 25% keeping load at other nodes unchanged. Total 14 cases are obtained for IEEE-14 system. FCM of these 14 cases are compared. It is observed that four distinct flow-coverage patterns are repeated in these 14 cases. Load increment at 1, 4, 5, 6, 7, and 9 nodes gives FCM-pattern 1. Similarly, load increment on 3 and 13 gives FCM-pattern 2. FCM-pattern 3 is obtained by increasing the load at nodes 2, 8 and 14. However, FCM-pattern 4 results when load at bus 10, 11, and 12 is changed. Transpose of these four FCM-patterns are given in Table 3.5, 3.6, 3.7 and 3.8. In all cases flow-coverage criteria of 75% is considered.

Table 3.5
Transpose of FCM-pattern 1

	1	**2**	**3**	**4**	**5**	**6**	**7**	**8**	**9**	**10**	**11**	**12**	**13**	**14**
1	1	1	1	1	0	1	1	1	1	1	1	1	1	1
2	0	1	0	1	0	0	0	0	0	0	0	0	0	0
3	0	0	1	0	0	0	0	0	0	1	1	1	1	0
4	0	0	0	1	0	0	0	0	0	0	0	0	0	0
5	0	0	0	0	1	0	0	0	0	0	0	0	0	0
6	0	0	0	0	0	1	0	0	0	0	0	0	0	0
7	0	0	0	0	0	0	1	0	0	0	0	0	0	0
8	0	0	1	0	0	0	0	1	0	1	1	1	1	0
9	0	0	0	0	0	1	0	0	1	0	0	0	0	0
10	0	0	0	0	0	0	0	0	0	1	0	0	0	0
11	0	0	0	0	0	0	0	0	0	1	1	0	0	0
12	0	0	0	0	0	0	0	0	0	0	0	1	0	0
13	0	0	0	0	0	0	0	0	0	0	0	0	1	0
14	0	0	0	0	0	0	0	0	0	0	0	0	0	1

Table 3.6
Transpose of FCM-pattern 2

	1	2	3	4	5	6	7	8	9	10	11	12	13	14
1	1	1	1	1	0	1	1	1	1	1	1	1	1	1
2	0	1	0	1	0	0	0	0	0	0	0	0	0	0
3	0	0	1	0	0	0	0	0	0	0	1	1	1	0
4	0	0	0	1	0	0	0	0	0	0	0	0	0	0
5	0	0	0	0	1	0	0	0	0	0	0	0	0	0
6	0	0	0	0	1	1	0	0	0	0	0	0	0	0
7	0	0	0	0	0	0	1	0	0	0	0	0	0	0
8	0	0	1	0	0	0	0	1	0	0	1	1	1	0
9	0	0	0	0	0	1	1	0	1	0	0	0	0	0
10	0	0	0	0	0	0	0	0	0	1	0	0	0	0
11	0	0	0	0	0	0	0	0	0	0	1	0	0	0
12	0	0	0	0	0	0	0	0	0	0	0	1	0	0
13	0	0	0	0	0	0	0	0	0	0	0	0	1	0
14	0	0	0	0	0	0	0	0	0	0	0	0	0	1

Table 3.7
Transpose of FCM-pattern 3

	1	2	3	4	5	6	7	8	9	10	11	12	13	14
1	1	1	1	1	0	1	1	1	1	1	1	1	1	1
2	0	1	0	1	0	0	0	0	0	0	0	0	0	0
3	0	0	1	0	0	0	0	0	0	1	1	1	1	0
4	0	0	0	1	0	0	0	0	0	0	0	0	0	0
5	0	0	0	0	1	0	0	0	0	0	0	0	0	0
6	0	0	0	0	1	1	0	0	0	0	0	0	0	0
7	0	0	0	0	0	0	1	0	0	0	0	0	0	0
8	0	0	1	0	0	0	0	1	0	1	1	1	1	1
9	0	0	0	0	0	1	1	0	1	0	0	0	0	0
10	0	0	0	0	0	0	0	0	0	1	0	0	0	0
11	0	0	0	0	0	0	0	0	0	1	1	0	0	0
12	0	0	0	0	0	0	0	0	0	0	0	1	0	0
13	0	0	0	0	0	0	0	0	0	0	0	0	1	0
14	0	0	0	0	0	0	0	0	0	0	0	0	0	1

Table 3.8

Transpose of FCM-pattern 4

	1	**2**	**3**	**4**	**5**	**6**	**7**	**8**	**9**	**10**	**11**	**12**	**13**	**14**
1	1	1	1	1	0	1	1	1	1	1	1	1	1	1
2	0	1	0	1	0	0	0	0	0	0	0	0	0	0
3	0	0	1	0	0	0	0	0	0	0	1	1	1	0
4	0	0	0	1	0	0	0	0	0	0	0	0	0	0
5	0	0	0	0	1	0	0	0	0	0	0	0	0	0
6	0	0	0	0	0	1	0	0	0	0	0	0	0	0
7	0	0	0	0	0	0	1	0	0	0	0	0	0	0
8	0	0	1	0	0	0	0	1	0	0	1	1	1	0
9	0	0	0	0	0	1	0	0	1	0	0	0	0	0
10	0	0	0	0	0	0	0	0	0	1	0	0	0	0
11	0	0	0	0	0	0	0	0	0	0	1	0	0	0
12	0	0	0	0	0	0	0	0	0	0	0	1	0	0
13	0	0	0	0	0	0	0	0	0	0	0	0	1	0
14	0	0	0	0	0	0	0	0	0	0	0	0	0	1

Transpose of FCM-pattern 1 (Table 3.5) is similar to transpose of base case FCM (Table 3.4).

3.3 FORMULATION FOR PMU PLACEMENT

The PMU placement problem is considered as a problem to identify those nodes in the system, where the demand covered is maximum. For a system having *n* nodes, consider the two sets of binary variables x_i and y_i .The $x_i(i=1\cdots n)$ is placement variable and denotes the buses where PMU has to be placed, and $y_i(i=1,2\cdots n)$ is the demand variable depicting whether the demand at node *i* is covered or not. To understand PMU placement under different flow patterns, PMU placement problem is first formulated for a single fixed pattern and later same formulation is extended for various flow patterns.

3.3.1 Formulation for Single Pattern

For a given power system, for a single fixed pattern the PMU placement problem is formulated as given below.

Maximize demand

$$\sum_{i}^{n} d_i y_i \tag{3.1}$$

Subject to following placement and coverage constraints

$$\sum x_i \le NP \qquad i = 1, 2, \cdots n \tag{3.2}$$

$$\sum \overline{C}_{i,j} x_i - y_i \ge 0 \qquad j = 1, 2, \cdots n \tag{3.3}$$

Where

NP = Number of PMUs to be placed,

d_i =Demand at node *i*

$\overline{C}_{i,j}$ = Transpose of FCM. In above formulation x_i=0 where $d_i = 0$

For IEEE-14 bus system equations (3.1), (3.2), and (3.3) are given as

$$\text{Maximize:} \quad \begin{aligned} &0.217 * y_2 + 0.112 * y_3 + 0.918 * y_4 + 0.2894 * y_7 + 0.0696 * y_8 + 0.4488 * y_9 + \\ &0.0855 * y_{10} + 0.035 * y_{11} + 0.600 * y_{12} + 0.133 * y_{13} + 0.14 * y_{14} \end{aligned} \tag{3.4}$$

$$\text{Subjected to:} \quad x_2 + x_3 + x_4 + x_7 + x_8 + x_9 + x_{10} + x_{11} + x_{12} + x_{13} + x_{14} \le 1 \tag{3.5}$$

Equations (3.1) and (3.2) are represented as (3.4) and (3.5) respectively, for IEEE-14 system. However, coverage constraint of (3.3) is presented in matrix form as (3.6)

$$\begin{bmatrix} 1 & 1 & 1 & 1 & 0 & 1 & 1 & 1 & 1 & 1 & 1 & 1 & 1 & 1 \\ 0 & 1 & 0 & 1 & 0 & 0 & 0 & 0 & 0 & 0 & 0 & 0 & 0 & 0 \\ 0 & 0 & 1 & 0 & 0 & 0 & 0 & 0 & 0 & 1 & 1 & 1 & 1 & 0 \\ 0 & 0 & 0 & 1 & 0 & 0 & 0 & 0 & 0 & 0 & 0 & 0 & 0 & 0 \\ 0 & 0 & 0 & 0 & 1 & 0 & 0 & 0 & 0 & 0 & 0 & 0 & 0 & 0 \\ 0 & 0 & 0 & 0 & 0 & 1 & 0 & 0 & 0 & 0 & 0 & 0 & 0 & 0 \\ 0 & 0 & 0 & 0 & 0 & 0 & 1 & 0 & 0 & 0 & 0 & 0 & 0 & 0 \\ 0 & 0 & 1 & 0 & 0 & 0 & 0 & 1 & 0 & 1 & 1 & 1 & 1 & 0 \\ 0 & 0 & 0 & 0 & 0 & 1 & 0 & 0 & 1 & 0 & 0 & 0 & 0 & 0 \\ 0 & 0 & 0 & 0 & 0 & 0 & 0 & 0 & 0 & 1 & 0 & 0 & 0 & 0 \\ 0 & 0 & 0 & 0 & 0 & 0 & 0 & 0 & 0 & 1 & 1 & 0 & 0 & 0 \\ 0 & 0 & 0 & 0 & 0 & 0 & 0 & 0 & 0 & 0 & 0 & 1 & 0 & 0 \\ 0 & 0 & 0 & 0 & 0 & 0 & 0 & 0 & 0 & 0 & 0 & 0 & 1 & 0 \\ 0 & 0 & 0 & 0 & 0 & 0 & 0 & 0 & 0 & 0 & 0 & 0 & 0 & 1 \end{bmatrix} \begin{bmatrix} x_1 \\ x_2 \\ x_3 \\ x_4 \\ x_5 \\ x_6 \\ x_7 \\ x_8 \\ x_9 \\ x_{10} \\ x_{11} \\ x_{12} \\ x_{13} \\ x_{14} \end{bmatrix} - \begin{bmatrix} y_1 \\ y_2 \\ y_3 \\ y_4 \\ y_5 \\ y_6 \\ y_7 \\ y_8 \\ y_9 \\ y_{10} \\ y_{11} \\ y_{12} \\ y_{13} \\ y_{14} \end{bmatrix} \ge 0 \tag{3.6}$$

The demands d_i for the given fixed pattern are taken from Table 3.2, real load column. However, $\overline{C}_{i,j}$ values are taken from Transpose of Table 3.4. Placement variables x_1, x_5 and x_6 are equal to zero because d_1, d_5 and d_6 are zero. Equation (3.4) shows that each demand-coverage variable is weighted by demand at that node. However, equation (3.5) depicts that placement variable is restricted by total number of PMUs (i.e. *NP*). Gradual increment in value of *NP* is made to install PMUs sequentially in the system. For IEEE-14 bus system, consider third row of (3.6), which relates placement variables and demand variable at node 3 as

$$x_3 + x_{10} + x_{11} + x_{12} + x_{13} - y_3 \geq 0 \tag{3.7}$$

According to above equation, demand at node 3 is covered by placing PMU at any bus, from the group 3, 10, 11, 12, and 13. Similarly, all other coverage constraints are explained. For multiple flow patterns, above formulation cannot be implemented directly. Single flow pattern formulation is modified for multiple flow patterns in following manner.

3.3.2 Formulation for Multiple Pattern

For multiple flow patterns, objective function of (3.1) and constraints of (3.2) and (3.3) are modified as

$$\text{Maximize} \quad \sum_{p=1}^{P}\sum_{i=1}^{n} d_{ip} y_{ip} \tag{3.8}$$

Subject to following placement constraint and coverage constraints

$$\sum x_i \leq NP \tag{3.9}$$

$$\sum \overline{C}_{i,j}^{p} x_i - y_{ip} \geq 0 \tag{3.10}$$

Where, $i = j = 1, 2, 3 \cdots n$

NP = Number of PMUs to be placed,

d_{ip} =Demand at node *i* for pattern *p*

$\overline{C}_{i,j}^{p}$ = Transpose of Flow-coverage-matrix (*FCM*) for p^{th} pattern.

P = Total number of patterns obtained and *n* =total number of nodes in the system. In above formulation $x_i = 0$ if $d_{ip} = 0$

In equation (3.8) y_{ip} is a demand variable at node *i* corresponding to pattern *p*. Similarly, d_{ip} is demand at node *i* for pattern *p*. Various flow patterns are obtained by varying the load at

different nodes. The load increment at different nodes results in similar flow pattern. In such case d_{ip} equals to average value of all those demands which gives similar flow pattern. The demand d_{ip}, for similar pattern is determined as described below.

Let increase in the load at nodes $k_1, k_2, \cdots k_m$ gives same pattern, say p^{th} pattern. Define $k = [k_1, k_2, \cdots k_m]$. Let a= length of vector *k* i.e. number of elements in vector *k*. Therefore equivalent demand at node *i* of p^{th} pattern are determined as

$$d_{ip} = \frac{\sum_{l=1}^{a} d_i^{k(l)}}{a} \quad \text{where } i = 1, 2 \cdots n \tag{3.11}$$

For IEEE-14 bus system, 25% load increment at 6 buses i.e. at bus-1, bus-4, bus-5, bus-6, bus-7 and bus-9 gave similar flow pattern i.e. FCM-pattern 1. Therefore, $k = [1,4,5,6,7,9]$ and *a*=6. Further, demand d_{ip} or d_{i1} corresponding to flow pattern-1 are given by following equation

$$d_{i1} = \left(d_i^1 + d_i^4 + d_i^5 + d_i^6 + d_i^7 + d_i^9\right)/6 \tag{3.12}$$

Where d_i^1 is demand at i^{th} node when load/demand at 1st bus is increased by 25%. Similarly d_i^4, d_i^5, d_i^6, d_i^7 and d_i^9 corresponds to 25% increment in demands at 5th , 6th ,7th and 9th node respectively. Likewise, for FCM-pattern 2, 3 and 4, d_{ip} are given by equation (3.13), (3.14), and (3.15).

$$d_{i2} = \left(d_i^3 + d_i^{13}\right)/2 \tag{3.13}$$

$$d_{i3} = \left(d_i^2 + d_i^8 + d_i^{14}\right)/3 \tag{3.14}$$

$$d_{i4} = \left(d_i^{10} + d_i^{11} + d_i^{12}\right)/3 \tag{3.15}$$

Demands at various nodes for four different FCM-patterns based on above equations are computed and are given in Table 3.9.

Equations (3.2) and (3.9) are same, which means that placement variable for single and multiple patterns remain same. However, objective function and coverage constraints based on coverage matrix are modified.

Table 3.9

Demands for various flow patterns

	Demand for Pattern 1	Demand for Pattern 2	Demand for Pattern 3	Demand for Pattern 4
1	0	0	0	0
2	0.4340	0.1447	0.2351	0.2170
3	0.2240	0.0840	0.1120	0.1120
4	1.9390	0.6202	0.9265	0.9189
5	0	0	0	0
6	0	0	0	0
7	0.690	0.1949	0.2913	0.2894
8	0.1456	0.0484	0.0777	0.0694
9	0.9663	0.3087	0.4584	0.4486
10	0.1777	0.0593	0.0885	0.0949
11	0.0700	0.0233	0.0350	0.0379
12	0.1210	0.0403	0.0603	0.0649
13	0.2681	0.1006	0.1337	0.1331
14	0.2911	0.0971	0.1568	0.1421

For IEEE-14 bus system, when all four flow-coverage patterns are considered, the objective function is given as

Maximize:

$$0.4340*y_{21}+0.2240*y_{31}+1.9390*y_{41}+0.690*y_{71}+0.1456*y_{81}+0.9663*y_{91}+0.1777*y_{101}+0.0700*y_{111}+0.1210*y_{121}+0.2681*y_{131}+0.2911*y_{141}+0.1447*y_{22}+0.0840*y_{32}+0.6202*y_{42}+0.1949*y_{72}+0.0484*y_{82}+0.3087*y_{92}+0.0593*y_{102}+0.0233*y_{112}+0.0403*y_{122}+0.1006*y_{132}+0.0971*y_{142}+0.2351*y_{23}+0.1120*y_{33}+0.9265*y_{43}+0.2913*y_{73}+0.0777*y_{83}+0.4584*y_{93}+0.0885*y_{103}+0.0350*y_{113}+0.0603*y_{123}+0.1337*y_{133}+0.1568*y_{143}+0.217*y_{24}+0.112*y_{34}+0.918*y_{44}+0.2894*y_{74}+0.0694*y_{84}+0.4486*y_{94}+0.0949*y_{104}+0.0379*y_{114}+0.649*y_{124}+0.1331*y_{134}+0.1421*y_{144}$$

(3.16)

Flow-coverage constraints are modified according to equation (3.10). For example, coverage constraint of equation (3.7) is modified according to each pattern as

$$x_3 + x_{10} + x_{11} + x_{12} + x_{13} - y_{31} \geq 0 \quad (3.17)$$

$$x_3 + x_{11} + x_{12} + x_{13} - y_{32} \geq 0 \quad (3.18)$$

$$x_3 + x_{10} + x_{11} + x_{12} + x_{13} - y_{33} \geq 0 \quad (3.19)$$

$$x_3 + x_{11} + x_{12} + x_{13} - y_{34} \geq 0 \quad (3.20)$$

Similarly, all other coverage constraints are modified for each flow patterns. For IEEE 14 bus system total number of constraints is 40.The optimization problem formulated above is solved using GAMS Mixed Integer Programming (MIP) solver.

Various steps involved in sequential placement of PMUs are summarized below

1. Input all bus data and line data of the system
2. Run load flow to obtain real power flow of the system at a fixed load conditions
3. Compute all flow fractions for the given pattern and form FFM
4. Select Flow-coverage-criterion and obtain FCM from FFM
5. To obtain various flow patterns, set *N*=total number of bus in the system and set *j*=1
6. Increase load at j^{th} bus by 25% and keep load at other buses constant
7. Repeat steps 2 to 4
8. If *j<N, j=j+1* and go to step 6 otherwise go to step 9
9. Compare all FCMs and find similar patterns
10. Compute Demands for each pattern and set *NP=1*
11. Carry out PMU optimization according to equation 3.8, 3.9, and 3.10
12. Compute all those nodes, which are covered by PMU placement, and calculate the total demand covered by these nodes
13. Check whether whole demand is covered or not, if yes finish otherwise *NP=NP+1* and go to step 11.

3.4 CASE STUDIES

The PMU placement formulation described in the previous sections are implemented on IEEE-14 and New England 39 bus system. For both the systems, PMU placement problem is carried out according to formulation explained in section 3.3 for different flow patterns.

3.4.1 IEEE-14 Bus System

Based on the load flow analysis, real power flows are obtained by increasing load at each node by 25% keeping load at other nodes constant. Based on these real power flows, FFMs are formed. The 75% Coverage criterion is considered to develop the FCMs for various flow patterns. When all 14 FCMs are compared, four different FCM-patterns are observed which are given in Table 3.5, 3.6, 3.7 and 3.8. Based on the flow-coverage matrices the placement problem is formulated as an optimization problem as given in section.3.3.

IEEE-14 bus system have 11 demand nodes i.e. node 2, 3, 4, 6, 7, 8, 10, 11, 12, 13 and 14. Locations for PMU placement is obtained by solving equation (3.8), (3.9), and (3.10). To cover the total demand, PMUs are added gradually in the system. The number of PMU's is varied from 1 to 6. Initially NP in equation (3.9) is selected 1 *i.e.* one PMU's to be placed in the system. Then the value of NP is changed gradually from 1 to 6. For each case, placement buses are identified and maximum percentage of load demand covered by placing the PMU's is obtained.

Table 3.10 gives the different number of PMUs placed and the maximum percentage of the load demand covered by these PMU's. The column 'node covered' represents the demand node covered by the PMU placement. The result shows that as the number of PMU's increases in the system the load demand covered by PMU's also increases.

Table 3.10

Number of nodes and total demand covered in IEEE-14 bus system

Number of PMUs	Placement nodes	Nodes covered	Percentage of demand coverage
1	4	2,4	18%
2	4,9	2,4,9	33%
3	4,9,13	2,3,4,8,9,13	50%
4	4,7,9,13	2,3,4,7,8,9,13	58%
5	4,7,9,12,14	2,3,4,7,8,9,12,13,14	83.3%
6	4,7,9,10,12,14	2,3,4,7,8,9,10,12,13,14,11	100%

Similar analysis is performed on New England system, which is given in next section.

3.4.2 New-England 39 Bus System

The New England (NE) 39 bus system has 11 generator buses and 19 load buses. Details for the system are given in APPENDIX-C. For the system, load-flow calculation is performed. The 25% of load at each bus of the system is increased to get different flow-coverage patterns, three distinct patterns are found. Pattern 1 results when load is increased at 7^{th} and 8^{th} node. Pattern-2 is obtained when load is increased at bus 20. Pattern 3 is dominant pattern, which is found when load at remaining 36 buses are increased. FCMs are developed considering the 75% coverage criterion. Using FCMs PMU placement problem is solved by adding PMUs gradually in the system. Number of PMU's varies from 1 to 15 for New England bus system. Results obtained from this analysis are shown in Table.3.11. It is observed from the results that as the number of PMUs varies from 1 to 15, the total demand covered varies from 5% to 100%. The locations of PMU's are given in Table 3.11.

Table 3.11

Number of nodes and total demand covered in NE-39 bus system

Number of PMUs	Placement Nodes	Nodes covered	Percentage of demand coverage
1	39	39	5.2%
2	20,39	20,39	10.52%
3	20,24,39	20,23,24,39	21%
4	8,20,24,39	8,20,23,24,39	26%
5	8,15,20,24,39	8,15,16,20,23,24,39	36.8%
6	4, 8,15,20,24,39	4,8,15,16,20,23,24,39	42.1%
7	4, 8,15,20,24,28,39	4,8,15,16,20,23,24,28,29,39	52.3%
8	4, 8,15,20,24,27,28, 39	4,8,15,16,20,23,24,26,27, 28,29,39	63%
9	3,4, 8,15,20,24,27, 28,39	3,4,8,15,16,20,23,24, 26,27,28,29,39	68%
10	3,4,8,15,20,21,24,27, 28,39	3,4,8,15,16,20,21,23, 24,26,27,28,29,39	73%
11	3,4,7,8,15,20,21,24, 27,28,39	3,4,7,8,15,16,20,21, 23,24,26,27,28,29,39	78%
12	3,4,7,8,15,20,21,24, 25,27,28,39	3,4,7,8,15,16,20,21,23, 24,25,26,27,28,29,39	84%
13	3,4,7,8,15,18,20,21, 24,25,27,28,39	3,4,7,8,15,16,18,20,21, 23,24,25,26,27,28,29,39	90%
14	3,4,7,8,15,16,18,20, 21,24,25,27,28,39	3,4,7,8,15,16,18,20,21, 23,24,25,26,27,28,29,39	96%
15	3,4,7,8,15,16,18, 20,21,24,25,27,28, 31,39	3,4,7,8,12,15,16,18,20,21,23,24,25,26,27,28,29,31, 39	100%

3.5 CONCLUSION

- Sequential placement of PMU is reported in present chapter, proposed method selects PMU locations based on power-flow patterns and demand. Proposed work also considers demand and flow pattern variations. Further, proposed method is successfully tested on IEEE-14 and NE-39 bus system.
- Possible application of proposed work is in congestion management where both demand and power flow patterns plays significant role. Further, for complete observability, IEEE-14 bus system requires four PMUs, as given in Table 2.1. However, with proposed scheme same system requires six PMUs. Therefore, proposed technique is beneficial when utilities have PMUs in large amount.
- Literature shows that for a fixed budget, PMUs should be added in the system in such a manner that previous PMU locations should be proper subset of the final PMU locations. PMUs placements with this kind of relationship are termed as robust. However, placement results obtained through proposed technique are not robust in nature. Therefore, there is requirement of a robust placement scheme dealing practical power system application.

CHAPTER-4
Ranking of PMU locations based on control strategy for small signal stability and mode identification using PMU measurements

4.1 INTRODUCTION

For secure operation of power system, monitoring and control of Small Signal Stability (SSS) is of immense importance. PMU measurements are widely used for SSS Analysis [15, 13, 44,128, 113, 24, 125, 52, 57, 58, 46]. However, little work is reported to place them according to SSS analysis. This chapter describes ranking of PMU Placement locations in a given network for SSS studies. This chapter proposes PMU placement according to power system application [51, 37, 32, 33, 70]. The PMU placement proposed in chapter-3 did not ensure complete observability and robustness. Because of aforesaid disadvantages of the previous method, in present chapter, a ranking scheme is proposed for PMU locations. The proposed ranking technique helps in monitoring and control of small signal stability after first stage placement. The placement results obtained are robust and make system completely observable.

The proposed ranking scheme is divided into three steps. The optimal PMU number and locations are determined in first step using Integer Linear Programming (ILP), such that each bus is observable at least by two PMUs. In the second step, Eigen value analysis is carried out to compute the inter area modes responsible for small signal instability. For each inter area mode, location of controllers and feedback signals are determined through participation factors and controllability indices. Buses associated with controller locations or feedback input signals are identified as critical buses. All optimal PMU locations obtained through first step are ranked in the third step. Three criteria's namely Generator Bus Observability (GBOI), Tie Line Bus Observability (TLBOI), and Bus Observability Indices (BOI) are utilized in the Analytical Hierarchy Process (AHP) to compute priority based Final Performance Indices (FPI). Based on these FPI's PMUs are ranked. All critical buses identified in step 2 are given the highest priorities in ranking the PMU locations. Further, important tie lines of the system are also determined and given the next higher priority. First five sections of the chapter gives detailed description of these ranking steps.

Another possible application of PMU placement and measurement is to capture inter-area system dynamics, which involve identification of inter area modes through these direct

measurements. Therefore, this chapter in its last sections describes mode identification using Wavelet and PMU measurements.

4.2 FORMULATION FOR PMU PLACEMENT

The problem of optimal PMU location for complete observability is formulated according to section 2.2.2. of Chapter 2. Basic objective function is given by equation (2.1). However, constraint equation of (2.7) is modified as (4.1)

$$Subject\ \ to\ AX \geq 2, \qquad a_{ij} = \begin{cases} 1, if\ \ i = j\ or\ if\ i\ and\ \ j\ are\ connected \\ 0, otherwise \end{cases} \tag{4.1}$$

In (4.1) right hand side of inequality ensures that each bus in the system is observed by two PMUs, such that any loss of the line or a line outage will not affect complete observability of the system [103]. Presence of conventional measurements reduces the number of PMUs required for complete observability [28], therefore zero injection measurements are also incorporated in above formulation as explained in chapter 2. The above ILP problem is solved using the algorithm described in chapter 2, to obtain optimal allocations for PMUs.

4.3 CONTROL AND IDENTIFICATION OF CRITICAL BUSES

In multi-machine power system, small signal oscillations are the result of group of the generators in one area swinging against a group of generators in another area. To prevent system from these oscillations, wide area damping controllers are generally provided [15,13]. In this chapter, a control scheme is presented, which comprises of selection of controller location and selection of controller input signals. However, in chapter 5, designing of these wide-area damping controllers are discussed in details. The following sub-sections give a detailed description of proposed scheme for control, selection of input signals, and controller locations.

4.3.1 Selection of Input Signals

In the control scheme of a wide area network, proper selection of feedback signals is of utmost importance. In this work, generator speed signals are considered as input signals for damping controllers. Therefore, selection of the input signal is the selection of generator speed signal. The input signals selected for wide area controllers should affect the inter area modes that are responsible for small signal oscillations. To determine inter-area modes, Eigen value analysis has been carried out. According to reference [39], to modify a mode of oscillation by the

feedback, the chosen input must excite the mode, and it must be visible in chosen output. The measures of these two properties are controllability and observability [7]-[8]. Consider the state space model of a system as.

$$\dot{x} = Ax + Bu \tag{4.2}$$

$$y = C^T x \tag{4.3}$$

Where x is the state vector, *y* is the output vector, *u* is the control vector, *A* is the state matrix, *B* is the input matrix and *C* is the output matrix. The controllability [7] of i^{th} mode of (4.2) from the j^{th} input is proportional to the cosine of the angle between b_j and q_i. This relationship is called as modal Controllability Index (CI) and is given as

$$CI = \cos\left[\theta\left(q_i, b_j\right)\right] = \frac{\left|q_i^T b_j\right|}{\left\|q_i\right\|\left|b_j\right|} \tag{4.4}$$

Where the symbol | | means that the absolute value of a scalar and || || means the standard 2-norm of a vector. q_i is the left eigen vector of A (state matrix) satisfying equation $A^T q_i = \lambda_i q_i$ and b_j, is the j^{th} column of B (input matrix). The selections of appropriate wide area feedback signals required for the controllers are done through the modal CI given by equation (4. 4). Thus, a higher value of CI for a particular mode indicates that the chosen input signal will be effective in controlling the mode.

4.3.2 Selection of Controller Locations

In wide area network, controllers are needed with machines that have the largest effect over oscillating modes of interest. Reference [24] utilized joint controllability and observability modal indices for selecting the location of wide area controller. Reference [8] relates participation factors of selective modal analysis with modal controllability and observability index. Therefore, participation factors are utilized in the proposed work to determine suitable controller location.

$$\rho_{ki} = p_{ki} q_{ki} \tag{4.5}$$

Where ρ_{ki} the participation factor of the i^{th} mode of the k^{th} state variable, p_{ki} is the k^{th} entry of i^{th} right eigenvector of (4.2) and q_{ki} is the k^{th} entry of i^{th} left eigenvector of (4.2). Machine having highest participation factor for a particular mode is selected as suitable location to place damping controller.

4.3.3 Control Scheme for Small Signal Stability

In proposed control scheme, speed signals of the machines, which are having the highest

controllability index are treated as wide area signals. These remote signals are communicated via PMUs to other areas, if the generator bus is observed by PMUs directly or in directly [42]. The controller is placed with the machine, which has highest participation factor, and the speed feedback is taken from the machine having highest controllability index (CI). Differences between speed signals of generators, which are having highest controllability index and participation factor, for a given mode are calculated. These speed deviations and derivative of speed deviations are given as inputs to wide area fuzzy controllers described in next chapter. Output signals of controllers are fed back to the generator, through the exciter.

Let the given system is sub-divided into *n* distinct areas, say $A_1, A_2, \cdots A_n$. Each area can have any number of machines. Let the total number of machines in the system is *P*. Let *k* modes are responsible for inter area oscillations, which are determined using modal /Eigen value analysis. Let for r^{th} mode $G_{rj}^{A_n}$ denotes the generator, which has the highest participation factor. For same mode, $G_{ri}^{A_m}$ denotes the generator, which has the highest controllability index.

Where $i \in P, P \text{ depicts total no. of generators present in given system } j \in P, j \neq i$,

$A_n \text{ and } A_m \text{ are two different areas}$

In Fig 4.1 for mode *1, 2...k*, $G_{1i}^{A_N}$, $G_{2i}^{A_1}$ and $G_{ki}^{A_2}$ are assumed to be those machines, which are having the highest controllability index. S_{1i}, S_{2i} *and* S_{ki} represents speed signals of these machines respectively. These signals are measured by PMUs and are communicated to wide area controllers through a communication medium. Generators i.e. $\left(G_{1j}^{A_1}, G_{2j}^{A_2} \text{ and } G_{kj}^{A_N}\right)$, which are having highest participation factors for given modes have speed signals $\left(S_{1j}, S_{2j} \text{ and } S_{kj}\right)$. Differences between the speed signals $\left(S_{1j}, S_{2j} \text{ and } S_{kj}\right)$and $\left(S_{1i}, S_{2i} \text{ and } S_{ki}\right)$of other areas are calculated. These speed deviations and derivative of speed deviations are given as inputs to wide area fuzzy controllers. Output signals of controllers $\left(C_1, C_2 \cdots C_k\right)$are fed back to each generator through exciters. Therefore, excitation system along with fuzzy controller is used to control load angles of generators to maintain synchronism. The communication delays for each communicated signal are shown separately in Fig 4.1 as d_1, d_2, and d_k. These delays can take similar values, if the communication medium used is same. These delays are significant, while designing damping controllers, which are discussed in next chapter.

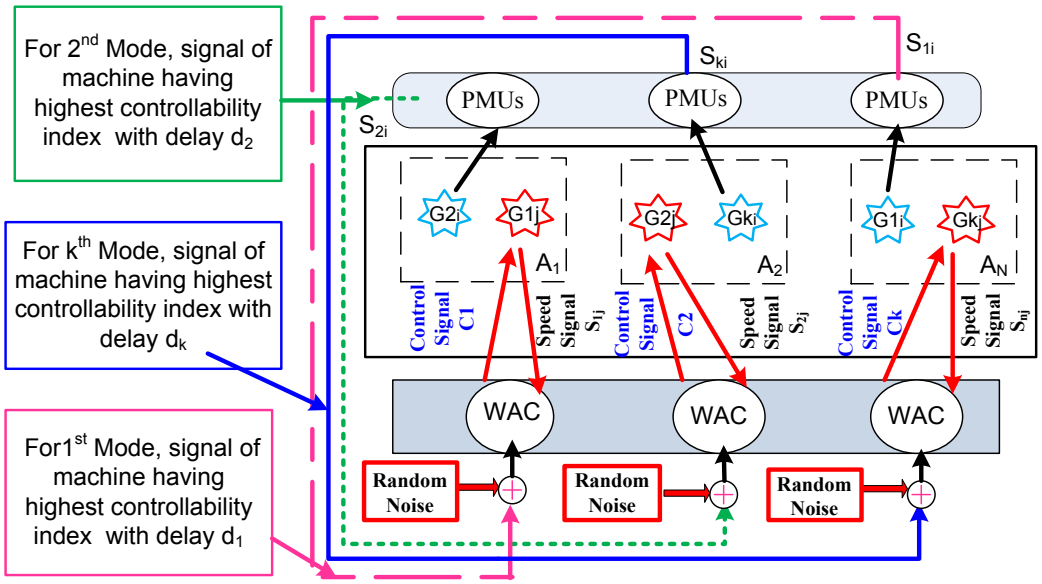

Figure 4.1 Basic Control Scheme for Wide Area Network

From above control scheme, it is observed that, there are certain buses that are critically important, such as generator buses to which controller is attached or generator buses from which feedback signals are taken or tie line buses to monitor inter tie performance. Therefore, all such buses are termed as critical buses of the given network. In such cases, PMUs are placed at these preferred buses in initial stages. Rests of the buses are made observable in later stages.

4.4 RANKING OF OPTIMAL PMU LOCATION

To rank locations, three criteria's namely, Generator Bus, Tie-line, and Bus observability criteria are proposed to monitor and control small signal stability. For small signal stability monitoring, tie line observability criterion is considered and for control, generator-bus observability criterion is considered. However, bus observability criterion depends on topological connectivity of the bus. These criteria are utilized in Analytic Hierarchy Process [116] to rank PMU locations.

Few Important considerations

- It is observed that, every optimal location (obtained in step1), is either a generator or tie line or simple load bus, and may or may not be a significant bus.
- It is also noted that, all generator, tie line, and load buses present in optimal locations are not critical buses. Therefore, to distinguish between critical and non-critical buses, each criterion (i.e. generator, tie line, and bus observability) is further divided into two criteria, one for critical buses, and another for non-critical buses.

- It may happen that a critical bus does not belong to the optimal locations. In such case, nearest optimal bus is considered as critical bus and highest priority is assigned to that bus.

4.4.1 Generator Bus Observability Index

In a power system, the angular separation between generators indicates that whether system will be leading to angular instability or not. Also, to improve inter tie performance wide area damping controllers are generally provided with generators [13], [24]. According to reference [24] generator speeds, terminal bus frequency and active power are the most commonly used control input signals, which can be used in designing damping controllers. Therefore, it is important to monitor the generator buses directly or indirectly using the PMUs. It is to be noted here, there may be few buses that are strategically important and are not present in optimal locations obtained through section 4.2. In such a case, nearest or second nearest optimal location to that critical bus is given priority.

According to the control scheme described in the previous section 4.3, there may be situations, when a generator bus is having controller or providing speed feedback signals. In such situation, these generator buses are of prime importance and termed as critical buses. Therefore, all generator buses present in optimal locations are divided into two groups i.e. critical generator buses and non-critical generator buses. For critical generator bus, the generator observability index is represented as GBOIS and is given as:

$$GBOIS^k = \left(wc_1 * \sum_{\forall gen} U^k_{\ gen} \right) + \left(wc_2 * \sum_{\forall Ngen} U^k_{Ngen} \right) + \left(wc_3 * \sum_{\forall NNgen} U^k_{NNgen} \right) \quad (4.6)$$

Where $GBOIS^k$ is the generator bus observability index for k^{th} bus, which has more significance for SSS analysis. U^k_{gen} represents number of generator buses connected to k^{th} bus. Similarly, U^k_{Ngen} and U^k_{NNgen} represents the number of neighboring and neighbor to neighboring buses connected to bus k. wc_1, wc_2 and wc_3 are constant weights related to GBOIS and assigned higher values.

In case of non-critical generator bus, the generator-bus observability index is indicated as GBOI and is given by following expression:

$$GBOI^k = \left(w_1 * \sum_{\forall gen} U^k_{gen} \right) + \left(w_2 * \sum_{\forall Ngen} U^k_{Ngen} \right) + \left(w_3 * \sum_{\forall NNgen} U^k_{NNgen} \right) \quad (4.7)$$

Where $GBOI^k$ is the generator bus observability index for any k^{th} bus. w_1, w_2 and w_3 are constant weights, which are having lower values as compared to wc_1, wc_2 and wc_3.

4.4.2 Tie Line Bus Observability Index

In large power systems, performances of damping controllers are observed through dynamic changes in inter-ties. Therefore, to monitor tie-line response, PMUs should be placed on the tie lines. To observe tie lines seven different cases are considered. Six cases are directly taken from reference [103]. Details of these six cases are not included in this work. However, first and second case is described here for understanding. For example, P and Q are end buses of a tie line. R and S are the neighboring buses of P and Q respectively. In the first case, both end buses of the tie line (P and Q) belongs to optimal PMU locations, obtained in the first stage. Since PMUs are to be placed on both the end buses. Both buses will have equal importance, therefore tie line bus observability indices will be $TLBOI^P = TLBOI^Q = 1$. Likewise, in the second case, the first end of the tie-line and neighbor of second end are present in PMU locations. To monitor tie line performance at least from one end, $TLBOI^P$ has been given higher priority than $TLBOI^S$ [103].

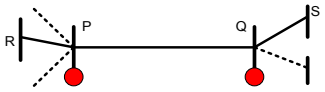

Case a: When both Tie line buses have PMUs

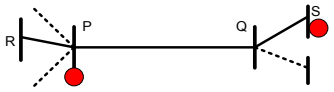

Case b: When one Tie line bus has PMU

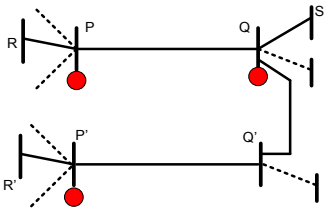

Case c: When two different Tie lines are neighbor

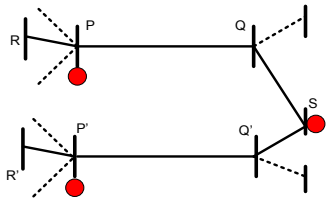

Case d: When two Tie lines are having same neighbor

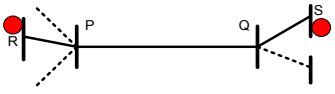

Case e: None of Tie line buses have PMUs

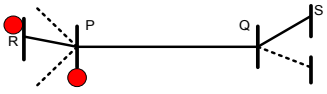

Case f: When one Tie line and adjacent bus have PMUs

Figure 4.2 Various cases to determine TLBOI

In a similar manner, PMU locations are prioritized in seventh case, which is additionally introduced in this work. In this particular case, one end bus of tie line (P) and its adjacent bus (R) at same end both is candidate of optimal PMU sites. As stated before, tie line bus is of great importance. Therefore, tie line bus observability index of tie line bus (P) is $TLBOI^P = 1.5$ and observability index of its adjacent bus (R) is $TLBOI^R = 0.25$.

All cases are summarized in Table 4.1 and Fig 4.2. For a given system, each tie line will satisfy any one condition, from stated seven conditions. TLBOI for k^{th} tie line or its neighboring bus is given by expression (4.8).

$$TLBOI^k = \begin{cases} TL, & if\ kth\ bus\ is\ tie\ line\ or\ its\ neighboring\ bus, \quad TL\ value\ is\ taken\ from\ Table\ 1 \\ 0, & otherwise \end{cases} \tag{4.8}$$

As mentioned before, not all tie lines have significance in SSS analysis. Therefore, tie lines are also divided into critical and non-critical tie lines. According to [39], critical tie lines can be identified based on coherency. Based on coherency property, a system can be divided into coherent group. Tie-lines between two coherent groups are weak connections which are critical. Tie line observability index for critical and non-critical tie line buses are represented as TLBOIS and TLBOI respectively.

Table 4.1

Various cases for Tie Line Bus Observability Index (TLBOI)

Case a	When both Tie line buses (P,Q) have PMUs	$TLBOI^P = TLBOI^Q = 1$
Case b	When one Tie line bus (P) and neighboring bus of other end (S) have PMUs	$TLBOI^P = 1.5$ $TLBOI^S = 0.5$
Case c	When two different Tie lines are neighbor ({P-Q}and {P'-Q'})	$TLBOI^Q = TLBOI^{P'} = 1.5$ $TLBOI^P = 1$
Case d	When two different Tie lines are having same neighbor ({P-Q}and {P'-Q'})	$TLBOI^P = TLBOI^Q = 1.5$ $TLBOI^S = 1$
Case e	None of Tie line buses (P,Q) have PMUs	$TLBOI^R = TLBOI^S = 2$
Case f	When one Tie line bus (P) and adjacent bus of the same end (R) have PMUs	$TLBOI^P = 1.5$ $TLBOI^R = 0.25$
Case g	When Tie line is not present in optimal PMU locations (obtained through step 1).	$TLBOI^P = TLBOI^Q = 0$

Table 4.1 and Fig.4.2 gives tie line observability indices for non-critical tie lines. However, in case of critical tie line, TLBOI of the higher priority end is assigned value greater than or equal to 2. For example, if an important tie line belongs to Case 'b', then its higher priority end, TLBOI (i.e. $TLBOI^P$) is modified as TLBOIS and a value greater than or equal to 2 is assigned to it. Likewise, TLBOI of every significant tie line or its neighbor is modified and renamed as TLBOIS and is represented as:

$$TLBOIS^k = \begin{cases} TLS, & if\ kth\ bus\ is\ significant\ tie\ line\ or\ its\ neighboring\ bus,\quad TLS > TL\ and\ TLS \geq 2 \\ 0, & otherwise \end{cases} \tag{4.9}$$

4.4.3 Bus Observability Index

Bus observability index depends upon the topological connectivity of the bus. Like other two indices, this index is also divided into two indices. Bus observability Index for non-critical bus is represented as BOI. However, for critical bus, the bus observability index is abbreviated as BOIS. BOI for a PMU bus *k* is defined as the number of buses directly connected to k^{th} bus and mathematically expressed as:

$$BOI^k = \sum_{\substack{j=1 \\ j \neq k}}^{N} G_{kj} = \begin{cases} 1, if\ \ j\ and\ \ k\ are\ connected \\ 0, otherwise \end{cases} \tag{4.10}$$

This criterion, prioritize those buses which have maximum connectivity in the given system. Bus Observability indices for critical buses are given as:

$$BOIS^k = 1 * BOI^k,\ \ if\ \ kth\ bus\ itself\ \ is\ significant\ \ \ generator\ \ \ bus \tag{4.11}$$

However, if a significant generator does not belong to optimal placement locations (obtained in stage-1), then its immediate neighbor bus BOI (BOI^{nk}), is modified as BOIS.

$$BOIS^{nk} = 1 * BOI^{nk} \tag{4.12}$$

Where nk is the neighbor bus of the significant generator bus. From above expression, it is clear that, BOI of significant buses are separated from the rest of BOI's though they have same formulation. This is done to distinguish between critical and non-critical buses. This distinction is

useful for analysis, particularly while assigning priority in AHP. After computing, all six criteria's and optimal PMU locations, AHP is applied, which is described in the following sub section.

4.4.4 Analytical Hierarchical Process

AHP is a structured technique for analyzing complex decision problems. In AHP, the problem is broken into various criteria's and alternatives [116]. In PMU placement problem, optimal placement locations obtained through first step are treated as alternatives and various observability indices are criteria. In AHP, first pair wise matrix (*PM*) is constructed, which selects relative importance of different criteria. According to SSS problem, GBOIS is given highest priority, TLBOIS is given second highest and BOIS is assigned third highest priority whereas GBOI, TLBOI, and BOI are given lower priorities, as shown in Fig 4.3.

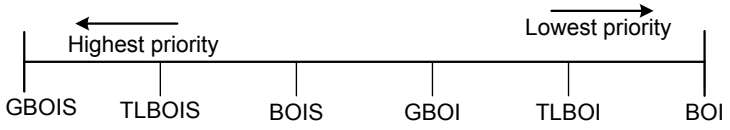

Figure 4.3 Priority Scale

All six criteria are prioritized using 15 priority rules, which are derived from priority scale and are given in Table 4.2. A PM is constructed based on these rules.

Table 4.2

Priority Matrix Rules

GBOIS is 6 times more important than GBOI	GBOI is 3 times more important than BOI
GBOIS is 2 times more important than TLBOIS	TLBOIS is 6 times more important as TLBOI
GBOIS is 4 times more important than BOIS	TLBOIS is 2 times more important than BOIS
GBOIS is 7 times more important than TLBOI	TLBOIS is 7 times more important than BOI
GBOIS is 9 times more important than BOI	BOIS is 5 times more important than TLBOI
TLBOIS is 4 times more important than GBOI	TLBOI is 2 times more important than BOI
GBOI is 2 times more important than TLBOI	BOIS is 5 times more important as BOI
BOIS is 5 times more important than GBOI	

PM is given in Table 4.3. In this table, the second element of first row depicts that GBOIS is six times more important than GBOI (as per 1st priority rule). Likewise, all entries of the Table 4.3 are derived from Table 4.2. PM is then utilized to compute weights for each criterion.

To calculate weights, Eigen values of PM are determined. Eigenvector associated with the largest Eigen value of PM, gives W i.e. the weight vector $W = [w_1, w_2, w_3, w_4, w_5, w_6]$. Weights for all criteria are normalized by utilizing expression (4.13).

Table 4.3

Pair wise Matrix (PM) for the sixteen- bus system

	GBOIS	GBOI	TLBOIS	TLBOI	BOIS	BOI
GBOIS	1	6/1	2/1	7/1	4/1	9/1
GBOI	1/6	1	1/4	2/1	1/5	3/1
TLBOIS	1/2	4/1	1	6/1	2/1	7/1
TLBOI	1/7	1/2	1/6	1	1/5	2/1
BOIS	1/4	5/1	1/2	5/1	1	5/1
BOI	1/9	1/3	1/7	1/2	1/5	1

$$nw_j = \frac{w_j}{\sum^6 w_j} \qquad j = 1,2,3,4,5,6 \tag{4.13}$$

After computing weights for each criterion, all six criteria's (i.e. GBOIS, TLBOIS, BOIS, GBOI, TLBOI, and BOI) are further normalized using (4.14) for each PMU location.

$$NI_{kj} = \frac{\left(I_{kj} - I_{\min,j}\right)}{\left(I_{\max,j} - I_{\min,j}\right)} \qquad j = 1,2,3,4,5,6 \tag{4.14}$$

Where NI_{kj} represent normalized value of j^{th} criterion for k^{th} optimal location. $I_{\min,j}$ and $I_{\max,j}$ is the mini-mum and maximum value of j^{th} criterion respectively. However, I_{kj} is the actual value of j^{th} criterion for k^{th} optimal location. Normalized values of weights and criteria are used to compute the Final Performance Index (FPI) for each optimal PMU location, which is given as

$$FPI_k = \sum_{j=1}^{6} nw_j NI_{kj} \qquad k = 1,2,3 \ldots K \tag{4.15}$$

Where NI_{kj} are normalized value of all six indices, nw_j is the normalized weight for each criterion and FPI_1, $FPI_2 \ldots FPI_k$ corresponds to final performance indices for each PMU location and K represents the total number of optimal locations. These FPIs prioritize the PMU locations. Now for a fixed number of phases, priority placement is done to make all generators, tie line, and load buses observable.

4.5 CASE STUDY

The proposed ranking scheme is applied on five-area sixteen-machine test system, which is shown in Fig 4.4. The system represents New England and New York Interconnection. [39] The test system based on coherency [39] can be divided into 5 groups. Generators 14, 15 and 16 each forms a single generator group. However, group 4 consists of New England system (generator 1-9) and group5 (generators 10-13) consists of New York system. Other details are included in APPENDIX-D

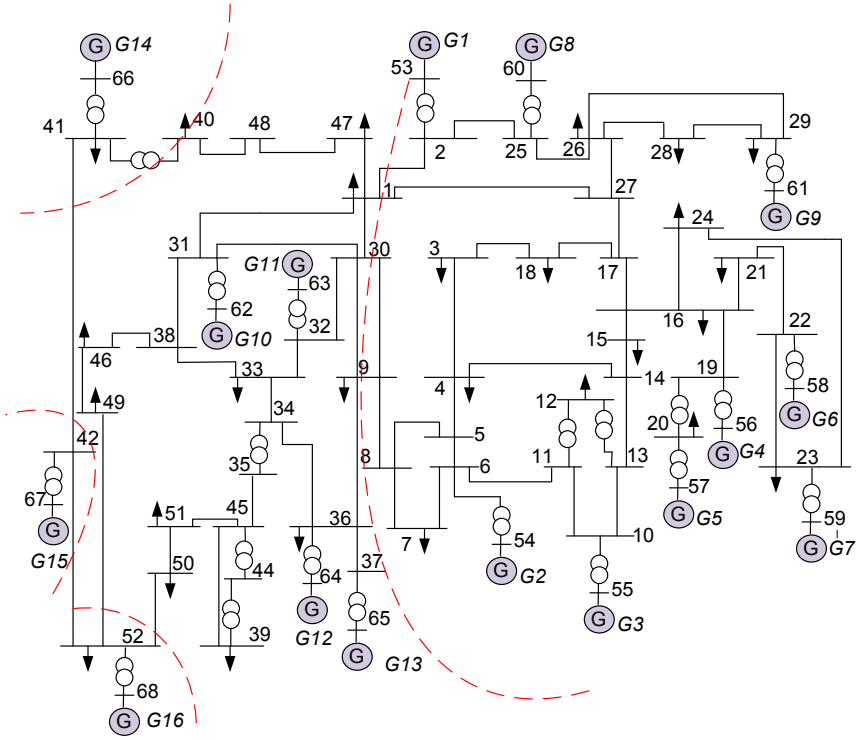

Figure 4.4 Five-area sixteen-bus system

Simulation studies have been carried out utilizing Power System Toolbox (PST) [48] and MATLAB [84].

4.5.1 Optimal PMU Placement

As described in the section 4.2, the optimal placement locations of PMUs are found according to equation (2.1) and (4.1). To achieve the complete observability of the given system, total 42 PMUs are required. The optimal locations for these PMUs are: 6, 8, 11, 12, 14, 16, 17, 19, 20, 22, 23, 25, 26, 29, 31, 32, 34, 36, 37, 41, 42, 44, 45, 46, 47, 48, 49, 51, 52, 56, 57, 58, 59, 60,

61, 62, 63, 64, 65, 66, 67, 68. Placing PMUs on these locations will make the system completely observable at least by two PMUs, even when single transmission line or PMU is lost.

4.5.2 Eigen Value Analysis and Identification of Critical buses

To prevent the system from small signal instability, first inter area modes are determined from Eigen value analysis, which are given in Table 4.4. This table shows that three inter area modes and one unstable mode are present.

Table 4.4

Eigen Value Analysis of Sixteen Machine Systems

Unstable Mode	**Eigen Values**	**Frequency**	**Damping**
1	0.3264±6.8364i	1.0880	-0.0477
Inter area Mode	**Eigen Values**	**Frequency**	**Damping**
1	-0.2251±2.393i	0.3809	0.0936
2	-0.2782±3.280i	0.5221	0.0845
3	-0.1781±4.219i	0.6715	0.0422

To implement the control scheme for above inter area modes, speed participation factors and controllability indices are computed.

Participation factors determine the suitable location for placing the damping controller and controllability index determines the feedback signal selection. Fig. 4.5 (a-d) shows speed participation factors corresponding to unstable and inter-area modes of Table 4.4.

Fig.4.5 (a) corresponds to unstable mode and shows that unstable mode is coupled to 9^{th} generator (G9). Therefore, placing damping controller with generator 9 will make the system more stable. Fig. 4.5 (b) shows that for 1^{st} inter area mode damping controller can be placed with any generator because each generator has a positive speed participation factor. However, the 13th generator (G13) has the highest participation so it is the best candidate for placing damping controller. Similarly, Fig.4.5 (c) and (d) shows that 16^{th} and 13^{th} generators have the highest participation for 2^{nd} and 3^{rd} mode respectively. Therefore, 9^{th}, $13^{th,}$ and 16^{th} generators are three possible locations, which are selected for the wide area-damping controller.

To select the appropriate feedback signal for three proposed damping controllers, controllability indices are computed corresponding to each mode. Results so obtained are shown in Table 4.5.

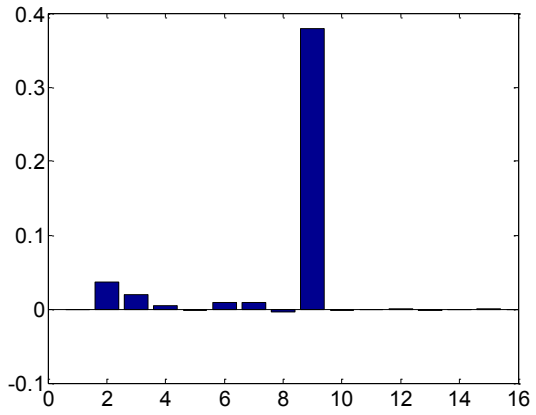

(a) Participation factors for unstable mode

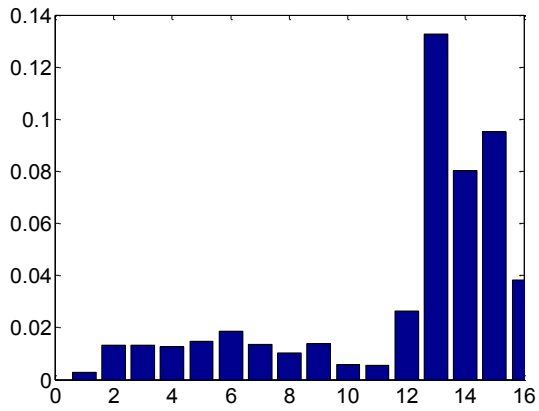

(b) Participation factors for 1st inter area mode

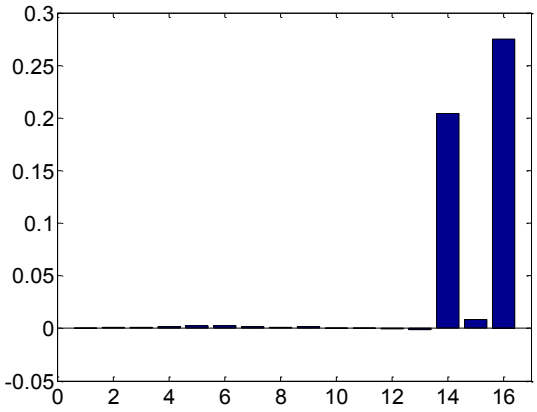

(c) Participation factors for 2nd inter area mode

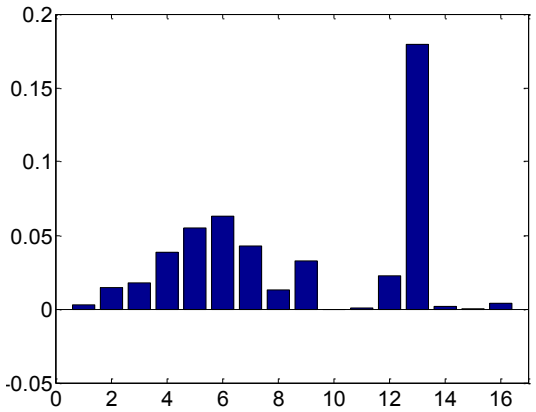

(d) Participation factors for 3rd inter area mode

Figure 4.5 Participation factors for unstable and inter area modes

Table 4.5

Controllability Index Table (e-1)

Generator	1	2	3	4	5	6	7	8	9	10	11	12	13	14	15	16
Unstable Mode	1.9	2.5	2.1	0.4	0.6	0.8	0.7	1.1	0.8	4.1 e-1	1.1 e-1	0.2	1.4 e-2	1.2 e-2	1.2 e-2	2.1 e-2
Inter area Mode1	0.4	0.6	1.2	9.2	0.6	0.3	0.5	0.1	0.4 e-1	2.0 e-1	0.8 e-1	0.1 e-1	1.6 e-3	2.8 e-4	6.3 e-4	2.8 e-4
Inter Area Mode2	1.7	0.4	2.5	0.1	0.1	0.1	0.1	1.6	0.3	4.6	1.2	2.4	3.7 e-1	0.3	0.3 e-2	1.6
Inter area Mode3	4.4	0.3	0.3	0.2	5.0	4.4	0.3	5.8	0.4	0.6	2.3 e-3	0.2	4.5 e-4	1.6 e-3	7.5 e-5	4.1 e-3

For unstable mode, 2nd generator (G2) has the highest controllability index. For 1st and 3rd inter area modes, a single damping controller is placed with generator 13 (G13). The controllability index table shows that generator 4 (G4) signal has highest CI compared to generator 8 (G8). Therefore, generator 4 speed signals should be fed to damping controller placed with 13th generator. Likewise, for 2nd mode, 10th generator (G10) speed signal is selected as feedback signal and damping controller is placed with 16th generator (G16).

From above Eigen value analysis, it is clear that, six generators 2nd, 4th, 9th, 10th, 13th and 16th are of immense importance for small signal stability. Hence, it becomes essential to place PMUs on these generator buses in the initial phases.

4.5.3 Phased PMU Placement

In this work, it is considered that PMUs are placed in the network in four phases. In first three phases, 11 PMUs are placed in each phase, while in fourth phase, 9 PMUs are placed. There are 16 generator buses and 8 tie lines in the given system (as shown in Table 6). From the small signal stability viewpoint, only 6 and 4 tie lines are of importance [39]. Third column of Table 4.6 shows, placement scheme according to various cases of TLBOI.

Table 4.6

Tie line buses in the sixteen- bus system

Tie Line Data		
From Bus	**To Bus**	**Placement scheme**
1	2	No PMUs on tie line end buses
1	27	No PMUs on tie line end buses
1	47	Second end bus of tie line will have PMU
8	9	First end bus of tie line will have PMU
42	41	Both buses of tie line are with PMUs
52	42	Both buses of tie line are with PMUs
46	49	Both buses of tie line are with PMUs
50	51	Second end bus of tie line will have PMU

For each PMU location, values of GBOIS, TLBOIS, BOIS, GBOI, TLBOI, and BOI criteria are computed and normalized according to normalization expressions given in section 4.4.

Pair wise matrix (PM) is formed to compare the relative importance of each criterion. Further, PM is utilized to calculate the weight vector W, which is Eigenvector associated with largest

Eigen values of *PM.* In this paper, W i.e weight vector is [0.7976, 0.1278, 0.4779, 0.0873, 0.3286, 0.0590] and final performance indices (FPI) are computed according to (4.15).

Table 4.7 shows normalized values of each criterion for every PMU location, and FPI are also given in eighth column of Table 4.7. Ninth and tenth column of the same table depicts ranking and prioritized FPI respectively.

Table 4.7

Normalized values of criteria's and final placement indices for sixteen- bus system

OPP vector	TLBOI (Normalized)	GBOI (Normalized)	BOI (Normalized)	TLBOIS (Normalized)	GBOIS (Normalized)	BOIS (Normalized)	FPI	Rank	Priority FPI	Final Priority Placement
6	0	0.375	0	0	0	1	0.205	10	0.468	56
8	0	0	0.60	1	0	0	0.271	7	0.468	61
11	0	0.625	0.60	0	0	0	0.060	25	0.468	62
12	0	0	0.40	0	0	0	0.012	42	0.468	65
14	0	0	0.60	0	0	0	0.018	40	0.468	68
16	0	0.312	1	0	0	0	0.052	33	0.343	51
17	0	0	0.60	0.571	0	0	0.163	12	0.271	8
19	0	0.687	0.60	0	0	0	0.064	20	0.211	26
20	0	0.687	0.40	0	0	0	0.058	32	0.209	25
22	0	0.687	0.60	0	0	0	0.064	21	0.205	6
23	0	0.687	0.60	0	0	0	0.064	22	0.194	31
25	0	0.687	0.60	0.571	0	0	0.209	9	0.163	17
26	0	0.625	0.80	0.571	0	0	0.211	8	0.156	47
29	0	0.375	0.60	0	0	0	0.043	34	0.130	42
31	0	0.375	0.80	0.571	0	0	0.194	11	0.115	52
32	0	0.375	0.60	0	0	0	0.043	35	0.109	41
34	0	0.312	0.60	0	0	0	0.039	37	0.086	36
36	0.333	0.687	0.80	0	0	0	0.086	17	0.073	66
37	0	0.687	0.60	0	0	0	0.064	23	0.073	67
41	1	0.687	0.60	0	0	0	0.109	16	0.064	19
42	1	1	0.60	0	0	0	0.130	14	0.064	22
44	0	0	0.60	0	0	0	0.018	41	0.064	23
45	0.166	0	0.80	0	0	0	0.032	38	0.064	37
46	0.666	0	0.40	0	0	0	0.042	36	0.063	49
47	0	0	0.40	0.571	0	0	0.156	13	0.060	11
48	0.166	0	0.40	0	0	0	0.019	39	0.058	57
49	0.666	0.312	0.40	0	0	0	0.063	24	0.058	58
51	0	0	0	1	0	0.50	0.343	6	0.058	59
52	1	0.687	0.80	0	0	0	0.115	15	0.058	60
56	0	0	0	0	1	0.25	0.468	1	0.058	63
57	0	0.781	0.20	0	0	0	0.058	26	0.058	64
58	0	0.781	0.20	0	0	0	0.058	27	0.058	20
59	0	0.781	0.20	0	0	0	0.058	28	0.052	16
60	0	0.781	0.20	0	0	0	0.058	29	0.043	29
61	0	0	0	0	1	0.25	0.468	2	0.043	32
62	0	0	0	0	1	0.25	0.468	3	0.042	46
63	0	0.781	0.20	0	0	0	0.058	30	0.039	34
64	0	0.781	0.20	0	0	0	0.058	31	0.032	45
65	0	0	0	0	1	0.25	0.468	4	0.019	48
66	0.333	0.781	0.20	0	0	0	0.073	18	0.018	14
67	0.333	0.781	0.20	0	0	0	0.073	19	0.018	44
68	0	0	0	0	1	0.25	0.468	5	0.012	12

Phased PMU placement for sixteen-bus system is given in Table 4.8. For the given 16 machines bus system, tie lines 1-27, 1-2, 8-9, and 50-51 are most important tie lines [39]. Eigen value analysis shows that, generator buses 54, 56, 61, 62, 65, and 68 corresponding to generators G2, G4, G9, G10, G13, and G16 are the critical buses for controlling small signal instability.

Table 4.8

Phased PMU placement for sixteen bus system

No. of PMUS	Phase-1	Phase-2	Phase-3	Phase-4
1.	56	17	37	29
2.	61	47	49	32
3.	62	42	11	46
4.	65	52	57	34
5.	68	41	58	45
6.	51	36	59	48
7.	8	66	60	14
8.	26	67	63	44
9.	25	19	64	12
10.	6	22	20	-
11.	31	23	16	-

A close inspection of phase-1 of Table 4.8 reveals that, in phase-1 itself, all important tie lines and generators are having PMUs, to aid wide area monitoring and control. First, five locations correspond to generators which are important for small signal stability. Bus 51 aids in monitoring tie line between areas 1 and 4. PMU placement at bus 8 will help in monitoring tie line 8-9. Similarly, 25 and 26 PMU locations help in monitoring tie lines connecting buses 1-2 and 1-27 respectively, which are between area 4 and 5. Tenth location of phase-1 will provide measurements from generator-2 from depth first. Last location in phase-1, provides measurements for tie line 46-49. However, by the end of phase-1, all critical tie line buses and critical generator buses are observed, either by placing PMU directly on bus or on the neighboring buses connected to critical buses. After 2^{nd}, 3^{rd}, and 4^{th} stage placement, whole system is made observable. Proposed phased PMU placement approach makes all generators and tie line buses observable, which assists in small signal monitoring in the initial phases.

Based on above, it can be concluded that, instead of placing PMUs on all generator buses [15, 13, 44, 128, 113, 24, 125], it is good to place few PMUs on significant generator buses. From

proposed method, significant PMU locations are easily identified based on control scheme designed for small signal stability.

Presented method is also compared with probabilistic technique of reference [52]. In [52], authors have only taken account of fast and slow dynamic observability of the system utilizing probabilistic approach. Complete topological observability is not considered, in the work. Authors of [52] have identified PMU locations for New England system, which only satisfy dynamic observability criteria. However, proposed ranking and placement approach deals simultaneously with complete-topological observability and small signal dynamics.

In addition to above, both small signal and transient stability analysis requires real-time rotor measurements. Therefore, in proposed work, Generator bus observability index (GBOI) is introduced for small signal analysis. This GBOI is given highest priority, which ensures PMU placement on generator buses. Consequently, proposed technique can be applied for transient stability studies also, without any significant changes.

There may be situation, when a tie line bus and its adjacent bus are suitable candidate for PMU locations. Tie line bus observability index for this situation is not reported in [103]. In present work, TLBOI for this particular case is also introduced. Proposed ranking technique is robust because it satisfies the robustness criteria for different placement budget mentioned in [70]. Since PMUs are added sequentially in the system and phase-1 is always subset of phase- 2, 3, and 4.

Further, in [57] authors have used Monte Carlo based Probabilistic Eigen value analysis for various operating conditions and uncertainties. In terms of performance, the proposed ranking and placement will also work well for different operating scenarios. Ranking methodology presented in this paper, totally depends on control scheme employed. If there is any change in control algorithm, ranking of PMUs will change. In such situation, problem of changing operating conditions can be solved by employing a suitable adaptive control scheme, without affecting ranking. For example, variation in loading conditions, results into multiple operating conditions. At different operating conditions, generator speed signals will be different. According to proposed control scheme, this speed variation will vary speed error and error derivative. This speed error will be reflected as variation in universe of discourse of fuzzy inputs (in case of fuzzy controllers, which are described in next chapter). An adaptive controller like fuzzy controller dealing with this variation will work well for various operating scenarios, as described in reference [24].

Suggested PMU placement technique ensures complete observability with high redundancy. Therefore, once placement is accomplished, any changes in operating conditions will not affect system performance as system is completely observable.

4.6 MODE IDENTIFICATION USING PMU MEASUREMENTS

To explore more benefits of the proposed placement scheme, consider first phase placement locations given in Table 4.8. From the table, it is observed that after first phase, tie lines 8-9, 50-51, 1-27, 1-2, and 46-49 are with PMUs. According to Y. Chompoobutrgool *et.al* PMU measurements contains "actual" system modes. These measurements are able to capture the non-liner dynamics of the system more accurately, which is not possible with conventional Eigen value analysis [129]. In this sub-section, PMU measurements obtained through first stage placement are utilized to identify inter-area modes. It is to be noted here that mode identification method is directly taken from [56]. Continuous wavelet Transform (CWT) is used to analyze inter-area modes and a comparative study is carried out with conventional method to present multi utility of proposed placement scheme and PMU measurements. For analysis, time domain simulated signals are considered as PMU "synthetic measurements" or actual measurements [129]. Present section gives details about the wavelet transform. However, next section describes the case studies.

4.6.1 Continuous Wavelet Analysis

Literature reveals [9,76,50,43,88,49,97,89,105,56,107] that wavelets have multi resolution properties, which are useful for recognizing the features of a signal in both the time and frequency domains. Wavelet means small wave or an oscillatory function of a finite length. In wavelet analysis, given finite signal is multiplied with the wavelet function. Continuous wavelet transform of a continuous signal *f(t)* is mathematically defined as follows:

$$W_h f(a,b) = \frac{1}{\sqrt{a}} \int_{-\infty}^{\infty} f(t) h^*\left(\frac{t-c}{a}\right) dt \tag{4.16}$$

Wavelet transform of *f(t)* is a function of *b* and *a*. Where *b* is time shift parameter or translation parameter and *a* is scale parameter or dilation parameter. *h(t)* is mother wavelet function and $h^*(t)$is its complex conjugate. Mother wavelet is a prototype for generating other wavelets. Thus, CWT is the sum over all time of the signal *f(t)* multiplied by scaled and shifted version of mother wavelet. These shifted versions are known as son wavelets. Wavelet transform decompose a signal *f(t)* into wavelet coefficients using the basis of son wavelets. Consequently it provides valuable information about *f(t)* at different levels of resolution and measures the similarity between *f (t)* and each son wavelet [120]. The difference between these wavelets is

mainly due to the different lengths of filters that define the wavelet and scaling functions.The CWT possesses localization properties in both time and frequency domains, which defines it multi resolution property. Because of this property, CWT automatically filter out the noise from *f (t)*, therefore no additional filters are needed [110]. Complete procedure of CWT is summarized in following steps:

Steps of Continuous Wavelet Transform

Step 1: The Wavelet is placed at the beginning of the signal, and set a=1(the most compressed wavelet)

Step 2: The wavelet function at scale "1" is multiplied by the signal and integrated over all times

Step 3: Shift the wavelet to t=b and get the transform value at t=b and a=1

Step 4: Repeat step 3 for every value of t

Step 5: Scale 'a' is increased by a sufficiently small value and procedure is repeated for all values of a.

4.6.2 Mother Wavelet Function

As mentioned earlier, Mother-Wavelet function is a prototype for generating the other wavelet functions. Different types of mother wavelet functions are available in literature [96], which are selected according to the nature of the signal to be analyzed. Complex Morlet wavelet is well-suited for the analysis of ring down signals [56] [96].

The complex Morlet wavelet is defined as

$$h(t) = \frac{1}{c_M} e^{j2\pi f_c t} e^{-t^2/2} \tag{4.17}$$

Where f_C is the central frequency parameter of the wavelet and c_M is a normalization factor. Normalization factor is commonly assigned the value $\sqrt[4]{\pi}$ of to ensure that the wavelet has unit energy [96]. By substituting (4.17) in (4.16), it can be noticed that c_M constitutes a multiplier to the computed wavelet transform. Therefore, unity value is used in this work for c_M. This is done, to avoid alteration of the wavelet transform modulus and erroneous estimation of modal parameters.

Complex Morlet wavelet can be considered as a linear band pass filter whose bandwidth is proportional to $1/a$ or to the central frequency [56], which is given by its Fourier transform in following equation.

$$\hat{h}(\omega) = \sqrt{2\pi} e^{-(w-2\pi f_c)^2/2} \tag{4.18}$$

Dilated Fourier transform of above equation is represented as

$$\hat{h}(a\omega) = \sqrt{2\pi} e^{-(aw-2\pi f_c)^2/2} \tag{4.19}$$

It is noticed from above expression that $\hat{h}(a\omega)$ has maximum value at $a\omega = 2\pi f_c$. In addition, only the i^{th} oscillatory mode is strongly related to the scale $a = 2\pi f_c/\omega$. Modification in complex Morlet wavelet is done according to [56] by introducing a bandwidth parameter f_b, which controls the shape of the wavelet. Therefore, modified complex Morlet wavelet is given as follows:

$$h(t) = e^{j2\pi f_c t} e^{-t^2/f_b} \tag{4.20}$$

A proper value of f_b gives a narrower spectrum for better resolution in the detection of inter-area modes. Values of f_b are taken greater than 10 for proper resolution in both time and frequency.

4.6.3 Modal Parameters Identification using Wavelets

Small signal oscillations are termed as sum of damped signals. Mathematically they are represented as:

$$f(t) = Me^{-\alpha t}\cos(\omega t + \theta) \tag{4.21}$$

$$f(t) = A(t)\left[\frac{e^{j(\omega t+\theta)} + e^{-j(\omega t+\theta)}}{2}\right] \tag{4.22}$$

$$A(t) = Me^{-\alpha t} \tag{4.23}$$

Where *t* is time interval, α is exponential decay constant, ω is angular frequency, θ is mode's phase shift and M is mode's relative amplitude.

$A(t)$ is expended by Taylor series in the neighbor hood of the reference point *t=b,* as

$$A(t) = A(b) + \sum_{n=1}^{\infty} (t-b)^n \frac{A^{(n)}(b)}{n!} \tag{4.24}$$

The use of (4.23) and (4.24) makes a better approximation of the signal $f(t)$. By using (4.16) and (4.22), the Morlet wavelet-transform of $f(t)$ can be expressed as

$$W_h x(a,b) = \frac{1}{\sqrt{a}} \int_{-\infty}^{\infty} A(t) \left[\frac{e^{j(\omega t+\theta)} + e^{-j(\omega t+\theta)}}{2} \right] h^*\left(\frac{t-b}{a} \right) dt \tag{4.25}$$

Providing the condition that Morlet Mother Wavelet's duration is limited and its average value is zero. Amplitude $A(t)$ is truncated at point where son wavelet has maximum value. For first term it will be around *t=b*. Therefore (4.25) is modified as

$$W_h x(a,b) = \frac{M}{\sqrt{a}} \int_{-\infty}^{\infty} e^{-\alpha b} \left[\frac{e^{j(\omega t+\theta)} + e^{-j(\omega t+\theta)}}{2} \right] h^*\left(\frac{t-b}{a} \right) dt \tag{4.26}$$

By substituting $r = (t-b)/a$, $dt = adr$ and substituting (4.20) into (4.26)

$$W_h x(a,b) = \frac{\sqrt{a} M e^{-\alpha b}}{2} \int_{-\infty}^{\infty} \left[e^{j[\omega(ar+b)t+\theta]} + e^{-j[\omega(ar+b)t+\theta]} \right] e^{-j2\pi f_c r} e^{\frac{-r^2}{f_b}} dr \tag{4.27}$$

According to reference [56], after few substitutions previous equation is represented as

$$W_h x(a,b) = \frac{\sqrt{\pi a f_b} M e^{-\alpha b}}{2} e^{-f_b/4(a\omega - 2\pi f_c)^2 + j(b\omega+\theta)} \tag{4.28}$$

If the i^{th} mode, which belongs to the k^{th} scale makes a important involvement to (4.28), the expression $e^{-f_b/4(a\omega-2\pi f_c)^2}$ has its maximum value at $a_k = 2\pi f_c/\omega$ and (4.28) becomes (4.29)

$$W_h x(a,b) = \frac{\sqrt{\pi a f_b} M e^{-\alpha b}}{2} e^{j(b\omega+\theta)} \tag{4.29}$$

After substituting *t* for *b*, (4.29) is rewritten in the form of phase angle and time varying amplitude as

$$W_h x(a_k,t) = \frac{\sqrt{\pi a_k f_b} M e^{-\alpha t}}{2} e^{j(\omega t+\theta)} \tag{4.30}$$

By applying logarithm on the modulus of $W_h x(a,b)$, equation (4.31) is obtained

$$\ln|W_h x(a_k,t)| = -\alpha t + \ln\left(\frac{\sqrt{\pi a_k} f_b M}{2} \right) \tag{4.31}$$

Equation (4.31) represents a straight line whose slope is termed as real part of i^{th} mode. However,

$$\arg\left[W_h x(a_k,t)\right] = \omega t + \theta \tag{4.32}$$

Equation (4.32) represents a straight line whose slope is termed as imaginary part of the i^{th} mode. These real and imaginary parts of a mode ($\lambda = \alpha + j\omega$) are further computed using (4.31) and (4.32) in following manner

$$\alpha = \frac{m\sum_{i=1}^{m} b_i \ln\left|W_h x(a_k,b_i)\right| - \sum_{i=1}^{m} b_i \sum_{i=1}^{m} \ln\left|W_h x(a_k,b_i)\right|}{m\sum_{i=1}^{m} b_i^2 - \left(\sum_{i=1}^{m} b_i\right)^2} \tag{4.33}$$

$$\omega = \frac{m\sum_{i=1}^{m} b_i \arg\left|W_h x(a_k,b_i)\right| - \sum_{i=1}^{m} b_i \sum_{i=1}^{m} \arg\left|W_h x(a_k,b_i)\right|}{m\sum_{i=1}^{m} b_i^2 - \left(\sum_{i=1}^{m} b_i\right)^2} \tag{4.34}$$

4.6.4 Selection of Wavelet Parameters

Morlet CWT-based method depends upon the proper selection of the values of some parameters. These parameters are bandwidth parameter f_b, center frequency parameter f_c, scale parameter a, and translation parameter *b*. In present thesis, these parameters are directly taken from reference [56].

Typical frequency range for Inter-area modes is from 0.2 to 0.6 Hz. Therefore, centre frequency f_c is taken from this range. Authors of [56] proved that bandwidth parameter f_b should be chosen greater than 9. The centre frequency parameter turns into f_c / a, when the complex Morlet mother wavelet is expanded by a scaling parameter. If the signal has a sampling period of Δt then the scale a related to the modal frequency f_a is defined as:

$$a = \frac{f_c}{f_a \Delta t} \tag{4.35}$$

Therefore, a valid range for oscillatory modes is computed based on above formula.

Frequency of modes can also be, identified by the chart of wavelet coefficient. In wavelet analysis lower scales corresponds to fast varying signal i.e. high frequency components. However, higher scale values are used to identify low frequency components. Wavelet

scalogram of a given signal creates large wavelet coefficients at those values of scales where the oscillation correlates better to the low frequency signal. These large values or peaks represents dominant inter area modes. Scale value corresponding to this peak value of wavelet coefficients $|W_h x(a_k,t)|$ is termed as a_k. At last, for determination of the real and imaginary terms for i^{th} mode, translation parameter *b* is taken in the positive range of small values. The range of *b* includes the linear region of plot $\ln|W_h x(a_k,t)|$ versus time.

4.7 CASE STUDIES

To understand mode-identification by CWT, first CWT is applied on a synthetic signal, as explained in [56]. Later, same analysis is conducted on five-area system.

4.7.1 Case-1 Synthetic Signal Analysis

Two-mode synthetic test signal is considered in the present work. The parameters of this test signal are as follows:

For Mode 1) M_1=1.0, $\theta_1 = 0$, and f_1=0.30 Hz

For Mode 2) M_2=1.0, $\theta_2 = 0$, and f_2=0.70 Hz

Where M is amplitude θ is phase shift and *f* is frequency. The synthetic test signal is shown in Fig 4.6.

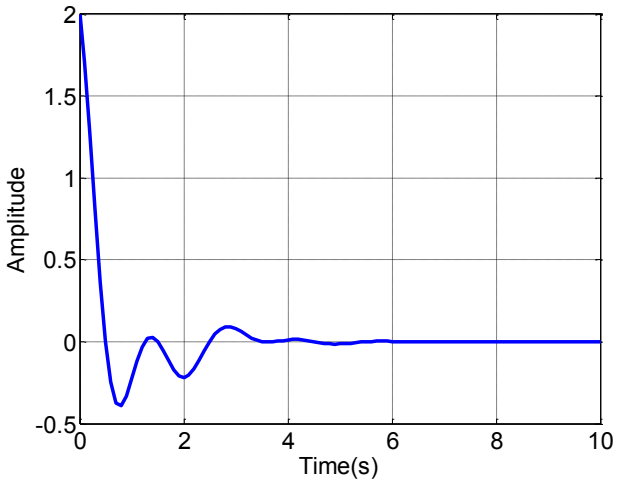

Figure 4.6 Two-mode synthetic test signal

It is to be noted here that wavelet contour plot is generally a three-dimensional plot between wavelet coefficients, scale, and time. However, in this thesis two-dimensional plots between

these three parameters are given. The plot between magnitude of wavelet coefficients and scale parameter for two-mode test signal for scale range 1-30 is shown in Fig 4.7.

It is observed, that there are two peaks in the plot. Every peak of scale parameter is associated with the frequency of a mode. The highest peak is noted on scale factor 7, which is closely related to the mode of frequency 0.7143Hz. The 2nd highest peak is noted on scale factor 16, which is closely related to the 2nd mode of frequency 0.3125Hz. Mode frequencies are computed using equations (4.34). In (4.34) parameter b is taken from linear region of plots given in Fig 4.9 and 4.10. Linear region is 4 to 7s and 3 to 5.6s for first and second mode respectively.

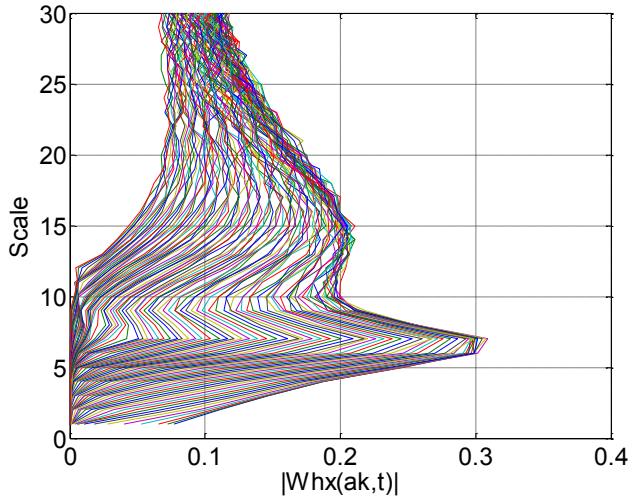

Figure 4.7 Plot between magnitude of wavelet coefficients and scale parameter

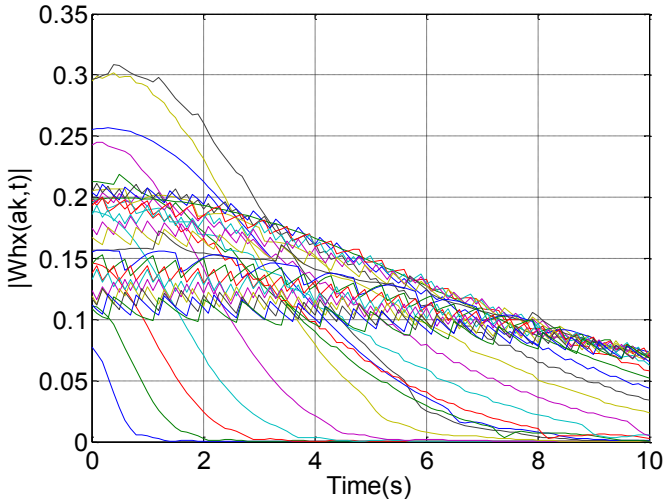

Figure 4.8 Plot between magnitude of wavelet coefficients and Time

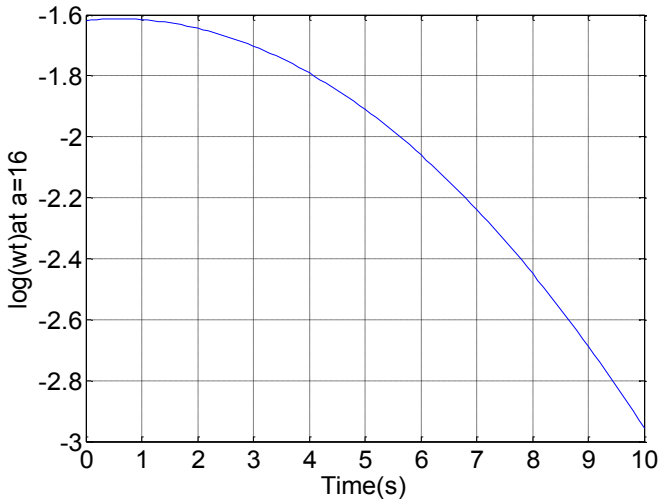

Figure 4.9 Plot between log of magnitude of wavelet coefficient at a=16 and Time

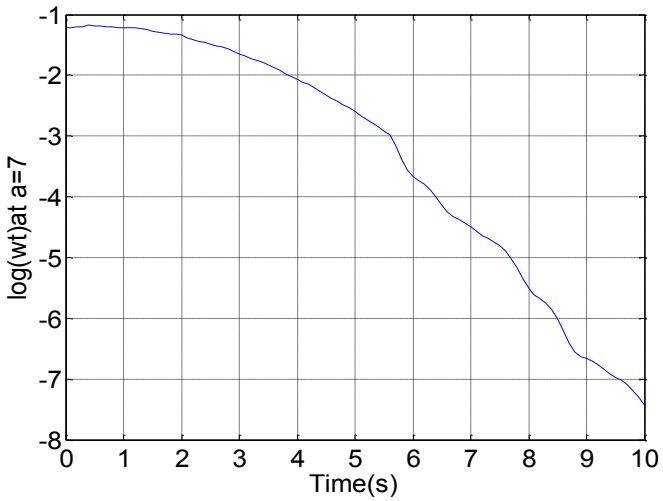

Figure 4.10 Plot between log of magnitude of wavelet coefficient at a=7 and Time

Results obtained from above analysis are approximately equal to the original value of frequency of modes, which signifies that wavelet analysis on direct PMU measurements are able to identify inter area modes.

4.7.2 Case- 2 Analysis of Sixteen-Bus System

Similar analysis is conducted on five-area sixteen bus system. The active power flow on the line 8-9 is taken as data for analysis and is shown in Fig 4.11. This data is obtained from The PMU, which is placed on bus 8 in first stage of Table 4.8. Morlet wavelet analysis is carried out on this

ring up signal. The Plot between magnitude of wavelet coefficients and scale parameter between 1 and 150 is shown in Fig. 4.12.

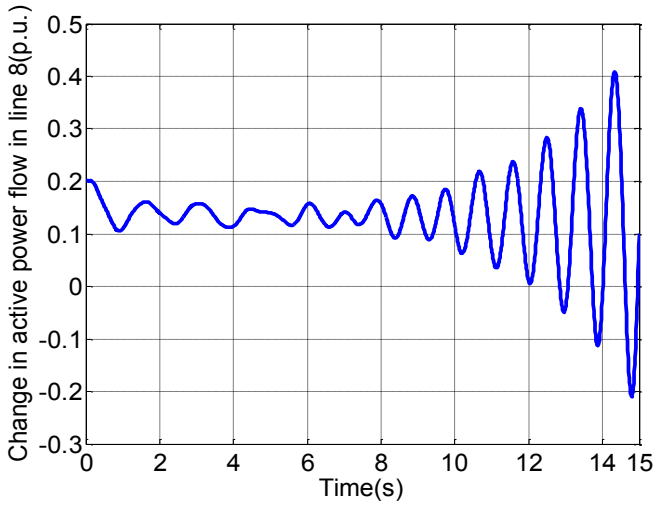

Figure 4.11 Active Power responses to disturbance

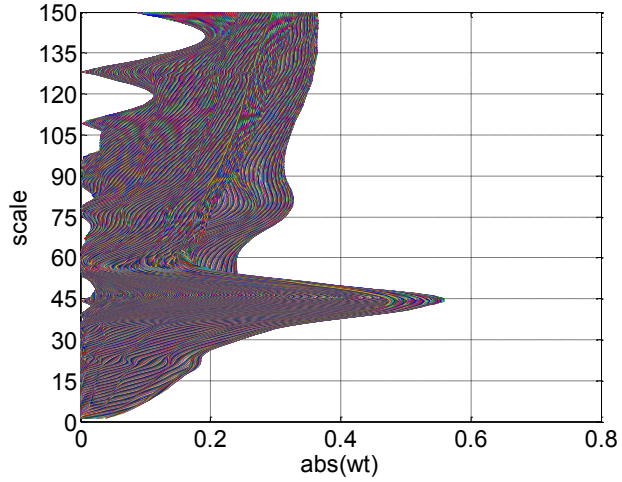

Figure 4.12 Plot between magnitude of wavelet coefficients and scale parameter

The peaks of Fig. 4.12 are taken as the scaling factors, which are associated to each mode separately. The highest peak is noted and it is associated to the unstable mode of frequency 1.1408Hz. The 2nd highest peak is noted which is associated to the 1st inter area mode of frequency 0.3803Hz. The 3rd highest peak is associated to the 2nd inter area mode of frequency 0.5238Hz and the 4th highest peak is associated to the 3rd inter area mode of frequency 0.6755Hz. Results obtained from above analysis are shown in Table 4.9.

This table also compares the wavelet analysis results with Eigen value analysis results, given in Table 4.4 of previous section.

Table 4.9

Comparison between Wavelet and Eigen value Analysis

Unstable Mode	Frequency		Damping	
	Eigen value Analysis	Wavelet Analysis	Eigen value Analysis	Wavelet Analysis
1	1.0880	1.1408	-0.0477	-0.0542
Inter area Mode				
1	0.3809	0.3803	0.0936	0.0954
2	0.5221	0.5238	0.0845	0.0987
3	0.6715	0.6755	0.0422	0.0416

From Table 4.9, it is observed that inter area mode estimation from Morlet CWT are approximately equal to the values obtained from linear Eigen analysis.

4.8 CONCLUSION

- Multi staged PMU placement scheme has been proposed to monitor and control small signal instability in a large network. In the proposed approach, first optimal placement sites are computed, which make the system completely observable, even under loss of one PMU or transmission line. For the given control scheme, critical buses are determined based on modal controllability and participation factors. Generator, Tie line, and Bus observability criteria are developed and optimal locations are ranked according to these criteria. AHP algorithm is utilized and PMU placements are done to make all generators and Tie lines observable.
- From placement results, it is observed that all critical generator and tie line buses are observed in first-stage itself. Therefore, control scheme can be implemented after first-stage placement, which will benefit in wide area small signal stability analysis.
- The proposed scheme is robust for different stage budget and satisfies robustness criterion of [70]. Results show that, the proposed placement scheme provides a maximum advantage in terms of observability and stability of a large system.

- Proposed approach without any significant changes can be applied for transient stability studies, because transient stability studies also require real-time generator rotor-angle information.
- Further, first-stage PMU placement on tie-lines helps in getting accurate identification of the inter area modes. The results obtained from wavelet based mode identification approach are verified with the results of Eigen value analysis. This confirms the potential benefit of proposed placement approach and PMU measurements.

CHAPTER-5
Design of Wide area fuzzy damping controllers using PMU measurements to control small signal instability

5.1 INTRODUCTION

Apart from real-time monitoring, phasor measurements also plays significant role in real-time control of small-signal-rotor angle instability [64]. In past years, it is established that PMU measurements can effectively damp inter-area modes [15, 13, 44, 128, 113, 24, 125, 52, 57, 58, 46, 122, 45, 35, 123]. In previous chapter, a control scheme is proposed to monitor small signal stability by judiciously placing PMUs on generator terminals. In present chapter, considering same control scheme, wide area damping controllers are designed. Designed controllers provide additional damping to control and prevent inter-tie oscillations. As a result, inter tie performance is enhanced and transmission corridors are able to transport more power to nearby areas.

In this chapter, Wide Area Controllers (WACs) based on fuzzy systems are designed. Three different types of damping controllers i.e. Mamdani or Type-1, Adaptive Neuro Fuzzy Inference systems (ANFIS), and Type-2 Fuzzy Inference Systems (Type-2 FIS) are described. First Mamdani or Type-1 controllers are designed for the two test systems. Later, information of Type-1 is utilized to design other two types of controllers. Signal selection and control scheme procedure is same for all three types of controllers. Further, communication delays [123, 11, 119, 124], parameter variations, and various measurement uncertainties [85, 47, 41, 75, 91, 79, 98, 60] associated with PMU measurements are considered in this work while designing these controllers. Details of aforesaid factors are presented in subsequent sections of this chapter.

5.2 DAMPING CONTROLLERS AND COMMUNICATION DELAY

5.2.1 Control Scheme and Controller Signal Selection

To have effective control on small-signal (SS) instability, it is important to select controllers input signals, output signals, and suitable location of the controllers in a wide area network. Control scheme discussed in previous chapter-4 sub-section 3 has been utilized to implement the controllers. In this chapter, controllers are designed for two test systems namely, two-area four-machine system and five-area sixteen-machine system.

For five-area sixteen-machine system, Eigen value analysis, participation factors and controllability indices for selection of controller locations and feedback signals is presented in preceding chapter, sub section 4.5.2. However, for two-area four-machine system similar analysis is performed, and is presented in sub-section 5.5.1.

5.2.2 Communication Delays in Wide Area Network

In a wide area network, phasor measurements are communicated from one area to another area to implement control algorithm. These remote measurements always have time latencies. These time-delays are the time interval taken by phasor measurements from data-acquisition layer to the application layer via data-management layer. In order to have good damping of SS instability, damping controllers should be designed to compensate both time latencies and inter area oscillations simultaneously. These time delays are represented in proposed control scheme (given in section 4.3.3) as d_1, d_2 ... d_k for different areas. In this work, it is assumed that communication medium is same in all cases. Therefore, time latencies are equal and time constant in their nature. Maximum time latency in a wide area network is 1 second [15], [113], depending on distance, protocol, mode of transmission and various other factors. Therefore, 1 s latency is the maximum time delay considered in this work.
Considering aforesaid latency problem, first mamdani /type-1 fuzzy controllers are designed as wide area damping controllers. Details of controllers are included in next section.

5.3 MAMDANI OR TYPE-1 FUZZY DAMPING CONTROLLERS

Due to non-linearity and large size of wide area network system, it is difficult to design conventional controllers for them. Past studies have shown that, Fuzzy Logic Controller (FLC) is most suitable controllers, where conventional controller based on complex mathematics fails to give desired performance or are difficult to design [71]. FLC is generally two-input and a single output component. According to the small signal problem, difference between speeds of two different generators is treated as input feedback error. This error and its derivative are treated as two fuzzy input variables to FLC. However, output is the additional stabilizing signal, which is feed to exciters to control rotor angles as explained before in section 4.3.3. Mamdani or type-1 FLC generally comprises of four components namely Fuzzifier, Knowledge base, Inference-engine and Defuzzifier. The basic functional block diagram of a typical FLC is shown in Fig. 5.1

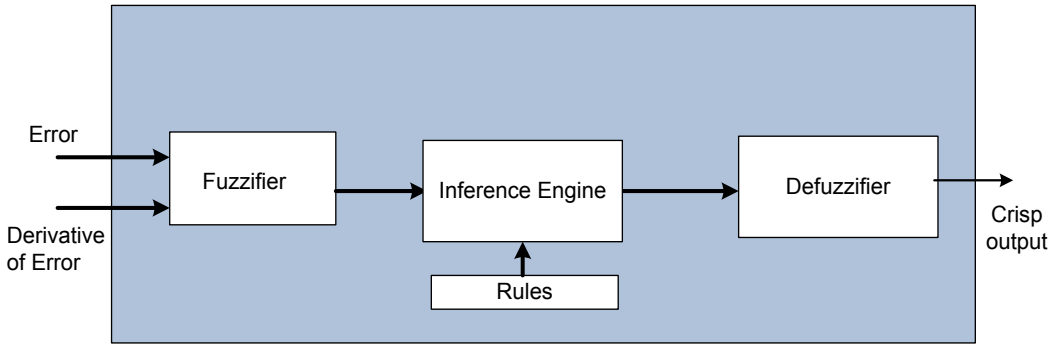

Figure 5.1 Basic structure of Type-1 Fuzzy Logic Controller

As stated before, error and its derivative are fed to Fuzzifier of the FLC. The Fuzzifier transforms these crisp inputs to fuzzy linguistic variables or type-1 fuzzy sets. In this chapter, each input and output signal is expressed into five linguistic variables namely NB, NS, Z, PS, and PB which stands for negative big, negative small, zero, positive small and positive big respectively. Each linguistic variable has a Membership Function (MF) attached with it. In this work, Gaussian membership functions are considered for all fuzzy sets. This is because Gaussian MF provides smooth control surface [71,115].

In fuzzy systems, knowledge of the given systems is expressed as fuzzy rule base. The fuzzy rule base is a collection of "if-then rules", in which antecedents and consequents are linguistic variables. Mathematically, these rules are generally expressed as R^l having structure $R^l : If\ e\ is\ NB \cdots AND\ de\ is\ NB,\quad THEN\ z\ is\ NB$

Where e is speed error, de is derivative of error, and z is output of the controller. The rules describe what action or output should be taken in terms of currently observed information. Therefore, a fuzzy rule associates a condition using input variables and fuzzy variables to an output set or conclusion. These rules are combined in the inference engine, to produce fuzzy output. The inference engine provides conceptual framework of fuzzy logic. Fuzzy inference mechanism, involves fuzzy implication and rule aggregation to derive fuzzy outputs. All fuzzy implication rules are generated from fuzzy conjuction, disjunction, or fuzzy implication by using t-norms and co-norms [115]. Therefore, fuzzy inference system computes the degree to which input data matches the condition of a rule.

Defuzzifier is the last processing unit of type-1 FLC. The defuzzifier converts fuzzy output back to desired crisp or classical output to control the system under study. Literature provides many methods for defuzzification. However, in this work Center of Gravity method is used [115].

5.3.1 Design of Mamdani /Type 1 FLC for two-area four-machine system

In this thesis, mamdani/type-1FLC is derived from Proportional Integral Derivative (PID)

controller. To design type-1 FLC, the universe of discourse or range of input/output variables should be limited. This is done to avoid saturation and instability. Therefore, the universe of discourse of FLC is derived from conventional Proportional Integral Derivative (PID) input and output responses. The PID controller is optimally tuned with Genetic Algorithm, as described in [25]. Gains of PID controllers are transferred to Fuzzy controllers, according to [115]. These derived input/output domains are divided equally into five Gaussian MFs. Each membership set is finally adjusted with hit and trial, to get the best response. In type-1 FLC, Gaussian MF is specified by two parameters, i.e. center and standard deviation, which are denoted as {c, σ}[71].

$$\mu_A(x) = e^{-\frac{1}{2}\left(\frac{x-c}{\sigma}\right)^2} \tag{5.1}$$

Where *c* represents the MFs center and *σ* represents MFs standard deviation. Centers and standard deviations of type-1 MFs for input and output signals of two-area system are shown in the Table 5.1.

Table 5.1

Standard Deviations and Centers of Input and Output Variables for Type-1 FLC (Two-area system)

	Error Input		**Derivative of Error Input**		**Output**	
Fuzzy MFs	Standard deviation (1e-4)	Center of MF (1e-4)	Standard deviation (1e-4)	Center of MF (1e-3)	Standard deviation (1e-3)	Center of MF (1e-3)
NB	1.03	-6.50	9.30	-5.05	2.52	-14.7
NM	1.37	-3.32	9.93	-2.68	2.84	-8.83
Z	1.01	-0.10	1.00	-1.85	2.80	- 1.26
PM	1.31	3.11	9.09	2.26	3.11	5.68
PB	1.01	6.29	9.29	4.84	3.16	14.0

After fuzzy MFs, Fuzzy rules are designed. Fuzzy rules for two-area system are given in Table 5.2.

To understand working of fuzzy rules, consider a rule

$$e \text{ is } NB \cdots AND \text{ } de \text{ is } NB, \quad THEN \text{ } zo \text{ is } NB$$

Where, *e= (speed of generator-remote generator speed)*

Above rule signifies that when feedback speed is more than speed of generators and generators are accelerating, then controller output should follow the remote feedback signal to keep generators in synchronism.

Table 5.2

Fuzzy Rules for Type-1 and Type-2 Fuzzy Controllers (Two-area system)

de / e	NB	NS	Z	PS	PB
NB	NB	-	Z	-	-
NS	-	NS	Z	-	-
Z	-	-	Z	-	-
PS	-	-	Z	PS	-
PB	-	-	Z	-	PB

5.3.2 Design of Mamdani /Type 1 FLC for five-area sixteen-machine system

Like two-area system, in five-area system also, first PID controller is tuned and system is stabilized. Later, PID controller is replaced with fuzzy controller by changing gains.Type-1 fuzzy controllers are designed, for the system utilizing fuzzy rules of Table 5.3. However, standard deviations and centers for Mamdani FLCs are given in Table 5.4.

Table 5.3

Fuzzy Rules for Type-1 and Type-2 Fuzzy Controllers (Five-area system)

de / e	NB	NS	Z	PS	PB
NB	NB	NB	NS	NS	Z
NS	NB	NS	NS	Z	PS
Z	NS	NS	Z	PS	PS
PS	NS	Z	PS	PS	PB
PB	Z	PS	PS	PB	PB

Table 5.4

Standard Deviations and Centers of Input and Output Variables for Type-1 FLC (Five- area system)

	Error Input		**Derivative of Error Input**		**Output**	
Fuzzy MFs	Standard deviation (1e-2)	Center of MF (1e-2)	Standard deviation (1e-2)	Center of MF (1e-2)	Standard deviation (1e-2)	Center of MF (1e-2)
NB	1.359	-6.50	1.381	-6.50	1.708	-6.50
NM	1.782	-3.25	1.694	-3.25	1.703	-3.06
Z	0.949	0.00	0.803	0.00	0.832	0.00
PM	1.607	3.25	1.724	3.25	1.895	2.73
PB	1.383	6.50	1.382	4.84	1.650	6.50

5.3.3 Limitations of Mamdani /Type 1 FLCs

Many researchers have used Mamdani fuzzy controllers to damp inter-area oscillations [24]. However, while designing Mamdani FLC, it is observed that if universe of discourse and MFs are not selected properly, system will become unstable. This problem increases with increase in size of the system. Therefore, in a large system, designing fuzzy rules is a difficult task. Literature shows that Adaptive Neuro Fuzzy Inference System (ANFIS) can successfully model complex problems where the relationship between model variables is unknown [63]. Fuzzy membership functions of ANFIS are determined by input-output training patterns, which makes ANFIS based controller adaptive and fast. Further, compared to other intelligent techniques, ANFIS requires less amount of training data. Therefore, wide area damping controller based on ANFIS is designed here to damp inter-tie oscillations and latency effects. Later, Case studies show comparative analysis between conventional PID, Mamdani, and ANFIS controller.

5.4 ADAPTIVE NEURO FUZZY INFERENCE SYSTEMS

Adaptive neuro fuzzy inference system [63, 62] is a kind of neural network that is based on Takagi–Sugeno fuzzy inference system. Since it integrates both neural networks and fuzzy logic principles, it has potential to capture the benefits of both in a single framework.

5.4.1 Structure of ANFIS

To understand the ANFIS architecture, consider two fuzzy if-then rules based on a first-order Sugeno model:

Rule 1: If (x is $F1$) and (y is $L1$), then ($f1 = p1x + q1y + r1$)

Rule 2: If (x is $F2$) and (y is $L2$), then ($f2 = p2x + q2y + r2$)

Where x and y are the inputs, F_i and L_i ($i=1, 2$) are the fuzzy sets, f_i are the outputs within the fuzzy region specified by the fuzzy rule. p_i, q_i and r_i are the design parameters that are determined during the training process. In the proposed scheme, x and y inputs correspond to speed deviation (ω) and derivative of speed deviation $(d\omega/dt)$ which are fed to ANFIS. Control output of the proposed controller, i.e. f_i is given to generators to provide sufficient damping torque. However, consequent parameters (p, q, and r) are obtained during training of ANFIS.

The structure of ANFIS is shown in Fig. 5.2. In this figure, *A1, A2, B1, B2, C1, C2, M, N,* and *S* are called the nodes. A node is either a fixed node, or an adaptive node. Symbol O_1^1 means output signal of first node of first layer. Where, superscript corresponds to layer number and subscript to the node number. Similarly, other output signals are defined.

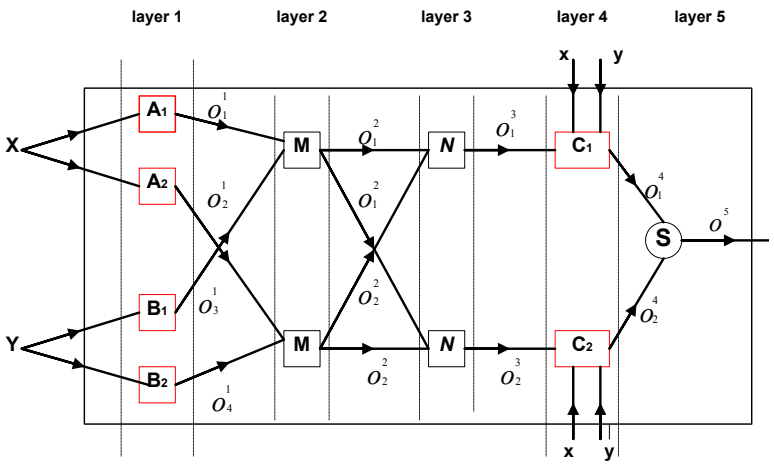

Figure 5.2 Architecture of Adaptive Neuro Fuzzy Inference Systems

First layer of ANFIS, have adaptive nodes. The outputs of layer 1 are the fuzzy membership grade of the inputs, which are given by:

$$O_i^1 = \mu_{Ai}(x) \qquad i = 1, 2 \tag{5.2}$$

$$O_j^1 = \mu_{Bj}(y) \qquad j = 3, 4 \tag{5.3}$$

Where, $\mu_{Ai}(x)$, $\mu_{Bj}(y)$ can adopt any fuzzy membership function. For ANFIS controller, bell-shaped membership function are considered, which are given by $\mu_{Ai}(x)$ and $\mu_{Bj}(y)$:

$$\mu_{Ai}(x) = 1 \Big/ 1 + \left\{ \left(\frac{x - c_i}{a_i} \right) \right\}^{b_i} \tag{5.4}$$

$$\mu_{Bj}(y) = 1 \Big/ 1 + \left\{ \left(\frac{x - c_j}{a_j} \right) \right\}^{b_j} \tag{5.5}$$

Where a_i, a_j, b_i, b_j and c_i, c_j are called as premise parameters, and depend on membership function. Second layer, have fixed nodes *M*, indicating that they are simple multiplier nodes. Outputs of this layer are known as firing strength, which is represented as:

$$O_1^2 = \mu_{Ai}(x)\mu_{Bj}(y) \qquad i = 1 \quad \& \; j = 3 \tag{5.6}$$

$$O_2^2 = \mu_{Ai}(x)\mu_{Bj}(y) \qquad i = 2 \quad \& \; j = 4 \tag{5.7}$$

In third layer also, nodes are fixed and are labeled with *N*. This layer normalizes the output of previous layer. Therefore, outputs of third layer are called normalized firing strengths and represented as:

$$O_k^3 = O_k^2 / \left(O_1^2 + O_2^2\right) \qquad k = 1, 2 \tag{5.8}$$

Fourth layer has adaptive nodes. The output of each node in this layer is simply the product of the normalized firing strength and a first-order polynomial (for a first-order Sugeno model). The outputs of this layer are given by:

$$O_k^4 = O_k^3 f_k = O_k^3 \left(p_k x + q_k y + r_k\right) \qquad k = 1, 2 \tag{5.9}$$

Fifth layer has a single fixed node labeled with *S*. This node performs the summation of all incoming signals. The overall output of the model is given by:

$$O^5 = \sum_{k=1}^{2} O_k^3 f_k = \frac{\sum_{k=1}^{2} O_k^3 f_k}{O_1^2 + O_2^2} \tag{5.10}$$

In ANFIS architecture, first layer has three variables $\{a_i, b_i, c_i, a_j, b_j, c_j\}$, which are related to the input membership functions and called premise parameters. Fourth layer has three variables $\{p_i, q_i, r_i\}$, pertaining to the first-order polynomial, which are known as consequent parameters.

5.4.2 Learning Algorithm of ANFIS

The objective of the learning algorithm for ANFIS architecture is to tune all the variables, namely $\{a_i, b_i, c_i, a_j, b_j, c_j\}$ and $\{p_i, q_i, r_i\}$, to make the ANFIS output match the training data. When the premise parameters a_i, a_j, b_i, b_j and c_i, c_j of the membership function are fixed, the output of the ANFIS model can be written as:

$$f = \frac{O_1^2}{O_1^2 + O_2^2} f_1 + \frac{O_2^2}{O_1^2 + O_2^2} f_2 \tag{5.11}$$

Substituting Eq. (5.8) into Eq. (5.11) yields:

$$f = O_1^3 f_1 + O_2^3 f_2 \tag{5.12}$$

Substituting the fuzzy if-then rules into Eq. (5.12), it becomes:

$$f = O_1^3 \left(p_1 x + q_1 y + r_1\right) + O_2^3 \left(p_2 x + q_2 y + r_2\right) \tag{5.13}$$

After rearrangement, the output is expressed as:

$$f = \left(O_1^3 x\right) p_1 + \left(O_1^3 y\right) q_1 + \left(O_1^3\right) r_1 + \left(O_2^3 x\right) p_2 + \left(O_2^3 y\right) q_2 + \left(O_2^3\right) r_2 \tag{5.14}$$

This is a linear combination of the consequent parameters p_1, q_1, r_1, p_2, q_2 and r_2. The optimal values of these parameters are obtained by using any optimal approach. According to [63], when the premise parameters are not fixed, the search space becomes large. Because of large

search space, convergence of the training becomes slow. To solve this problem, a hybrid algorithm combining the least square's method and the gradient descent [62] is used, which is explained in Appendix-F.

5.4.3 Design of ANFIS Controller

ANFIS controller requires input/output data for training. In present work, this training data is generated from input and output responses of the type-1 FLC. Therefore, first, wide area fuzzy controller based on mamdani inference is designed according to section 5.3.1. Later, Sugeno-ANFIS is designed using subtractive clustering, based on the training data obtained by type-1. It is to be noted that performance of ANFIS controller depends upon the nature of training data. In this work, training data is obtained at various operating conditions by taking input/output response of type-1 controller at different conditions, which are simulated by varying loading of the buses by 5 percent. For both systems, i.e. two-area and five-area systems ANFIS controllers are designed in similar manner. A comparative analysis is carried out in next section to check performance of type-1 and ANFIS controllers for both systems.

5.5 CASE STUDIES

Two cases are considered in present section, to check performance of controllers. In Case-1, time latencies in PMU measurements are taken in account. However, Case-2 considers parameter variations along with time latencies. In parameter variations, few machine parameters like inertia, leakage reactance, *d* axis, and *q* axis transient reactances are varied by 5 percent. In simulation results, mamdani fuzzy controller is represented as Wide area fuzzy controller 1 (WAFC1) and ANFIS based controller is termed as Wide area fuzzy controller 2 (WAFC2).

5.5.1 Two-area four-machine test system

The Two-area four-machine system is shown in the Fig 5.3 [34]. The system consists of two fully

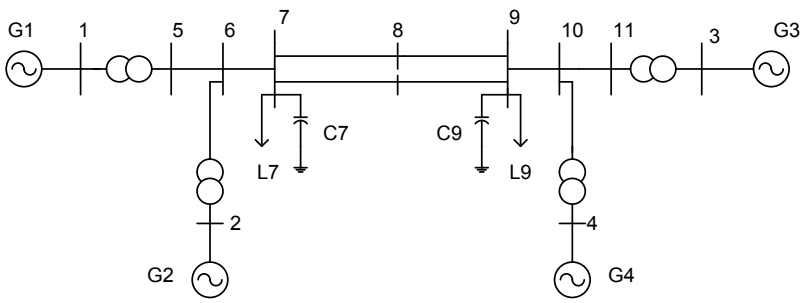

Figure 5.3 Two-area Four-Machine System

symmetrical areas linked together by two 230 kV tie lines of 220 km length. Each area is equipped with two identical round rotor generators rated 20 kV/ 900 MVA.

Line, bus and dynamic information of the system is given in Appendix-B. This system is naturally unstable without PSS, even for small disturbances as shown in Fig 5.4.

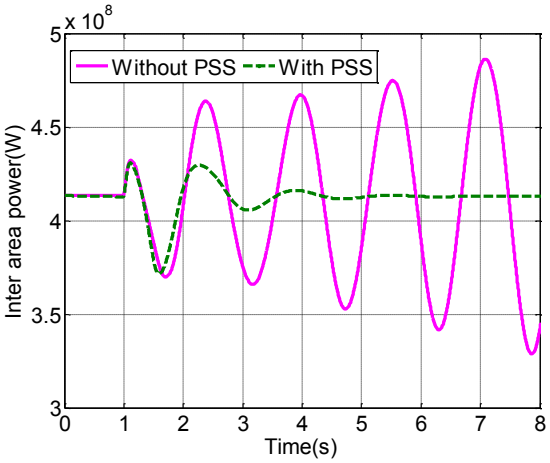

Figure 5.4 Tie line Power Dynamic Response with and without PSS

Eigen value analysis is carried out on the given system and inter area mode is determined. Parameters of inter area mode are given in Table 5.5.

Table 5.5

Eigen value analysis of Two-area four-machine System

Inter area Mode	Eigen Values	Frequency	damping
1	-0.7735±4.2214i	.6719	0.180

From Table 5.5 it is clear that only one critical inter area mode is present. To design damping controller for this single critical inter area mode, controllability index is computed corresponding to inter area mode for all four generators according to equation (4.4) of section 4.3. These controllability indices are shown in Table 5.6.

Table 5.6
Controllability Index Table

Inter area Mode	1	2	3	4
1	0.5168	0.5045	0.4573	0.5005

From Table 5.6, it is observed that machine 1 has highest controllability index. Therefore, speed signal of machine 1 is chosen as feedback signal. To select the appropriate location of controller, speed participation factors are evaluated for the given system and are depicted in Table 5.7.

Table 5.7

Participation Factors for Inter Area Mode

Generators	1	2	3	4
Inter area Mode	0.0946	0.0628	0.1585	0.1347

From Table 5.7, it is clear that damping controller can be placed with any generator since all generators have positive real participation factors. However, generator 3 has the highest participation in inter area mode. Therefore, generator 3 is the most suitable candidate to place the fuzzy controller. Similar to five-area system, generator 1 and 3 are important for implementing proposed control scheme in two-area system.

To simulate the system for small signal stability a disturbance of 5% increase in reference voltage of generator 1 has been considered between time t =1.0s to t=1.2s. To check the performance of the proposed controllers dynamic changes in the tie-line power transferred from area 1 to area 2 is considered. Tie line power transfer from area 1 to area 2 is shown in Fig. 5.4, this figure shows that system is inherently unstable without PSS's. System response improves when all generators are equipped with PSS. Though involvement of PSS's improves system response, however it does not gives satisfactorily results for inter-area oscillations.

Improvements in inter-area oscillations are obtained by employing Wide Area Controllers (WACs) i.e. Proportional Integral Derivative (PID), Wide Area Fuzzy Controller-1(WAFC1), and Wide area Fuzzy Controller-2(WAFC2), which are able to provide sufficient damping to the system and are shown in Fig 5.5.

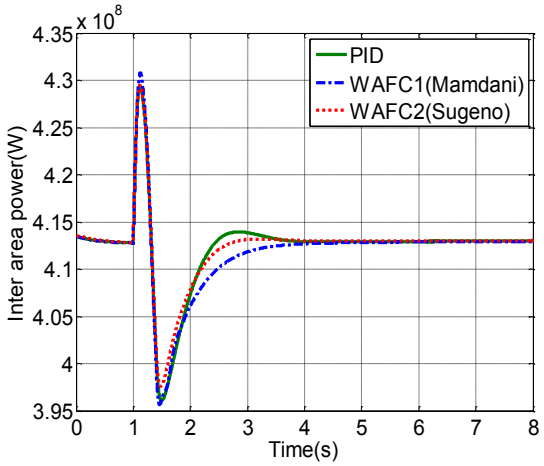

Figure 5.5.Tie Line Power Dynamic Response (Latency effect neglected)

Results so obtained, shows that WAFC1 and WAFC2 out performs PID. However, in this case WAFC1, which is based on Mamdani fuzzy inference systems, performs best among all the controllers.

Case-1 (With Time Latency only)

To simulate the latency effect of communication network equal time delay from area 1 to area 2 is considered. A delay of 0.5s is considered in the communication network. Dynamic response of the tie line power with delay is shown in Fig 5.6, which shows that inclusion of delay deteriorates the system performance. Wide Area Controller based on conventional PID configuration almost fails to maintain stability. However, WAFC1 and WAFC2 perform satisfactorily for given time delay.

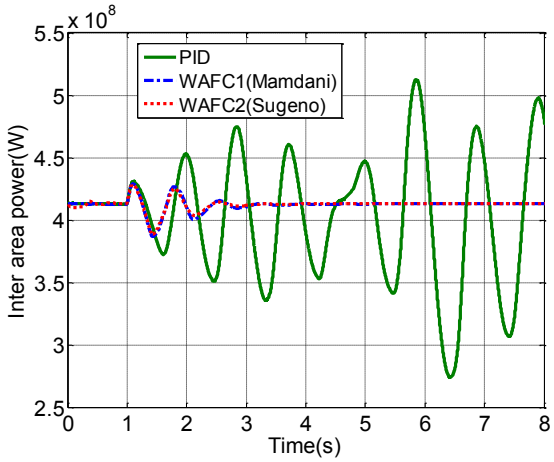

Figure 5.6 Tie Line Power Dynamic Response with 0.5s Delay

Further, from Fig 5.6, it is concluded that the performance of WAFC1 and WAFC2 is almost same for delay of 0.5 s. In further analysis, magnitude of these time delays is increased to 1 s, for all wide area signals. Result so obtained for 1 s time delay is shown in Fig 5.7.

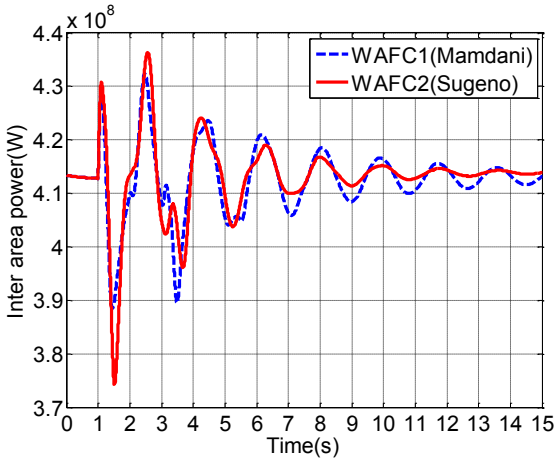

Figure 5.7 Tie Line Power Dynamic Response with 1s Delay

Further, PSS response with time delay is not included because PSS are for local control. Time delays in local signals are generally not encountered. PSS response becomes unbounded with delays, as shown in Fig 5.8 for two-area system.

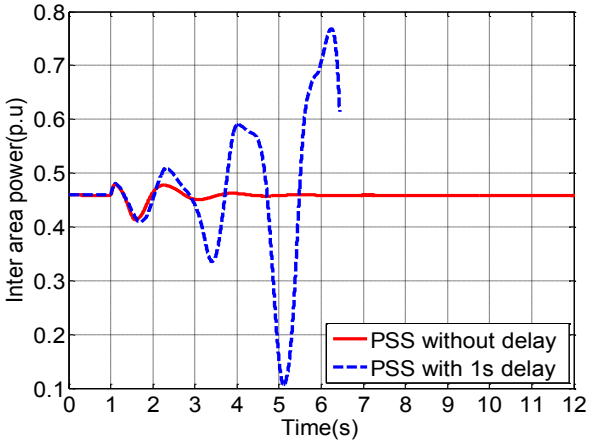

Figure 5.8 Tie Line Power Responses of PSS with and without 1 s Delay in Two- Area System

The performance parameters of the proposed FLC's i.e. overshoot, settling time, and damping are compared in Table 5.8

Table 5.8

Response Characteristics of Controllers with Delay (Two-area system)

Delay (Magnitude)	Type of Controller	Overshoot (percentage)	Settling Time(s)	Damping
500ms delay	WAFC1 (Mamdani)	4.298	4.98	0.493
	WAFC2 (Sugeno)	4.297	4.59	0.494
1s delay	WAFC1 (Mamdani)	4.324	9.35	0.462
	WAFC2 (Sugeno)	4.365	9.20	0.423

It is observed from the Table 5.8, that percentage overshoot is always high for WAFC2 and are within prescribed 10% bound. Settling time of the system increases with increase in time delay magnitude. However for 500ms and 1s time latency, WAFC2 settling time is less as compared to WAFC1. However, response is more oscillatory for WAFC1 as shown in Fig 5.7. The above results show that WAFC2 performs better as compared to WAFC1, for larger time delays.

Case-2 (With Time Latency and Parameter variation)

To check robustness of the proposed controllers, parameters of machines 2 and 4 are varied by 5 percent. Responses of the controllers are shown in Fig 5.9 and performance parameters are given in Table 5.9.

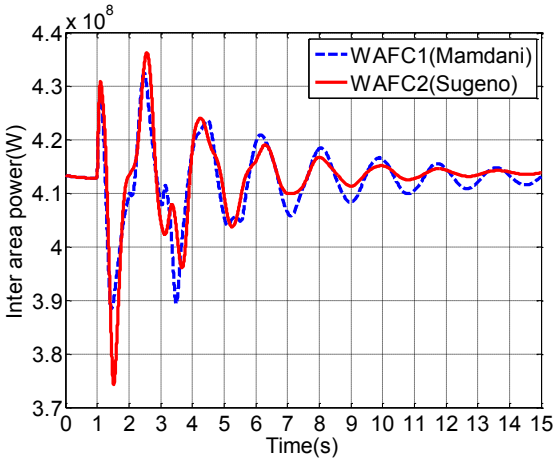

Figure 5.9 Tie Line Powers Dynamic Response with 1s Delay and Parameter Variation

Table 5.9

Response Characteristics of Controllers with delay and parameter variation (Two-area system)

Delay (Magnitude)	Type of Controller	Overshoot (percentage)	Settling Time(s)	Damping
1s delay	WAFC1 (Mamdani)	4.326	13.01	0.460
	WAFC2 (Sugeno)	4.367	10.3	0.423

From Fig 5.9 and Table 5.9, it can be concluded that, WAFC2 is more robust compared to WAFC1 as the settling time for Sugeno type controller is 10.3, which less as compared to Mamdani type controller's 13.01s.

5.5.2 Five-area sixteen-machine test system

WAFC1 and WAFC2 controllers are also designed for five-area sixteen-machine system. For this system controller locations and feedback signal locations are already selected in chapter 4 subsection 5.2. To simulate the system for small signal stability a disturbance of 5% increase in magnitude of reference voltage of generator-1 is considered between t=2.0s to 2.5s. The system is initially unstable even for small disturbances as shown by Fig 5.10.

This figure, presents speed response of 9^{th} generator to the disturbance. Responses of other machines are also similar to machine 9. According to participation factor analysis (section 4.3), 9^{th}, $13^{th,}$ and 16^{th} generators are suitable location for wide area controller placement. A comparative analysis has been done by placing PID, WAFC1, and WAFC2 on these locations without considering any time delay.

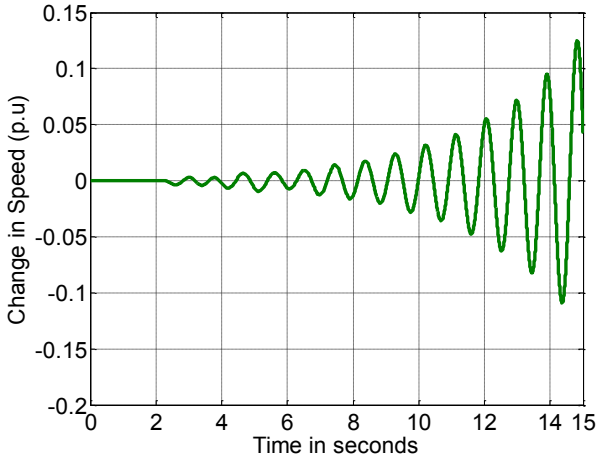

Figure 5.10 Speed Response obtained without control

Fig 5.11 shows performance of PID and fuzzy controllers on four major tie lines of 16-machine system.

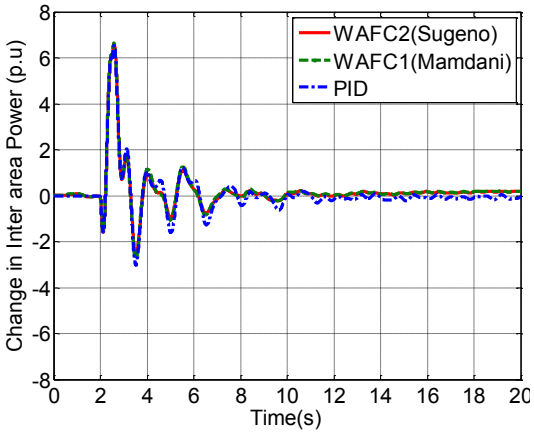

(a) Tie line between buses 1-2 (area4,5)

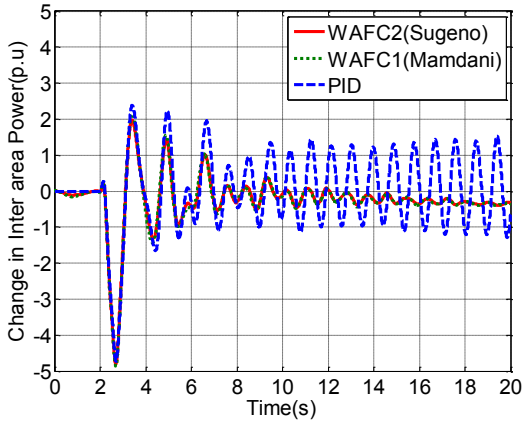

(b) Tie line between buses 8-9 (area4,5)

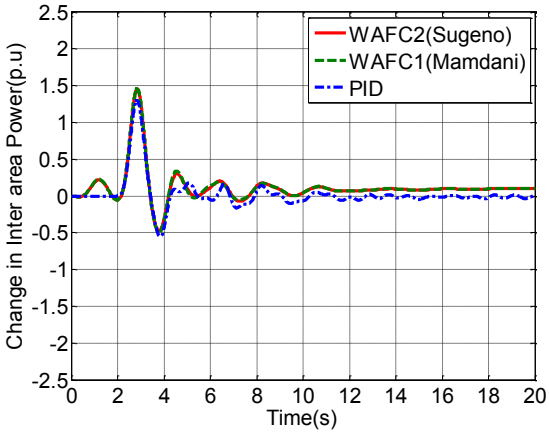

(c) Tie line between buses 42-41 (area1,2)

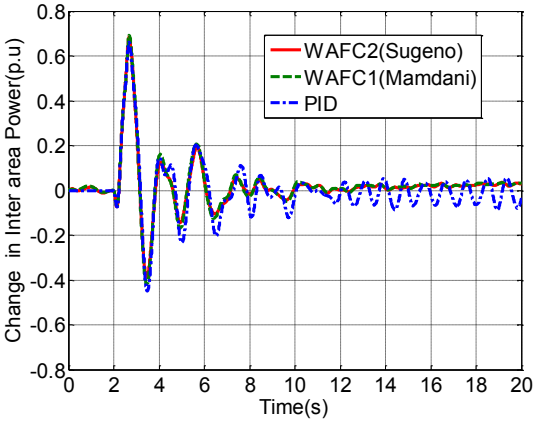

(d) Tie line between buses 1-27 (area4,5)

Figure 5.11.Change in Tie-Line Power Without delay

From above response, it can be concluded that fuzzy controllers are better than PID. However, responses of WAFC1 and WAFC2 are almost same without delay. This might be because training data of WAFC2 is obtained from WAFC1 itself.

Case-1 (With Time Latency only)

To simulate the latency effect of communication network equal time delay of 500ms are considered in all wide area measurement signals. Responses of four tie lines with PID, WAFC1, and WAFC2 are shown in Fig 5.12(a) to (d).

From Fig 5.12, it is observed that, delay deteriorates the system performance. Conventional PID controller almost fails to maintain stability of the system, as response become oscillatory as apparent from 5.12 (a), (b),(c) and (d). However, fuzzy controllers perform well.

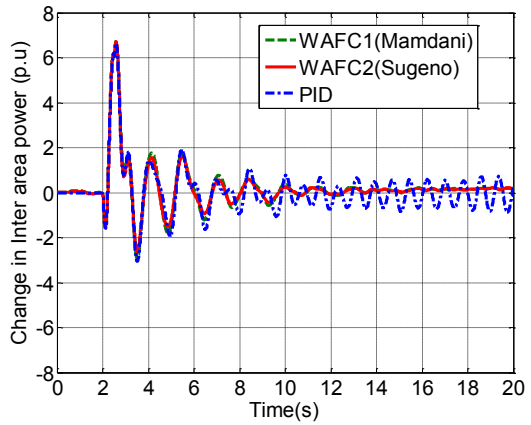

(a) Tie line between buses 1-2 (area4,5)

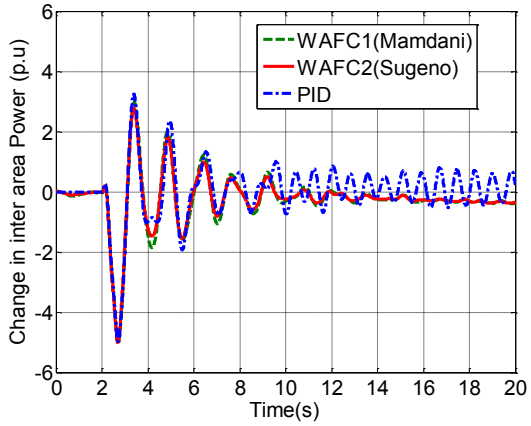

(b) Tie line between buses 8-9 (area4,5)

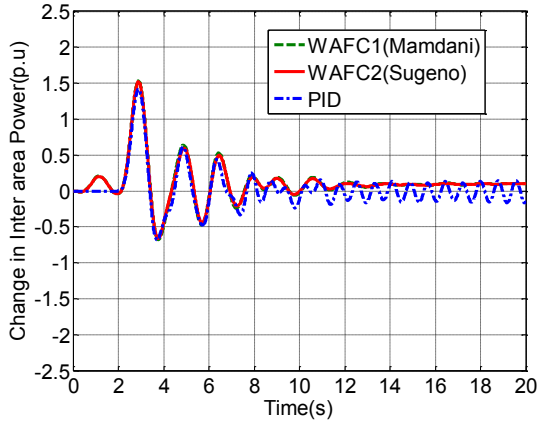

(c) Tie line between buses 42-41 (area1,2)

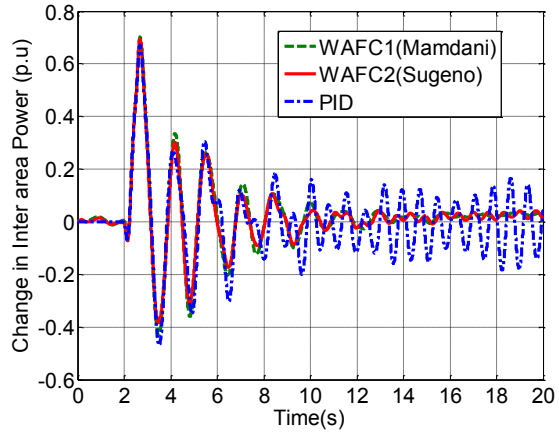

(d) Tie line between buses 1-27 (area4,5)

Figure 5.12.Change in Tie line Power with 0.5 s Delay

To compare performance of WAFC1 and WAFC2 controllers, magnitude of time latency is increased from 500ms to 1 s. Simulation results so obtained are shown in Fig 5.13(a) to (d) respectively for WAFC1 and WAFC2.

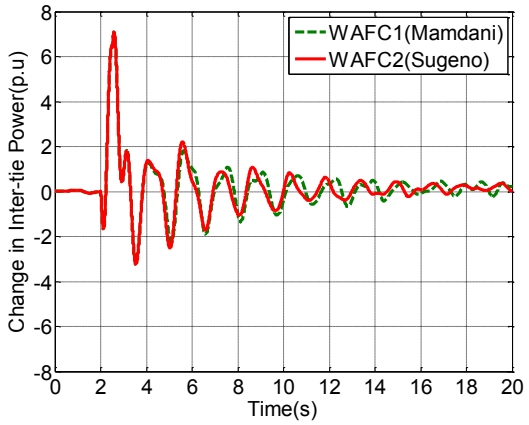

(a) Tie line between buses 1-2 (area4,5)

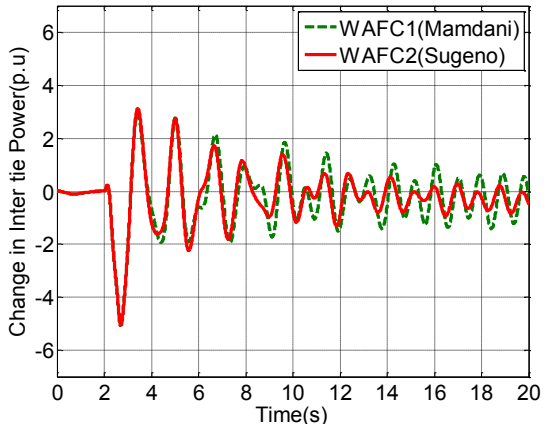

(b) Tie line between buses 8-9 (area4,5)

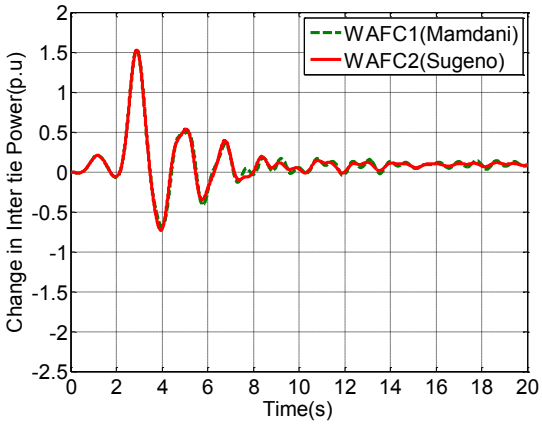

(c) Tie line between buses 42-41 (area1,2)

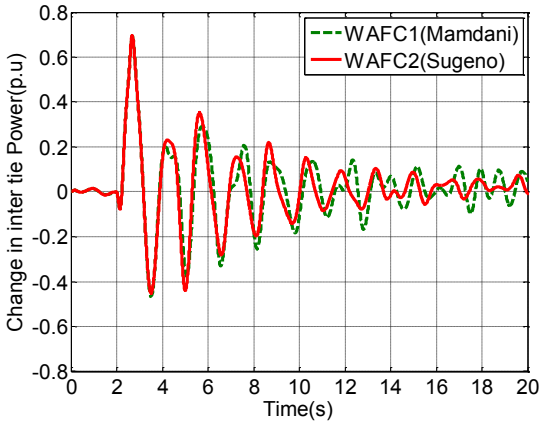

(d) Tie line between buses 1-27 (area4,5)

Figure 5.13.Change in Tie Line Power with 1 sec Delay

A close inspection of Fig 5.13 shows that the performance of WAFC2 is better than WAFC1 with increase in time delays. Performances of two controllers are compared in terms of peak overshoot, settling time and damping which is given in Table 5.10.

From above table, it can be concluded that, as the time delay increases, controllers based on ANFIS performs better as magnitude of percentage overshoot and settling time are less for WAFC2. In addition, improvement in damping is also obtained.

Table 5.10

Response Characteristics of Controllers with Delay (Five-area System)

Delay (Magnitude)	Type of Controller	Overshoot (percentage)	Settling Time(s)	Damping
500ms delay	WAFC1 (Mamdani)	6.710	11.15	0.512
	WAFC2 (Sugeno)	6.715	11.075	0.514
1s delay	WAFC1 (Mamdani)	6.735	13.83	0.522
	WAFC2 (Sugeno)	6.717	13.01	0.526

Case-2 (With Time Latency and Parameter variation)

Robustness of the proposed controllers is also checked for parameter variation. The parameters of machines 3, 6, 9, 10, 14 and 16 are varied by 5 percent. Responses of the controllers are shown in Fig.5.14, and performance characteristics are given in Table 5.11.

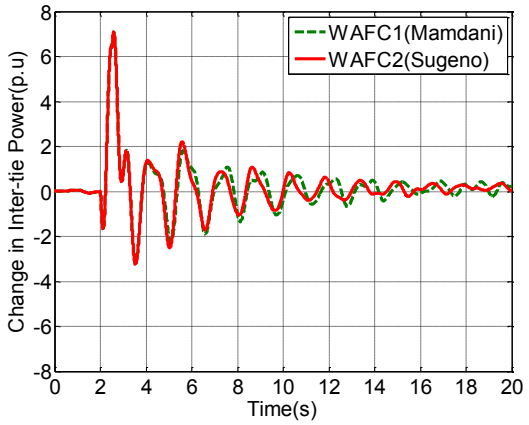

(a) Tie line between buses 1-2 (area4,5)

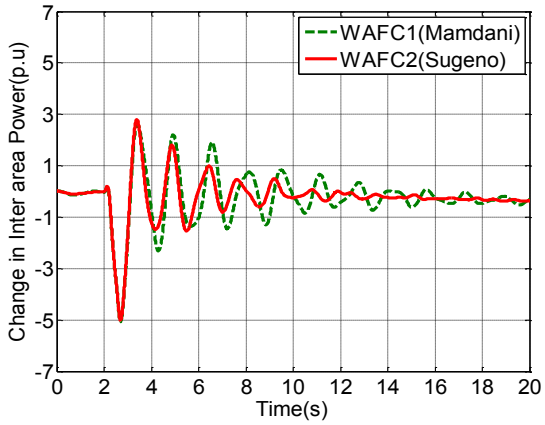

(b) Tie line between buses 8-9 (area4,5)

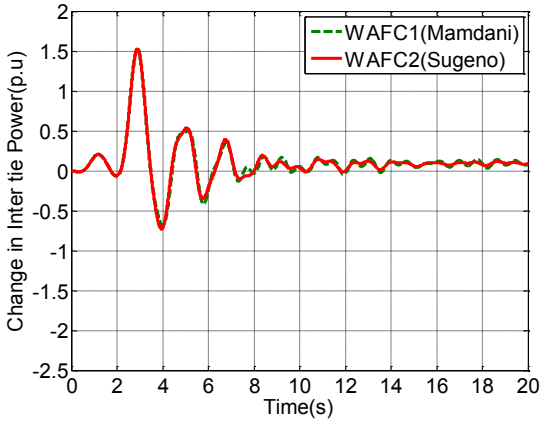

(c) Tie line between buses 42-41 (area1,2)

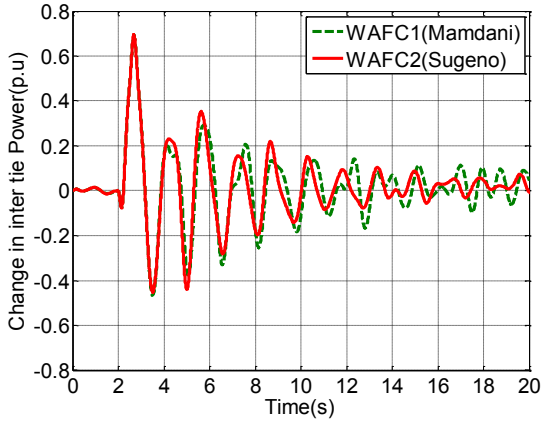

(d) Tie line between buses 1-27 (area4,5)

Figure 5.14.Change in Tie Line Power with 1 sec Delay with Parameter Variation

Table 5.11

Response Characteristics of Controllers with delay and parameter variation (Five-area system)

Delay (Magnitude)	Type of Controller	Overshoot (percentage)	Settling Time(s)	Damping
1s delay	WAFC1 (Mamdani)	7.0875	17.6	0.522
	WAFC2 (Sugeno)	7.088	17.3	0.526

From these results, it is observed that fuzzy controller WAFC2 based on ANFIS is more robust than WAFC1.

5.6 PMU MEASUREMENTS UNCERTAINITIES

Recent available literature [47, 75, 60] supports the presence of measurement uncertainties in PMU measurements. Presence of these uncertainties is generally neglected while designing damping controllers. However, if these uncertainties are left untreated, sometimes may contribute to instability. As stated before, fuzzy logic provides much easier way to handle randomness. According to Castilo et. al. [92] Type-1 fuzzy systems are able to model the uncertainties of linguistic variables. However, in comparison to type-1, type-2 is capable of modeling uncertainties in their membership functions and linguistic variables simultaneously. Type-1 fuzzy is a special case of type-2. In type-2 fuzzy systems, uncertainties are incorporated in MF through Foot of Uncertainty (FOU). Therefore, type-2 fuzzy systems are more reliable for practical power systems because they are able to provide higher order realization of uncertainty when compared to type-1 counterpart [92].

In remaining sections of this chapter, type-2 FLC are explored as wide area damping controller. In this work, communicated measurement uncertainties are modeled in the FOU of type-2. Details regarding modeling of FOU are also presented in subsequent subsections.

5.6.1 Interval Type-2 Fuzzy Membership Functions

Concept of type-2 fuzzy sets was introduced by Zadeh [71] as an extension of an ordinary type-1 fuzzy set. In type-2, corresponding to each primary membership there are secondary membership grades [92, 72, 59, 90]. For example, $\tilde{A}$ denotes a type-2 fuzzy set, $\tilde{\mu}_A(x)$ denotes the membership grade of *x* in the type-2 fuzzy set $\tilde{A}$. The elements of the domain $\tilde{\mu}_A(x)$ are called primary memberships of *x* in $\tilde{A}$. However, type-2 MF is represented as

$\tilde{\mu}_A(x,u) = \int_u f_x(u)/u$, where $u \in J_x \subseteq [0,1]$, x and u are primary and secondary variables. Secondary variable has the domain J_x, which is the primary membership of x.

This secondary uncertainty in primary membership of a type-2 fuzzy set consists of a bounded region, which is named as Foot of Uncertainty (FOU), as shown in Fig.5.15. This foot of uncertainty of an interval type-2 set is the union of all primary memberships and is given as:

$$FOU(\tilde{A}) = \bigcup_{x \in X} J_x$$

Upper Membership Functions and Lower Membership Functions are two type-1 MFs, which bounds FOU. The Upper MF is a subset, which has the maximum membership grade of the FOU. Similarly, Lower MF is also a subset, which consists of minimum membership grade of FOU. Since, FOU is bounded by two type-1 MFs. This means, FOU is able to handle uncertainty in a particular range bounded by type-1 MFs.

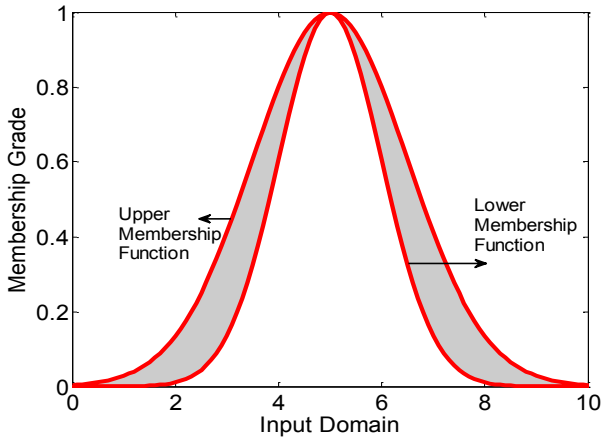

Figure 5.15 Foot of Uncertainty of Type-2 Membership Function

Based on numerical value of uncertainty or range of uncertainty, FOU can be extended only up to a fixed limit. Too narrow FOU is equivalent to type-1 MF, without modeling uncertainty, which can deteriorate performance. On the other hand, performance also depreciates, when FOU is increased significantly in comparison to uncertain information. Therefore, type-2 fuzzy systems require proper definition of FOU for the given system.

5.6.2 Interval Type-2 Fuzzy Logic Systems

Interval type-2 Fuzzy Logic System (FLS) is quite similar to type-1 FLS in its structure. However, type-1 and type-2 have different type of MFs and type-reducer in their output- processing unit [92].The basic structure of the interval type-2 Fuzzy Logic Controller (FLC) is shown in Fig. 5.16.

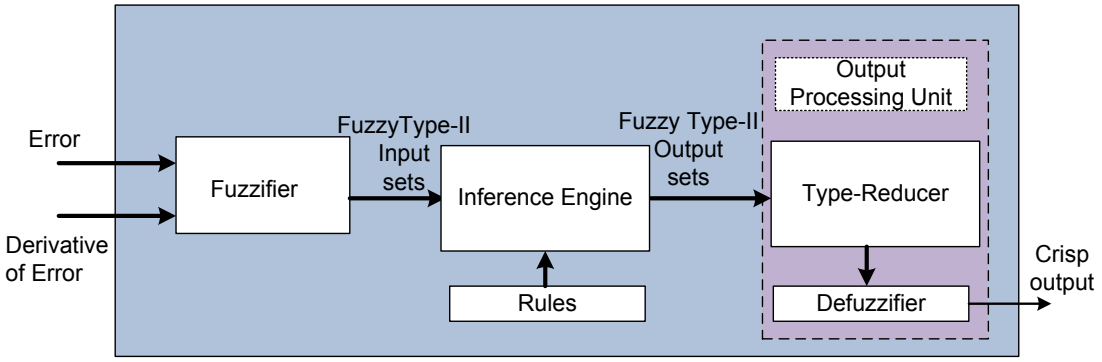

Figure 5.16 Basic Structure of Type-2 Fuzzy Logic System

Like type-1, in an interval type-2 fuzzy system also, knowledge is expressed in terms of rules. A general structure for l^{th} rule is given below.

$R^l : If\ x_1 is\ \tilde{P}_1^l\ and\ x_2\ is\ \tilde{P}_2^l\ and \cdots x_n\ is\ \tilde{P}_n^l$, *then y is* $\tilde{D}^l$

Where $x_1, x_2 \ldots x_n$ corresponds to the input variable, $\tilde{P}_1^l, \tilde{P}_2^l \cdots \tilde{P}_n^l$ are *n* antecedent variables for rule *l*, y is output variable and $\tilde{D}^l$ is consequent set corresponding to output variable *y* for rule *l.*

The Inference engine computes the MF for output interval type-2 fuzzy set $\tilde{B}$, corresponding to l^{th} rule. This output set is calculated using minimum or product t–norms [92] as shown below

$$\mu_{\tilde{B}^l}(y) = \mu_{\tilde{D}^l}(y) \prod P^l, y \in Y \tag{5.15}$$

In an interval type-2, *Meet* and *Join* operations of interval sets are determined by the two endpoints of each interval set, which are upper and lower MFs [92, 72, 81].Therefore, (5.15) is expressed as

$$\mu_{\tilde{B}_l} = \int_{b^l \in \left[\underline{p^l} * \underline{\mu_{\tilde{D}^l}}(y), \overline{p^l} * \overline{\mu_{\tilde{D}^l}}(y)\right]} 1/b^l \tag{5.16}$$

Where $\underline{\mu_{\tilde{D}^l}}(y)$ and $\overline{\mu_{\tilde{D}^l}}(y)$ are lower and upper membership grades of $\mu_{\tilde{D}^l}(y)$, $\underline{p^l}$ and $\overline{p^l}$ are lower n upper membership grade of P^l. Suppose *N* out of the *M* rules are fired, where *N*≤ *M*, then corresponding output fuzzy set $\mu_{\tilde{B}}(y)$ for a type-2 FLS is given as

$$\mu_{\tilde{B}}(y) = \coprod_{l=1}^{N} \mu_{\tilde{B}^l}(y), \qquad y \in Y \tag{5.17}$$

Thus combined output fuzzy set $\mu_B(y)$, is obtained by combining the fired output consequent sets, which is computed by taking the union of the rule R^l fired output consequent sets. Hence, output interval set with domain *b* is given by expression (5.18). Interval type-2 reduction is discussed in detail in [90]. According to Karnik *et.al*, type reducer converts interval type-2 output fuzzy sets to type-1 fuzzy sets.

$$\mu_{\tilde{B}}(y)=\int_{b\in}\begin{bmatrix}\left[\underline{p}^1*\underline{\mu_{\tilde{D}^1}}(y)\right]\cdots\left[\underline{p}^N*\underline{\mu_{\tilde{D}^N}}(y)\right],\\ \left[\overline{p}^1*\overline{\mu_{\tilde{D}^1}}(Y)\right]\cdots\left[\overline{p}^N*\overline{\mu_{\tilde{D}^N}}(y)\right]\end{bmatrix}1/b \tag{5.18}$$

After type reduction, crisp outputs are evaluated by computing the centroid of type reduced set. Since a type reduced set is an interval set, centroid is the midpoint of its domain, i.e. average of upper and lower membership values of reduced set.

5.6.3 PMU Measurement Uncertainties and Type-2 Controller

According to the proposed control scheme, speed error and derivative of error are the two inputs to the FLC. Error in the speed signal of two generators, without any delay is represented as

$$e_1 = s_j(t) - s_i(t) \tag{5.19}$$

However, error having the delay of *d* sec and the noise s_{noise}, is formulated as

$$e_2 = s_j(t) - \left[s_i(t+d) + s_{noise}\right] \tag{5.20}$$

Where $s_j(t)$ is the speed signal of the generator, which is having the controller. $s_i(t)$ is the speed signal of the generator, which is measured by PMU and communicated from remote locations as a feedback signal.

When a fuzzy controller is designed for the fixed range of error e_1, crisp membership functions will work well. However, crisp memberships will not give good results for equation (5.20). From equation (5.19) and (5.20), it can be concluded that e_2 is more disturbed and uncertain. Due to uncertainties of e_2 (i.e. s_{noise}+*d*), each membership will be uncertain and variable. This uncertainty in type-2 MF is modeled as FOU. Therefore, in type-2 it is important to determine FOU for given uncertainty. According to author's best knowledge, very little literature is available for FOU tuning. Therefore, in proposed work, FOU is increased in discrete steps to check type-2 performance. For example, 10% uncertainty in communicated signal is accounted by 10% change in FOU of interval type-2 MF.

5.7 DESIGN OF INTERVAL TYPE-2 FUZZY SYSTEMS

5.7.1 Important Considerations

Few important considerations are made in this work for designing fuzzy controllers, which are given below

- Both type-1 and type-2 FLCs use same rule base. However, rule base for different

systems are different.

- Both speed error and derivative of error in type-2 are represented by five Gaussian fuzzy sets, which are Negative Big (*NB*), Negative Small (*NS*), Zero (*Z*), Positive Small (*PS*), and Positive Big (*PB*) as shown in Fig.5.17.

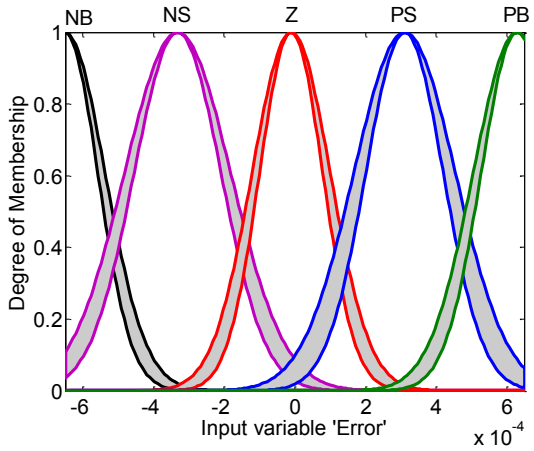

Figure 5.17.Type-2 Fuzzy Sets for Error Input

- In case of type-2 fuzzy systems, Gaussian MFs with a fixed center and uncertain standard deviation [92], $\sigma \in [\sigma_1, \sigma_2]$ are considered in present work. Therefore, Gaussian MF of (5.1) is modified as (5.21).

$$\mu_A(x) = e^{-\frac{1}{2}\left(\frac{x-c}{\sigma}\right)^2} \qquad \sigma \in [\sigma_1, \sigma_2] \tag{5.21}$$

$$Upper\ MF, \qquad \mu_{\tilde{A}}(x) = e^{-\frac{1}{2}\left(\frac{x-c}{\sigma_1}\right)^2} \tag{5.22}$$

$$Lower\ MF, \qquad \mu_{\tilde{A}}(x) = e^{-\frac{1}{2}\left(\frac{x-c}{\sigma_2}\right)^2} \tag{5.23}$$

- Since type-1 and type-2 differ in their membership functions. Therefore, type-2 MFs are derived from type 1 MFs by changing standard deviations.
- To have type-2 MF with 10% FOU, upper and lower MFs are computed in following manner

  For Gaussian MF with constant center,

  Standard Deviation of upper MF= 10% increment in the Standard Deviation of type-1 MF

  Standard Deviation of lower MF= 10% decrement in the Standard Deviation of type-1 MF.

In a similar manner, membership functions with 20% and 30% FOU are computed.

5.7.2 Design of Type-2 controller for Two-area four-machine system

Type-2 MFs for input and output variables are derived from type-1 as given in preceding sub section 5.7.1. Type-1 FLC parameters are given in Table 5.1. These parameters are used to derive type-2 parameters. Derived type-2 parameters are given in Table 5.12, 5.13, and 5.14. Furthermore, controller uses fuzzy rules already mentioned in Table 5.2.

TABLE 5.12

Standard Deviations of Type-2 FLC for Error Input (Two-area System)

	10% Standard deviation(1e-4)		**20% Standard deviation(1e-4)**		**30% Standard deviation(1e-4)**	
	σ1	σ2	σ1	σ2	σ1	σ2
NB	1.140	0.093	1.244	0.082	1.348	0.072
NM	1.509	1.234	1.646	1.097	1.783	0.096
Z	1.111	0.089	1.212	0.080	1.313	0.070
PM	1.443	1.100	1.574	1.049	1.705	0.091
PB	1.243	1.017	1.356	0.090	1.469	0.079

TABLE 5.13

Standard Deviations of Type-2 FLC for Derivative of Error Input (Two-area System)

	10% Standard deviation(1e-3)		**20% Standard deviation(1e-3)**		**30% Standard deviation(1e-3)**	
	σ1	σ2	σ1	σ2	σ1	σ2
NB	1.023	0.083	1.111	0.074	1.209	0.065
NM	1.092	0.089	1.191	0.079	1.290	0.069
Z	1.100	0.090	1.200	0.080	1.300	0.070
PM	1.109	0.080	1.210	0.080	1.311	0.070
PB	0.095	0.077	1.036	0.061	1.123	0.060

TABLE 5.14

Standard Deviations of Type-2 FLC for Control Output (Two-area System)

	10% Standard deviation(1e-3)		**20% Standard deviation(1e-3)**		**30% Standard deviation(1e-3)**	
	σ1	σ2	σ1	σ2	σ1	σ2
NB	2.777	2.468	3.024	2.016	3.276	1.764
NM	3.124	2.556	3.408	2.272	3.692	1.988
Z	2.828	2.520	3.360	2.240	3.640	1.960
PM	3.421	2.799	3.732	2.488	4.043	2.177
PB	3.476	2.844	3.792	2.528	4.108	2.212

5.7.2 Design of Type-2 controller for Five-area sixteen-machine system

As described in earlier section, type-2 FLC is designed for 10%, 20%, and 30% increment in FOU. For designing type-2, type-1 FLC's centers and standard deviations of input and output signals are given in Table 5.4. However, different FOUs parameters for type-2 are computed and tabulated in Tables 5.15, 5.16, and 5.17. Designed type-2 controller uses Fuzzy rules given in Table 5.3.

TABLE 5.15

Standard Deviations of Type-2 FLC for Error Input (Five-area System)

	10% Standard deviation(1e-2)		20% Standard deviation(1e-2)		30% Standard Deviation(1e-2)	
	σ1	σ2	σ1	σ2	σ1	σ2
NB	1.494	1.223	1.630	1.080	1.766	0.952
NM	1.960	1.603	2.130	1.420	2.316	1.247
Z	1.043	0.854	1.130	0.756	1.234	0.664
PM	1.760	1.440	1.920	1.280	2.089	1.124
PB	1.521	1.244	1.650	1.100	1.797	0.968

TABLE 5.16

Standard Deviations of Type-2 FLC for Derivative of Error Input (Five-area System)

	10% Standard deviation(1e-2)		20% Standard deviation(1e-2)		30% Standard Deviation(1e-2)	
	σ1	σ2	σ1	σ2	σ1	σ2
NB	1.510	1.240	1.650	1.104	1.795	0.960
NM	1.860	1.520	2.030	1.355	2.202	1.185
Z	0.880	0.720	0.963	0.647	1.043	0.563
PM	1.890	1.550	2.060	1.370	2.241	1.206
PB	1.520	1.240	1.650	1.105	1.790	0.967

TABLE 5.17

Standard Deviations of Type-2 FLC for Control Output (Five-area System)

	10% Standard deviation(1e-2)		20% Standard deviation(1e-2)		30% Standard Deviation(1e-2)	
	σ1	σ2	σ1	σ2	σ1	σ2
NB	1.878	1.537	2.049	1.366	2.220	1.190
NM	1.873	1.532	2.043	1.362	2.213	1.192
Z	0.915	0.748	0.999	0.666	1.082	0.582
PM	2.080	1.705	2.274	1.516	2.463	1.326
PB	1.815	1.485	1.980	1.320	2.145	1.155

5.8 CASE STUDIES

The Fuzzy controllers described in preceding sections are tested on two-area four-machine and five-area sixteen-machine systems. The proposed controllers are tested for two cases, in Case-1, only time-latencies are considered in feedback signals, and in Case-2 measurement uncertainty and time delays are considered simultaneously. In Case-2, small amount of noise is deliberately added to feedback signals to represent various uncertainties and noise of measured signals. For both the systems, results of fuzzy type-2 are compared with fuzzy type-1 controllers discussed in section 5.3.

5.8.1 Two-area four-machine system

Case-1 (Without noise)

Two-area system is simulated according to sub-section 5.5.1. Improvements in inter-area oscillations are obtained by employing Wide Area Controllers (WACs) i.e. Fuzzy Type-1(FT1) and Fuzzy Type-2 (FT2) are shown in Fig.5.18.

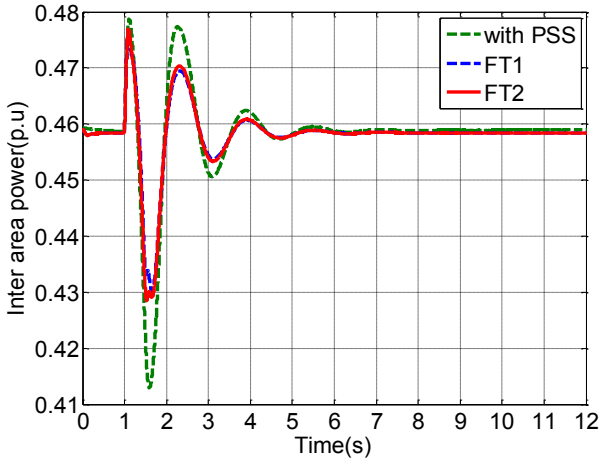

Figure 5.18 Tie -Line Power Dynamic Response without Delay

Fig.5.18 represents that FT1 and FT2 without time latency have almost the same performance. To simulate the latency effect of communication network, equal time delay of 1 s is considered in all wide area measurement signals from area 1 to area 2 and vice-versa. In this case, the delay is considered without any measurement uncertainty and noise. Results of fuzzy controllers with the time latency are shown in Fig. 5.19.

From Fig. 5.19, it is observed that for delayed wide area signals, FT2 performs better than FT1.

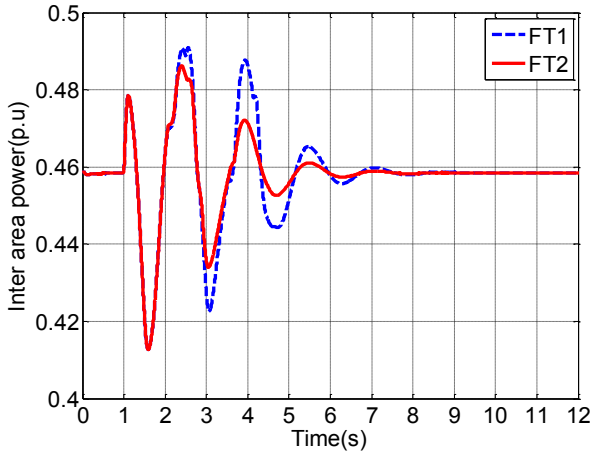

Figure 5.19 Tie -Line Power Dynamic Response with 1s Delay

Case- 2 (With noise)

To model measured signal uncertainties, type-2 FLCs are varied under different FOUs. FOUs are increased by 20%, and 30%, according to section 5.7.1, which are given in Tables 5.12, 5.13, and 5.14. In this case, noise signals of 10dB and 30 dB SNR are added with feedback signals to check the performance of controllers. Dynamic response of proposed controllers for 1 s latency along with communication uncertainty and noise (10dB SNR) are shown in Fig.5.20.

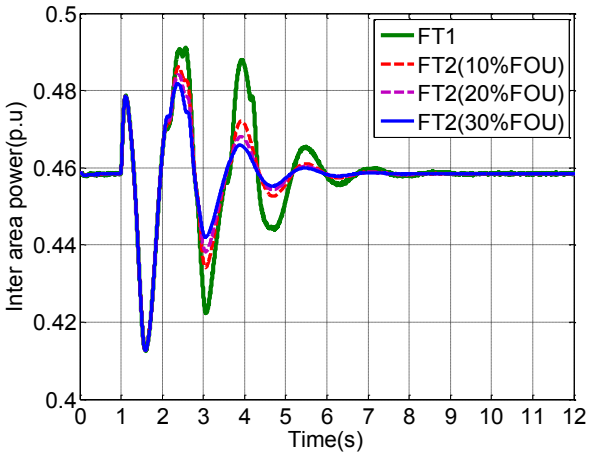

Figure 5.20 Change in Inter-area Power with 1s Delay and 10dB Noise

Fig. 5.20 shows that type-2 controllers are able to reduce 10 dB noises effectively. Response becomes better as foot of uncertainty is increased. However, for FOU above 30%, type-2 performance deteriorates. Similar results are obtained with 30 dB SNR, which is shown in Fig 5.21.

Various performance parameters like overshoot and settling time of the proposed FLCs are compared and are given in Table 5.18.

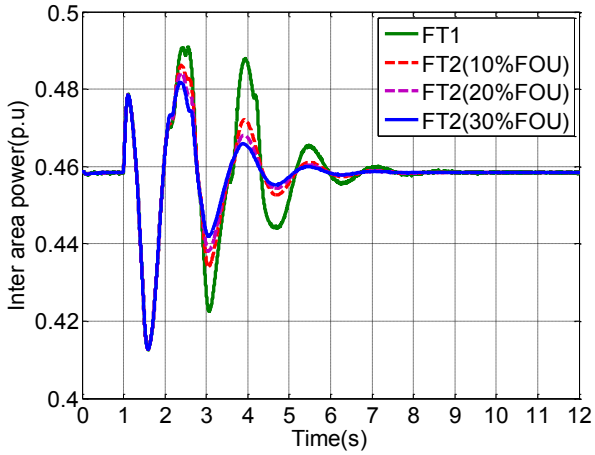

Figure 5.21 Change in Inter-area Power with 1s Delay and 30dB Noise

Table 5.18 depicts that FT2 performs well, in terms of peak overshoot and settling time. Further, damping factor is considerably improved with FT2.

TABLE 5.18

Response Characteristics of Controllers (Two- area System)

Without Delay	Peak Overshoot	Settling Time	Damping Factor
With PSS	0.478	4.15	0.480
FT1	0.475	3.40	0.510
FT2	0.477	3.40	0.516
With 1s Delay	Peak Overshoot	Settling Time	Damping Factor
FT1	0.491	6.10	0.366
FT2	0.486	5.15	0.413
With 1s Delay &10dB noise	Peak Overshoot	Settling Time	Damping Factor
FT1	0.491	6.11	0.366
FT2 (10%FOU)	0.486	5.45	0.413
FT2 (20%FOU)	0.484	5.01	0.434
FT2 (30%FOU)	0.481	4.95	0.455

5.8.2 Five-area sixteen-machine system

Case- 1 (Without noise)

Similar to section 5.5.2, five-area system is simulated in similar manner. Fig. 5.22 shows the performance of PSS and fuzzy controllers on four major tie lines of the five- area system. These tie lines are 1-2(area4- area5), 8-9(area4-area5), 50-51 (area1-area4), and 1-27(area4- area5).

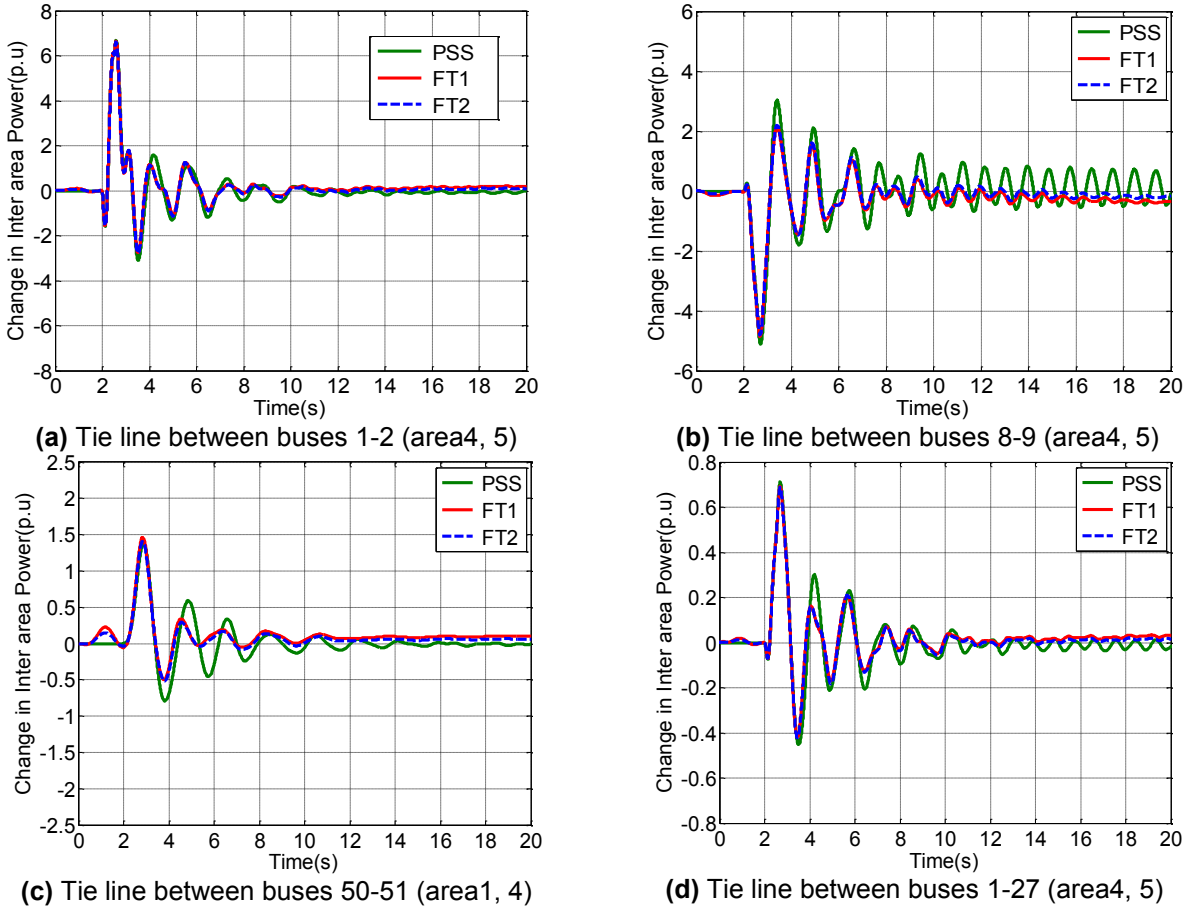

(a) Tie line between buses 1-2 (area4, 5)

(b) Tie line between buses 8-9 (area4, 5)

(c) Tie line between buses 50-51 (area1, 4)

(d) Tie line between buses 1-27 (area4, 5)

Figure 5.22 Change in Inter-area Power without Delay

Fig. 5.22 response indicates that fuzzy controllers are better than PSS. However, responses of type-1 and type-2 for noise free signal are same, since both controllers have the same structure. To simulate the latency effect of communication network equal time delays of 1s are taken in measurement signals, without any uncertainty and noise. Responses of four tie lines with FT1, FT2 (10% FOU) and FT2 (20% FOU) are depicted in Fig.5.23 (a) - (d).

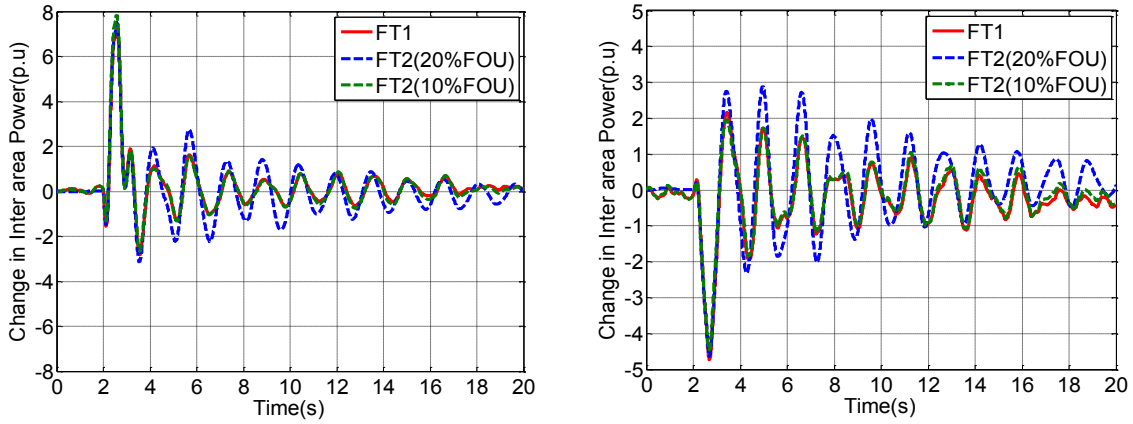

(a) Tie line between buses 1-2 (area4, 5)

(b) Tie line between buses 8-9 (area4,5)

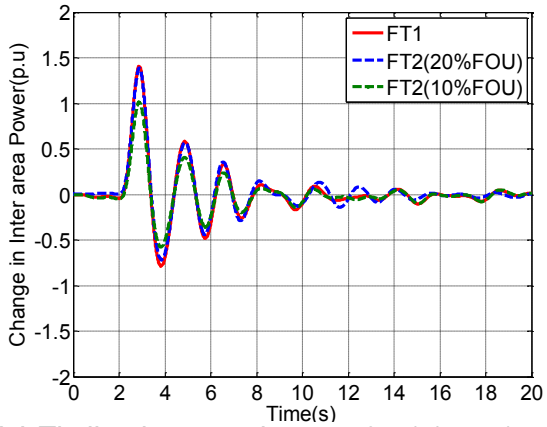

(c) Tie line between buses 50-51 (area1, 4)

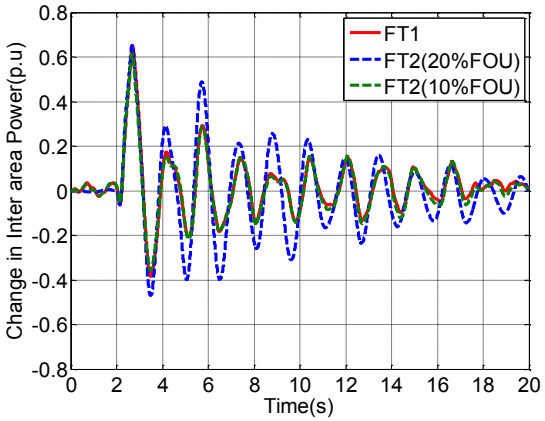

(d) Tie line between buses 1-27 (area4, 5)

Figure 5.23 Change in Inter-area power with 1s delay

From Fig. 5.23, it is observed that responses of FT1and FT2 with 10 % FOU are very similar in nature. Further, when FOU is increased by 20%, the response becomes oscillatory. However, with 30% increment in FOU, the outputs of controllers become out of bounds.

Case- 2 (With noise)

For the given system, FOUs of type-2 FLCs are varied for uncertain and noisy feedback signals. Noise signals of 10dB SNR is added to the input signal. Standard deviations corresponding to lower and upper memberships for type-2 are taken from Tables 5.15, 5.16, and 5.17. Dynamic response on four major tie lines with proposed controllers for 1s latency along with communication uncertainty and noise (10 db SNR) is shown in Fig. 5.24 (a)-(d).

A close inspection Fig.5.24 shows that when the noise of 10dB is added to the system, performances of FT2 controllers are better than FT1 with 10%, 20%, and 30% FOU. It is observed from above response that as FOU increases beyond 10%, the response of FT2 deteriorates compared to FT2 with 10% FOU.

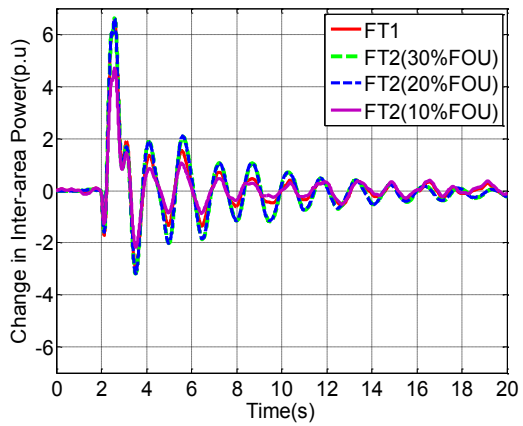

a) Tie line between buses 1-2 (area4, 5)

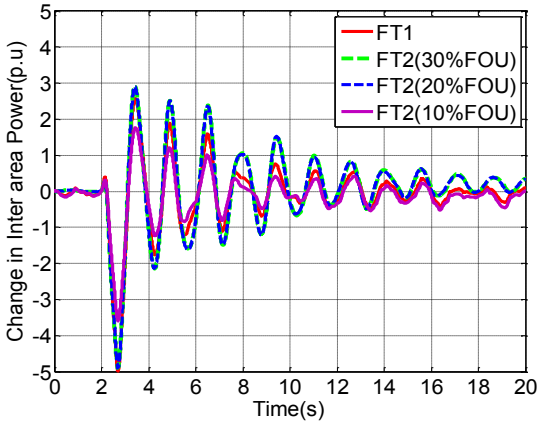

(b) Tie line between buses 8-9 (area4, 5)

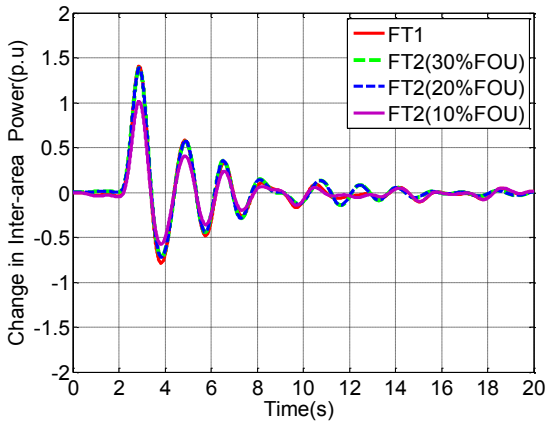

(c) Tie line between buses 50-51 (area1, 4)

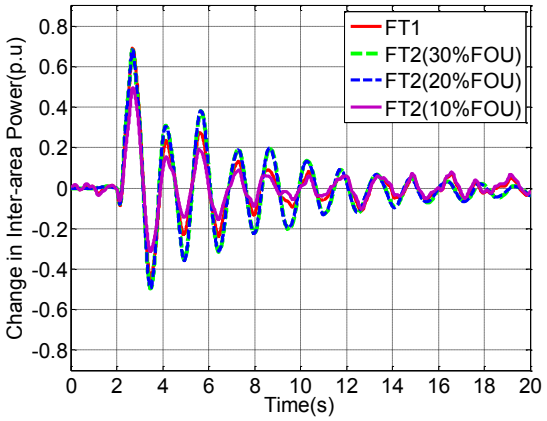

(d) Tie line between buses 1-27 (area4, 5)

Figure 5.24 Change in Inter-area Power with 1s Delay and 10dB Noise

Similar results are obtained for 30 dB of noise. Therefore, it is concluded that FOU can be increased up to a limit to nullify the noise effect. However, when FOU is continuously increased, type-2 fuzzy controller's response deteriorates. Performance parameters for given system are presented in Table 5.19.

TABLE 5.19

Response Characteristics of Controllers for Tie Line 1-2 (Five- area System)

Without Delay	Peak Overshoot	Settling Time	Damping Factor
With PSS	6.680	10.12	0.510
FT1	6.647	9.80	0.509
FT2	6.622	9.96	0.511
With 1s Delay	Peak Overshoot	Settling Time	Damping Factor
FT1	4.800	16.20	0.421
FT2	4.780	15.56	0.422
With 1s Delay &10dB noise	Peak Overshoot	Settling Time	Damping Factor
FT1	6.600	17.95	0.505
FT2 (10%FOU)	4.700	17.89	0.441
FT2 (20%FOU)	6.620	18.12	0.513
FT2 (30%FOU)	6.621	18.14	0.513

Table 5.19, indicates that significant improvement in peak overshoot, settling time, and the damping factor is obtained with type-2 controller compared to type-1.

5.9 CONCLUSION

- In this chapter, Mamdani/Type-1, ANFIS, and robust Type-2 fuzzy damping controllers are proposed for communication delay, uncertainty, and noise of PMU measurements to improve small signal stability analysis of the power system. Modal analysis of earlier chapter is used to find inter area modes. For each inter area mode, the controller is placed on the machine, which has the highest participation factor. Speed signal of the machine having the highest controllability index is feedback to the controller via PMUs. Output signals of wide area controllers are given to the exciters of alternators to improve the inter tie dynamic response. Communication delays of 1s are taken in all wide area signals. Further, PMU uncertainties and noise signal of 10dB and 30dB SNR is considered to check the performance of the controllers for different FOUs. In present work, performance of ANFIS and type-2 controller are not compared with each other. Both of them are separately compared with type-1 controller. The proposed controllers are successfully tested on two-area four-machine and five-area sixteen-machine systems.
- From the simulation results of section 5.5 and performance characteristics given in Table 5.8, 5.9, 5.10, and 5.11, it can be concluded that ANFIS based controllers are more robust at various operating conditions, parameter variations and time delays and are more suitable for practical power systems.
- From the simulation results of section 5.8, it is observed that fuzzy controller based on type-2 FLCs performs better than type-1 FLCs for delayed, uncertain, and noisy measurements. However, type-2 controllers have good response, only when the FOU is increased within certain limits. In present work, FOU is increased in discrete steps, to check controller's performance. Further, damping factor is improved by type-2 controllers, which means type-2 FLCs are more efficient and reliable for practical power systems.

CHAPTER-6
Fast Transient Stability Predictor using PMU Measurements

6.1 INTRODUCTION

Today power system is subjected to both small and large rotor angle excursions. These rotor angle deviations when small are controlled with the help of damping controllers, as mentioned in previous chapter. Large-angle excursions or transients are biggest threats to power system stability. To prevent system from these transients, generally transient predictors are employed [34, 112, 100, 4, 73, 3, 38]. These predictors are capable to predict transients before there occurrence. Existing works establishes that with PMU measurements, "real-time early-warning" systems are easy to build [95, 53, 36, 130, 31, 127, 77, 34, 112, 100, 4]. Present chapter, discusses designing of such fast and accurate transient predictor utilizing synchro phasor measurements. Further, existed predictors require rotor angle measurements of all generators, which are ensured through placement scheme suggested in chapter-4. Since, PMU provides direct voltage and current phasor measurements. Therefore, proposed predictors make use of voltage phasors to predict transient stability of the system.

In this work, RVM based transient stability predictor is proposed. Three different inputs namely generator bus voltage magnitudes, angles or combination of voltage and angle (i.e. complete voltage phasors) are utilized in classification. First, simulations are carried out to develop training data with different operating conditions. Stability index for each simulation is calculated and a label is assigned for each simulation. Later, performances of RVM predictors are compared with SVM classifiers. Effect of measurement errors on performance of predictor is further considered. Proposed predictor is tested on New England 39 bus system.

6.2 RVM BASED TRANSIENT STABILITY PREDICTION SCHEME

When a disturbance occurs in a system, generator angles and speeds are most affected, therefore for transient stability analysis generator rotor angles are generally used for stability prediction [93]. However, generator voltages are also affected significantly after a fault. During a fault the bus voltages dip, however, when fault is cleared the bus voltages recover. The initial rate of recovery and final voltage values at the buses can indicate the final stability status of the system. A slower recovery rate and lower final voltages are signs of transient instability problem [3]. In this work, a binary RVM classifier is designed to predict the stability status of the given

system using post fault voltage and angle information. The system after fault will be either 'stable' or 'unstable', therefore a two class RVM predictor is trained using training data, which is generated through offline simulations.

6.2.1 Input Features for Classification

Prediction accuracy of transient stability predictor depends on the input features, which are used for classification. In proposed binary classification problem, three different input features are used to train the classifiers. These input features are generator bus-voltage magnitudes, angles and complete/combined phasors (i.e. both voltage magnitudes and generator angles). It is assumed that these generator voltage magnitudes and angles, are the outputs of PMUs which are connected at each generator bus. These PMU measurements are sampled and these sample values just after fault clearing are taken as input vector as shown in Fig 6.1. Number of samples are gradually increased from 2 to 7 to improve classification by transient predictors.

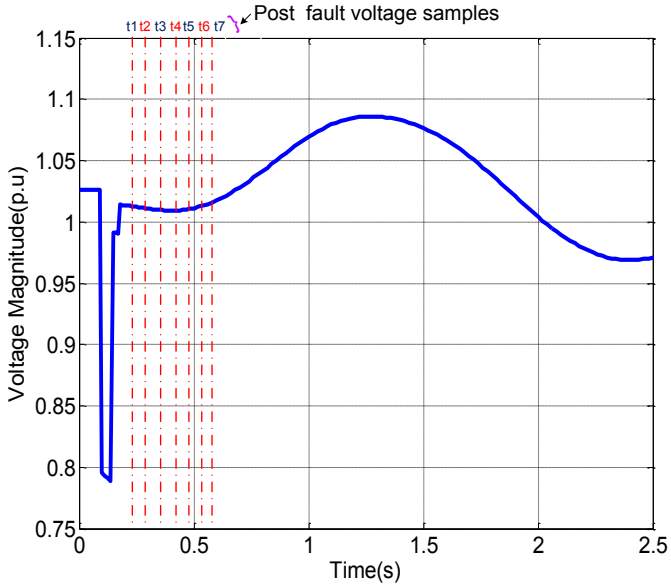

Figure 6.1 Feature selections from voltage profiles

6.2.2 Creation of Training Data

Performance of a machine learning algorithms are always based on past knowledge. This past knowledge, is obtained through large number of off-line simulations in the form of input and output data. Different operating conditions are simulated for various operating conditions, by changing fault-type, clearing time and loading. Various types of faults like three-phase to ground, line to line and line to ground faults are simulated. Fault clearing time is varied from 5 to 11 cycles. Further loading conditions are also changed from 5 to 10 percent. The data obtained through these simulations is randomly divided into training and testing data set.

6.2.3 Transient Stability Index

Stability of the power system is determined by utilizing the binary classifier. This classifier assigns class labels to the post-fault input vector. These class labels are 'stable' and 'unstable' depicting that whether system is moving towards stability or instability. In order to assign these labels to input data, a transient stability index is determined [38] as given below

$$C = \frac{360 - |d_{\max}|}{360 + |d_{\max}|} \times 100$$

Where $|d_{\max}|$ is the maximum angle of separation between any two machines during post fault response. When stability index C, satisfies condition $C > 0$ system is considered stable. Similiarly if $C < 0$ the system is unstable.

Classification algorithmn proposed in this chapter is shown in Fig 6.2. block diagram

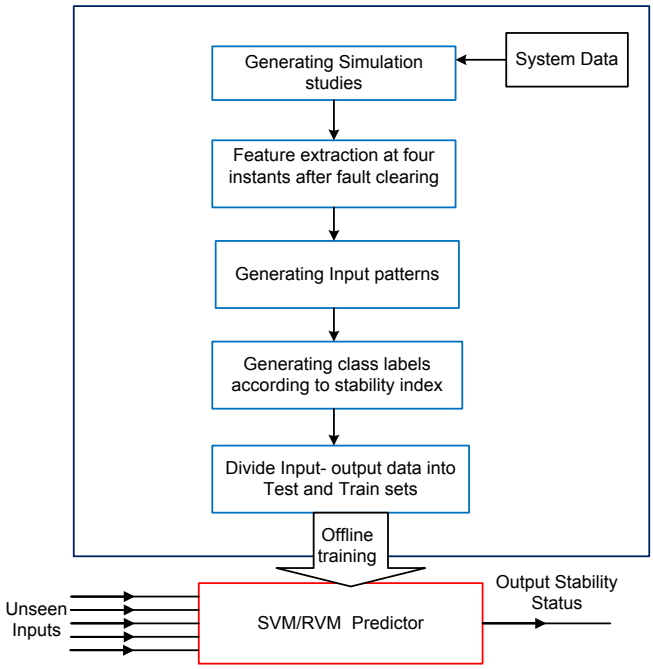

Figure 6.2 Proposed Classification Scheme

6.3 RELEVANCE TRANSIENT STABILITY PREDICTOR

The transient predictor predicts the stability status of the given system, for various fault conditions. To understand working of transient predictor, a fault condition is considered. For example, a three-phase fault occurs on transmission line 1-2 of New England 39 bus system, which is shown in Fig 6.3. This fault will bring considerable changes in voltage and angle profiles

of all 10 generators. Consider that the three post-fault sample values are taken for prediction. Input vector of predictor, corresponding to generator voltage/angles will be of dimension [10X3] and corresponding to this input vector there will be one binary output (0/1). If 105 such fault cases are considered then, input vector will be [1050X3] and output vector will be a vector having 105 entries. When voltage magnitudes or angles are considered input vector, dimension of input vector will be [10X3], however, for complete phasor case this dimension will be [20X3]. In general, for any fault input vector, x_j will be of dimension [AXB], where A is the number of generators in the system and B is the number of post fault samples of input. The output t_j will be either 0 (stable) or 1(unstable) depending upon stability of the system.

6.3.1 Relevance Vector Machine (RVM) for Prediction

Relevance Vector Machine (RVM) is a probability based machine-learning technique developed by M.E Tipping [83]. RVM is widely used for regression and classification problems. It is a bayesian treatment Support Vector Machines (SVM), which is another widely used machine learning approach. Both RVM and SVM have same functional form. However, RVM utilizes fewer kernel functions and is faster than SVM. To have better understanding, first RVM predictor for regression is explained. RVM for binary classification is discussed in subsequent section.

An intelligent predictor learns from input-output pairs and tries to predict output (*t*) for an unknown input (*x*). In an intelligent supervised learning process, learning is accomplished through model weights 'w' and 'model function'. In SVM [118], this 'model function' is 'kernel function'. The output of a SVM predictor $y(x)$ for single input is expressed as.

$$y(x) = \sum_{i=1}^{M} w_i K(x, x_i) + w_0 \tag{6.1}$$

Where, w_i denotes model weights, $K(x, x_i)$ represents kernel function, w_0 is the bias, *x* denotes the input vector and *M* denotes total number of inputs. Above expression shows, that predictor output is linear weighted sum of kernel functions. Tipping in [82] has summarized disadvantages of SVM predictor and potential benefits of probabilistic Bayesian approach for prediction and classification. In Bayesian approach, conditional probability $P(t_j / x_j)$ represents the probability of obtaining the output t_j when input x_j is given. This probability is assumed to have a Gaussian distribution over t_j with mean $y(x_j)$ and variance σ^2.

$$P(t_j / x_j) = G(t_j / y(x_j), \sigma^2) \tag{6.2}$$

As stated earlier, RVM is probabilistic treatment of SVM and follows same functional model (6.1). Output of predictor $y(x_j)$ is related to actual target value t_j with the help of expression

$$t_j = y(x_j) + \in_j \tag{6.3}$$

Where $\in_j$ corresponds to noise process, which is assumed to have zero mean Gaussian distribution with σ^2 variance. When all fault cases are considered, then likelihood of getting output stability status, from input are given as

$$P(t/w,\sigma^2) = (2\pi\sigma^2)^{-\frac{M}{2}} \exp\left\{-\frac{1}{2\sigma^2}\|t-\varphi w\|^2\right\} \tag{6.4}$$

Where $t = (t_1 \cdots t_M)^T$, $w = (w_0 \cdots w_M)^T$ and φ is called as design matrix. This design matrix is further defined as $\varphi = [\varphi(x_1), \varphi(x_2) \cdots \varphi(x_M)^T]$ and $\varphi(x_j) = [1, K(x_j, x_1), K(x_j, x_2) \cdots K(x_j, x_M)]^T$. From above expression, it is clear that as number of fault cases increases, number of parameters involved in the model also increases, and will lead to severe over fitting. To avoid this, extra constraints are applied on parameters. These extra constraints are applied by assigning prior probabilities to weights [81].

$$P(w/\alpha) = \prod_{i=0}^{M} Q(w_i/0, \alpha_i^{-1}) \tag{6.5}$$

Where α represents vector of hyper-parameters and each hyper parameter is independently associated with every weight. Similarly, hyper-priors are attached with noise variance σ^2. These hyper-priors are assumed to have gamma distributions. Further, these hyper-priors have gamma parameters a, b, c and d [82].

$$p(\alpha) = \prod_{i=0}^{M} Gamma(\alpha_i/a,b) \tag{6.6}$$

$$p(\beta) = Gamma(\beta/c,d) \quad where\ \beta = \sigma^{-2} \tag{6.7}$$

To simplify (6.6) and (6.7) a, b, c and d have assigned very small value, in order to make hyper priors uniform. According to [82], to make prediction for a new unknown input (voltage/angle/complete phasor) x*, corresponding output (stability status) is t*. In probabilistic sense, t* can be obtained by the expression

$$P(t^*/t) = \int P(t^*/\alpha,\sigma^2) P(w,\alpha,\sigma^2/t) dw\, d\alpha\, d\sigma^2 \tag{6.8}$$

Expression (6.8) gives, likelihood of getting output-status for unknown input (t*), when output status vector for all known inputs (t) are given. To compute (6.8), second term on right hand side is decomposed and written as

$$P\left(w,\alpha,\sigma^2/t\right)=P\left(w/t,\alpha,\sigma^2\right)P\left(\alpha,\sigma^2/t\right) \tag{6.9}$$

$P\left(\alpha,\sigma^2/t\right)$ and its inverse probability are related by Baye's theorem and expression (6.10) is derived

$$P\left(\alpha,\sigma^2/t\right)\propto P\left(t/\alpha,\sigma^2\right)P(\alpha)P\left(\sigma^2\right) \tag{6.10}$$

Assuming uniform hyper priors and ignoring $P(\alpha)$ and $P\left(\sigma^2\right)$ and $P\left(\alpha,\sigma^2/t\right)\propto P\left(t/\alpha,\sigma^2\right)$ and now replacing $P\left(\alpha,\sigma^2/t\right)$ in (6.9),

$$P\left(w,\alpha,\sigma^2/t\right)=P\left(w/t,\alpha,\sigma^2\right)P\left(t/\alpha,\sigma^2\right) \tag{6.11}$$

Once again applying Baye's theorem in first part of right hand term expression in (6.9)

$$P\left(w/t,\alpha,\sigma^2\right)=\frac{P\left(t/w,\sigma^2\right)P(w/\alpha)}{P\left(t/\alpha,\sigma^2\right)} \tag{6.12}$$

Above expression on simplification gives

$$P\left(w,\alpha,\sigma^2/t\right)=P\left(w/t,\alpha,\sigma^2\right)P\left(t/\alpha,\sigma^2\right)=P\left(t/w,\sigma^2\right)P(w/\alpha) \tag{6.13}$$

$$P\left(t/\alpha,\sigma^2\right)\equiv P(t/\alpha,\beta)=\int P\left(t/w,\sigma^2\right)P(w/\alpha)dw \tag{6.14}$$

Expression (6.14) gives marginal likelihood, which is further solved by substituting (6.4) and (6.5). This marginal likelihood expression is maximized with respect to α and β. Evidence Approximation Procedure [82] is used to find optimal values of hyper-parameters. For stability problem, (6.14) gives likelihood of getting stability status when hyper parameters of the model are known. After finding optimal values, marginal likelihood is used to evaluate prediction distribution over *t* (known output vector) for unknown phasor input x^* with the help of expression (6.8) as

$$P\left(t^*/t\right)=\int P\left(t^*/w,\sigma_{OP}^2\right)P\left(w,\alpha_{OP},\sigma_{OP}^2/t\right)dw \tag{6.15}$$

According to given transient problem, $P\left(t^*/w,\sigma_{OP}^2\right)$ is probability of transient status for unknown new input when RVM weights and optimal model parameters are known. Similarly, $P\left(w,\alpha_{OP},\sigma_{OP}^2/t\right)$ term depicts probability of having model weights and optimal parameter values for known output vector (t). Since stability status problem is a binary classification problem, few modifications are made in above RVM prediction method, which is for regression.

6.3.2 Relevance Vector Machine (RVM) for classification

For two class problem, posterior probability of membership of one class (instability cases) with input data *x* is written as

$$p(t_j = 1/x) \approx \sigma\{y(x;w)\} \tag{6.16}$$

Where

$y(x;w) = \sum_{j=1}^{M} w_j \varphi_j(x) + w_0$ and $\sigma(y) = 1/(1+e^{-y})$

The bernoulli distribution is applied for $P(t/w)$ [81] and therefore likelihood is given by expression

$$P(t/w) = \prod_{j=1}^{M} \sigma\{y(x_j;w)\}^{t_j} \left[1-\sigma\{y(x_j;w)\}\right]^{1-t_j} \tag{6.17}$$

Targets $t_j \in [0,1]$and there is no noise variance in classification. Weights cannot be integrated out analytically in classification like regression. Therefore, an approximation technique based on laplace method [30] is used. A prior distribution is introduced over the vector model parameters or weights, as given by (6.6) and (6.7). Posterior distribution of weights from Bayes rule $P(w/t,\alpha)$ is proportional to product of $P(t/w)P(w/\alpha)$. Thus optimal value of *w* is computed, which is equivalent to maximum of log likelihood function

$$\log P(t/w)P(w/\alpha) = \sum_{j=1}^{M}\left[t_j \log y_j + (1-t_j)\log(1-y_j)\right] - \frac{1}{2} w^T A w \tag{6.18}$$

Where $A = diag(\alpha_0, \alpha_1, \cdots \alpha_N)$

The values of optimal parameters are obtained using a technique 'iteratively-reweighted least squares algorithm [81]. Laplace's method is used to obtain a Guassian approximation to the posterior density of the weights. The hyper parameters are updated in order to maximize marginal likelihood. This process is repeated until an appropriate convergence criterion [98] is met. The maximization of the marginal likelihood or evidence for the hyper parameters alpha leads to the hyper parameters associated with the uninformative features becoming very large. This in turn forces the value of the associated weight essentially to zero, allowing redundant features to be easily identified and pruned from the model. Laplace approximation effectively maps the binary classification problem to a regression one, with the inverse noise variance given by

$$\beta_j = \sigma\{y(x_j)\}\left[1-\sigma\{y(x_j)\}\right] \tag{6.19}$$

6.4 SIMULATION STUDIES

The Transient stability classifier described in previous sections is tested on New-England 39 bus system [39]. This test system consists of 39 buses, 10 generators, 19 load buses, and 34 transmission lines as shown in Fig 6.3

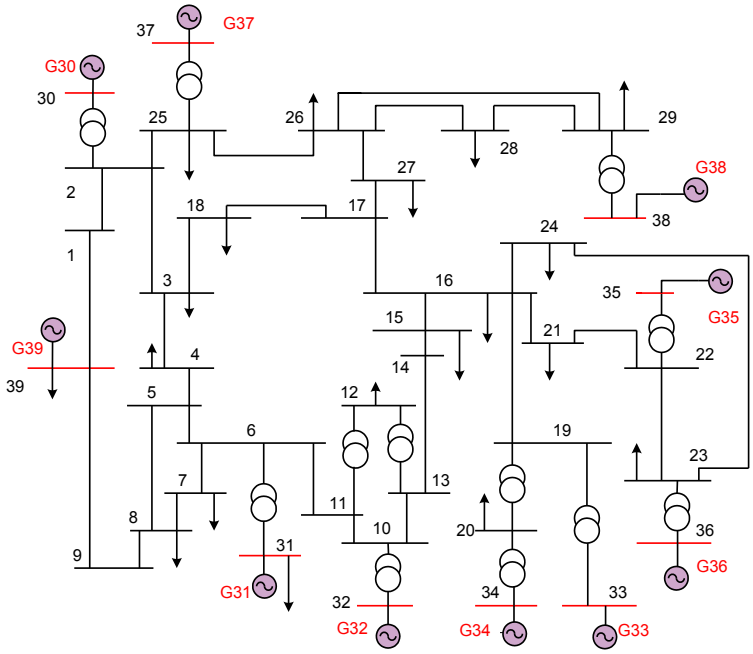

Figure 6.3 New England 39 bus system

All machine data and other system information are given in Appendix-C. For the given system, binary classifier based on SVM and RVM are designed. Training and testing data are generated from off line simulations. Different types of faults like three-phase to ground, line to line and line to ground faults are considered for simulation. As mentined before, for each type of fault, fault clearing time is varied from 5 cycles to 11 cycles and loading is varied by 5-10%, to generate data covering all operating conditions of the system.

For each type of fault 1840 cases are generated, i.e. 1840 cases are created for L-L, L-G and three phase fault, considering load and fault clearing time. From the data obtained via simulation, it is found that data is highly unbalanced, which means there are more number of stable cases than unstable cases. Therefore, to balance the data, unstable cases are replicated and a balanced data is generated.

This balanced data is randomly divided into training and testing set in 80:20 ratio, such that 2000 cases are used as training set and 500 cases are treated as test set. Generated training set is utilized to train SVM and RVM classifiers, and testing sets are used to check the performances of two classifiers for unseen input patterns.Since data is randomly divided into two

sets, it may happen that unstable/stable cases in test set may vary. This simply means that some of unstable/stable cases have migrated to training set, during random division. Therefore, for same type of fault, stable/unstable cases in test set may vary. This variation should not be confused with data discrepancy, it simply means data division for training and testing data is random. Further, when fault type is different, unstable and stable sets are different.

As described in previous sections, three different features are considered in this work. Generator bus voltage magnitude are computed from bus voltage profiles. Generator bus angles are assumed to be obtained by generator rotor angle profiles. However, complete/combined phasor information is obtained by combining generator bus angle and voltage measurements. Typical voltage profiles and generator angular deviation for I0 generator system after three phase fault are shown in Fig 6.4 and Fig 6.5 respectively. Training and testing of transient predictors are carried out, with normal input data and with noisy input data.

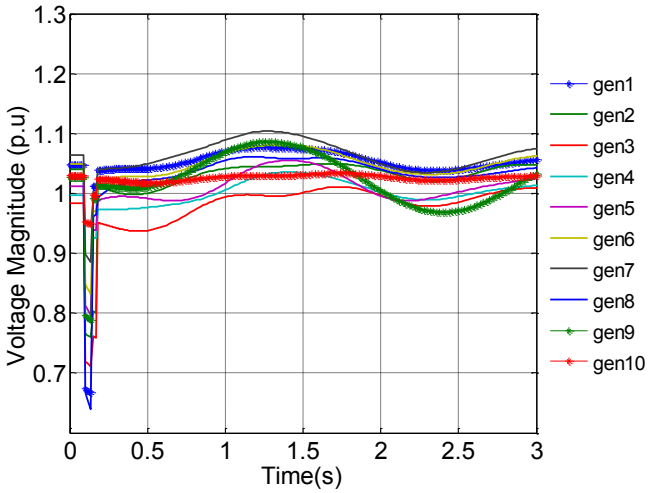

Figure 6.4 Voltage profiles of all generators after three-phase fault

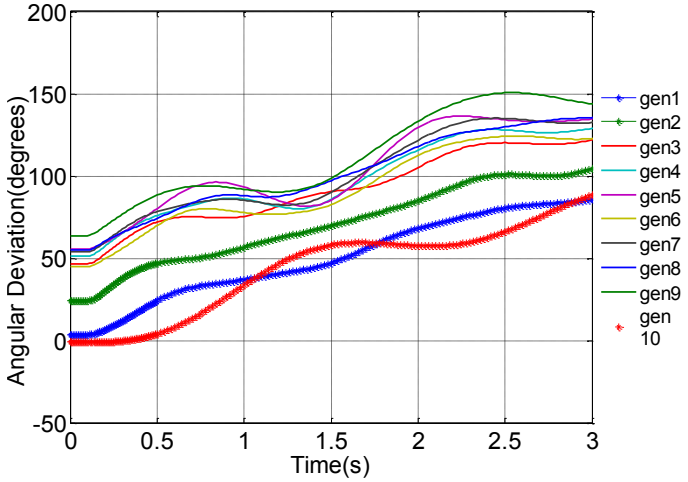

Figure 6.5 Angular profiles of all generators after three-phase fault

6.4.1 Training and Testing of Predictor with Normal Data

To train RVM and SVM predictors, three cases are considered. In Case-1 voltage magnitudes are used to train SVM and RVM predictor. In Case-2 and Case-3 angle magnitudes and combined phasors are considered, respectively.

Cross validation method is used to find optimal values of soft margin parameter (C) and width of gaussian kernel in SVM and RVM predictors. Comparitive analysis for all cases is performed by calculating the prediction error. For example, if two samples of input voltage magnitudes features are selected the prediction error is 77.83% in SVM and 6.88% in RVM for three phase faults. Similarly, the prediction error for all cases are determined and shown in Table 6.1,6.2, and 6.3.

Table 6.1

Comparison between SVM and RVM predictor for three- phase faults

Type of Phasor	Number of Samples	SVM		RVM	
		Error	Support Vectors	Error	Relevance Vectors
Voltage Phasor	2	77.83	1358	6.88	119
	3	13.19	1128	6.88	86
	4	7.61	1358	6.88	21
	5	7.39	1329	6.88	24
	6	6.30	1322	6.75	68
	7	6.74	1297	6.75	48
Angle Phasor	2	92.6	1368	7.88	27
	3	14.13	1234	7.75	32
	4	6.30	1380	7.63	30
	5	8.04	1350	7.12	21
	6	8.04	1315	7.25	23
	7	8.04	1149	6.38	24
Combined Phasor	2	26.09	992	6.88	13
	3	13.9	695	6.88	14
	4	12.17	638	6.88	18
	5	11.09	709	6.88	10
	6	9.35	964	6.88	15
	7	8.04	976	6.63	19

Table 6.2

Comparison between SVM and RVM predictor for line-to-line faults

Type of Phasor	Number of Samples	SVM		RVM	
		Error	Support Vectors	Error	Relevance Vectors
Voltage Phasor	2	72.39	1380	3.50	80
	3	9.57	1167	3.50	27
	4	4.78	1339	3.38	10
	5	5.2	1292	3.38	7
	6	5.2	1242	3.25	6
	7	4.78	1314	3.25	11
Angle Phasor	2	95.65	1380	5.88	31
	3	8.48	1204	5.75	29
	4	5.87	1227	5.38	26
	5	3.04	1372	4.0	18
	6	3.91	1371	3.88	17
	7	3.70	1313	3.50	13
Combined Phasor	2	85.0	1352	3.75	11
	3	6.0	1340	3.75	15
	4	5.6	897	3.62	15
	5	6.52	1380	3.62	13
	6	4.78	1380	3.88	15
	7	4.35	1372	3.62	21

Table 6.3

Comparison between SVM and RVM predictor for line- to- ground faults

Type of Phasor	Number of Samples	SVM		RVM	
		Error	Support Vectors	Error	Relevance Vectors
Voltage Phasor	2	74.35	1173	2.50	119
	3	10.43	1151	2.25	86
	4	5.22	1316	2.0	21
	5	6.09	756	1.75	24
	6	4.57	951	2.0	68
	7	4.35	1081	2.0	48
Angle Phasor	2	93.91	1377	5.50	29
	3	5.65	1379	5.25	29
	4	3.7	1305	5.25	29
	5	5.0	1380	4.00	18
	6	5.43	1329	3.75	21
	7	4.35	1346	3.50	13
Combined Phasor	2	20.43	1301	3.75	11
	3	4.78	1325	3.75	15
	4	5.22	824	3.62	15
	5	5.22	1127	3.62	13
	6	4.57	1236	3.88	17
	7	4.35	1306	3.62	21

From Table 6.1, 6.2, and 6.3, it is observed that as numbers of sample increases, a gradual improvement in classification is obtained. A close inspection of SVM error reveals that at least four sample values are required for correct classification (error less than 10%), as misclassification error at 2nd and 3rd sample is very large. However, from 4th sample value deviation in error is small. RVM error column shows that even 2nd and 3rd sample value are quite near to final error values. It is concluded from this result that RVM predictor is able to make accurate predictions even with three sample values with an overall accuracy of 95.20%. RVM errors are always less than SVM errors for every fault case. Further, number of relevance vectors required for classification is very less as compared to support vectors, which makes RVM predictor faster compared to SVM predictor.

Results shows that, magnitude of generator bus voltage and complete phasor are the best input feature vector for transient stability prediction. Voltage magnitude inputs and complete phasors results in good classification in both RVM and SVM based predictors. From results, it is observed that magnitude of errors are significantly small in case of RVM stability predictor than SVM stability predictor.

RVM predictor is able to make accurate predictions even with three sample values. Therefore, to check the prediction accuracy on testing data, three sample values of generator voltage magnitudes or complete phasors are taken for various faults.

Table 6.4 presents three phase fault results when three samples of the normal data (without measurement errors) are used for both training and testing. Results show that, RVM predictor is able to predict all stable (292) cases accurately. However, two unstable (2/208) cases are misclassified as stable, when combined phasors are considered. When voltage magnitude is considered, all unstable cases are accurately predicted (230/230) however, two stable cases are misclassified as unstable (2/270).

Table 6.4

RVM prediction for three-phase faults without measurement errors

Condition	Prediction Accuracy on Testing Data			
	Combined Phasor		Voltage magnitudes	
	Classified as Stable	Classified as Unstable	Classified as Stable	Classified as Unstable
Stable cases	292/292	0/292	268/270	2/270
Unstable cases	2/208	206/208	0/230	230/230

Similarly, Table 6.5 and 6.6 represents results for line-to-ground and line-to-line faults respectively. From above results, it can be concluded again that the best-input feature for RVM predictor is generator-bus voltage magnitudes and complete phasor.

Table 6.5

RVM prediction for line- to-ground faults without measurement errors

Condition	Prediction Accuracy on Testing Data			
	Combined Phasor		Voltage magnitudes	
	Classified as Stable	Classified as Unstable	Classified as Stable	Classified as Unstable
Stable cases	332/332	0/332	315/315	0/315
Unstable cases	0/168	168/168	0/185	185/185

Table 6.6

RVM prediction for line-to-line faults without measurement errors

Condition	Prediction Accuracy on Testing Data			
	Combined Phasor		Voltage magnitudes	
	Classified as Stable	Classified as Unstable	Classified as Stable	Classified as Unstable
Stable cases	333/333	0/333	315/315	0/315
Unstable cases	0/167	167/167	0/185	185/185

6.4.2 Training and Testing of Predictor with Noisy Data

According to [47] total vector error for PMUs should be less than 1%, which means voltage measurements can have maximum error of 1%. To check the performance of RVM predictor for these measurement errors, random error between 0 to 1% is added to all bus voltages and a noisy database is generated. Two different cases are considered in this work for noisy data. In Case-1, normal data is utilized for training and noisy data for testing, and Case-2 considers noisy data for training and testing of RVM predictors. In each case, three input samples are taken as input feature vector. Classification results so obtained are shown in Tables 6.7- 6.11.

Table 6.7 shows, results when training is done with the normal data, and testing is carried out with noisy data, for three phase faults. From this table, it is observed that RVM predictor accurately predicts all stable cases (280/280) and (270/270) for the complete phasors and voltage magnitudes respectively. For the complete phasor, unstable misclassification is (46/220), which means 46 unstable cases are misclassified as stable and (174/220) are predicted correctly. However, 116 unstable cases are misclassified as stable (116/230) for voltage magnitudes.

Table 6.7 (CASE-1)

RVM prediction for three-phase faults with measurement errors

(Training with normal data)

Condition	Prediction Accuracy on Testing Data			
	Combined Phasor		Voltage magnitudes	
	Classified as Stable	Classified as Unstable	Classified as Stable	Classified as Unstable
Stable cases	280/280	0/280	270/270	0/270
Unstable cases	46/220	174/220	116/230	114/270

Table 6.8, depicts prediction results for three-phase fault, when training and testing both is carried out with noisy data.

Table 6.8(CASE-2)

RVM prediction for three- phase faults with measurement errors

(Training with noisy data)

Condition	Prediction Accuracy on Testing Data			
	Combined Phasor		Voltage magnitudes	
	Classified as Stable	Classified as Unstable	Classified as Stable	Classified as Unstable
Stable cases	300/300	0/300	297/297	0/297
Unstable cases	0/200	200/200	1/230	229/230

Table 6.8 shows significant improvement in misclassification error, only single unstable case is predicted stable (1/230) for voltage magnitudes. All stable and unstable cases are correctly classified, with zero classification error for the complete phasor input. Likewise, prediction results are obtained for line to line and line to ground fault for 3 sample values, results for all cases are given in Tables 6.9, 6.10, 6.11 and 6.12.

Table 6.9 (CASE-1)

RVM prediction for line- to- ground faults with measurement errors

(Training with normal data)

Condition	Prediction Accuracy on Testing Data			
	Combined Phasor		Voltage magnitudes	
	Classified as Stable	Classified as Unstable	Classified as Stable	Classified as Unstable
Stable cases	333/333	0/333	315/315	0/315
Unstable cases	51/167	116/167	54/185	131/185

Table 6.10 (CASE-2)

RVM prediction for line-to-ground faults with measurement errors

(Training with noisy data)

Condition	Prediction Accuracy on Testing Data			
	Combined Phasor		Voltage magnitudes	
	Classified as Stable	Classified as Unstable	Classified as Stable	Classified as Unstable
Stable cases	332/332	0/332	358/358	0/358
Unstable cases	0/168	168/168	0/144	144/144

Table 6.11(CASE-1)

RVM prediction for line-to-line faults with measurement errors

(Training with normal data)

Condition	Prediction Accuracy on Testing Data			
	Combined Phasor		Voltage magnitudes	
	Classified as Stable	Classified as Unstable	Classified as Stable	Classified as Unstable
Stable cases	333/333	0/333	315/315	0/315
Unstable cases	51/167	116/167	54/185	131/185

Table 6.12 (CASE-2)

RVM prediction for line- to- line faults with measurement errors

(Training with noisy data)

Condition	Prediction Accuracy on Testing Data			
	Combined Phasor		Voltage magnitudes	
	Classified as Stable	Classified as Unstable	Classified as Stable	Classified as Unstable
Stable cases	332/332	0/332	357/358	1/358
Unstable cases	0/168	168/168	0/144	144/144

The above results show that RVM trained with noisy data gives the accurate results. Results obtained either by voltage magnitudes or complete phasors as inputs are almost the same.

6.5 CONCLUSION

- In this chapter, a fast RVM based transient stability predictor is proposed. The proposed scheme is faster and more accurate compared to SVM predictor. Generator bus voltage

or generator bus angle or complete phasor has been taken as the input to the RVM transient stability predictor. Number of samples of these inputs are varied from 2 to 7 for training and testing. Output of the PMU's are taken as input to the RVM predictor. Data avialable from the PMU can have the noise. Therefore, a RVM transient stability predictor for noise data has also been proposed in this work. The proposed RVM transient stability predictor for normal and noisy data has been successfully tested on 39 bus New England system.

- Results shows that RVM predictor is more accurate with voltage magnitude or complete phasor input. Therefore, it is concluded from the results that either the bus voltage magnitude or complete phasor can be used as input to the predictor. From Table 6.1-6.12, it is observed that RVM classifier can efficiently predict the transient stability of a given power system with 95% accuracy with only three samples of input feature vector.

CHAPTER-7
Conclusion and Future Scope

7.1 GENERAL

In interconnected and geographically distributed power systems, it is essential to have a synchronized measurement technique to have global view of the system. Further, to carry out various operations and analysis in real-time, measurement- telemetry of the system should be fast and accurate. Wide-area monitoring systems (WAMS) with Phasor measurements units (PMUs) provide synchronized phasors with fast reporting rates and are most suitable choice for today's ever-changing power system. Therefore, the aim of this dissertation is to study the various issues regarding, optimal placement of phasor measurement units and utilization of PMU measurements for control of rotor-angle stability problem. Proposed PMU allocation techniques will be beneficial in monitoring power system and other applications. Since, proper allocation of PMU plays a decisive role in rotor angle stability. Therefore, developed methodologies will be useful for monitoring and control of rotor angle stability in real-time. Thus, presented work will be helpful in preventing system from severe angular catastrophes

In present chapter, various findings of the conducted research work are summarized first and later few suggestions for future work in this area are discussed.

7. 2 SUMMARY OF THE IMPORTANT FINDINGS

In chapter 2, Binary Particle Swarm Optimization (BPSO) based quadratic technique is proposed considering observability, redundancy, and conventional measurements together in a single objective function. With formulated objective function, optimal PMU locations are computed for four test systems, which are IEEE-7, 14, 30, and 57 bus systems. Complete and incomplete observability cases are considered for each test system. Results with proposed approach are compared with results of references [17, 16, 108] and with solutions obtained through GAMS-MIP solver. From results, obtained in this chapter following conclusions are drawn

- Proposed approach is able to find optimal number of PMUs for given systems accurately. Results with proposed technique are in complete agreement with references [17,16, 108] and GAMS-MIP solver.
- In most systems, proposed approach successfully provides optimal number of PMUs. However, it is unable to provide optimal locations in the given system i.e. PMU locations may vary in the system with same number of PMUs.
- In general, with increase in size of the network, ambiguity in PMU locations increases more.

With swift development in synchrophasor technology, utilities want to place PMUs to assist real-time power system applications. In Chapter 3, a new approach is proposed to sequentially place the PMUs in the power system for monitoring power flows. Demand and Flow coverage concept is introduced. Based on conventional load flow, flow pattern are generated. In proposed PMU placement scheme, those demand nodes are selected, which maximizes the demand-coverage and flow-coverage simultaneously. The results, obtained on IEEE-14 and NE 39 bus systems, provide following conclusions

- The proposed strategy can be utilized by utilities in applications where power flows and demands plays significant role for example in congestion management
- With proposed method significant demand nodes and maximum flow of the given network can be monitored
- Proposed method is quite general and can be applied for various operating conditions. Formulation is extended for multiple flow patterns and is successfully applied on two test systems for deployment of PMUs.
- In comparison to traditional observability results, proposed placement scheme requires large number of PMUs to achieve complete flow coverage and demand coverage. Further, it is observed that PMU locations in a particular phase may vary from previous phase/stage.

To assist power system rotor-angle stability, it is essential to place PMU on generator terminals to have real-time values of the rotor angle. However, placing PMUs on all generator buses are not feasible. Further, in small signal analysis, it is essential to observe tie-lines also. Therefore, in chapter 4, a ranking scheme is proposed based on control strategy for small signal stability. First modes causing inter area oscillations are identified and later a control scheme is proposed to nullify these modes of oscillations. Based on control scheme, critical generator and tie lines

are selected. PMUs are placed in stages, such that these critical buses are observed in first stages only. Following are important findings of this work

- Proposed approach is quite general and can be applied without any significant changes to transient stability analysis
- Proposed scheme guarantees complete observability of the system as well as it also helps in control and monitoring of small signal stability, by placing PMUs on all critical generator, load and tie-lines within phase of placement
- After first stage of placement, PMU measurements can be utilized further, to identify inter area modes using direct measurement based mode identification technique.
- Placement results obtained from proposed technique are robust in nature. This means that every location of n^{th} stage is a subset of $(n+1)^{th}$ stage.

In Chapter 5, remote measurements from PMUs are utilized to damp inter area oscillations prevailing in a wide area network. Wide area damping controllers based on fuzzy systems are designed. Mamdani, Adaptive Neuro Fuzzy Inference systems (ANFIS) and Fuzzy type-2 controllers are designed. Communication delay and various measurement uncertainties are further considered in designing these controllers. From simulation results obtained on two area four machine and five- area sixteen machine system, following conclusions are derived.

- The proposed damping controllers based on Mamdani inference systems are able to damp out inter oscillation effectively compared to local PSS with delayed feedback signals.
- In large systems, designing of fuzzy rules is difficult, in such situations; proposed ANFIS based controllers are quite successful. Further, these controllers are quite robust towards parameter variation and delays.
- Proposed Type-2 controllers can model uncertainties in their structure. Therefore, they are capable to model uncertain and delayed remote measurements. Hence, damping controllers based on type-2 system can nullify the effects of inter area modes quite efficiently, with proper tuning of FOU.

In chapter 6, a new transient stability predictor based on Relevance Vector Machine (RVM) is designed to predict transients in the system. Since, PMU provides voltage and current phasors. Therefore, sampled values of voltage phasors are utilized to predict transient stability. A comparative analysis is also conducted between SVM and proposed RVM predictors. Prediction results of NE-39 bus system, provides following conclusions

- It is observed from prediction results that RVM predictor provides much better results than SVM predictor.
- RVM Predictors are able to make accurate predictions even with less number of sample values and kernel functions, with an overall accuracy of 95.20%. This means that proposed controllers are fast and accurate.
- From prediction results, it is concluded that complete voltage phasors and voltage magnitudes are effective inputs to predict transient stability, compared to angle magnitudes.

7.3 SCOPE FOR FUTURE RESEARCH

As a result, of the investigations carried out in this thesis, following topics are identified for future research in this area:

- ❖ Proposed PMU placement schemes can be extended by considering number of PMU channels, which is recent topic of interest.
- ❖ Placement scheme to monitor power flows can be extended for congestion management application.
- ❖ Performance of proposed fuzzy type-2 controllers can be improved by tuning each FOU separately using optimization techniques like Genetic Algorithm or PSO.
- ❖ In present work, Type-1 ANFIS controllers are designed as damping controller. However, in future Type-2 ANFIS controllers can be designed, which will be robust and adaptive in nature.
- ❖ Proposed transient stability predictor is a binary classifier, which can be extended to predict relative stability through stability margin.
- ❖ Present thesis primarily focused on application of synchrophasors to the angular stability. The work can be extended for other possible applications in the power systems.

REFERENCES

[1] Abur ,“Optimal placement of phasor measurements units for state estimation”, PSERC Publication 06-58, October 2005

[2] A. Prince, N. Senroy , R Balasubramanian, “Targeted approach to apply masking signal-based empirical mode decomposition for mode dynamic power system wide area measurement signal data”, IET generation, transmission and distribution,vol.5, no.10,pp 1025-1032, October 2011

[3] A.D. Rajapakse, F.R. Gomez, K. Nanayakkara, P.A. Crossley, and V.T. Terzija, “Rotor Angle Instability Prediction Using Post-Disturbance Voltage Trajectories”, IEEE Transactions on Power Systems, vol. 25, no. 2, pp. 947–956, May 2010

[4] A.E. Gavoyiannis, D.G. Vogiatzis, D.R. Georgiadis, and N.D. Hatziargyriou, “Combined support vector classifiers using fuzzy clustering for dynamic security assessment”, IEEE Power Engineering Society Summer Meeting, vol. 2, pp. 1281–1286, July 2001

[5] A.G. Phadke, J. S. Thorp, and K. J. Karimi, “State Estimation with Phasor Measurements”, IEEE Transactions on Power Systems, vol. 1, no. 1, pp. 233-238, February 1986

[6] A.G. Phadke, J.S. Thorp, R.F. Nuqui and M. Zhou, “Recent Developments in State Estimation with Phasor Measurements” IEEE/PES Power Systems Conference and Exposition, pp. 1-7, April 2009

[7] A.M.A Hamdan, A.M. Elabdalla, On the coupling measures between modes and state variables and subsynchronous resonance”, Electric Power System Research, vol. 13, no.3, pp.165-171, December 1987

[8] A.M.A Hamdan, A.M. Elabdalla,“Geometric measures of modal controllability and observability of power system models”, Electric Power System Research, vol. 15, no. 2, pp. 147-155, October 1988

[9] A.R. Messina, Inter area oscillation in power systems: A Non linear and Nonstationary perspective, Springer, 2009

[10] A.R. Messina, V. Vittal, G.T. Heydt, T.J. Browne, “Nonstationary Approaches to Trend Identification and Denoising of Measured Power System Oscillations”, IEEE Transactions on Power Systems, vol.24, no.4, pp.1798,1807, November 2009

[11] B. Naduvathuparambil, M.C. Valenti, A. Feliachi, “Communication delays in wide area measurement systems”, Thirty-Fourth Southeastern Symposium on System Theory, pp. 118-122, 2002

[12] B. Changaroon, S.C. Srivastava, D.Thukaram, “A neural network based power system stabilizer suitable for on-line training-a practical case study for EGAT system”, IEEE Transactions on Energy Conversion, vol.15, no.1, pp.103-109, March 2000

[13] B. Chaudhuri, B.C. Pal, “Robust damping of multiple swing modes employing global stabilizing signals with a TCSC ”, IEEE Transactions on Power System, vol. 19, no.1, pp. 499-506, Februrary 2004

[14] B. Chaudhuri, B.C. Pal, A.C. Zolotas, I. M. Jaimoukha, T. C. Green, “Mixed-sensitivity approach to H-infinity control of power system oscillations employing multiple FACTS devices”, IEEE Power Engineering Society General Meeting, vol.4, pp.13-17 July 2003

[15] B. Chaudhuri, R. Majumder, B.C. Pal, “Wide-Area Measurement-Based Stabilizing Control of Power System Considering Signal Transmission Delay”, IEEE Transactions on Power System, vol.19, no. 4, pp. 1971-1979, November 2004

[16] B. Gou, “Generalized Integer programming formulation for optimal PMU placement,” IEEE Transactions on Power Systems, vol. 23, no. 3, pp. 1099-1104, August 2008

[17] B. Gou, “Optimal placement of PMUs by integer linear programming,” IEEE Transactions on Power Systems, vol. 23, no. 3, pp. 1525-1526, August 2008

[18] B. Ravikumar, D. Thukaram, H.P. Khincha, “Application of support vector machines for fault diagnosis in power transmission system,” IET Generation, Transmission and Distribution, vol. 2, no.1, pp.119-130, January 2008

[19] B. Xu and A. Abur, “Observability analysis and measurement placement for systems with PMUs,” IEEE/ PES Power Systems Conference and Exposition, vol. 2, pp. 943-946, October 2004

[20] B.H. Lee, R.A. Deininger , “Optimal Locations of monitoring stations in water distribution systems”, Journal of Environmental Engineering, vol. 118, no. 1, pp. 4-17, February1992.

[21] B.K. Saha Roy, A.K. Sinha, A.K. Pradhan, “An optimal PMU placement Technique for power system observability”, International Journal of Electrical Power and Energy Systems, vol.42, no.1, pp. 71-77, November 2012

[22] B.K. Saha Roy, A.K. Sinha, A.K. Pradhan, “Synchrophasor Assisted Prediction of Stability/Instability of a power system”, International Journal of Emerging Electric Power and Energy Systems, vol. 14, no.1, pp.1-8, May 2013

[23] B.P. Padhy, S.C. Srivastava, N.K. Verma, “A Coherency-Based Approach for Signal Selection for Wide Area Stabilizing Control in Power Systems”, IEEE Systems Journal, vol.7, no.4, pp.807-816, December 2013

[24] B.P. Padhy, S.C. Srivastava, N.K. Verma, “Robust wide area TS fuzzy output feedback controller for enhancement of stability in multimachine Power System”, IEEE Systems Journal , vol. 6, no. 3, pp. 426-435, September 2012

[25] C. Sharma, B. Tyagi, “Wide area fuzzy controller design considering time latencies in communication networks”, National Power System Conference (NPSC-2012), IIT BHU, Varanasi, 12-14, pp.1-4, December 2012

[26] C. Su, Z. Chen, “Optimal Placement of Phasor Measurement Units with New Considerations”, Asia-Pacific International Conference on Power and Energy Engineering, pp. 1-4, March 2010

[27] C.W. Liu, J. Thorp, “Application of Synchronized Phasor Measurements to Real-time Transient Stability Prediction ”, IEE Generation Transmission Distribution, Vol. 142. No. 4, pp.355-360, July 1995

[28] Dua, S. Dambhare, R.K. Gajbhiye, and S.A. Soman, “Optimal multistage scheduling of PMU placement: an ILP approach”, IEEE Transactions on Power Delivery, vol. 23, no.4 , pp. 1812–1820, October 2008

[29] D.J. Trudnowski, “Estimating Electromechanical Mode Shape From Synchrophasor Measurements”, IEEE Transactions on Power Systems, vol.23, no.3, pp.1188-1195, August 2008

[30] D.J.C. Mackay, “The Evidence Framework Applied to classification networks”, Neural Computaion, vol.4, no.5, pp.720-736, 1992

[31] D.R. Vega and M. Pavella, “A Comprehensive Approach to Transient Stability Control. I. Near Optimal Preventive Control ”, IEEE Transactions on Power System, vol. 18, no.4, pp. 1446–1453 , November 2003

[32] F. Aminifar, F. Fotuhi, M. Shahidehpour, A. Khodaei, “Observability enhancement by optimal PMU placement considering random power system outages”, Energy Systems, vol. 2, no.1 , pp. 45-65, 2011

[33] F. Aminifar, S.S. Bagheri, F.M. Fotuhi, M. Shahidehpour, “Reliability Modeling of PMUs Using Fuzzy Sets”, IEEE Transactions on Power Delivery, vol. 25, no. 4, pp. 2384-2391, 2010

[34] F. Hashiesh, H.E. Mostafa, M.M. Mansour, A.R. Khatib and I. Helal, “Wide Area Transient Stability Prediction using On-line Artificial Neural Networks”, IEEE Electric Power Conference, pp.1-7, October 2008

[35] FA. Snyder, N. Hadjsaid, D. Georges, L. Mili, A. G. Phadke, O. Faucon, and S. Vitet, “ Inter-area oscillation damping with power system stabilizers and synchronized phasor measurements,” International Conference on Power System Technology, vol. 2, pp. 790-794, 1998

[36] F.F. Song, T.S. Bi, and Q.X. Yang, “Study on Wide Area Measurement System Based Transient Stability Control for Power Systems”, 7th International Power Engineering Conference, vol. 2, pp. 757–760, December2005

[37] F.H. Fesharaki, R.A. Hooshmand, A. Khodabakhshian, “A new Method for simultaneous optimal placement of PMUs and PDCs for maximizing data transmission reliability along with providing the power system observability”, Electric Power System Research, vol. 100, pp. 43-54, July 2013

[38] F.R. Gomez, A.D. Rajapakse, U.D. Annakkage, and I.T. Fernando, “ Support Vector Machine-Based Algorithm for Post-Fault Transient Stability Status Prediction Using Synchronized Measurements”, IEEE Transactions on Power Systems, vol. 26, no. 3, pp. 1474-1483, August 2011

[39] G. Rogers, Power System Oscillations, Kluwer: Norwell MA, 2000

[40] G.E. Boukarim, S. Wang, J.H. Chow, G.N.Taranto, N. Martins, “A comparison of classical, robust, and decentralized control designs for multiple power system stabilizers”, IEEE Transactions on Power Systems, vol.15, no.4, pp.1287-1292, November 2000.

[41] G.Yu, B. Zang, Z. Bo, H. Xie, C.Wang, “Nonlinear robust control of power system considering wide-area signals delay and incompletness”, European Transactions on Electric Power, vol. 19, no.3, pp. 433-446, March 2009

[42] H. Dongchen, V. Venkatasubramanian, “New wide-area algorithms for detection and mitigation of angle instability using synchrophasors”, IEEE Power Engineering Society General Meeting, pp. 1-8, June 2007

[43] H. Ghasemi, “On-line monitoring and oscillatory stability margin prediction in power systems based on system identification,” Ph.D. dissertation, Univ. Waterloo, Waterloo, ON, Canada, 2006

[44] H. Ni, G.T. Heydt, L. Mili, “ Power System Stability Agents Using Robust Wide Area Control”, IEEE Transactions on Power System, vol.17 , no.4 , pp.1123-1131, November 2002

[45] Hu Zhijian, "H_∞ control of inter-area oscillations based on WAMs considering signals transmission delay", 2nd IEEE Conference in Industrial Electronics and Applications, pp. 1453-1458, May 2007

[46] H.M. Behbehani, J. Bialek, Z. Lubosny, "Enhancement of Power System Stability using Fuzzy Logic based Supervisory Power System Stabilizer", 2nd IEEE International Conference on Power and Energy, pp. 479-484, December 2008

[47] IEEE Standards for synchrophasors for Power Systems, IEEE Std. C37.118-2005 (Revision of IEEE Std.1344-1995), 2006

[48] J.H Chow and G. Rogers, Power System Toolbox Version 3.0. Cobourg, ON, Canada, Cherry Tree Scientific Software, 2008 [Online]. Available: http://www.etk.ee.kth.se

[49] J.F. Hauer, ''Application of Prony analysis to the determination of modal content and equivalent models for measured power system response,'' IEEE Transactions on Power Systems, vol. 6, no. 3, pp. 1062–1068, August 1991

[50] J.D. Trudnowski and J. W. Pierre, "Overview of algorithms for estimating swing modes form measured responses," IEEE Power and Energy Society General Meeting, pp. 1–8, July 2009

[51] J. Zhang, G. Welch, G. Bishop, "Observability and estimation uncertainty analysis for PMU placement alternatives", North American Power Symposium (NAPS 2010), Arlington, TX, U.S.A., pp.1-8, September 2010

[52] J.C. Cepeda, J.L. Rueda, I. Erlich, D.G. Colome, "Probabilistic Approach - Based PMU Placement for Real-Time Power System Vulnerability Assessment", IEEE/ PES Innovative Smart Grid Technologies Europe, pp. 1-8, October 2012

[53] J.D.L. Ree, V. Centeno, J.S. Thorp, and A.G. Phadke, "Synchronized Phasor Measurement Applications in Power Systems", IEEE Transactions on Smart Grid, vol. 1, no. 1, pp. 20-27, June 2010

[54] J.H. Chow, K.W. Cheung, "A toolbox for power system dynamics and control engineering education and research", IEEE Transactions on Power Systems, vol.7, no.4, pp.1559-1564, November 1992

[55] J.L Rueda, W.H Guaman, J.C.Cepeda, I Erlich, A Vargas , "Hybrid Approach for Power System Operational Planning With Smart Grid and Small-Signal Stability Enhancement Considerations", IEEE Transactions on Smart Grid, vol.4, no.1, pp.530-539, March 2013

[56] J.L. Rueda, C.A. Juárez, and I. Erlich,"Wavelet-Based Analysis of Power System Low-Frequency Electromechanical Oscillations" IEEE Transactions on power systems, vol. 26, no. 3, August 2011

[57] J.L. Rueda, I. Erlich, “Probabilistic framework for risk analysis of power system small signal stability”, Journal of Risk and Reliability, Special Issue Paper, vol. 226, pp.118-133, October 2011

[58] J.L. Rueda, J.C. Cepeda, I. Erlich, A. Vargas, “Hybrid approach for power system operational planning with smart grid and small-signal stability enhancement considerations”, IEEE Transactions on Smart Grid, vol. 4, no. 1, pp. 530-539, March 2013

[59] J.M Mendel, R.I John, F. Liu, “Interval type-2 fuzzy logic systems made simple”, IEEE Transactions on Fuzzy Systems, vol. 14, no.6, pp. 808-821, December 2006

[60] J.R. Hockenberry, B.C. Lesieutre, “Evaluation of uncertainty in dynamic simulations of Power system models: the probabilistic collocation method”, IEEE Transactions on Power System, vol.19, no.3, pp.1483-1491, August 2004

[61] J.S. Thorp, A.G. Phadke, S.H. Horowitz, M.M. Begovic, “Some Applications of Phasor Measurements to Adaptive Protection”, IEEE Transactions on Power Systems, vol.3, no.2, pp.791-798, May 1988

[62] J.S.R. Jang, “ ANFIS: adaptive-network-based fuzzy inference system,” IEEE Transactions on Systems, Man and Cybernetics, vol.23, no.3 , pp.665-685, June 1993

[63] J.S.R. Jang, “Self-learning fuzzy controllers based on temporal backpropagation,” IEEE Transactions on Neural Networks, vol. 3,no.5 , pp. 714-723, September 1992

[64] J.S.Throp and A.G.Phadke, Synchronized phasor measurement and thier applications, Spinger, 2008

[65] J.W. Stahlhut, T.J. Browne, G.T. Heydt, V.Vittal, “Latency viewed as a stochastic process and its impact on wide area power system control signals”, IEEE Transactions on Power System, vol. 23, no.1, pp. 84-91, Februrary 2008

[66] K. Mazlumi, H. Vahedi, S.M. Ezzati, “Optimal Placement of Pmus in Power Systems Using Heuristic Algorithms and Mixed Integer Non Linear Programming Methods”, International Conference on Electrical Engineering/Electronics Computer Telecommunications and Information Technology (ECTI-CON), pp. 805-809, 19-21 May 2010.

[67] K. Seethalaksmi, S.N. Singh, S.C.Srivastava, “Wide Area Protection and Control: Present Status and Key Challenges”, in Proceeding of 15th National Power System Conference, IIT- Bombay, pp.169-175, December 2008

[68] K. Uhlen, L. Vanfretti, M. M. De Oliveira, A.B. Leirbukt, V. H. Aarstrand, J. O. Gjerde, “Wide-Area Power Oscillation Damper implementation and testing in the Norwegian transmission network”, IEEE Power and Energy Society General Meeting, pp.1-7, 22-26 July 2012

[69] L. Chunyan, D. Changhong, S. Yuanzhang, C. Xiangyi, “An on-line transient stability emergency control strategy based on PMU forecasted trajectory”, International Power Engineering Conference, pp.807-812, 3-6 December 2007

[70] L. Qiao, C. Tao, W. Yang, N. Rohit, F. Franz, D.I. Marija, “ An Information - Theoretic Approach to PMU Placement in Electric Power Systems”, IEEE Transactions on Smart Grid, vol. 4, no.1 , pp. 446-456, March 2013

[71] L.A Zadeh, “The concept of a linguistic variable and its application to approximate reasoning-II”, Information Sciences, vol. 8, no.4, pp. 301-357, 1975

[72] L.Qilian, J.M Mendel, “Interval type-2 fuzzy logic systems: theory and design”, IEEE Transactions on Fuzzy Systems, vol.8, no.5, pp. 535-550, October 2000

[73] L.S. Moulin, A.P.A. da Silva, M.A. El-Sharkawi, and R.J. Marks II , “Support Vector Machines for Transient Stability Analysis of Large-Scale Power Systems”, IEEE Transactions of Power System, vol. 19, no.2, pp. 818–825, May 2004

[74] Li Husheng, Lai Lifeng, Zhang Weiyi, “Communication Requirement for Reliable and Secure State Estimation and Control in Smart Grid”, IEEE Transactions on Smart Grid, vol.2, no.3, pp.476-486, September 2011

[75] M. Chenine, L. Nordstrom, “Modeling and simulation of wide-area communication for centralized PMU-based applications”, IEEE Transactions on Power Delivery, vol. 26, no.3, pp.1372-1380, July 2011

[76] M.J. Gibbard, N. Martins, J. J. Sanchez-Gasca, N. Uchida, V. Vittal, and L.Wang, “Recent applications of linear analysis techniques,” IEEE Transactions on Power System, vol. 16, no. 1, pp. 154–162, February 2001

[77] M. Pavella, D. Ernst, and D. Ruiz-Vega, Transient Stability of Power Systems: A Unified Approach to Assessment and Control, Boston, MA: Kluwer, 2000

[78] M. Ruofei, C. Hsiao-Hwa, H. Yu-Ren, M. Weixiao, “Smart Grid Communication: Its Challenges and Opportunities”, IEEE Transactions on Smart Grid, vol.4, no.1, pp.36-46, March 2013

[79] M. Shahraeini, M.H. Javidi, M.S. Ghazizadeh,“Comparison between communication infrastructures of centralized and decentralized wide area measurement systems”, IEEE Transactions on Smart Grid, vol. 2, no.1, pp. 206-211, March 2011

[80] M.A. Pai, Energy Function Analysis for Power System Stability. Boston, MA: Kluwer, 1989

[81] M.E. Tipping, “Bayesian Inference: An Introduction to Principles and Practice in Machine Learning”, In O. Bousquet, U. von. Luxburg, G. Ratsch (Eds), Advanced Lectures on Machine Learning, Springer, pp. 41-62, 2004

[82] M.E. Tipping, “Sparse Bayesian Learning and The Relevance Vector Machine”, Journal of Machine Learning Research, vol. 1, pp. 211-244, June 2001

[83] M.E. Tipping, “The Relevance Vector Machine, In S.A. Solla, T.K. Leen and K.R.(Eds) ”, Advances in Neural Information Processing Systems, vol. 12, pp. 652-658 , 2000

[84] Matlab User Guide, The Math Works, Inc., Natick MA, 1998.

[85] Molina, G.K. Venayagamoorthy, J. Liang, “Intelligent local area signals based damping of power system oscillations using virtual generators and approximate dynamic programming”, IEEE Transactions on Smart Grid, vol. 4, no. 1, pp. 498-508, March 2013

[86] N. Lin, D.Z. Gang, Z.J Gua, “Real-Time Transient Stability Prediction Based on Relevance Vector Learning Mechanism for Large-Scale Power System”, IEEE Conference on Electronics and Applications, pp.147-152, May 2007

[87] N. Martins, “Efficient Eigen-value and Frequency Response Methods Applied to Power System Small-Signal Stability Studies”, IEEE Transactions on Power Systems, vol.1, no.1, pp.217-224, February 1986

[88] N. Zhou, D. J. Trudnowski, J. W. Pierre, and W. A. Mittelstadt, “Electromechanical mode online estimation using regularized robust RLS methods,” IEEE Transactions on Power System, vol. 23, no. 4, pp. 1670–1680, November. 2008

[89] N. Zhou, J. W. Pierre, D. J. Trudnowski, R. T. Guttromson, ‘‘Robust RLS methods for online estimation of power system electromechanical modes,’’ IEEE Transactions on Power Systems, vol. 22, no. 3, pp. 1240–1249, August 2007

[90] N.N Karnik, J.M Mendel, L.Qilian, “Type-2 fuzzy logic systems”, IEEE Transactions on Fuzzy Systems, vol. 7, no.6, pp. 643-658, December 1999

[91] Novosel, “Benefits of PMU technology for various Applications”, Presented at the CIGRE-7th Symposium on Power System Management, pp. 1-13, Nov 2006

[92] O.Castillo, P. Melin, Type-2 Fuzzy Logic:Theory and Applications. Springer, 2008

[93] P. Kundur, Power System Stability and Control, Mc Graw-Hill: New York, 1994

[94] P. Korba, K. Uhlen, “Wide-area monitoring of electromechanical oscillations in the nordic power system: practical experience”, IET Generation, Transmission & Distribution, vol.4, no.10, pp.1116-1126, October 2010

[95] P. Kundur, J. Paserba, V. Ajjarapu, G. Anderson, A. Bose, C. Canizares, N. Hatziargyriou, D. Hill, A. Stankovic, C. Taylor, T.V. Caustem and V. Vittal, “ Defination and Classification of Power System Stability”, IEEE Transactions on Power System, vol. 19, no. 2, pp. 1387-1401, August 2004

[96] PS. Addison, J. N. Watson, and T. Feng, “Low-oscillation complex wavelets,” Journal of Sound and Vibration, vol. 254, no. 4, pp. 733–762, July 2002

[97] P. Tripathy, S. C. Srivastava and S. N. Singh, ‘‘A Noise Space decomposition based Method for Identifying Low frequency Oscillations using Synchro-Phasor Measurements,” IEEE General Meeting , Minnesota,USA, pp.1-6, July 2010

[98] P. Tripathy, S.C. Srivastava, S.N. Singh, “A divide by difference filter based algorithm for estimation of generator rotor angle utilizing synchrophasor measurements”, IEEE Transactions on Instrumentation and Measurement , vol. 59, no. 6, pp. 1562-1570, June 2010

[99] Performance of Three PSS for inter area oscillations , Mathworks, Matlab.

[100] Q. Gao, and S.M. Rovnyak, “Decision Trees Using Synchronized Phasor Measurements for Wide- Area Response-Based Control”, IEEE Transactions on Power Systems, vol. 26, no. 2 pp. 855-861, May 2011

[101] R. Gupta, B. Bandyopadhyay, A.M. Kulkarni, “Design of Power System Stabilizer for Single Machine System using Robust Periodic output Feedback Controller”, IET Generation, Transmission and Distribution,vol.150,no.2, pp. 211-216, March 2003

[102] R. Majumder, B. Chaudari, B.C. Pal, “Implementation and Test of a Wide-area Measurement-Based Controller for Damping Inter area Oscillations Considering Signal - Transmission Delay”, IET Generation, Transmission and Distribution,vol.1,no.1, pp. 1-7, January 2007

[103] R. Sodhi, S.C. Srivastava, and S.N. Singh, “Multi-criteria decision- making approach for multistage optimal placement of phasor measurement units”, IET Generation Transmission Distribution, vol. 5, no. 2 , pp. 181–190, February 2011

[104] R. Sodhi, S.C. Srivastava, and S.N. Singh, “Optimal PMU placement method for complete topological and numerical observability of power system”, Electric Power System Research, vol. 80, no. 9, pp. 1154–1159, September 2010

[105] R. W. Wies, J. W. Pierre, D. J. Trudnowski, ‘‘Use of ARMA block processing for estimating stationary low-frequency electromechanical modes of power systems,’’ IEEE Transactions on Power Systems, vol. 18, no. 1, pp. 167–173, Februrary 2003

[106] R.F. Nuqui and A.G. Phadke, “Phasor measurement unit placement techniques for complete and incomplete observability,” IEEE Transactions on Power Delivery, vol. 20, no. 4, pp. 2381-2388, October 2005

[107] S. Avdakovic, A. Nuhanovic, M. Kusljugic, M. Music,"Wavelet transform applications in power system dynamics", Electric Power Systems Research , vol.83, no.1, pp. 237-245, Februrary 2012

[108] S. Chakrabarti and E. Kyriakides, "Optimal placement of phasor measurement units for power system observability", IEEE Transactions on Power System, vol. 23, no.3, pp.1433-1440, August 2008

[109] S. Chakrabarti, G.K. Venayagamoorthy, and E. Kyriakides, "PMU placement for power system observability using binary particle swarm optimization", Australasian Universities Power Engineering Conference, pp.1-5, December 2008

[110] S. Chen, J. Liu, and H. Lai, "Wavelet analysis for identification of damping ratios and natural frequencies," Journal of Sound and Vibration ,vol. 323, no. 1, pp. 130–147, March 2009

[111] S. Ghosh, N. Senroy, "The localness of electromechanical oscillations in power systems", International Journal of Electrical Power and Energy systems ,vol. 42,no.1,pp. 306-311, November 2012

[112] S. Kai, S. Likhate, V. Vittal, V.S. Kolluri, and S. Mandal, "An Online Dynamic Security Assessment Scheme using Phasor Measurements and Decision Trees", IEEE Transactions on Power System, vol. 22, no.4, pp. 1935–1943, November 2007

[113] S. Ray, G.K. Venayagamoorthy, "Real-time implementation of a measurement-based adaptive wide-area control system considering communication delays", IET Generation Transmission Distribution, vol.2, no.1, pp. 62-70, January 2008

[114] S.Chakrabarti, E.Kyriakides, D.G.Eliades, "Placement of Synchronized Measurements for Power System Observability", IEEE Transactions on Power Delivery, vol 24, no.1, pp. 12-19, January 2009

[115] T.J. Ross, Fuzzy Logic Engineering Applications,John Wiley 2005

[116] T.L. Saaty, "Decision making with Analytical Process", International Journal Services Sciences, vol. 1, no.1, pp. 83-98, 2008

[117] U.P. Mhaskar, A.M. Kulkarni, "Power oscillation damping using FACTS devices: modal controllability, observability in local signals, and location of transfer function zeros", IEEE Transactions on Power Systems, vol.21, no.1, pp.285-294, February 2006

[118] V.N. Vapnik, Statistical Learning Theory, Wiley, New York.1998

[119] W. Hongxia, N. Hui, G.T. Heydt, "The impact of time delay on robust control design in power systems", IEEE Power Engineering Society Winter Meeting, vol. 2, pp. 1511–1516, 2002

[120] W.J. Staszewski,“Identification Damping MDOF Syst. Using Time-Scale Decomposition”, Journal of Sound and Vibration, vol. 203, no. 2, pp. 283–305, June 1997

[121] W. Shaobu, M. Xiangyu, C. Tongwen, “Wide-Area Control of Power Systems Through Delayed Network Communication”, IEEE Transactions on Control Systems Technology, vol.20, no.2, pp.495-503, March 2012

[122] W.Huaren, W.Qi, and L.Xiaohui, “PMU based wide area damping control of power systems,” in Proc. Joint International Conference on Power system Technology and IEEE power India conference , 2008. pp.1-4

[123] W.Yao, L. Jiang, Q.H. Wu , J.Y. Wen, S.J.Cheng, “ Delay-Dependent stability analysis of the power system with a wide-area damping controller embedded”, IEEE Transactions on Power System, vol. 26, no.1, pp. 233-240, Februrary 2011

[124] W.Yao, L. Jiang, Q.H. Wu , J.Y. Wen, S.J.Cheng, “ Delay-Dependent stability analysis of the power system with a wide-area damping controller embedded”, IEEE Transactions on Power System, vol. 26, no.1, pp. 233-240, Februrary 2011

[125] Y.Chompoobutrgool, L. Vanfretti, M. Ghandhari, “Survey on power system stabilizers control and thier prospective applications for power system damping using synchrophasor-based wide area systems”, European Transactions on Electric Power, vol. 21, no.8, pp. 2098-2111, November 2011

[126] Y. del Valle, G. K. Venayagamoorthy, S. Mohagheghi, J. C. Hernandez, R. G. Harley, “Particle swarm optimization: basic concepts, variants and applications in power systems,” IEEE Trans. Evolutionary computation, vol. 12, no. 2, pp. 171-195, April 2008.

[127] Y. Xue, L. Wehenkel, R. Belhomme, P. Rousseaux, M. Pavella, E. Euxibie, B. Heilbronn, and J.F. Lesigne, “Extended Equal Area Criterion Revisited (EHV Power Systems)”, IEEE Transactions on Power System, vol. 7, no.3, pp. 1012–1022, August 1992

[128] Y. Ye, S .Yuanzhang, L. Guojie, “Evaluation of delayed input effects to PSS interarea damping control design”, IEEE Power Engineering Society General Meeting, pp.1-5, June 2007

[129] Y. Chompoobutrgool, L.Vanfretti, “Identification of power system dominant Inter-area oscillation paths,” IEEE Transactions on Power Systems, vol. 28, no. 3, pp. 2798–2807, August 2013

[130] Y.V. Markov, P. Du, T.B. Nguyen, X. Guo, J.W. Burns, J.F. Gronquist and M.A. Pai, “PMU-Based Wide Area Security Assessment: Concept, Method, and Implementation”, IEEE Transactions on Smart Grid, vol. 3, no.3, pp. 1325–1332, September 2012.

List of Publications

On the basis of research work carried out, following papers have been published/under review in international journals and published in proceedings of international/ National conferences.

INTERNATIONAL JOURNALS:

[1] Charu Sharma, Barjeev Tyagi," Ranking of Phasor Measurement Units based on Control strategy for Small signal Stability" *International Transactions on Electrical Energy Systems (Accepted)* May 2014.

[2] Charu Sharma, Barjeev Tyagi, "Fuzzy Type-2 Controller Design for Small Signal Stability Considering Time latencies and Uncertainties in PMU Measurements" *IEEE Systems Journal (Accepted)* June 2014.

[3] Charu Sharma, Barjeev Tyagi, "An Approach for Optimal placement using Binary particle Swarm Optimization with Conventional Measurements" *International Journal of Engineering, Science and Technology,* vol. 3, no.3, pp. 56-63, April 2011.

[4] Charu Sharma, Barjeev Tyagi, "Transient Stability Predictor based on Phasor Measurement" *Journal of Applied Soft Computing (Under-review).*

[5] Charu Sharma, Barjeev Tyagi, "Adaptive Neuro Fuzzy Wide Area Controller Design For Small Signal Stability" Expert Systems with Applications (*Under-review).*

INTERNATIONAL/NATIONAL CONFERENCES:

[1] Charu Sharma, Barjeev Tyagi, "Sequential PMU Placement To Monitor Power Flow In Integrated Power Systems" in Proceedings of *IEEE PES Transmission and Distribution Conference & Exposition-2014,* Chicago, USA, 9-14 April 2014.

[2] Charu Sharma, Barjeev Tyagi, "Transient Stability Status predictor based on Relevance Vector Machine" in Proceedings *of IEEE PES Innovative Smart Grid Technologies Conference(ISGT)-Asia*, Bangalore, 9-13 November, 2013.

[3] Charu Sharma, Barjeev Tyagi, "Fuzzy Controller Design Considering Time Latencies in Communication Networks" Proceedings of *17th* National Power

Systems Conference, (*NPSC-2012*), Department of Electrical Engineering, IIT-BHU Varanasi, 12 - 14 December 2012.

[4] Charu Sharma, Barjeev Tyagi, “An Approach For Optimal Placement Using Binary Particle Swarm Optimization With Conventional Measurements” Proceedings of National conference on Recent Advantages in Electrical Power and Energy System Management, (*RAEPSM-2011*), at M.M.M. Engineering College Gorakhpur (U.P.) on 25-26 March 2011.

[5] Charu Sharma, Yati Sharma, Barjeev Tyagi, “Identification of Inter area modes in an interconnected power systems using wavelets” Proceedings of IEEE conference INDICON, Indian Institute of Technology, Bombay, 10-13 December-2014.

APPENDIX-A
Data for IEEE- 14, IEEE- 30, AND IEEE- 57 bus systems

In this appendix, line data and bus data of IEEE-14, 30, and 57 bus system used in this thesis are given. For IEEE-14 bus system Line data and Bus data are presented in table A.1 and A.2 respectively. Bus data for 1EEE-30 bus system is given Table A.3. For same system, line data is given in A.4. Further, for IEEE-57 bus system line and bus data are given in Table A.5 and A.6 respectively.

Table A.1: Bus Data for IEEE-14 Bus System (in p.u.)

Bus	*Voltage*	P_G	Q_G	P_L	Q_L	*Bus type*
1	1.060	0	0	0	0	1
2	1.045	40	42.4	21.7	12.70	2
3	1.010	0	23.4	94.2	19.00	2
4	1	0	0	47.8	-3.90	3
5	1	0	0	7.60	1.60	3
6	1.070	0	12.2	11.2	7.50	2
7	1	0	0	0	0	3
8	1.090	0	17.4	0	0	2
9	1	0	0	29.5	16.6	3
10	1	0	0	9	5.80	3
11	1	0	0	3.50	1.80	3
12	1	0	0	6.10	1.60	3
13	1	0	0	13.5	5.80	3
14	1	0	0	14.9	5	3

Table A.2: Line Data for IEEE-14 Bus System (in p.u.)

From Bus	*To Bus*	*Resistance*	*Reactance*	*B shunt*	*Tap ratio*
1	2	0.01938	0.05917	0.0264	1
1	5	0.0540	0.22304	0.0246	1
2	3	0.0469	0.19797	0.0219	1
2	4	0.0581	0.17632	0.0170	1
2	5	0.0569	0.17388	0.0173	1
3	4	0.0670	0.17103	0.0064	1
4	5	0.0133	0.04211	0	1
4	7	0	0.20912	0	0.9780
4	9	0	0.55618	0	0.9690
5	6	0	0.25202	0	0.9320

6	11	0.0949	0.19890	0	1
6	12	0.1229	0.25581	0	1
6	13	0.0661	0.13027	0	1
7	8	0	0.17615	0	1
7	9	0	0.11001	0	1
9	10	0.0318	0.08450	0	1
9	14	0.1271	0.27038	0	1
10	11	0.0820	0.19207	0	1
12	13	0.2209	0.19988	0	1
13	14	0.1709	0.34802	0	1

Table A.3: Bus Data for IEEE-30 Bus System (in p.u.)

Bus	*Voltage*	P_G	Q_G	P_L	Q_L	*Bus type*
1	1.060	0	0	0	0	1
2	1.043	40	50	21.70	12.7	2
3	1	0	0	2.400	1.20	3
4	1.060	0	0	7.600	1.60	3
5	1.010	0	37	94.20	19	2
6	1	0	0	0	0	3
7	1	0	0	22.80	10.9	3
8	1.010	0	37.30	30	30	2
9	1	0	0	0	0	3
10	1	0	0	5.800	2	3
11	1.082	0	16.20	0	0	2
12	1	0	0	11.20	7.50	3
13	1.071	0	10.60	0	0	2
14	1	0	0	6.200	1.60	3
15	1	0	0	8.200	2.50	3
16	1	0	0	3.500	1.80	3
17	1	0	0	9	5.80	3
18	1	0	0	3.200	0.90	3
19	1	0	0	9.500	3.40	3
20	1	0	0	2.200	0.70	3
21	1	0	0	17.50	11.2	3
22	1	0	0	0	0	3
23	1	0	0	3.200	1.6	3
24	1	0	0	8.70	6.7	3
25	1	0	0	0	0	3
26	1	0	0	3.50	2.3	3
27	1	0	0	0	0	3
28	1	0	0	0	0	3
29	1	0	0	2.40	0.9	3
30	1	0	0	10.60	1.9	3

Table A.4: Line Data for IEEE-30 Bus System (in p.u.)

From Bus	*To Bus*	*Resistance*	*Reactance*	*B shunt*	*Tap ratio*
1	2	0.0192	0.0575	0.0264	1
1	3	0.0452	0.1652	0.0204	1
2	4	0.0570	0.1737	0.0184	1
3	4	0.0132	0.0379	0.0042	1
2	5	0.0472	0.1983	0.0209	1
2	6	0.0581	0.1763	0.0187	1
4	6	0.0119	0.0414	0.0045	1
5	7	0.0460	0.1160	0.0102	1
6	7	0.0267	0.0820	0.0085	1
6	8	0.0120	0.0420	0.0045	1
6	9	0	0.2080	0	0.978
6	10	0	0.5560	0	0.969
9	11	0	0.2080	0	1
9	10	0	0.1100	0	1
4	12	0	0.2560	0	0.932
12	13	0	0.1400	0	1
12	14	0.1231	0.2559	0	1
12	15	0.0662	0.1304	0	1
12	16	0.0945	0.1987	0	1
14	15	0.2210	0.1997	0	1
16	17	0.0824	0.1923	0	1
15	18	0.1073	0.2185	0	1
18	19	0.0639	0.1292	0	1
19	20	0.0340	0.0680	0	1
10	20	0.0936	0.2090	0	1
10	17	0.0324	0.0845	0	1
10	21	0.0348	0.0749	0	1
10	22	0.0727	0.1499	0	1
21	23	0.0116	0.0236	0	1
15	23	0.1000	0.2020	0	1
22	24	0.1150	0.1790	0	1
23	24	0.1320	0.2700	0	1
24	25	0.1885	0.3292	0	1
25	26	0.2544	0.3800	0	1
25	27	0.1093	0.2087	0	1
28	27	0	0.3960	0	0.968
27	29	0.2198	0.4153	0	1
27	30	0.3202	0.6027	0	1
29	30	0.2399	0.4533	0	1
8	28	0.0636	0.2000	0.0214	1
6	28	0.0169	0.0599	0.0650	1

Table A.5: Bus Data for IEEE-57 Bus System (in p.u.)

Bus	*Voltage*	P_G	Q_G	P_L	Q_L	*Bus type*
1	1.040	0	0	0	0	1
2	1.010	0	-0.80	3	88	2
3	0.985	40	-1	41	21	2
4	1	0	0	0	0	3
5	1	0	0	13	4	3
6	0.980	0	0.80	75	2	2
7	1	0	0	0	0	3
8	1.005	450	62.1	150	22	2
9	0.980	0	2.20	121	26	2
10	1	0	0	5	2	3
11	1	0	0	0	0	3
12	1.015	310	128.5	377	24	2
13	1	0	0	18	2.30	3
14	1	0	0	10.50	5.30	3
15	1	0	0	22	5	3
16	1	0	0	43	3	3
17	1	0	0	42	8	3
18	1	0	0	27.20	9.80	3
19	1	0	0	3.300	0.60	3
20	1	0	0	2.300	1	3
21	1	0	0	0	0	3
22	1	0	0	0	0	3
23	1	0	0	6.300	2.10	3
24	1	0	0	0	0	3
25	1	0	0	6.300	3.20	3
26	1	0	0	0	0	3
27	1	0	0	9.30	0.50	3
28	1	0	0	4.60	2.30	3
29	1	0	0	17	2.60	3
30	1	0	0	3.60	1.80	3
31	1	0	0	5.80	2.90	3
32	1	0	0	1.60	0.80	3
33	1	0	0	3.80	1.90	3
34	1	0	0	0	0	3
35	1	0	0	6	3	3
36	1	0	0	0	0	3
37	1	0	0	0	0	3
38	1	0	0	14	7	3
39	1	0	0	0	0	3
40	1	0	0	0	0	3
41	1	0	0	6.30	3	3
42	1	0	0	7.10	4.40	3
43	1	0	0	2	1	3
44	1	0	0	12	1.80	3
45	1	0	0	0	0	3
46	1	0	0	0	0	3

47	1	0	0	29.70	11.6	3
48	1	0	0	0	0	3
49	1	0	0	18	5.30	3
50	1	0	0	21	10.50	3
51	1	0	0	18	5.30	3
52	1	0	0	4.90	2.20	3
53	1	0	0	20	10	3
54	1	0	0	4.10	1.40	3
55	1	0	0	6.80	3.40	3
56	1	0	0	7.60	2.20	3
57	1	0	0	6.700	2	3

Table A.6: Line Data for IEEE-57 Bus System (in p.u.)

From Bus	*To Bus*	*Resistance*	*Reactance*	*B shunt*	*Tap ratio*
1	2	0.0083	0.0280	0.0645	1
2	3	0.0298	0.0850	0.0409	1
3	4	0.0112	0.0366	0.0190	1
4	5	0.0625	0.1320	0.0129	1
4	6	0.0430	0.1480	0.0174	1
6	7	0.0200	0.1020	0.0138	1
6	8	0.0339	0.1730	0.0235	1
8	9	0.0099	0.0505	0.0274	1
9	10	0.0369	0.1679	0.0220	1
9	11	0.0258	0.0848	0.0109	1
9	12	0.0648	0.2950	0.0386	1
9	13	0.0481	0.1580	0.0203	1
13	14	0.0132	0.0434	0.0055	1
13	15	0.0269	0.0869	0.0115	1
1	15	0.0178	0.0910	0.0494	1
1	16	0.0454	0.2060	0.0273	1
1	17	0.0238	0.1080	0.0143	1
3	15	0.0162	0.0530	0.0272	1
4	18	0	0.5550	0	0.970
4	18	0	0.4300	0	0.978
5	6	0.0302	0.0641	0.0062	1
7	8	0.0139	0.0712	0.0097	1
10	12	0.0277	0.1262	0.0164	1
11	13	0.0223	0.0732	0.0094	1
12	13	0.0178	0.0580	0.0302	1
12	16	0.0180	0.0813	0.0108	1
12	17	0.0397	0.1790	0.0238	1
14	15	0.0171	0.0547	0.0074	1
18	19	0.4610	0.6850	0	1
19	20	0.2830	0.4340	0	1
21	20	0	0.7767	0	1.043
21	22	0.0736	0.1170	0	1
22	23	0.0099	0.0152	0	1
23	24	0.1660	0.2560	0.0042	1

24	25	0	1.1820	0	1
24	25	0	1.2300	0	1
24	26	0	0.0473	0	1.043
26	27	0.1650	0.2540	0	1
27	28	0.0618	0.0954	0	1
28	29	0.0418	0.0587	0	1
7	29	0	0.0648	0	0.967
25	30	0.1350	0.2020	0	1
30	31	0.3260	0.4970	0	1
31	32	0.5070	0.7550	0	1
32	33	0.0392	0.0360	0	1
34	32	0	0.9530	0	0.975
34	35	0.0520	0.0780	0.00160	1
35	36	0.0430	0.0537	0.00080	1
36	37	0.0290	0.0366	0	1
37	38	0.0651	0.1009	0.00100	1
37	39	0.0239	0.0379	0	1
36	40	0.0300	0.0466	0	1
22	38	0.0192	0.0295	0	1
11	41	0	0.7490	0	0.955
41	42	0.2070	0.3520	0	1
41	43	0	0.4120	0	1
38	44	0.0289	0.0585	0.00100	1
15	45	0	0.1042	0	0.955
14	46	0	0.0735	0	0.900
46	47	0.0230	0.0680	0.00160	1
47	48	0.0182	0.0233	0	1
48	49	0.0834	0.1290	0.00240	1
49	50	0.0801	0.1280	0	1
50	51	0.1386	0.2200	0	1
10	51	0	0.0712	0	0.930
13	49	0	0.1910	0	0.895
29	52	0.1442	0.1870	0	1
52	53	0.0762	0.0984	0	1
53	54	0.1878	0.2320	0	1
54	55	0.1732	0.2265	0	1
11	43	0	0.1530	0	0.958
44	45	0.0624	0.1242	0.00200	1
40	56	0	1.1950	0	0.958
56	41	0.5530	0.5490	0	1
56	42	0.2125	0.3540	0	1
39	57	0	1.3550	0	0.98
57	56	0.1740	0.2600	0	1
38	49	0.1150	0.1770	0.00150	1
38	48	0.0312	0.0482	0	1
9	55	0	0.1205	0	0.94

APPENDIX-B
Data for Two area Four machine System

The two area system is shown in the Fig.5 [93]. The system consists of two fully symmetrical areas linked together by two 230 kV tie lines of 220 km length. Each area is equipped with two identical round rotor generators rated 20 kV/ 900 MVA. Generators 1 and 2 are in area one and generator 3 and 4 belongs to second area. Table B.1 and B.2 shows the bus data and line data respectively. Synchronous machine and exciter data are given in Table B.3 and Table B.4.

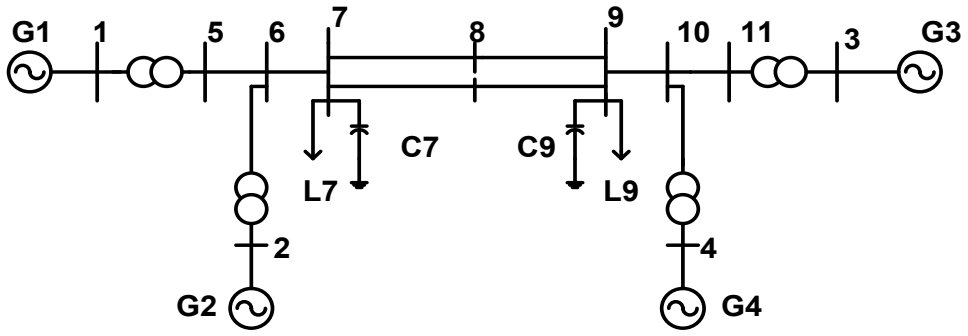

Figure.B.1 Two-area four-machine system

Table B.1 Bus Data (in p.u.)

Bus	*Voltage*	P_G	Q_G	P_L	Q_L
1	1.030	7	1.610	0	0
2	1.010	7	1.760	0	0
7	0.978	0	0	9.76	1
5	1.010	0	0	0	0
3	1.030	7.16	1.490	0	0
4	1.010	7	1.390	0	0
9	0.989	0	0	17.67	1
6	0.987	0	0	0	0
8	1	0	1.090	0	0
11	1.012	0	0	0	0
10	0.993	0	0	0	0

Table B.2 Line Data (in p.u.)

From Bus	*To Bus*	*Resistance*	*Reactance*	*Line charging*	*Tap Ratio*
1	5	0	0.0167	0	1
2	6	0	0.0167	0	1
7	6	0.001	0.0100	0.0175	1
7	8	0.011	0.1100	0.1925	1
7	8	0.011	0.1100	0.1925	1
5	6	0.0025	0.0250	0.0437	1
3	11	0	0.0167	0	1
4	10	0	0.0167	0	1
9	8	0.0110	0.1100	0.1925	1
9	8	0.0110	0.1100	0.1925	1
9	10	0.0010	0.0100	0.0175	1
11	10	0.0025	0.0250	0.0437	1

Table B.3 Synchronous Machine Data (in p.u.)

Gen No	*Bus No*	*MVA*	X_l	r_a	X_d	X'_d	X''_d	T'_{d0}	T''_{d0}	X_q	X'_q	X''_q	T'_{q0}	T''_{q0}	H
1	1	900	0.2	0.0025	1.8	0.3	0.25	8	0.03	1.7	0.55	0.25	0.4	0.05	6.5
2	2	900	0.2	0.0025	1.8	0.3	0.25	8	0.03	1.7	0.55	0.25	0.4	0.05	6.5
3	3	900	0.2	0.0025	1.8	0.3	0.25	8	0.03	1.7	0.55	0.25	0.4	0.05	6.5
4	4	900	0.2	0.0025	1.8	0.3	0.25	8	0.03	1.7	0.55	0.25	0.4	0.05	6.5

Table B.4 Exciter Data (in p.u.)

Gen no.	T_R	K_A	T_A	$V_{R\max}$	$V_{R\min}$
1	0	0.01	200	5	-5
2	0	0.01	200	5	-5
3	0	0.01	200	5	-5
4	0	0.01	200	5	-5

Table B.5 Power system stabilizer Data (in p.u.)

Gen no.	K	T_W	T_1	T_2	T_3	T_4
1	30	10	0.05	0.02	3	4
2	30	10	0.05	0.02	3	4
3	30	10	0.05	0.02	3	4
4	30	10	0.05	0.02	3	4

List of Symbols

P_G	Real power generated
Q_G	Reactive power generated
P_L	Real load
Q_L	Reactive load
X_l	Leakage reactance
r_a	resistance
X_d	d-axis synchronous reactance
X'_d	d-axis transient reactance
X''_d	d-axis sub transient reactance
T'_{d0}	d-axis open circuit time constant
T''_{d0}	d-axis open circuit sub transient time constant
X_q	q-axis synchronous reactance
X'_q	q-axis transient reactance
X''_q	q-axis sub transient reactance
T'_{q0}	q-axis open circuit time constant
T''_{q0}	q-axis open circuit sub transient time constant
H	Inertia Constant
d_0	Local damping coefficient
d_1	
T_R	Input filter time constant
K_A	Voltage regulator gain
T_A	Voltage regulator time constant
T_B	Voltage regulator time constant
T_C	Voltage regulator time constant
$V_{R\max}$	Max voltage regulator output

$V_{R\min}$	Min voltage regulator output
K_E	Exciter constant
T_E	Exciter time constant
E_1	
SE_1	Saturation function
E_2	
SE_2	Saturation function
K_F	Stabilizer gain
T_F	Stabilizer time constant
K	Gain
T_W	Washout time constant
T_1	Lead time constant
T_2	Lag time constant
T_3	Lead time constant
T_4	Lag time constant
$OUT_{\max}$	Maximum output limit
$OUT_{\min}$	Minimum output limit

APPENDIX-C
Data for 39-bus New England System

Simplified representation of New England (NE) 39-bus system is shown in Fig.C.1. The system is having 10 generators and 29 load buses. Table C.1 and C.2 shows the bus data and line data in p.u. Synchronous machine and exciter data is given in Tables C.3 and C.4, respectively.

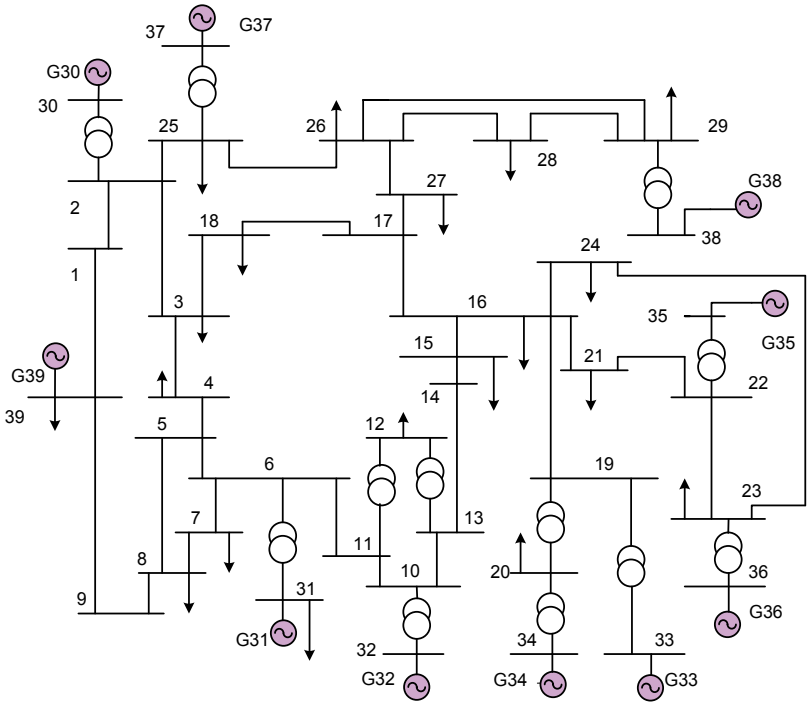

Figure C.1 New England 39 Bus system

Table C.1: Bus Data (in p.u.)

Bus	*Voltage*	P_G	Q_G	P_L	Q_L	*Bus type*
1	1.048	0	0	0	0	3
2	1.050	0	0	0	0	3
3	1.034	0	0	3.22	0.024	3
4	1.011	0	0	5	1.840	3
5	1.016	0	0	0	0	3
6	1.017	0	0	0	0	3
7	1.006	0	0	2.33	8.400	3
8	1.005	0	0	5.22	1.760	3
9	1.032	0	0	0	0	3
10	1.023	0	0	0	0	3
11	1.020	0	0	0	0	3

12	1.007	0	0	0.085	0.880	3
13	1.020	0	0	0	0	3
14	1.018	0	0	0	0	3
15	1.019	0	0	3.200	1.530	3
16	1.034	0	0	3.294	3.230	3
17	1.036	0	0	0	0	3
18	1.034	0	0	1.580	0.300	3
19	1.050	0	0	0	0	3
20	0.991	0	0	6.800	1.030	3
21	1.033	0	0	2.740	1.150	3
22	1.050	0	0	0	0	3
23	1.045	0	0	2.475	0.846	3
24	1.039	0	0	3.086	-0.922	3
25	1.058	0	0	2.240	0.4720	3
26	1.053	0	0	1.390	0.1700	3
27	1.039	0	0	2.810	0.7550	3
28	1.050	0	0	2.060	0.2760	3
29	1.050	0	1	2.835	1.2690	2
30	1.047	2.5	1.36	0	0	2
31	1.040	5.7	1.70	0.092	0.0460	2
32	0.983	6.5	1.75	0	0	2
33	0.997	6.3	1.03	0	0	2
34	1.012	5.0	1.64	0	0	2
35	1.049	6.5	2.08	0	0	2
36	1.063	5.6	0.96	0	0	2
37	1.027	5.4	-0.04	0	0	2
38	1.026	8.3	0.193	0	0	2

Table C.2: Line Data (in p.u.)

From Bus	*To Bus*	*Resistance*	*Reactance*	*Line Charging*	*Tap Ratio*
1	2	0.0035	0.0411	0.6987	0
1	39	0.0010	0.0250	0.7500	0
2	3	0.0013	0.0151	0.2572	0
2	25	0.0070	0.0086	0.1460	0
2	30	0	0.0181	0	1.025
3	4	0.0013	0.0213	0.2214	0
3	18	0.0011	0.0133	0.2138	0
4	5	0.0008	0.0128	0.1342	0
4	14	0.0008	0.0129	0.1382	0
5	8	0.0008	0.0112	0.1476	0
6	5	0.0002	0.0026	0.0434	0
6	7	0.0006	0.0092	0.1130	0
6	11	0.0007	0.0082	0.1389	0
7	8	0.0004	0.0046	0.0780	0
8	9	0.0023	0.0363	0.3804	0
9	39	0.0010	0.0250	1.2000	0
10	11	0.0004	0.0043	0.0729	0
10	13	0.0004	0.0043	0.0729	0

10	32	0	0.0200	0	1.070
12	11	0.0016	0.0435	0	1.006
12	13	0.0016	0.0435	0	1.006
13	14	0.0009	0.0101	0.1723	0
14	15	0.0018	0.0217	0.3660	0
15	16	0.0009	0.0094	0.1710	0
16	17	0.0007	0.0089	0.1342	0
16	19	0.0016	0.0195	0.3040	0
16	21	0.0008	0.0135	0.2548	0
16	24	0.0003	0.0059	0.0680	0
17	18	0.0007	0.0082	0.1319	0
17	27	0.0013	0.0173	0.3216	0
19	33	0.0007	0.0142	0	1.070
19	20	0.0007	0.0138	0	1.060
20	34	0.0009	0.0180	0	1.009
21	22	0.0008	0.0140	0.2565	0
22	23	0.0006	0.0096	0.1846	0
22	35	0	0.0143	0	1.025
23	24	0.0022	0.0350	0.3610	0
23	36	0.0005	0.0272	0	1
25	26	0.0032	0.0323	0.5130	0
25	37	0.0006	0.0232	0	1.025
26	27	0.0014	0.0147	0.2396	0
26	28	0.0043	0.0474	0.7802	0
26	29	0.0057	0.0625	1.0290	0
28	29	0.0014	0.0151	0.2490	0
29	38	0.0008	0.0156	0	1.025
31	6	0	0.0250	0	1

Table C.3: Synchronous Machine Data (in p.u.)

Gen. no	*Bus No.*	*MVA*	X_l	r_a	X_d	X'_d	X''_d	T'_{d0}	T''_{d0}	X_q
1	30	1000	0.125	0.0014	1	0.310	0	10.2	0	0.69
2	31	1000	0.350	0.0270	2.95	0.697	0	6.56	0	2.82
3	32	1000	0.304	0.0038	2.49	0.531	0	5.70	0	2.37
4	33	1000	0.295	0.0022	2.62	0.436	0	5.69	0	2.58
5	34	1000	0.540	0.0014	6.70	1.320	0	5.40	0	6.20
6	35	1000	0.224	0.0615	2.54	0.500	0	7.30	0	2.41
7	36	1000	0.322	0.0026	2.95	0.490	0	5.66	0	2.92
8	37	1000	0.280	0.0068	2.90	0.570	0	6.70	0	2.80
9	38	1000	0.298	0.0030	2.10	0.570	0	4.79	0	2.05
10	39	1000	0.030	0.0010	0.20	0.060	0	7	0	0.19

Gen. no	X'_q	X''_q	T'_{q0}	T''_{q0}	H	d_0	d_1
1	0.310	0	1.50	0	4.20	0	0
2	0.697	0	1.50	0	3.03	0	0
3	0.531	0	1.50	0	3.58	0	0
4	0.436	0	1.50	0	2.86	0	0
5	1.320	0	0.44	0	2.60	0	0
6	0.500	0	0.40	0	3.48	0	0
7	0.490	0	1.50	0	2.64	0	0
8	0.570	0	0.41	0	2.43	0	0
9	0.570	0	1.96	0	3.45	0	0
10	0.060	0	0.70	0	50	0	0

Table C.4: Exicter Data (in p.u.)

Gen no.	T_R	K_A	T_A	T_B	T_C	$V_{R\max}$	$V_{R\min}$	K_E	T_E	E_1	SE_1	E_2	SE_2	K_F	T_F
1	0	5	0.06	0	0	5	-5	-0.05	0.25	1.7	0.50	3	2	0	0.04
2	0	6.2	0.05	0	0	5	-5	0.63	0.41	3	0.66	4	0.88	0	0.06
3	0	5	0.06	0	0	5	-5	-0.02	0.50	3	0.13	4	0.34	0	0.08
4	0	5	0.06	0	0	5	-5	-0.05	0.50	3	0.08	4	0.31	0	0.08
5	0	40	0.02	0	0	10	-10	-0.04	0.78	3	0.03	4	0.91	0	0.03
6	0	5	0.02	0	0	5	-5	1	0.47	3	0.08	4	0.25	0	0.08
7	0	40	0.02	0	0	6.5	-6.5	1	0.73	3	0.03	4	0.74	0	0.03
8	0	5	0.02	0	0	5	-5	-0.05	0.52	3	0.09	4	0.28	0	0.09
9	0	40	0.02	0	0	10.5	-10.5	1	1.40	3	0.03	4	0.85	0	0.03

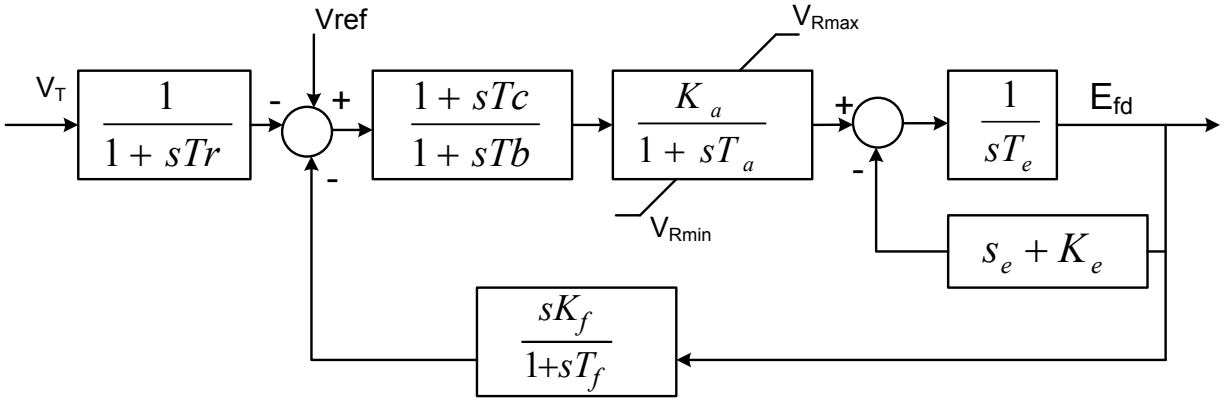

Figure C.2 D.C. Type-1 Exciter

APPENDIX-D
Data for 68-bus New England-New York Interconnected System

The single line diagram of 16-machine New England -New York System is given in Fig.D.1. This system is an interconnection of New England and New York power systems [39]. There are total 16 generators, G1-G9 in New England, G10-G13 in New York and G14-G16 in the neighborhood of New York. Table D1. and D.2 show the line and bus data . Synchronous machine and exciter data are given in Table D.3 and D.4 respectively. The parameters of the conventional type of power system stabilizers are given in D.5

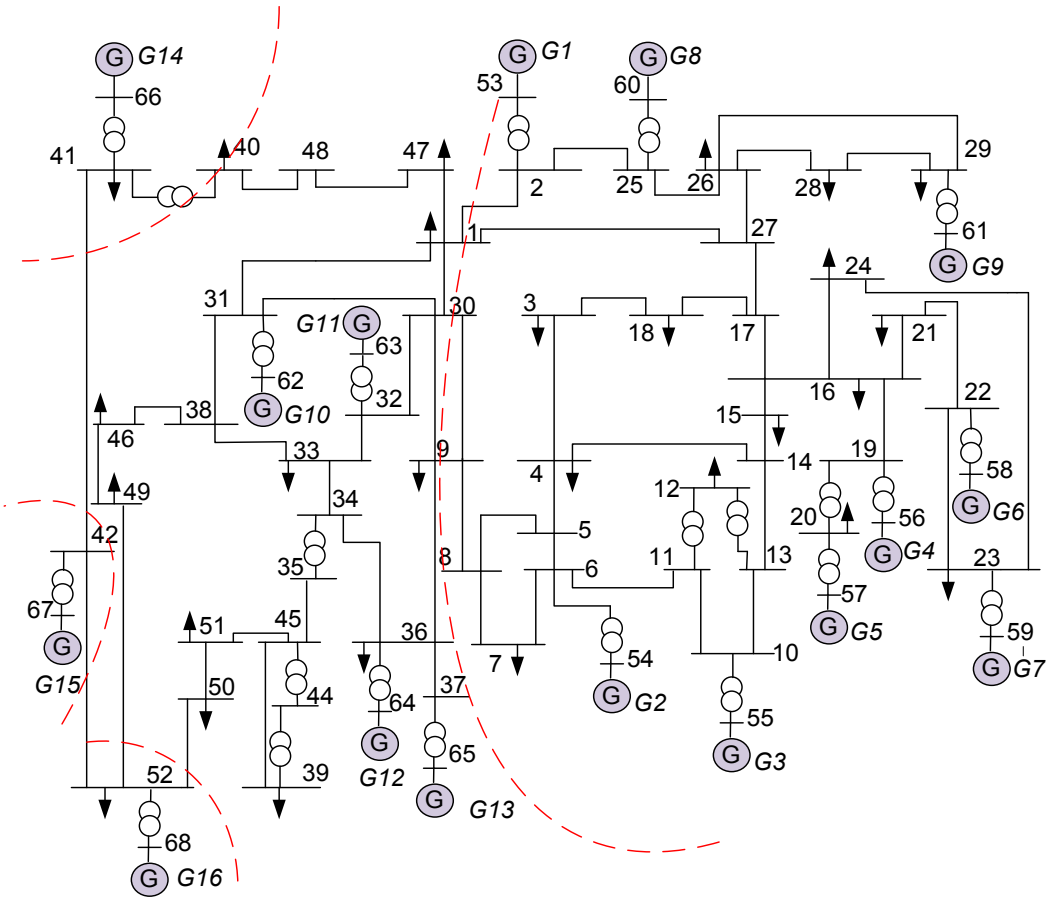

Figure D.1 Five-area sixteen-machine system

Table D.1: Bus Data (in p.u.)

Bus	*Voltage*	P_G	Q_G	P_L	Q_L	*Bus type*
1	1	0	0	2.527	1.1856	3
2	1	0	0	0	0	3
3	1	0	0	3.220	0.0200	3
4	1	0	0	5	1.8400	3
5	1	0	0	0	0	3
6	1	0	0	0	0	3
7	1	0	0	2.340	0.8400	3
8	1	0	0	5.220	1.7700	3
9	1	0	0	1.040	1.2500	3
10	1	0	0	0	0	3
11	1	0	0	0	0	3
12	1	0	0	0.090	0.8800	3
13	1	0	0	0	0	3
14	1	0	0	0	0	3
15	1	0	0	3.200	1.5300	3
16	1	0	0	3.290	0.3200	3
17	1	0	0	0	0	3
18	1	0	0	1.580	0.3000	3
19	1	0	0	0	0	3
20	1	0	0	6.800	1.0300	3
21	1	0	0	2.740	1.1500	3
22	1	0	0	0	0	3
23	1	0	0	2.480	0.8500	3
24	1	0	0	3.090	-0.920	3
25	1	0	0	2.240	0.4700	3
26	1	0	0	1.390	0.1700	3
27	1	0	0	2.810	0.7600	3
28	1	0	0	2.060	0.2800	3
29	1	0	0	2.840	0.2700	3
30	1	0	0	0	0	3
31	1	0	0	0	0	3
32	1	0	0	0	0	3
33	1	0	0	1.1200	0	3
34	1	0	0	0	0	3
35	1	0	0	0	0	3
36	1	0	0	1.0200	-0.1946	3
37	1	0	0	60	3	3
38	1	0	0	0	0	3
39	1	0	0	2.6700	0.1260	3
40	1	0	0	0.6563	0.2353	3
41	1	0	0	10	2.5000	3
42	1	0	0	11.500	2.5000	3
43	1	0	0	0	0	3
44	1	0	0	2.6755	0.0484	3
45	1	0	0	2.0800	0.2100	3
46	1	0	0	1.5070	0.2850	3

47	1	0	0	2.0312	0.3259	3
48	1	0	0	2.4120	0.0220	3
49	1	0	0	1.6400	0.2900	3
50	1	0	0	1	-1.470	3
51	1	0	0	3.3700	-1.220	3
52	1	0	0	24.700	1.230	3
53	1.045	2.50	0	0	0	2
54	0.980	5.45	0	0	0	2
55	0.983	6.50	0	0	0	2
56	0.997	6.32	0	0	0	2
57	1.011	5.05	0	0	0	2
58	1.050	7	0	0	0	2
59	1.063	5.60	0	0	0	2
60	1.030	5.40	0	0	0	2
61	1.025	8	0	0	0	2
62	1.010	5	0	0	0	2
63	1	10	0	0	0	2
64	1.015	13.5	0	0	0	2
65	1.011	35.9	0	0	0	1
66	1	17.8	0	0	0	2
67	1	10	0	0	0	2
68	1	40	0	0	0	2

Table D.2: Line Data (in p.u.)

From Bus	*To Bus*	*Resistance*	*Reactance*	*Line charging*	*Tap Ratio*
1	2	0.00350	0.0411	0.6987	0
1	30	0.00080	0.0074	0.4800	0
2	3	0.00130	0.0151	0.2572	0
2	25	0.00700	0.0086	0.1460	0
2	53	0	0.0181	0	1.0250
3	4	0.00130	0.0213	0.2214	0
3	18	0.00110	0.0133	0.2138	0
4	5	0.00080	0.0128	0.1342	0
4	14	0.00080	0.0129	0.1382	0
5	6	0.00020	0.0026	0.0434	0
5	8	0.00080	0.0112	0.1476	0
6	7	0.00060	0.0092	0.1130	0
6	11	0.00070	0.0082	0.1389	0
6	54	0	0.0250	0	1.0700
7	8	0.00040	0.0046	0.0780	0
8	9	0.00230	0.0363	0.3804	0
9	30	0.00190	0.0183	0.2900	0
10	11	0.00040	0.0043	0.0729	0
10	13	0.00040	0.0043	0.0729	0
10	55	0	0.0200	0	1.0700
12	11	0.00160	0.0435	0	1.0600
12	13	0.00160	0.0435	0	1.0600
13	14	0.00090	0.0101	0.1723	0

14	15	0.00180	0.0217	0.3660	0
15	16	0.00090	0.0094	0.1710	0
16	17	0.00070	0.0089	0.1342	0
16	19	0.00160	0.0195	0.3040	0
16	21	0.00080	0.0135	0.2548	0
16	24	0.00030	0.0059	0.0680	0
17	18	0.00070	0.0082	0.1319	0
17	27	0.00130	0.0173	0.3216	0
19	20	0.00070	0.0138	0	1.0600
19	56	0.00070	0.0142	0	1.0700
20	57	0.00090	0.0180	0	1.0090
21	22	0.00080	0.0140	0.2565	0
22	23	0.00060	0.0096	0.1846	0
22	58	0	0.0143	0	1.0250
23	24	0.00220	0.0350	0.3610	0
23	59	0.00050	0.0272	0	0
25	26	0.00320	0.0323	0.5310	0
25	60	0.00060	0.0232	0	1.0250
26	27	0.00140	0.0147	0.2396	0
26	28	0.00430	0.0474	0.7802	0
26	29	0.00570	0.0625	1.0290	0
28	29	0.00140	0.0151	0.2490	0
29	61	0.00080	0.0156	0	1.0250
9	30	0.00190	0.0183	0.2900	0
9	36	0.00220	0.0196	0.3400	0
9	36	0.00220	0.0196	0.3400	0
36	37	0.00050	0.0045	0.3200	0
34	36	0.00330	0.0111	1.4500	0
35	34	0.00010	0.0074	0	0.9460
33	34	0.00110	0.0157	0.2020	0
32	33	0.00080	0.0099	0.1680	0
30	31	0.00130	0.0187	0.3330	0
30	32	0.00240	0.0288	0.4880	0
1	31	0.00160	0.0163	0.2500	0
31	38	0.00110	0.0147	0.2470	0
33	38	0.00360	0.0444	0.6930	0
38	46	0.00220	0.0284	0.4300	0
46	49	0.00180	0.0274	0.2700	0
1	47	0.00130	0.0188	1.3100	0
47	48	0.00250	0.0268	0.4000	0
47	48	0.00250	0.0268	0.4000	0
48	40	0.00200	0.0220	1.2800	0
35	45	0.00070	0.0175	1.3900	0
37	43	0.00050	0.0276	0	0
43	44	0.00010	0.0011	0	0
44	45	0.00250	0.0730	0	0
39	44	0	0.0411	0	0
39	45	0	0.0839	0	0
45	51	0.00040	0.0105	0.7200	0
50	52	0.00120	0.0288	2.0600	0

50	51	0.00090	0.0221	1.6200	0
49	52	0.00760	0.1141	1.1600	0
52	42	0.00400	0.0600	2.2500	0
42	41	0.00400	0.0600	2.2500	0
41	40	0.00600	0.0840	3.1500	0
31	62	0	0.0260	0	1.0400
32	63	0	0.0130	0	1.0400
36	64	0	0.0075	0	1.0400
37	65	0	0.0033	0	1.0400
41	66	0	0.0015	0	1
42	67	0	0.0015	0	1
52	68	0	0.0030	0	1
1	27	0.03200	0.3200	0.4100	1

Table D.3: Synchronous Machine Data (in p.u.)

Gen. no	*Bus No.*	*MVA*	X_l	r_a	X_d	X'_d	X''_d	T'_{d0}	T''_{d0}	X_q
1	53	300	0.0030	0	1.0174	0.248	0.147	12.6	0.045	0.630
2	54	800	0.035	0	1.8900	0.4252	0.3050	6.56	0.050	1.8067
3	55	800	0.030	0	1.8900	0.3830	0.3246	5.70	0.050	1.7952
4	56	800	0.029	0	1.8900	0.2995	0.2404	5.69	0.050	1.8611
5	57	700	0.027	0	1.8900	0.3600	0.2727	5.40	0.050	1.7754
6	58	900	0.022	0	1.8900	0.3543	0.2834	7.30	0.050	1.7932
7	59	800	0.032	0	1.8900	0.2989	0.2440	5.66	0.050	1.8707
8	60	800	0.028	0	1.8900	0.3537	0.2793	6.70	0.050	1.8247
9	61	1000	0.029	0	1.8900	0.4871	0.3846	4.79	0.050	1.8397
10	62	1200	0.019	0	1.8900	0.4867	0.4260	9.37	0.050	1.2861
11	63	1600	0.010	0	1.8900	0.2531	0.1687	4.10	0.050	1.8161
12	64	1900	0.022	0	1.8900	0.5524	0.4455	7.40	0.050	1.7777
13	65	12000	0.003	0	1.8900	0.3344	0.2432	5.90	0.050	1.8261
14	66	10000	0.001	0	1.8900	0.2850	0.2300	4.10	0.050	1.8165
15	67	10000	0.001	0	1.8900	0.2850	0.2300	4.10	0.050	1.8165
16	68	11000	0.004	0	1.8900	0.3589	0.2780	7.80	0.050	1.7732

Table D.3 (cont...): Synchronous Machine Data (in p.u.)

Gen. no	X'_q	X''_q	T'_{q0}	T''_{q0}	H	d_0	d_1
1	0.250	0	0.035	0	3.570	0	0
2	0.366	0.3050	1.50	0.035	5.1968	0	0
3	0.360	0.3246	1.50	0.035	5.2104	0	0
4	0.274	0.2404	1.50	0.035	4.3710	0	0
5	0.327	0.2727	0.44	0.035	5.0050	0	0
6	0.318	0.2834	0.40	0.035	5.1562	0	0
7	0.274	0.2440	1.50	0.035	4.5430	0	0
8	0.310	0.2793	0.41	0.035	4.1107	0	0
9	0.427	0.3846	1.96	0.035	4.2383	0	0
10	0.479	0.4260	1.50	0.035	3.0561	0	0
11	0.210	0.1687	1.50	0.035	2.1055	0	0
12	0.499	0.4455	1.50	0.035	5.4380	0	0
13	0.304	0.2432	1.50	0.035	4.2821	4.0782	0
14	0.250	0.2300	1.50	0.035	3.1500	3	0
15	0.250	0.2300	1.50	0.035	3.1500	3	0
16	0.303	0.2780	1.50	0.035	4.6725	4.450	0

Table D.4: Exicter Data (in p.u.)

Gen no.	T_R	K_A	T_A	T_B	T_C	$V_{R\max}$	$V_{R\min}$
1	0	100	0.010	0	0	5	-5
2	0	100	0.010	0	0	5	-5
3	0	100	0.010	0	0	5	-5
4	0	100	0.010	0	0	5	-5
5	0	100	0.010	0	0	5	-5
6	0	100	0.010	0	0	5	-5
7	0	100	0.010	0	0	5	-5
8	0	100	0.010	0	0	5	-5
9	0	100	0.010	0	0	5	-5
10	0	100	0.010	0	0	5	-5
11	0	100	0.010	0	0	5	-5
12	0	100	0.010	0	0	5	-5
13	0	100	0.010	0	0	5	-5
14	0	100	0.010	0	0	5	-5
15	0	100	0.010	0	0	5	-5
16	0	100	0.010	0	0	5	-5

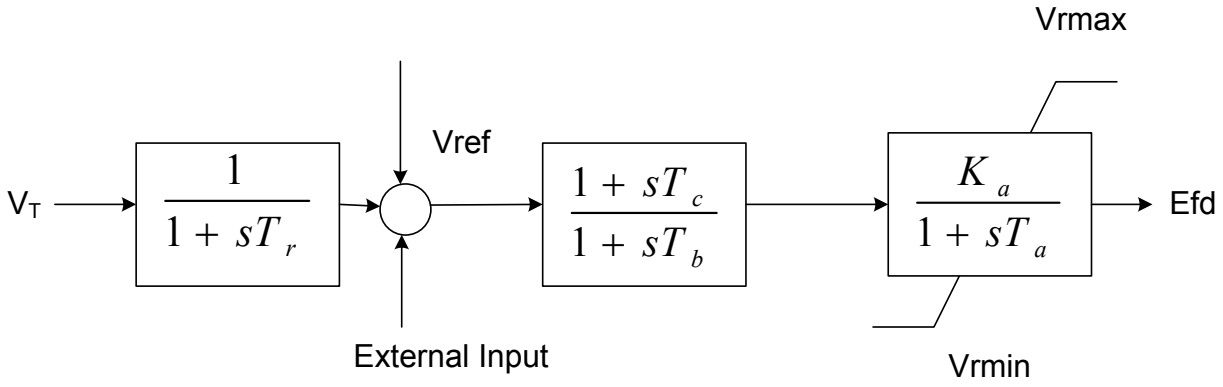

Fig.D.2. Simple Static Exciter

Table D.4: Power system stabilizer (PSS) Data (in p.u.)

Gen no.	K	T_W	T_1	T_2	T_3	T_4	$OUT_{\max}$	$OUT_{\min}$
7	100	10	0.080	0.020	0.080	0.020	0.20	-0.050
8	100	10	0.080	0.020	0.080	0.020	0.20	-0.050
9	100	10	0.050	0.020	0.020	0.010	0.20	-0.050
10	100	10	0.100	0.020	0.10	0.020	0.20	-0.050
11	50	10	0.080	0.030	0.05	0.010	0.20	-0.050
12	110	10	0.100	0.020	0.10	0.020	0.20	-0.050
7	100	10	0.080	0.020	0.08	0.020	0.20	-0.050
8	100	10	0.080	0.020	0.08	0.020	0.20	-0.050
9	100	10	0.050	0.020	0.02	0.010	0.20	-0.050
10	100	10	0.100	0.020	0.10	0.020	0.20	-0.050
11	50	10	0.080	0.030	0.05	0.010	0.20	-0.050
12	110	10	0.100	0.020	0.10	0.020	0.20	-0.050

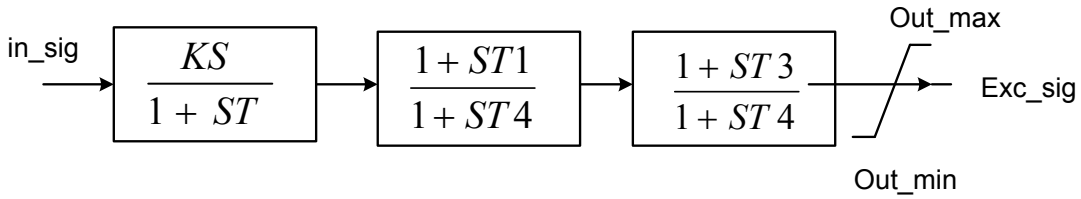

Figure D.3 Structure of Power system Stabilizer

APPENDIX-E
State Matrix Formulation for Large System

Power system consists of synchronous machines, excitation systems, transmission network, static and dynamic loads and various FACTS devices. Therefore, to analyze the complete system for small signal stability involves simultaneous solution of various ordinary differential and algebraic equations. The formulation of the state equations for small-signals analysis involves the development of linearized equations about an operating point and elimination of all variables other than the state variables. Therefore, the formulation of state equations requires a systematic procedure for treating the wide range of devices. Fig E.1 depicts the procedure:

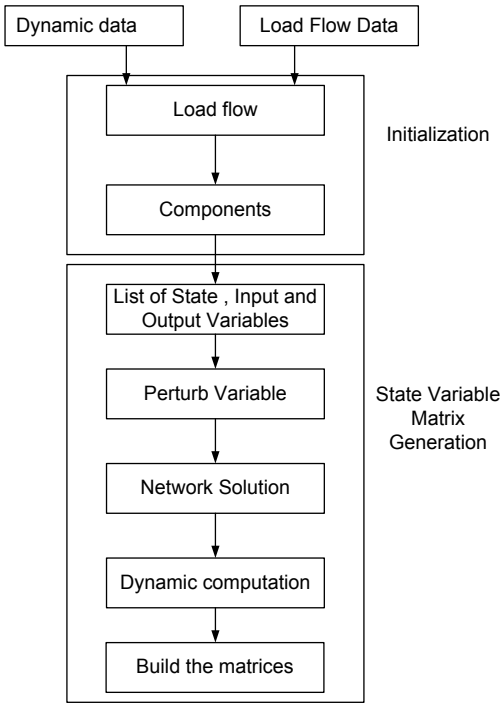

Figure E.1 Structure of Program of State Matrix Formulation [54]

First load flow of the given system using Newton-Rapson algorithm in polar co-ordinates is conducted. This load flow solution is used to initialize the state variables of the machine models and their control devices.

For network solutions, all voltages and currents are expressed in a common reference frame. Therefore, transformation from individual machine d-q axis to system reference coordinate is carried out for computing the network solution. Constant impedance loads are generally eliminated in the network solution. Further, voltages of these eliminated buses are computed

through voltage reconstruction matrix. In systems, having FACTs and SVCs, load buses are not removed in reduced Y matrix. However, Newton iteration method is utilized to obtain non-conforming load bus solution. In PST [48], the entries of state matrices are obtained by partial derivates, which are numerically obtained by dividing the state derivatives and output variable increments by small perturbations.

In an interconnected system each dynamic device can be represented as

$$\dot{x}_i = A_i x_i + B_i \Delta v \tag{E.1}$$

$$\Delta i_i = C_i x_i - Y_i \Delta v \tag{E.2}$$

Where

x_i are the perturbed values of the individual device state variables

i_i is the current injection into the network from the device

v is the vector of the network bus voltages

B_i and Y_i have non-zero elements corresponding to the terminal voltage of the device and any remote bus voltages used to control the device . The current $\dot{i}_i$ has two elements corresponding to the real and imaginary components. Similarly, the voltage vector v has two elements per bus associated with the device. Such state equations for all the dynamic devices in the system are further combined in the form

$$\dot{x} = A_D x + B_D \Delta v \tag{E.3}$$

$$\Delta \dot{i} = C_D - Y_D \Delta v \tag{E.4}$$

Where x is the state vector of the complete system, and A_D and C_D are the block diagonal matrices composed of A_i and C_i associated with the individual devices. The transmission network present in the power system is represented by node equation:

$$\Delta i = Y_N \Delta v \tag{E.5}$$

In above expression Y_N includes the effects of the non-linear static loads. Equating equations (E.4) to (E.5), following expression is obtained

$$C_D x - Y_D \Delta v = Y_N \Delta v \tag{E.6}$$

Above expression is further solved as

$$\Delta v = \left(Y_N + Y_D\right)^{-1} C_D x \tag{E.7}$$

Substituting, Δv from expression (E.7) to (E.3), overall system equation is obtained as

$$\dot{x} = A_D x + B_D \left(Y_N + Y_D\right)^{-1} C_D x \;=\; Ax \tag{E.8}$$

Where overall system A matrix is given by

$$A = A_D + B_D \left(Y_N + Y_D\right)^{-1} C_D \tag{E.9}$$

The method of building A_i, B_i, and Y_i matrices for synchronous machine and associated controls follow the above general approach. To speed up the computations instead of computing variables of each machine sequentially, the same variable of all machines are computed simultaneously.

APPENDIX-F
Hybrid Learning Rule of Adaptive Neuro Fuzzy Inference System

Hybrid learning rule of Adaptive Neuro Fuzzy Inference System (ANFIS) combines gradient descent method and least squares estimate (LSE) to identify various parameters of the network [62, 63].

Gradient descent method

In gradient-based learning rule, energy function for p^{th} entry of training data is represented as

$$E_p = \sum_{m=1}^{nL} \left(T_{m,p} - O_{m,p}^{L} \right)^2 \tag{F.1}$$

Where $T_{m,p}$ is the m^{th} component of p^{th} target output vector and $O_{m,p}^{L}$ is m^{th} component of actual output vector. L represents the total number of layers of the adaptive network , nL denotes number of nodes in layer L. Therefore total error over total training data P, is expressed as

$$E = \sum_{p=1}^{P} E_p \tag{F.2}$$

To implement gradient descent over parameter space, error rate is computed with respect to output node at (L,i)

$$\frac{\partial E_p}{\partial O_{i,p}^{L}} = -2\left(T_{i,p} - O_{i,p}^{L} \right) \tag{F.3}$$

Now expressing above equation in terms of network parameter

$$\frac{\partial E_p}{\partial \alpha} = \sum_{O^* \in S} \frac{\partial E_p}{\partial O^*} \frac{\partial O^*}{\partial \alpha} \tag{F.4}$$

Above expression in further solved and is expressed as

$$\Delta\alpha = -\eta \frac{\partial E}{\partial \alpha} \tag{F.5}$$

In above expression, for given step size sp, η is a learning rate, which is further given as

$$\eta = \frac{sp}{\sqrt{\sum_{\alpha} \left(\frac{\partial E}{\partial \alpha} \right)^2}} \tag{F.6}$$

Least Square Method

In least square estimate method, it is assumed that adaptive network had one output, which is of form

$$\text{output} = F(I, S) \tag{F.7}$$

Where, I is the set of input variables and S is the set of parameters. Now if there exists a function H such that the composite function $H \circ F$ is linear in some elements of S. These elements of S are identified using least squares method.

$$H(\text{output}) = H \circ F(I, S) \tag{F.8}$$

Parameter set S is further decomposed into two sets

$$S = S_1 \oplus S_2 \tag{F.9}$$

Now If $H \circ F$ is linear in the elements of S_2. With the given values of S_1 above expression (F.8) is represented as

$$AX = B \tag{F.10}$$

In (F.10) X is an unknown vector of parameters S_2. Above equation is solved using least square method as

$$X^* = \left(A^T A\right)^{-1} A^T B \tag{F.11}$$

To have efficient computation, sequential method of LSE is generally employed, which is given by following equation

$$X_{i+1} = X_i + S_{i+1} a_{i+1} \left(b_{i+1}^T - a_{i+1}^T X_i\right) \tag{F.12}$$

$$S_{i+1} = S_i - \frac{S_i a_{i+1} a_{i+1}^T S_i}{1 + a_{i+1}^T S_i a_{i+1}}, \quad i = 0,1,\cdots P-1 \tag{F.13}$$

In above expression S_i is called the covariance matrix and least square estimate X^* is equal to X_P.

Each epoch of hybrid learning rule consists of a forward and backward pass.

- In forward pass, input data and functional signals are used to calculate output matrices A and B of (F.10)
- Later parameters of S2 are computed using LSE through (F.12) and (F.13.) After identifying S2, error measure is calculated.
- In backward pass, error rates propagated from output to input are computed using (F.3) and (F.4).
- Finally, S1 are updated using error gradient method according to (F.5).